Luminescent lanthanide complexes for cellular applications

Poole, Robert

Luminescent Lanthanide Complexes for Cellular Applications

Robert Poole

A thesis submitted for the degree of Doctor of Philosophy

Department of Chemistry
University of Durham

2006

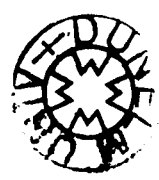

Declaration

The research described in this thesis was undertaken at the Department of Chemistry of the University of Durham between October 2003 and September 2006. All of the work is my own; no part of it has previously been submitted for a degree at this or any other university.

Statement of Copyright

Acknowledgements

Sincere thanks to:

Professor David Parker for giving me the opportunities to learn and do so much over the last three years, and for always being available to discuss my problems.

Dr Alan Kenwright, Catherine Hefferman and Ian McKeag for their assistance with NMR spectroscopy.

Dr Mike Jones and Lara Turner for help with mass spectrometry and for carrying out accurate mass determination.

Dr Aileen Congreve for the time she has given to sorting my many cells by flow cytometry.

Dr Bob Peacock for giving up his time to assist with CPL measurements and for allowing me to use his facilities at Glasgow University.

Dr Chris Ottley for carrying out ICP-MS measurements.

Dr Martin Cann for much help and advice with the more biological aspects of my work.

Collaborators at Cisbio: Gérard Mathis, Eric Trinquet, Laurent Lamarque, Michel Fink and Sraboni Ghose; Hervé Bazin for his advice and the time that he and Nathalie Gregor have given towards performing the HTRF assay; Michel Laget for his assistance in obtaining time resolved microscopy images; Emilie Blanche for help with an assessment of quenching behaviour using the Rubystar.

The current and past members of the DP lab, for their friendly advice, and for making the last three years so enjoyable.

My parents for their encouragement and support throughout my time in Durham.

Abstract

The tetraazatriphenylene chromophore, dpqC, efficiently sensitises europium(III) and terbium(III) emission. It has been incorporated into a series of ligands, based on the cyclen macrocycle, which saturate the coordination sphere of the metal ion and lead to complexes that exhibit high luminescent quantum yields in aerated aqueous media of the order of 15 – 50 %, with long emission lifetimes of the order of milliseconds. Dynamic quenching of the lanthanide excited state occurs with electron-rich donors (e.g. urate, ascorbate and iodide). The high efficiency of S_1 to T_1 intersystem crossing and the low susceptibility of the aryl triplet excited state to quenching by molecular oxygen, allowed an assessment to be made of the deactivation of the lanthanide excited state through a charge-transfer mechanism. Comparison has been drawn between structurally related complexes of differing charge and lipophilicity. Terbium(III) complexes were shown to be more strongly quenched than their europium(III) analogues. The order of sensitivity to quenching generally followed the ease of oxidation of the quenching anion, but urate was anomalous. In each case, it was shown to quench by an order of magnitude more strongly than ascorbate, despite having a redox potential of 0.59 V, compared to 0.30 V for ascorbate. These differences have been exploited in the development of a ratiometric assay for the determination of uric acid concentration in biological samples.

The complexes have been shown to be taken up by a number of eukaryotic cell lines and are amenable to time resolved fluorescence microscopy. The cationic and lipophilic complexes give brighter images '*in cellulo*' than their neutral and anionic analogues. However, determination of the intracellular lanthanide concentration has revealed that the complexes are taken up to a similar extent. By relating the structure of the complexes to their uptake and localisation profiles, it should be possible to design complexes for specific intracellular applications, for example, as probes or components in biological assays.

Contents

Abbreviations

Ala	alanine
Ar	aromatic
Boc	*tert*-butoxycarbonyl
bpy	bipyridyl
CCD	charge coupled device
CD	circular dichroism
CHO	chinese hamster ovary cells
COS	transformed african green monkey kidney fibroblast cells
COSY	correlation spectroscopy
CPL	circularly polarised luminescence
cyclen	1,4,7,10-tetraazacyclododecane
dd	doublet of doublets
DO3A	1,4,7,10-tetraazacyclododecane-1,4,7-triacetic acid
DOTA	1,4,7,10-tetraazacyclododecane-1,4,7,10-tetraacetic acid
dpq	dipyrido [3,2-f:2',3'-c] phenazine
dpqC	10,11,12,13-tetrahydrodipyrido-[3,2a:2',3'-c]-phenazine
DTPA	diethylenetriaminepentaacetic acid
eT	electron transfer
ET	energy transfer
FLIM	fluorescent lifetime imaging
FCS	foetal calf serum
FRET	fluorescent resonance energy transfer
GFP	green fluorescent protein
Glu	glutamic acid
GST	glutathione-S-transferase
h	hours
HDF	human dermal fibroblast cells
HeLa	human carcinoma cells
HEK	human embryonic kidney cells

HEPES	N-(2-hydroxyethyl)piperazine-N'-(2-ethanesulphonic acid)
HRMS	high resolution mass spectrometry
HSA	human serum albumin
HTRF	homogeneous time resolved fluorescence
ICP-MS	inductively coupled plasma – mass spectrometry
ICP-OES	inductively coupled plasma – optical emission spectroscopy
ILCT	intraligand charge transfer
ISC	intersystem crossing
LMCT	ligand-to-metal charge transfer
Ln	lanthanide
m	multiplet
M	mol dm^{-3}
m.p	melting point
m/z	mass/charge
Mol	moles
MLCT	metal-to-ligand charge transfer
MRI	magnetic resonance imaging
NCS	newborn calf serum
NIH 3T3	mouse skin fibroblast cells
NIR	near-infra red
NMR	nuclear magnetic resonance
NMRD	nuclear magnetic resonance dispersion
phen	1,10-phenanthroline
PMT	photomultiplier tube
poly(dAdT)	polydeoxyadenylic-deoxythymidylic acid
poly(dGdC)	polydeoxyguanylic-deoxycytidylic acid
q	quaternary
R_f	retention time
s	singlet
SAP	square anti-prism
TBP	trisbipyridyl
THF	tetrahydrafuran

TR-FAIM	time resolved – fluorescence anisotropy imaging
TSAP	twisted square anti-prism
VT	variable temperature

CHAPTER 1

Introduction

1 Introduction

Luminescent lanthanide complexes demonstrate a huge potential to complement and extend the current range of tags and probes that are available for the analysis of living biological systems. Our understanding of their unique photophysical properties and how these can be exploited through careful ligand design allows for the targeted synthesis of complexes for specific applications.

1.1 Luminescence Properties of the Lanthanides

Lanthanide ions exhibit line-like absorption and emission spectra that are characteristic of their $4f^n$ electronic configurations; the 4f oritals are effectively shielded by filled $5p^6 6s^2$ energy levels and 4f-4f transitions are forbidden by electric dipole selection rules leading to low molar absorbance coefficients ($< 3\ M^{-1}\ s^{-1}$), but long natural luminescence lifetimes. The contracted nature of these orbitals results in emission spectra that do not significantly broaden or shift in wavelength upon complexation: ligand field splittings are typically small, with values of the order of 100 cm^{-1}. The difference between the lowest lying excited state of the metal ion and the sub-levels of its ground state defines in which region of the spectrum the lanthanide will emit. (Figure 1.1)

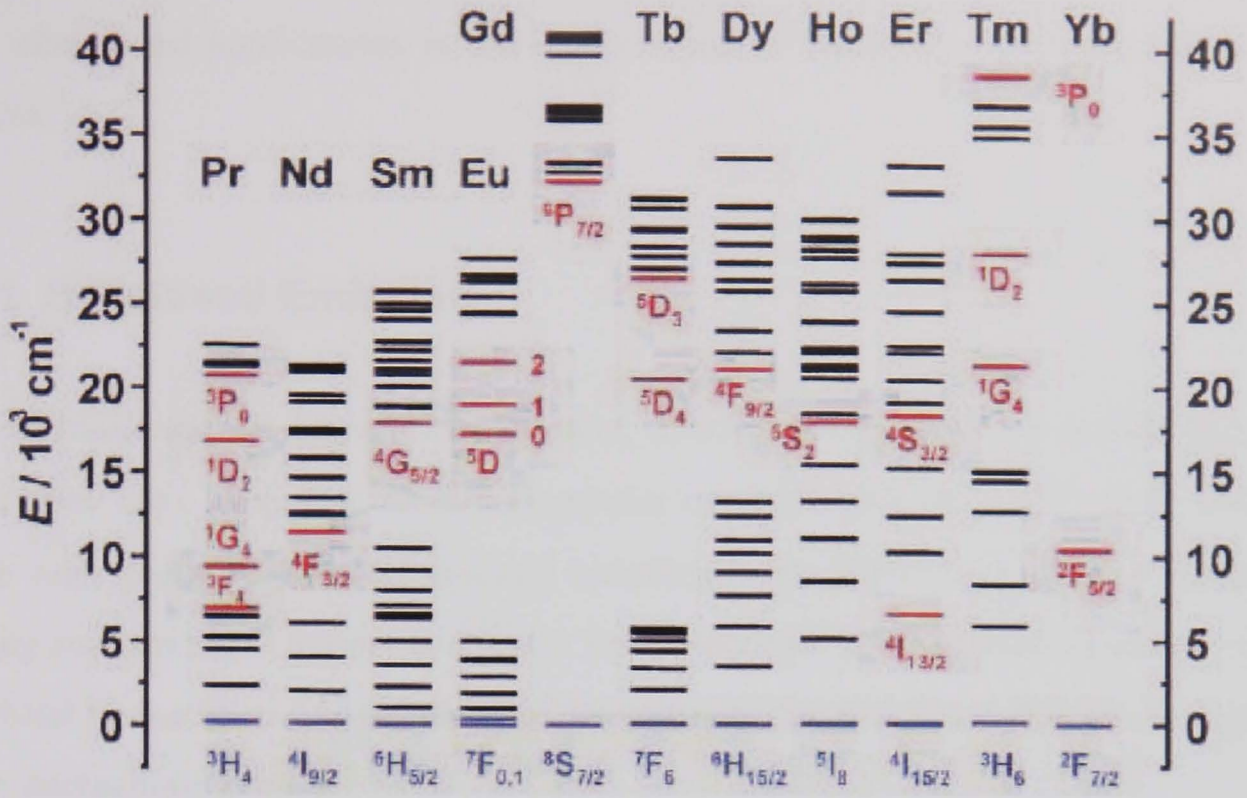

Figure 1. 1 - Partial energy diagram for the lanthanide aqua ions. Red lines indicate the main emissive levels, blue lines the ground state.

Europium(III), terbium(III), samarium(III) and dysprosium(III) complexes are all emissive in the visible region with energy gaps between the lowest emissive state and the ground-state manifold, ΔE = 12 300 ($^5D_0 \rightarrow {}^7F_6$), 14 800 ($^5D_4 \rightarrow {}^7F_0$), 7 400 ($^4G_{5/2} \rightarrow {}^6F_{11/2}$) and 7 850 ($^4F_{9/2} \rightarrow {}^6F_{3/2}$) cm^{-1} respectively.[1] In order for a compound to be useful in luminescence based applications, it is necessary to maximise the quantum yield of emission i.e. to minimise non-radiative deactivation pathways such as quenching through interaction with vibrational transitions of proximate molecular oscillators (e.g. O-H) and bound ligands.[2] The larger the energy gap between the ground and emissive state of the lanthanide ion, the less efficient these processes will be. Hence, it is not surprising that the majority of examples of luminescent lanthanide probes in the literature focus on europium(III) and terbium(III).[1] Some interest has also been shown in samarium(III) and dysprosium(III) complexes in the development of dual luminescent time-resolved immunoassays.[3] Apart from gadolinium(III), all of the remaining lanthanides have low emissive quantum yields in aqueous solution. Gd(III) emits in the UV, and is not useful as a luminescent probe for bioanalysis since the aromatic components of most biologically relevant molecules either absorb or emit in this region. Neodymium(III), holmium(III), erbium(III) and ytterbium(III) are interesting since they emit in the near-IR (NIR)

spectral range: a range in which biological tissue is relatively transparent.[4,5] They have also found applications in the construction of lasers and telecommunications devices.[1]

1.1.1 Sensitised Emission

4f -4f Transitions are Laporte (parity) and, in some cases also, spin forbidden. As a result they have very low molar absorption coefficients ($\varepsilon < 1\ M^{-1}\ cm^{-1}$) and are made only partially allowed through coupling with vibrational states, through J-mixing and mixing with opposite parity wavefunctions. The extent of shielding of the 4f orbital by the 6s and 5d orbitals and its contracted nature mean that the strength of these interactions is weak.

Excitation through the use of a high intensity source such as a laser is possible, but is not practicable if these compounds are to reach widespread applications as probes or sensors for biological systems. An alternative solution, which allows the use of lower intensity light, is sensitised emission whereby the excited state is reached following energy transfer from the triplet level of a suitable chromophore. (Figure 1.2)

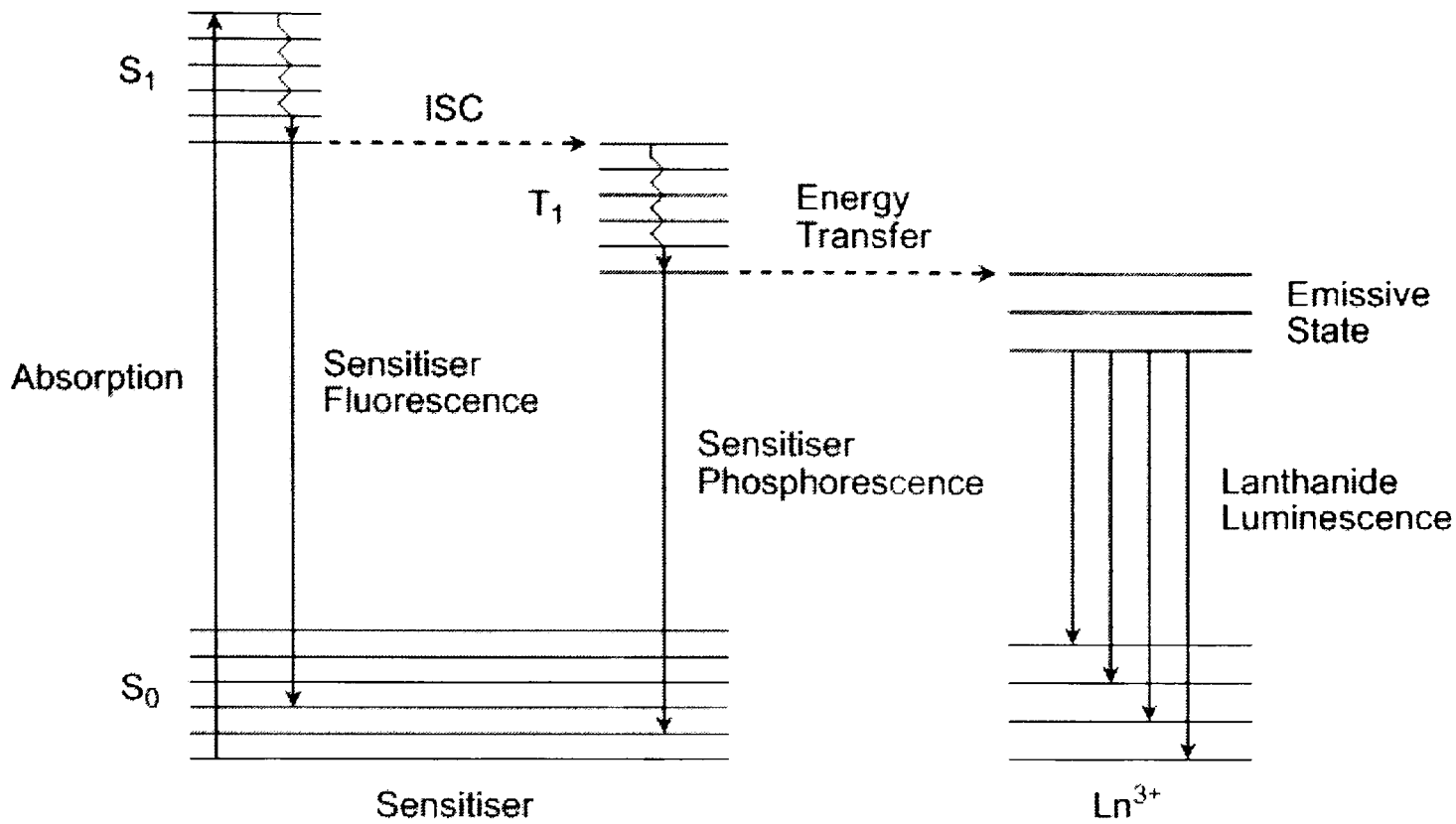

Figure 1. 2 – Jablonski diagram showing the indirect excitation of a lanthanide ion via an organic chromophore

A photon is first absorbed by the sensitiser, raising it to a vibrationally excited level of the S_1 band. Relaxation may occur through either non-radiative vibrational relaxation to the lowest level of the S_1 band followed by sensitiser fluorescence or by intersystem crossing to the triplet, T_1, band. From the T_1 state there are three competing processes: back intersystem crossing to the S_1 state; sensitiser phosphorescence; energy transfer to the lanthanide excited states. If the chromophore has a high molar absorption coefficient and the intersystem crossing and energy transfer processes are efficient, then the "effective" molar absorption coefficient of the metal is greatly increased and intense emission can be observed following excitation with conventional light sources.

For efficient sensitisation, the triplet energy of the chromophore should be slightly higher (> 1700 cm^{-1}) than the lanthanide emissive state ($^5D_0$ Eu = 17 240 cm^{-1}, $^5D_4$ Tb = 20 400 cm^{-1}). If the energy difference is too small i.e. less than 1500 cm^{-1} then thermally activated back energy transfer can occur leading to both a reduction in the emission intensity and lifetime. For europium, a photoinduced electron transfer from the chromophore to the metal can occur owing to the ease of reduction of Eu(III) to

Eu(II). This process often deactivates the singlet excited state of the sensitiser in a non-radiative way, thus reducing its efficiency as a sensitiser.

1.1.1.1 Mechanism of Energy Transfer[6]

There are two main classes of electronic energy transfer mechanism, radiative and non-radiative. Both the radiative and non-radiative processes rely on overlap between the emission spectrum of the donor and the absorption spectrum of the acceptor.

Radiative energy transfer involves the donor emitting light that is subsequently re-absorbed by the acceptor. This mechanism is favoured where the overlap is good and the quantum yield of emission of the donor and the light absorbing properties of the acceptor are maximised. For sensitised lanthanide emission, whilst there is good overlap between the chromophore triplet energy and the metal luminescent level, the low Ln(III) molar absorption coefficient makes this process unlikely.

A number of different mechanisms have been considered in an attempt to understand a non-radiative sensitiser-lanthanide energy transfer process. In principle, energy transfer can occur either from the chromophore singlet or triplet excited states; in most cases only the latter case is significant,[7] although some examples of direct energy transfer from the ligand first singlet excited state to the higher levels of europium(III) and terbium(III) ions have been reported in cases where the triplet state of the ligand lies below the emissive level of the metal.[8, 9] There are three mechanisms that are usually invoked for the energy transfer from the lowest band of the triplet manifold to the lanthanide(III) ion: i) the exchange (Dexter) mechanism; ii) a dipole-dipole (Förster) mechanism; iii) a dipole-multipole mechanism.

The exchange mechanism (Figure 1.3) involves mutual electron exchange between the sensitiser and acceptor, with conservation of multiplicity of the system. For this to occur the electronic orbitals of the donor and acceptor species must overlap.

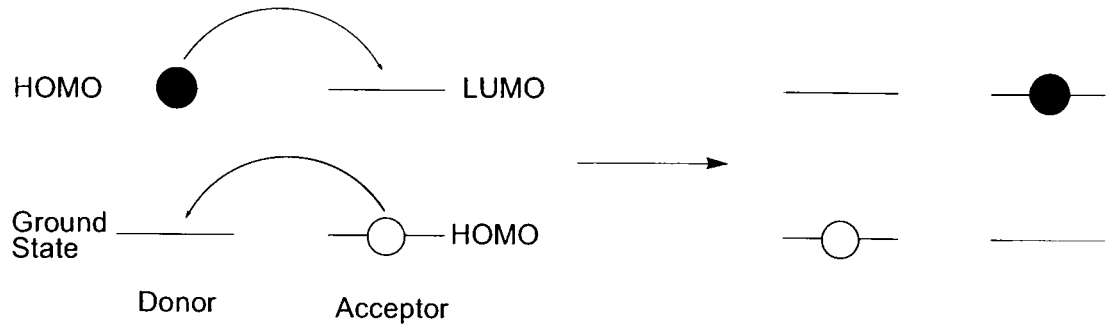

Figure 1. 3

The rate of energy transfer decreases exponentially with increasing separation between the donor and acceptor, R_{DA}.

The dipole-dipole and dipole-multipole mechanisms are through-space interactions between the electronic dipole moments of the sensitiser triplet state and the lanthanide 4f orbitals. The rate of energy transfer via the Förster mechanism exhibits a distance dependence of $1/R_{DA}^{6}$.

1.1.1.2 Alternative Routes to Sensitised Emission

Coordination of an organic chromophore with a suitable triplet energy to a lanthanide(III) ion is by far the most studied and well understood technique for sensitising emission. However, several other techniques have been demonstrated; the first requires the presence of available charge transfer states and as such is only valid for lanthanides that are able to accept electrons. This is true for Sm(III), Eu(III) and Yb(III) and involves transfer from a ligand-to-metal charge transfer (LMCT) state provided that it is of sufficient energy. Common examples involve the insertion of these compounds into inorganic matrices[1]; the second example relies on energy transfer from a transition metal. One example from Bünzli et al involves the use of Cr(III) both to sensitise Nd and Yb and to extent the lifetime of their emission into the millisecond range.[10] There are a number of other examples where transition metal complexes have been used to sensitise NIR emissive lanthanides mostly involving energy transfer from metal-to-ligand charge transfer (MLCT) states (e.g. through coordination of the Nd(III), Er(III) or Yb(III) to complexes of Ru(II), Re(I), Os(II) or

Pt(II)[11-13]; a final mechanism has been demonstrated by Faulkner *et al* where lanthanide complexes have been used to sensitise lanthanide emission, in this case Tb complexes being used to sensitise Yb emission.[14]

1.1.2 Minimising Competing De-activation Pathways

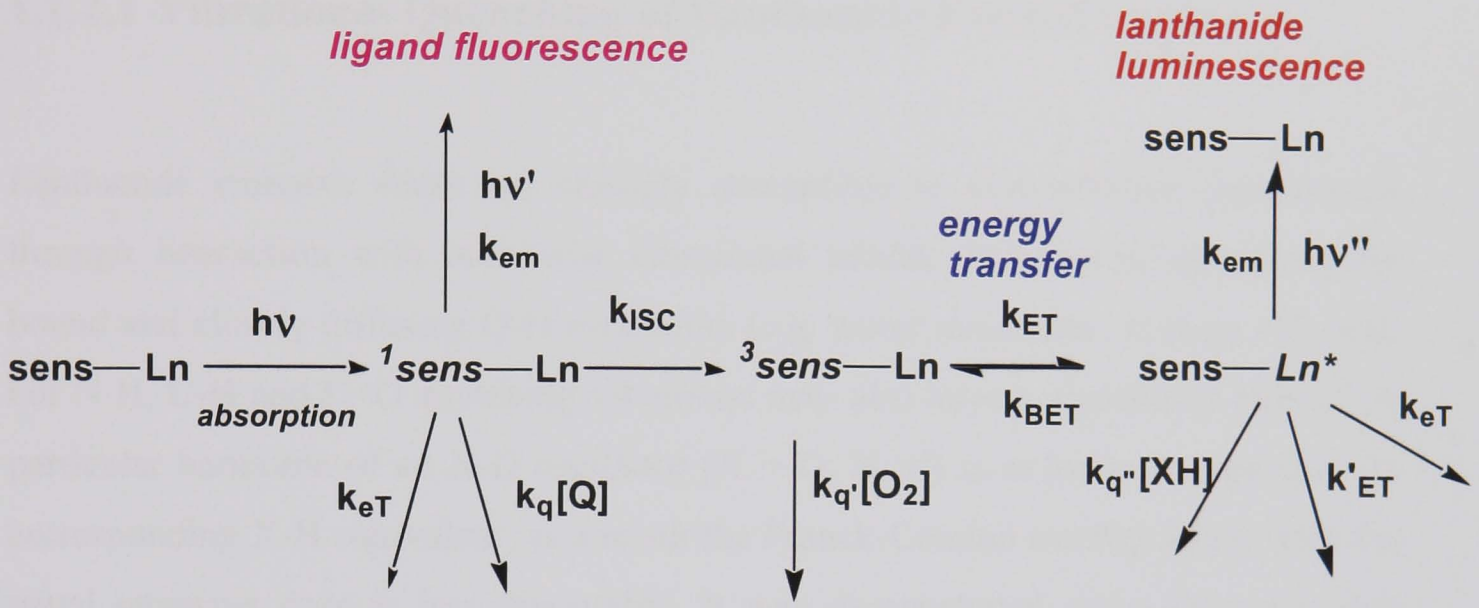

Figure 1. 4 – A diagram to show the competing deactivation pathways for sensitised lanthanide emission

The efficiency of energy transfer or emissive processes is usually expressed in terms of their quantum yields. For the case of sensitised lanthanide emission, we define the luminescence quantum yield as the ratio of the number of photons emitted through lanthanide luminescence to the number absorbed by the sample. This value is the product of the quantum yields of each of the individual energy transfer steps involved in reaching the lanthanide emissive state. Figure 1.4 depicts possible deactivation pathways for a lanthanide ion sensitised by an organic chromophore. There are three excited states that may be perturbed: the chromophore singlet and triplet states, and the lanthanide emissive state. In order to maximise the quantum yield, it is necessary to have fast intersystem crossing between the chromophore singlet and triplet levels and a high rate of energy transfer from the chromophore to the lanthanide. More particularly, the rates should be high when compared to those for competitive deactivation, through either radiative processes such as chromophore fluorescence or phosphorescence, or radiationless decay *via* electron/energy transfer

or by interaction with molecular quenching species. Examples of such processes include singlet state quenching by halide anions or by Eu(III) ions and triplet quenching by oxygen.[32-34] In addition to a high quantum yield, it is also desirable that the sensitising moiety should possess a high molar absorption coefficient to maximise the light output per unit concentration of sample.

1.1.2.1 Vibrational Quenching of Lanthanide Excited States

Lanthanide emissive states are strongly susceptible to non-radiative deactivation through interaction with molecular vibrational modes. In general, quenching by bound and closely diffusing O-H oscillators (e.g. water molecules) is most efficient, but N-H, C-H and C=O stretching vibrations may also have a significant effect.[16] A particular harmonic of an X-D oscillator (X = O, N, C) is at lower energy than its corresponding X-H equivalent; as a result the Franck-Condon overlap factor with the metal emissive state is less favourable. It was demonstrated some time ago that quenching of europium complexes observed in H_2O is greatly reduced in D_2O.[16, 17] Similarly, lanthanide ions with a comparatively larger energy gap between their ground and lowest energy excited states are less efficiently quenched; this accounts for the observation that terbium(III) complexes typically have higher emissive quantum yields than europium(III) complexes with the same ligand (Figure 1.5).

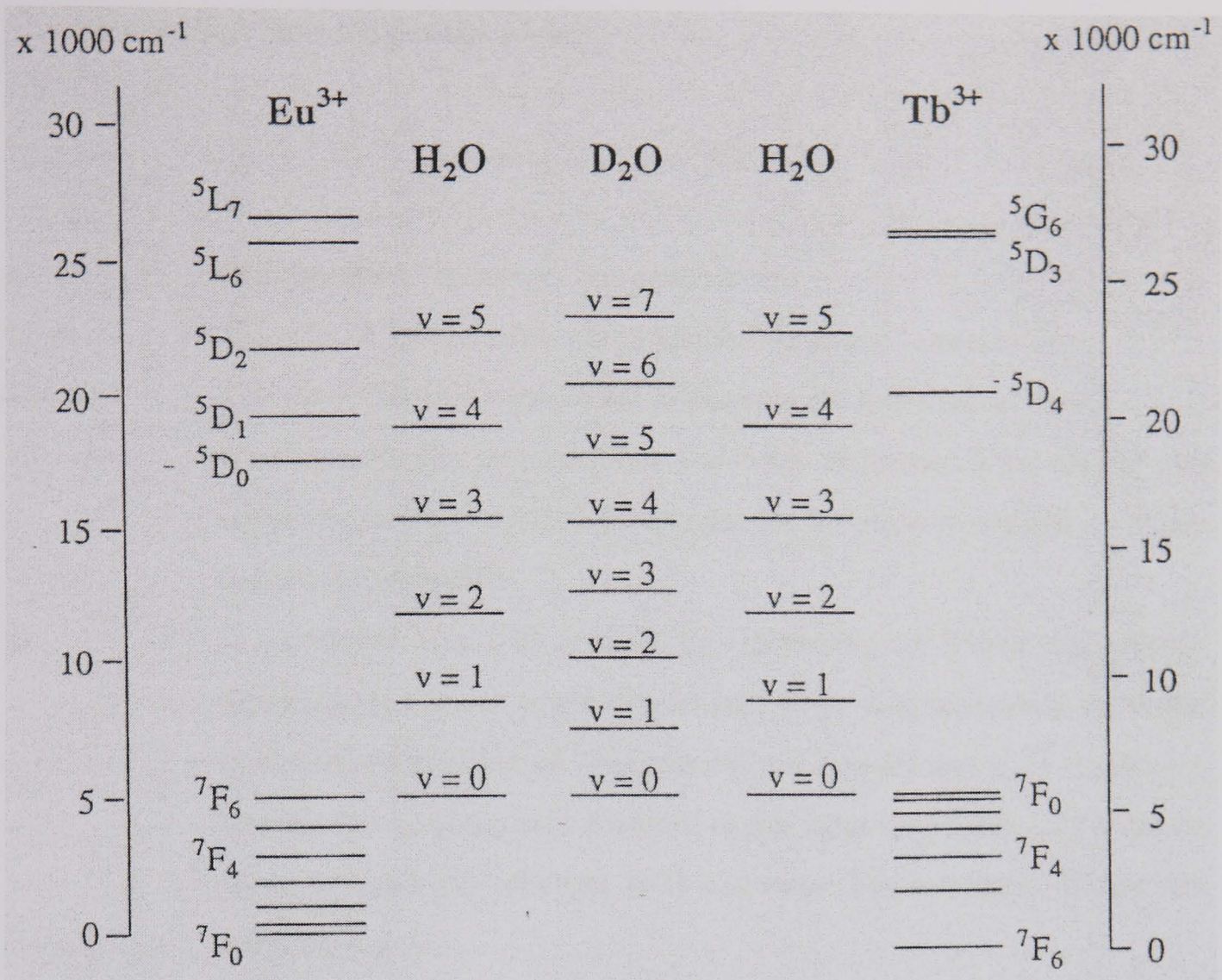

Figure 1. 5 - Energy level diagram showing correlation between the vibrational harmonic overtones of H_2O and D_2O relative to the emissive $^5D_0$ and $^5D_4$ states of europium and terbium respectively

Experimentally, the lower susceptibility of a complex to quenching in D_2O compared to H_2O is observed as an increase in lifetime and intensity of the metal-centred emission. The inverse of the emissive lifetime defines the rate constant for depopulation of the lanthanide excited state. Equations have been derived that allow the number of water molecules, q, directly coordinated to Nd(III), Sm(III), Eu(III), Tb(III) and Yb(III) lanthanide centres to be calculated; this is done through comparison between the rate constants for a given complex in H_2O and D_2O.[18-21] The basic assumptions of these relationships are that X-D oscillators do not contribute to de-activation and that all other competing pathways are the same in both D_2O and water (however, a number of correction factors are necessary).

The relationships have the general form:

$$q = A(k_{H2O} - k_{D2O} - B) - C$$

q	The number of unbound water molecules
k_{H2O}	The rate of deactivation of the lanthanide excited state in H_2O
k_{D2O}	The rate of deactivation of the lanthanide excited state in D_2O
A	A proportionality constant that scales the difference between the rate constants in D_2O and H_2O to account for the relative sensitivity of the particular lanthanide.
B	A correction factor to account for quenching by bound and closely diffusing oscillators: most importantly O-H, but depending upon the lanthanide, the effect of N-H (amine and amide) and C-H oscillators should also be taken into account; in the latter two cases care must be taken to establish whether H/D exchange has occurred. B has the same units as k
C	A further experimentally determined correction term to account for other Ln-dependent factors.

Quenching by O-H oscillators is predominant in aqueous media and the multipole-multipole mechanism that is thought to operate has a distance dependence of r^{-6} (where r is the distance between the energy donor and acceptor). Therefore, bound water molecules display the strongest effect. However, in order to obtain accurate q values, it is necessary to make corrections for contributions due to outer-sphere O-H quenching and deuterium exchangeable X-H oscillators, within the ligand structure.

The effect of second- and outer-sphere water molecules has been determined through analysis of a series of well characterised cyclen complexes that have been shown by X-ray crystallographic data to have no bound water molecules within their coordination sphere.[19] By comparing the radiative rate constants of complexes with the same ligand but different lanthanide ions in both H_2O and D_2O, an estimate can be made of the relative contribution of unbound O-H oscillators. The use of a number

of ligands of varying lipophilicity has been used to support the validity of these correction factors. As would be predicted from the difference in energy gap between their emissive state and ground state manifold, it follows that the order of sensitivities is Yb > Eu > Tb (correction factors are – 0.20 μs^{-1}, – 0.25 ms^{-1} and – 0.06 ms^{-1} respectively).[18, 19]

The quenching effect of other X-H oscillators needs to be taken into account only if they readily undergo H/D exchange. The use of amide based ligands is common with lanthanides: Eu(III) and Yb(III) centres are able to act as a charge sink, so that the N-H bonds of coordinated amide groups are able to undergo rapid H/D exchange (Figure 1.6). In contrast, for the other lanthanides where a 2+ oxidation state is of considerably higher energy, rates of NH/ND exchange may be much slower.

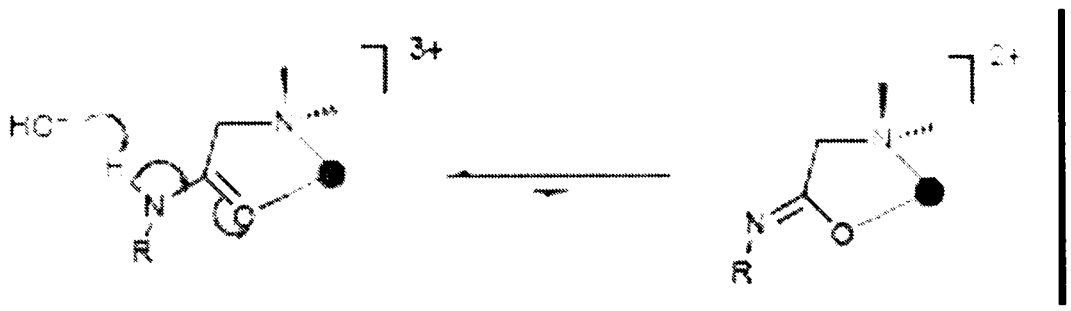

Figure 1. 6 – Base catalysed NH/ND exchange of coordinated amide NH bonds in Eu and Yb complexes, aided by the metal centre acting as a charge sink.[19]

In practice, correction is usually only necessary for europium complexes, since for ytterbium the quenching effect of N-H oscillators is small compared to the effect of proximate O-H oscillators. Comparison of a large number of tetraamide europium complexes has allowed the definition of the average quenching effect of an individual bound amide oscillator to be assessed as 0.075 ms^{-1}.

An example of the application of the general expression is provided in Chapter 2.

1.2 Ligand Design

The europium(III) and terbium(III) complexes that are the subject of the current work are intended for *in cellulo* fluorescence based applications as probes or as

components of biological assays. A number of factors need to be taken into consideration in the design of appropriate ligands which are considered in detail.

1.2.1 The Choice of Chromophore

As discussed in Section 1.1.1, due to the low molar absorption coefficients of the lanthanides (< 1 M^{-1} cm^{-1}), it is essential that a suitable sensitiser should be inserted into the ligand structure. The most important requirement is that the chromophore should have a high molar absorption coefficient at an excitation wavelength suitable for the intended application; for single photon excitation of biological samples this should be in the range 337 – 420 nm. The lower limit is set by the poor transparency of biological tissue to ultraviolet radiation and the harmful effects it has on live cells in microscopy; excitation in this range also obviates the need for quartz optics. The upper limit is defined by the excited state energies of the lanthanides. The $^5D_0$ europium(III) and $^5D_4$ terbium(III) excited states lie at 17200 and 20400 cm^{-1} respectively; the triplet energy of the chromophore should be at least 1500 cm^{-1} greater than the terbium $^5D_4$ state so as to prevent thermally activated back energy transfer. Generally, a requirement for such large triplet energies is that the chromophore S_1 – T_1 energy gap should be as small as possible. Excitation wavelengths that are particularly interesting are those that correspond to readily available laser lines (337, 355 or 405 nm for Eu/Tb), or those that are close in energy to the growing range of powerful light emitting diodes (e.g. 365 or 390 nm).[24]

In order to get efficient energy transfer to the lanathanide ion, the triplet state of the chromophore should be readily populated. This is achieved through having a fast rate of intersystem crossing compared to the rates of either radiative deactivation (i.e. fluorescence) or non-radiative decay processes. Furthermore, energy transfer is distance dependent and so the maximum quantum efficiency is achieved when the sensitiser-lanthanide distance is minimised. This is achieved through the use of a chromophore that can coordinate directly to the metal centre.

In recent years work in the Parker lab has focused on the use of tetraazatriphenylenes,[24-26] azaxanthones and azathiaxanthones[24, 27-28] but there are a number of other suitable examples, in particular those based on bi- and tri-pyridyls and their N-oxides.[29-31]

1.2.2 The Use of Macrocycles

The interactions between lanthanide ions and their ligands are mostly electrostatic. If a complex is to be used in any biological medium then there are significant concentrations of potentially competitive ligating molecules to consider (e.g. proteins, phospho-anions). In order to prevent metal ion dissociation it is essential that the complex should display high kinetic and thermodynamic stability, over a wide range of pH.

Lanthanide ions have high coordination numbers (8 or 9) and in aqueous solution are fully hydrated. Oxygen is a strong σ-donor and water is a good ligand for the lanthanides, often the enthalpy of bond formation does not fully compensate for the enthalpy of dehydration. A favourable Gibbs free energy term is still possible if there is a sufficient entropy change; this can be achieved through the use of a polydentate and in particular a macrocyclic ligand. Further stability can be provided by the incorporation of groups that provide strong electrostatic bonds by charge compensation upon complexation and the formation of stable 5 or 6 membered chelate rings.

1.2.3 Further considerations of Ligand Design

Further to the basic requirements that the ligand should be macrocyclic and incorporate a suitable chromophore, the design can be extended to include additional functionality through which the complex can be linked to another chemical compound or biological moiety. For example, to some form of targeting vector to be used for in cellular studies through coordination to an antibody or other component

in a fluorescence assay. [Much work has been carried out by Cisbio international in France towards the development of europium cryptates for use in heterogeneous time resolved fluorescence assays].[30]

1.2.4 Tetraazatriphenylenes: Highly Efficient Sensitisers for Europium and Terbium Emission

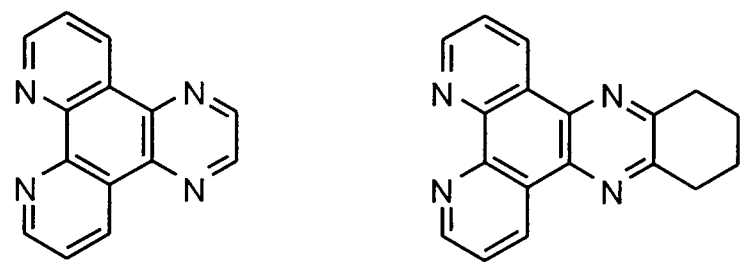

Figure 1. 7 Examples of tetraazatriphenylene chromophores dpq (left), dpqC (right)

Dipyrido[3,2-f:2',3'-h]quinoxaline (dpq) and 10,11,12,13-tetrahydrodipyrido[3,2-a:2',3'-c]phenazine (dpqC) (Figure 1.7) are excellent antenna chromophores.[31a, 31b] They absorb at 340 and 348 nm respectively; in both cases, their quantum yields of triplet formation are close to unity; They both have triplet state energies of about 23500 cm^{-1} (dpq 23800, dpqC 23400) which is sufficiently high for energy transfer to the emissive states of Eu(III) (17500 cm^{-1}) and Tb(III) (20400 cm^{-1}); They are reasonably strong ligands towards both Eu(III) and Tb(III) ions and as a result, the distance between donor and acceptor is small and the rate of energy transfer is high.

The dpqC chromophore was chosen for the current work since it has a longer wavelength first excited triplet state and has a significantly higher molar absorption coefficient in aqueous media (6440 M^{-1} cm^{-1} for dpqC cf. 3800 M^{-1} cm^{-1} for dpq).

1.2.5 Cyclen Based Ligand Systems[31c]

1,4,7,10-Tetraazacyclododecane (cyclen) based ligands are commonly used with the lanthanides since they afford well defined complexes with high thermodynamic and kinetic stability with respect to metal ion dissociation. Research in Durham has centred on this ligand system for a number of years and, as a result, its

functionalisation is well understood; this is usually done by coordinating pendent amide, carboxylic acid or phosphinate arms to the ring nitrogen atoms. Through the use of appropriate protecting strategies, the ring can be either mono, di, tri or tetra substituted; indeed attachment of up to four different arms is achievable. However, if conformational rigidity and a well defined structure are important, it is necessary that at least three of the four arms should be the same or very similar.

To understand the descriptions of conformation used with cyclen based ligands the commonly used example is 1,4,7,10-tetraazacyclododecane-N,N',N'',N'''-tetraacetic acid (DOTA). There are two elements of chirality that need to be defined: the conformation of the macrocyclic ring (λ or δ), associated with the N-C-C-N torsion angle (typically ± 60°) and the orientation of the acetate arms (Λ or Δ) associated with the N-C-C-O torsion angle (usually ± 30°).

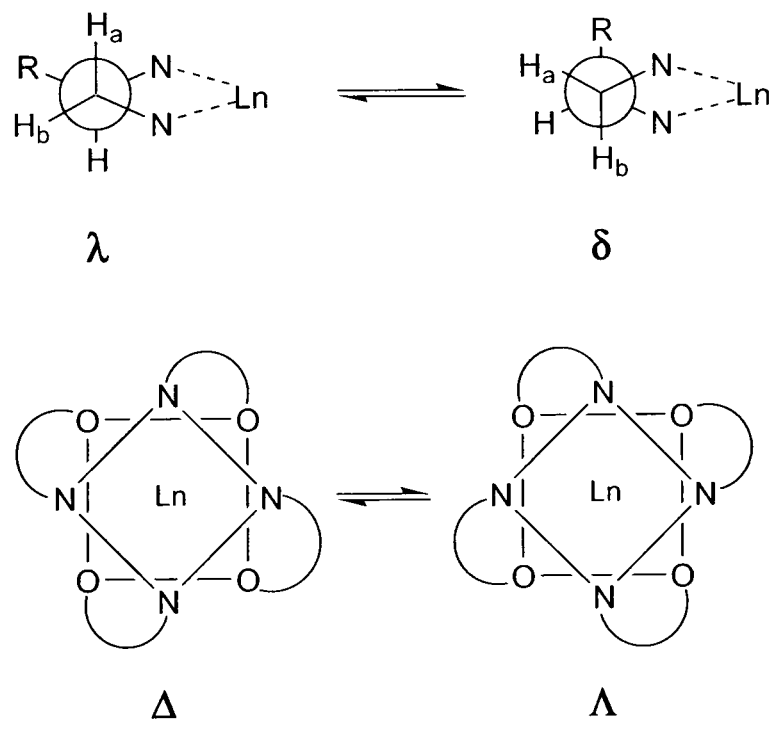

Figure 1. 8 DOTA conformations

As a result there are two possible macrocyclic ring conformations (Figure 1.8), λλλλ and δδδδ, and two conformations for the acetate arms, Λ or Δ giving rise to four stereoisomers that exist as two pairs of enantiomers. The stereoisomers adopt either a square antiprismatic geometry (SAP) with a twist angle of approximately 40° between the oxygen and nitrogen planes (Λ(δδδδ) and Δ(λλλλ)) or a twisted square antiprismatic geometry with a twist angle of approximately -30° (Λ(λλλλ) and

Δ(δδδδ)). In solution, the isomers can interconvert by either ring inversion (λλλλ to δδδδ) or arm rotation (Λ to Δ). Either process alone results in a change between the capped SAP and TSAP geometries whereas a combination of the two gives interconversion between the two enantiomers (Figure 1.9).

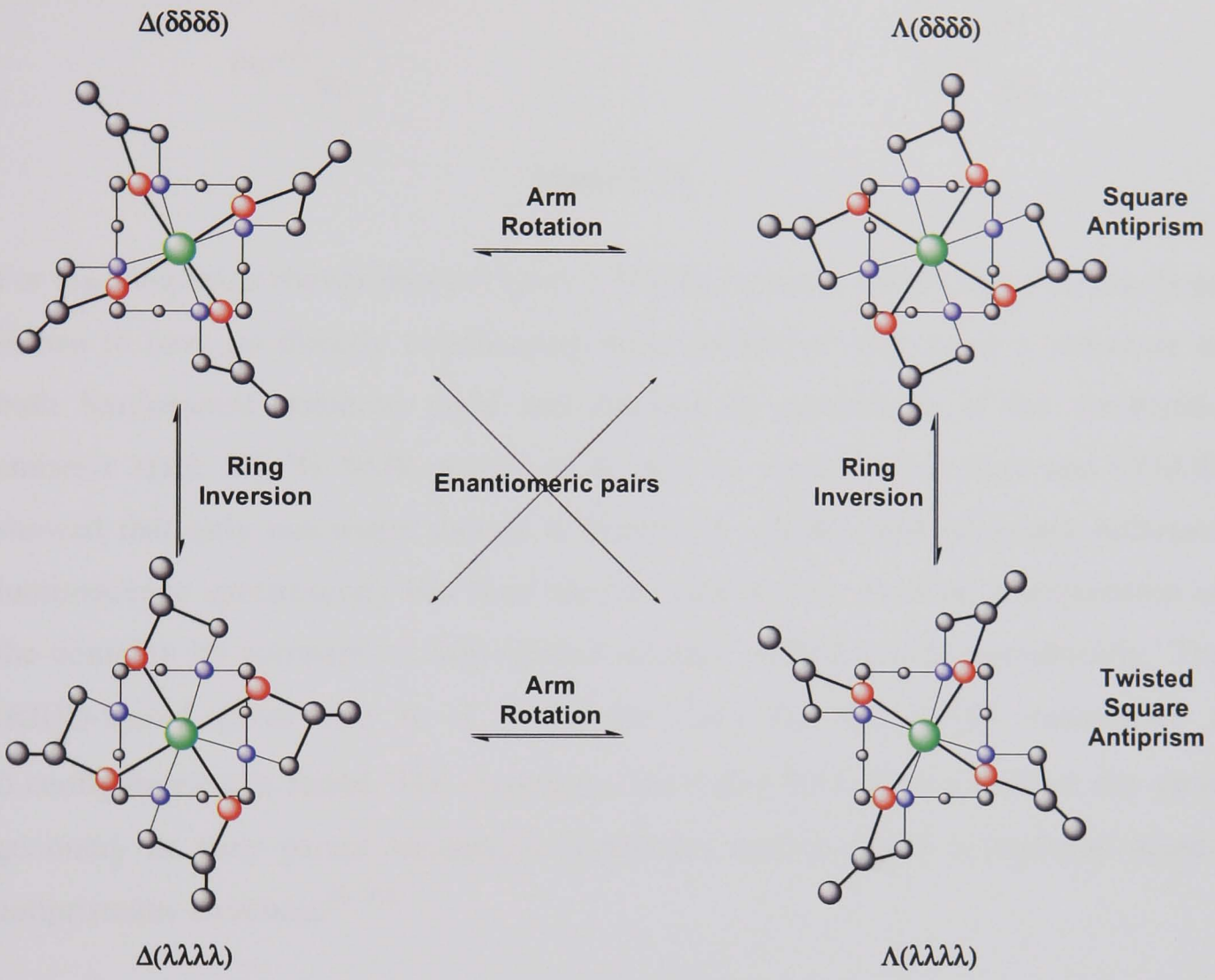

Figure 1. 9 Inversion between enantiomeric pairs through arm rotation and ring inversion

The introduction of a chiral centre δ to the ring nitrogen in tetraamide Ln(III) complexes imparts conformational rigidity.[31d] Arm rotation is inhibited, and ring inversion remains relatively slow (50 s^{-1} at 298 K); thus, one isomer may be preferred in solution. The configuration of the stereocentre determines the helicity of the complex, and the configuration of the macrocyclic ring, with the R and S isomers producing the Λ(δδδδ) and Δ(λλλλ) configurations respectively, in a regular square antiprismatic geometry.

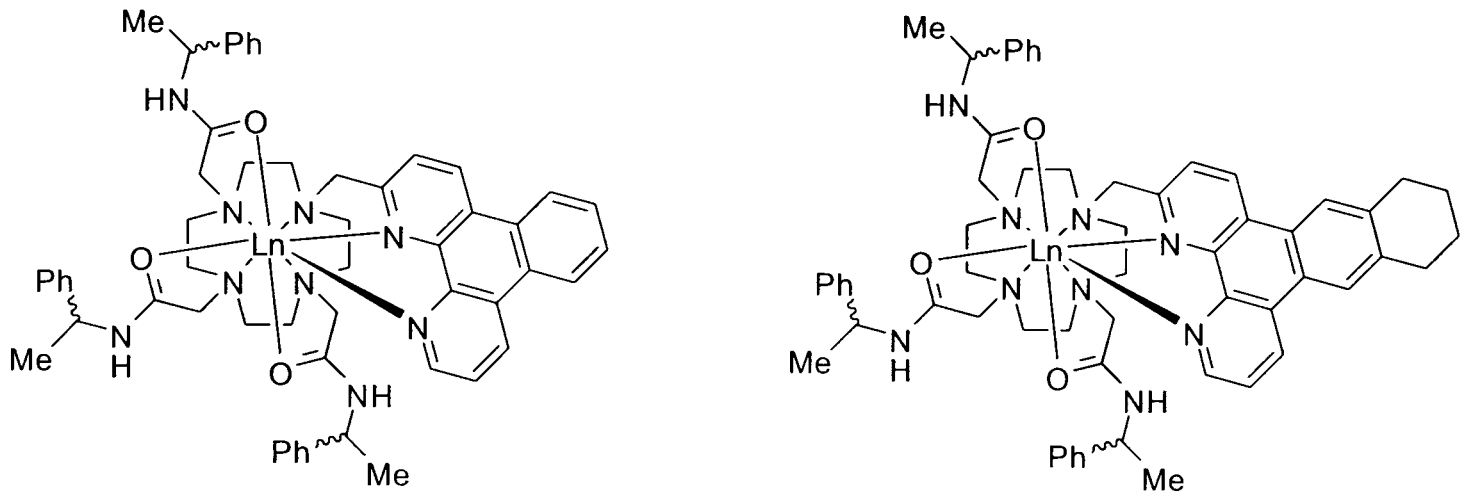

Figure 1. 10

For the complexes shown above (Figure 1.10) the ligand is nonadentate and has been shown to have no directly coordinating water molecules that cause a reduction in both luminescent quantum yield and lifetime by quenching of the lanthanide emissive state. VT ^{1}H NMR spectra of Δ- and Λ- complexes in D_2O and CD_3OD showed that only one major isomer is present in solution and circularly polarised luminescence spectroscopy has been used to confirm the absolute configuration of the complex by comparison with related systems studied crystallographically. The (RRR)-ligand gives rise to a Λ complex, and for the (SSS) enantiomer a Δ configurateion is found. The complexes have also been shown to have the same geometry as their parent tetraamide complexes and to adopt a preferred square antiprismatic structure.[26, 31e]

Lanthanide complexes incorporating phosphinate donors possess a stereogenic centre at P, leading to further series of enantiomeric pairs. A full discussion of the stereoisomerism of cyclen-based lanthanide complexes is provided in reference 31c.

1.3 Luminescence Microscopy

Fluorescence microscopy is an important tool that is used for the analysis of living biological systems, in particular for the imaging of live cells and the molecular events that occur within them. In fact, technology has now reached a level where through the use of an appropriate tag it is possible to monitor single molecules in real

time.[35] Essential to the use of luminescence microscopy is the availability of fluorescent stains, tags or probes to label particular molecules or compartments inside a cell or quantitatively probe the presence of specific analytes. The following sections will outline key microscopy techniques and the range of luminescent compounds that are currently in use or are in development, focusing particularly on luminescent lanthanide complexes.

1.3.1 Fluorescence Microscopy – The Basics

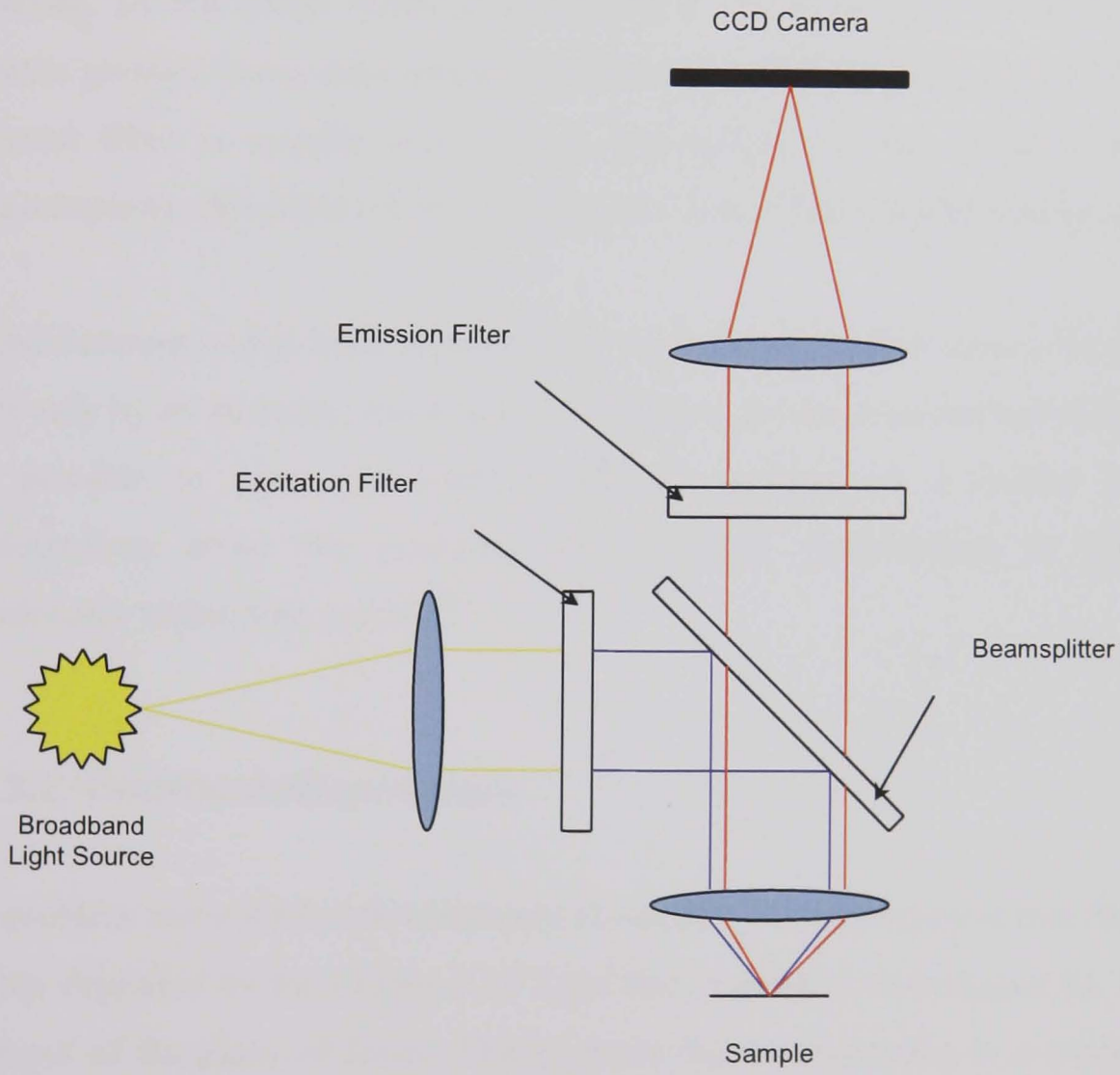

Figure 1. 11 – ***Schematic of a basic fluorescence microscope***

The figure above illustrates how a conventional fluorescence microscope operates. An external light source provides energy that is focussed through an objective onto the sample, where it is absorbed by a luminescent molecule raising this molecule to an excited state. Usually, a broad band excitation source (such as a Xe lamp) is used

and the excitation wavelength (or range of wavelengths) is chosen through the use of an appropriate filter. Emission from the molecule is observed as it relaxes back to its ground state; the light is focussed by the objective either to the eye or onto a CCD. Since the emitted light is of lower energy than that absorbed by the molecule, it allows discrimination between the excitation and the emission signal. Practically, this is done through the use of a dichroic mirror inclined at 45° to the direction of the excitation source. The mirror is chosen such that the excitation light is reflected, whilst the lower energy light emitted by the sample is allowed to pass through. However, often the absorption and emission spectra of fluorophores are broad and overlap, so that some reflected or scattered excitation light can pass through the mirror giving a lower than optimal signal/noise ratio and hence reduced sensitivity. A second filter is usually used that is appropriate for the emissive range of the chromophore; this allows more specific selection of the wavelengths of interest.[35]

Modifications to this basic system allow the luminescent emission to be characterised not only by its intensity, but also by its lifetime, polarisation and wavelength. Thus, it is possible to carry out multidimensional analysis of a system to determine information about the position, concentration, environment or interaction of molecules within that system.[36, 37]

1.3.2 Confocal Microscopy

A problem associated with traditional fluorescence microscopy is that the images are often degraded by the presence of light that is emitted or scattered by features that are out of the plane of focus. This problem can be overcome in a number of ways: through the use of image processing and deconvolution software,[38] through the use of an apotome (a commercially available attachment for most fluorescent microscopes) or through confocal imaging.[37]

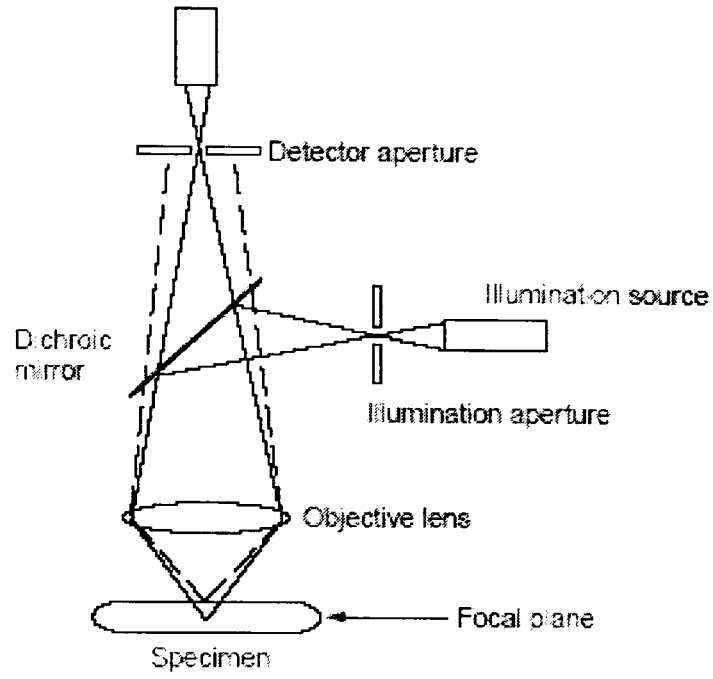

Figure 1. 12 The confocal principle

In a confocal microscope, both the illumination and detection systems are focussed on the same focal point within the sample. Out of focus light from the areas above or below the focal plane are simply eliminated through the use of a pinhole. The diagram illustrates how behind the objective lens, all of the light rays come together at a crossover point. The crossover point for light from the out-of-focus plane is above or below that for light from the in-focus plane. The insertion of a pinhole at the correct height allows the in-focus light to pass, but blocks nearly all of the dispersed light from planes that are higher or lower. Scattered light can inevitably still pass through the pinhole and it is for this reason that the excitation light is also focussed onto the focal point. If the light reaching regions above and below the focal plane is weak, then the intensity of scattered light will also be low. In confocal microscopy, the field of view is restricted to the size of the de-magnified pinhole; therefore, the image must be built up by scanning over the sample until the area of interest has been covered. Because a useful image often consists of 10^5 to 10^6 pixels, the time taken to record each pixel must be kept short and hence an intense source is necessary; this usually means that a laser must be used.[38] Whilst confocal microscopy gives the advantage of better resolution compared to traditional wide-field microscopy this advantage must be evaluated against the increased cost of the instrument and the limitations associated with the availability of a laser of appropriate wavelength for the fluorophore. In addition, the light intensity at the focal point is very high (MW/cm^2) and can cause strong photobleaching and

degradation of the specimen under study (above and below the focal plane). As a result, the light intensity should be carefully controlled so that it is of sufficient intensity to produce a high signal to background intensity, but should not be too high as to degrade the fluorescent tag or sample.

1.3.3 Multiphoton Excitation

The use of multiphoton excitation causes less photobleaching and damage to the sample than with single photon methods, since excitation is through ultrashort laser pulses (10^{-14} s). Whilst the laser energy is high, the sample is only illuminated for a very short period of time; practically this means that a much smaller area of the fluorescent specimen is being stimulated and consequently photobleaching only occurs in the focal plane.[37] However, it should also be noted that multiphoton excitation requires considerably higher laser intensities than for single photon methods: three photon excitation requires 5 to 10 times more laser power than for two photon excitation in order to observe the same intensity emission from the sample (exact values depend on the absorption cross section of the dye).[46]

An additional advantage of multiphoton excitation is that it allows excitation using light in the near-IR region of the spectrum, whilst still observing visible emission: biological tissue is most effectively penetrated in the range 710 – 820 nm in the near-IR region of the spectrum. This can increase the penetration depth of luminescence microscopies and may allow the method to be extended to *in vivo* applications. Whilst multiphoton excitation is becoming more accessible with the development of new and cheaper lasers capable of producing ultrafast pulses, it is not yet practicable to design probes for biological systems with the sole intention of using multiphoton methods. However, many of the europium and terbium complexes reported in the literature to have potential as sensors to signal the presence of analytes in solution require excitation in the near-UV, the use of two photon excitation could facilitate their use in the analysis of biological samples.

1.3.4 Time-Gated Detection

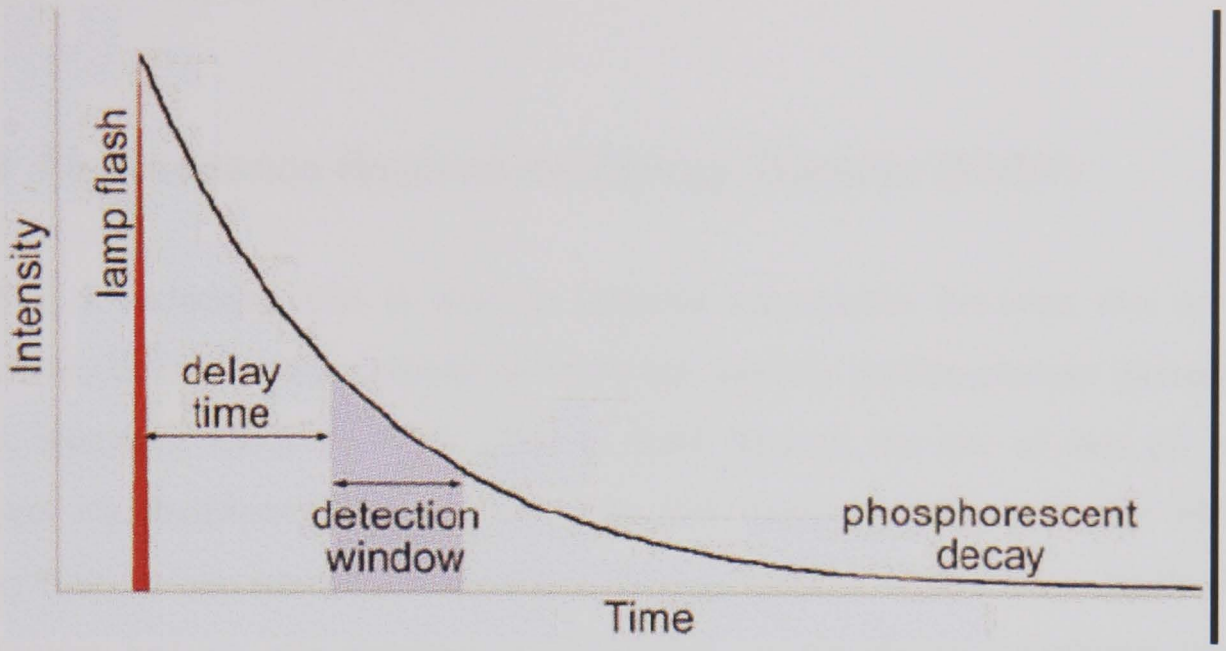

Figure 1. 13 Schematic showing the principle of time gated detection

4f-4f Transitions are Laporte forbidden. As a result, the lanthanides display long emissive lifetimes; for europium and terbium these values are of the order of milliseconds, much longer than the fluorescent background emission common to biological samples. The difference can be used to significantly enhance signal to noise and signal to background intensity ratios. Experimentally, this is done using a pulsed excitation source and an integrating camera. The excitation source is pulsed to excite the sample, a delay of the order of 10 – 100 ns is then introduced, over this time period the background emission intensity will decay to zero whilst the lanthanide intensity remains high. The camera then detects only emission from the lanthanide: scattered light does not reach the CCD, since the excitation is off whilst the signal is being acquired. The use of an integrating camera allows for the use of lower intensity excitation, since a number of pulses and detection cycles can be used.

1.3.5 Time-Resolved Fluorescence Microscopy[36, 39]

Fluorescence lifetime imaging (FLIM) and time-resolved fluorescence anisotropy imaging (TR-FAIM) are two techniques that take advantage of changes in the lifetime of emission to provide information about the environment of a fluorophore that would otherwise be difficult to obtain by fluorescence intensity imaging. FLIM

provides a map of lifetimes over a sample, whereas TR-FAIM tells us about the rotational mobility of a fluorophore.

1.3.6 Fluorescence Resonance Energy Transfer (FRET)

FRET is a technique that is used to monitor interactions between two or more molecules, often for the purpose of studying specific protein-protein interactions, lipids, enzymes, DNA or RNA. This is done through the use of two (or more) different chromophores with suitably matched energy levels, such that efficient energy transfer can occur between them. Energy transfer is through a dipole-dipole mechanism and its rate constant is dependent on the distance between the two chromophores, the extent of overlap between the emission spectum of the donor and the absorption spectrum of the acceptor, the quantum yield of the donor and the relative orientation of the donor and acceptor. Experimentally, what is normally quoted as the FRET efficiency can be defined as the ratio of the deactivation of the donor by energy transfer over all of the deactivation pathways. The acceptor does not need to be fluorescent, its deactivation can be either radiative or non-radiative (dark quenching). A limitation to the technique is the requirement for a short donor-acceptor distance. In practice, this should be in the range 2 – 8 nm.[39] In combination with microscopy it is possible to obtain both spatial information about the specific binding interaction and its time-course.[40]

A detailed example of the use of a lanthanide complex in a homogeneous time resolved fluorescence assay is provided in chapter 2.

1.4 Luminescent Compounds for in cellulo Fluorescence Based Applications

Over the years a number of different classes of compound have been used, or have been suggested to have potential application as probes for imaging and sensing both *in vivo* and *in cellulo*. Much of the understanding relating to the composition of cells and the processes that occur within them has been gained through the use of mutant

forms of green fluorescent protein (from *Aequorea victoria*) and from the application of commercially available organic dyes. More recently, the application of metal complexes and quantum dots has also shown promise.[51-72]

1.4.1 Fluorescent Proteins

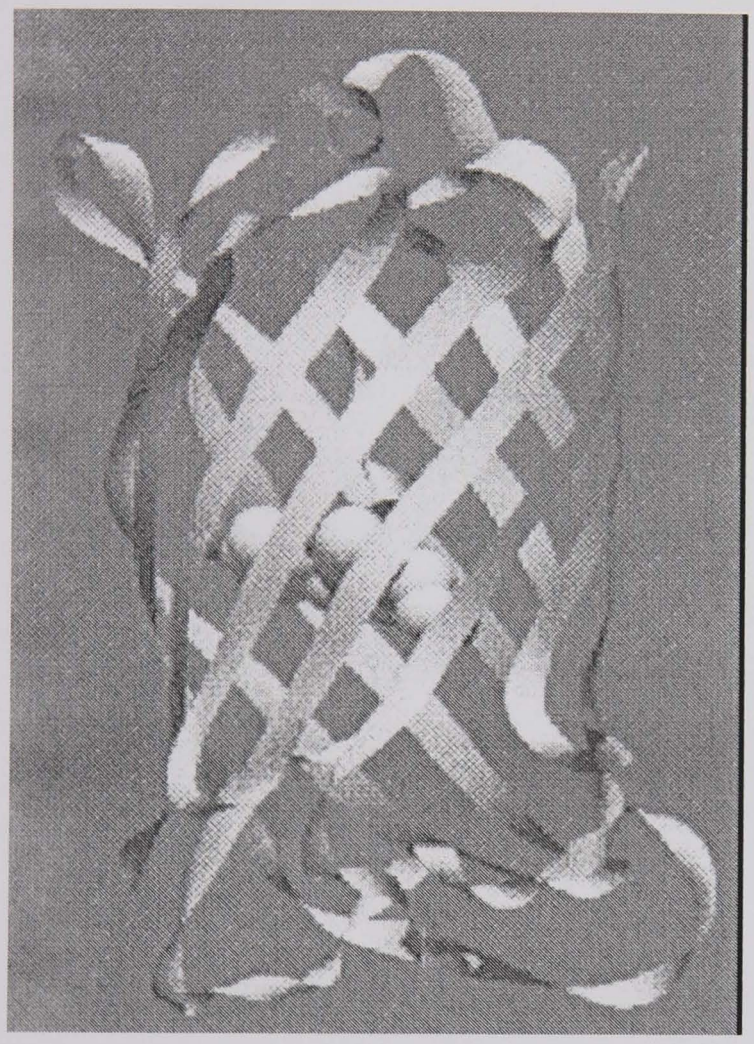

Figure 1. 14 Structure of GFP and its Fluorophore

The above figure displays the structure of green fluorescent protein and its chromophore. It is obtained from the bioluminescent jellyfish *Aequorea victoria*, the chromophore is contained within a barrel of β-sheet protein and forms spontaneously upon folding of the polypeptide chain.[38] Its absorption and emission spectra are at suitably long wavelengths: excitation is at greater than 350 nm and the emission is in the visible region of the spectrum. A range of fluorescent proteins is now available that span the visible spectrum: blue fluorescent protein (BFP), green fluorescent protein (GFP), yellow fluorescent protein (YFP), cyan fluorescent protein (CFP) and red fluorescent protein (RFP). Figure 1.15 gives the emission profiles for the range of

proteins (full lines) a comparison of the fluorophore structures for GFP and RFP is given.[44, 45]

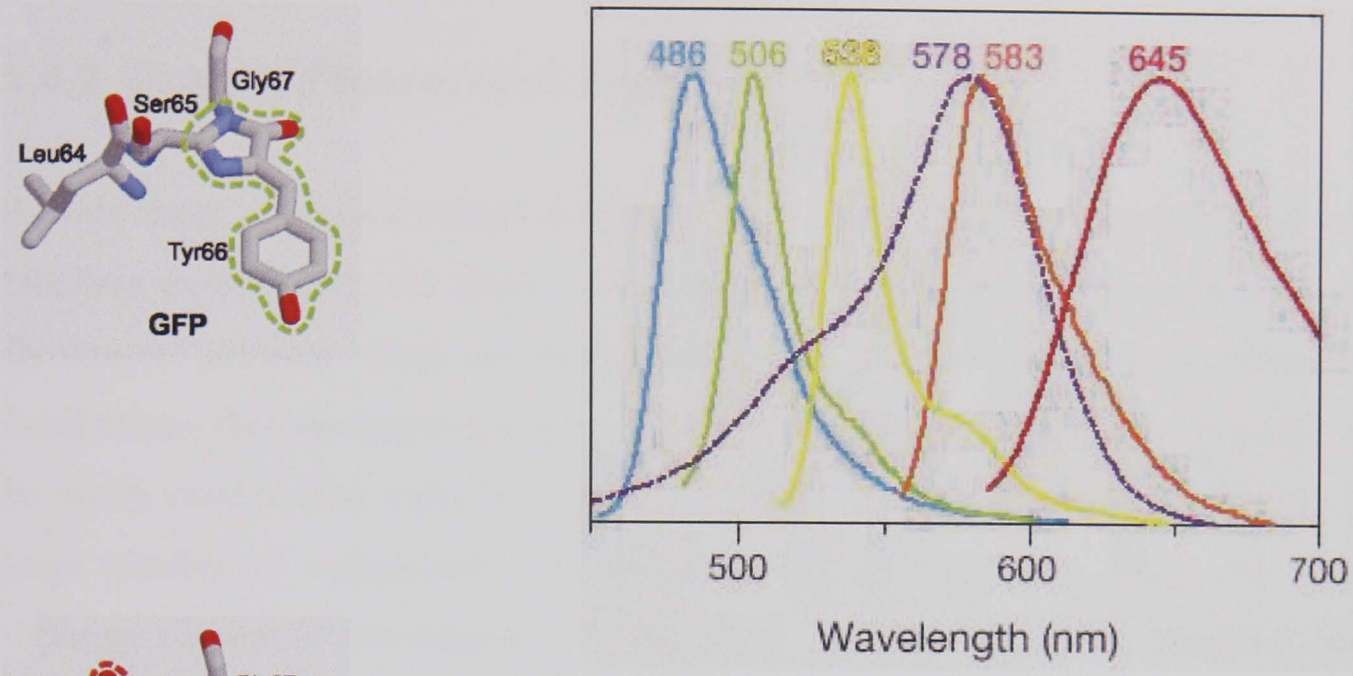

Figure 1. 15 – Emission spectra (solid lines) for a range of commercially available fluorescent proteins. Examples of chromophore structures are also provided

Fluorescent protein-based tags can be designed to respond to a wide variety of biological events and signals, targeted to sub-cellular compartments, introduced into a range of tissues and intact organisms and they rarely display any phototoxicity.[41] They are usually characterised by their fluorescent intensity, although the emissive lifetime of GFP is sensitive to changes in the refractive index of its environment and hence can be used to probe such changes.[36] The photophysical properties of *Aequorea* fluorescent proteins are complex, different mutant forms often have more than one emissive state with different fluorescent lifetimes.[42] Whilst FLIM of GFP and related proteins (with an average emissive lifetime of the order of 2-3 ns) has proved useful in some applications,[43] this complication can limit their application where multidimensional acquisition is desirable. In addition, their large steric bulk

(high MW) and slow rates of labelling mean that for many applications simple organic dyes have clear advantages.

1.4.2 Organic Fluorescent Dyes

A wide range of organic compounds is available for use as fluorescent probes or in labelling technologies; for many years they have constituted the main alternative to fluorescent proteins. They are highly emissive, they have large molar absorption coefficients, they are fast-responding and their structure and linking functionality can be easily modified in order to suite a particular application. However, despite the large number of compounds that are available, they all stem from only a few different classes of chromophore.[24] This is, in part, due to the requirements for a compound that is to be used for the fluorescence imaging of biological samples *i.e.*: they should be visible (or near-IR emissive); they should be amenable to excitation at wavelengths > 350 nm; their Stokes' shift should be as large as possible; their quantum efficiencies should be high and, importantly, they should also be water soluble. The relationship between chemical structure and photophysical properties is not yet at such a level where compounds can be designed to meet a set of physical requirements predictably, hence at present the route to new fluorophores is mostly empirical.[47,48] However, once a suitable chromophore has been found, the task of modulating its properties, for example, to blue shift or red shift the emission spectrum, is relatively facile.

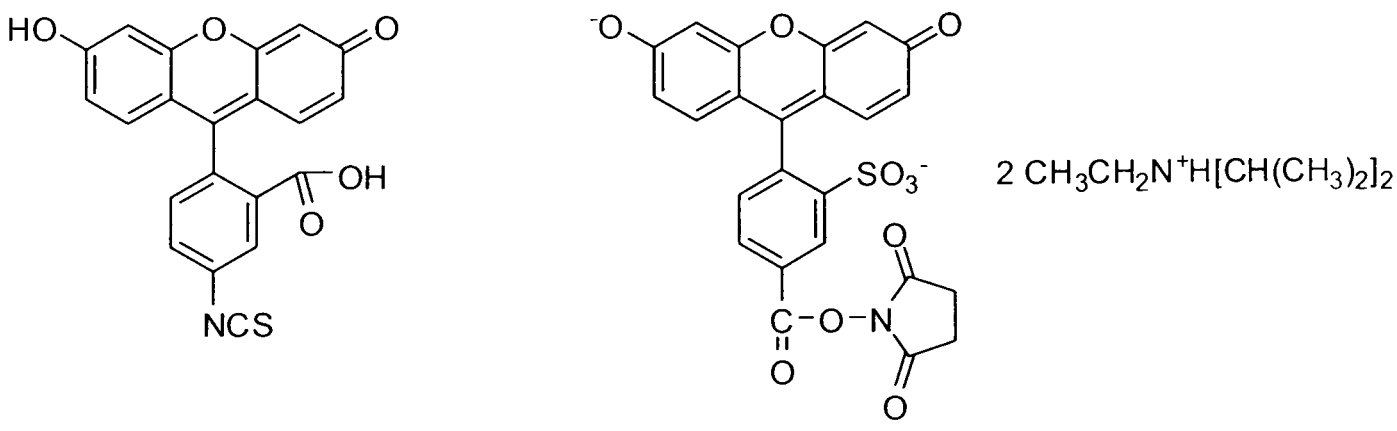

Figure 1. 16 Left: FITC 'isomer I' Right: reactive rhodamine green dye

Derivatives of fluorescein and rhodamine perhaps constitute the most well known class of fluorescent dyes.[47-49] They both have relatively high molar absorption coefficients, excellent fluorescent quantum yield and good water solubility. Fluorescein has an excitation maximum at 494 nm (close to the 488 nm argon laser line) and remains an important chromophore for confocal laser-scanning microscopy. Both can readily be used as labels by conjugating with their reactive ester or amine derivatives. Fluorescein dyes (and rhodamine to a lesser extent) have a number of limitations: a relatively high rate of photobleaching; pH sensitive fluorescence (fluorescein $pK_a \sim 6.4$), absorption and emission bands that are broad (limiting their use in multicolour applications) and fluorescence that can be quenched upon coordination to biopolymers. These problems have been reduced to some extent by the introduction of Alexa Fluor® and BODIPY® fluorescent dyes that are less susceptible to photobleaching and whose emission spectra display virtually no pH dependence (pH 4 – 9). In addition, they have high molar absorption coefficients (up to 200 000 M^{-1} cm^{-1}) and quantum yields that are often in excess of 0.7.[49, 50]

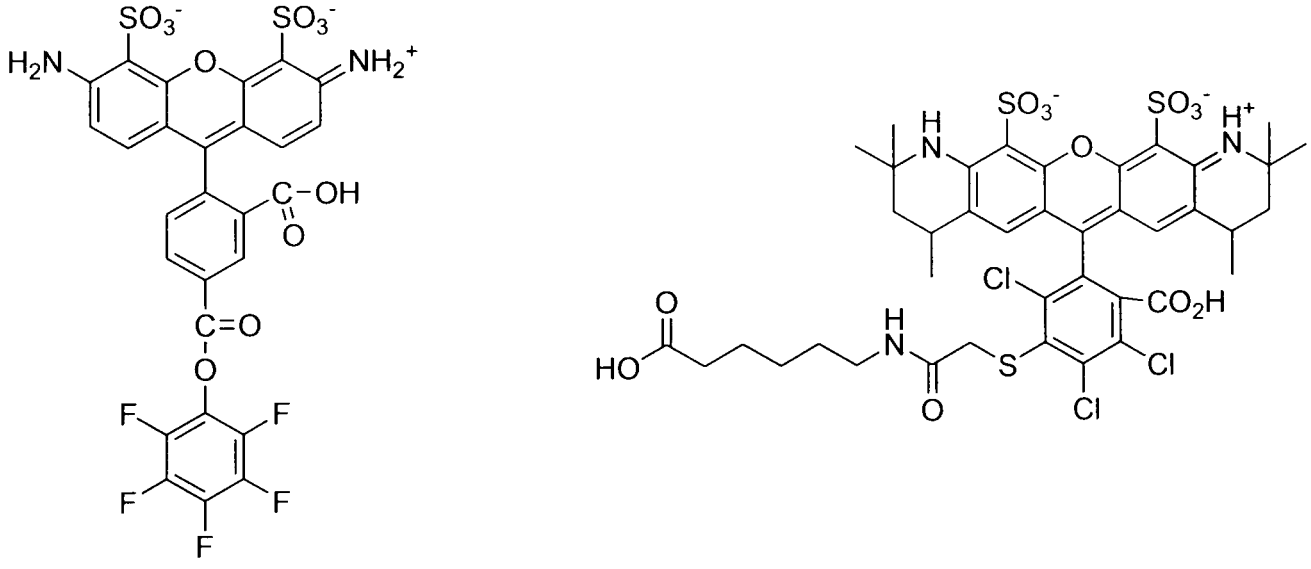

Figure 1. 17 Examples of two of the Alexa Fluor dyes, Left: Alexa Fluor 488 Right: Alexa Fluor 546

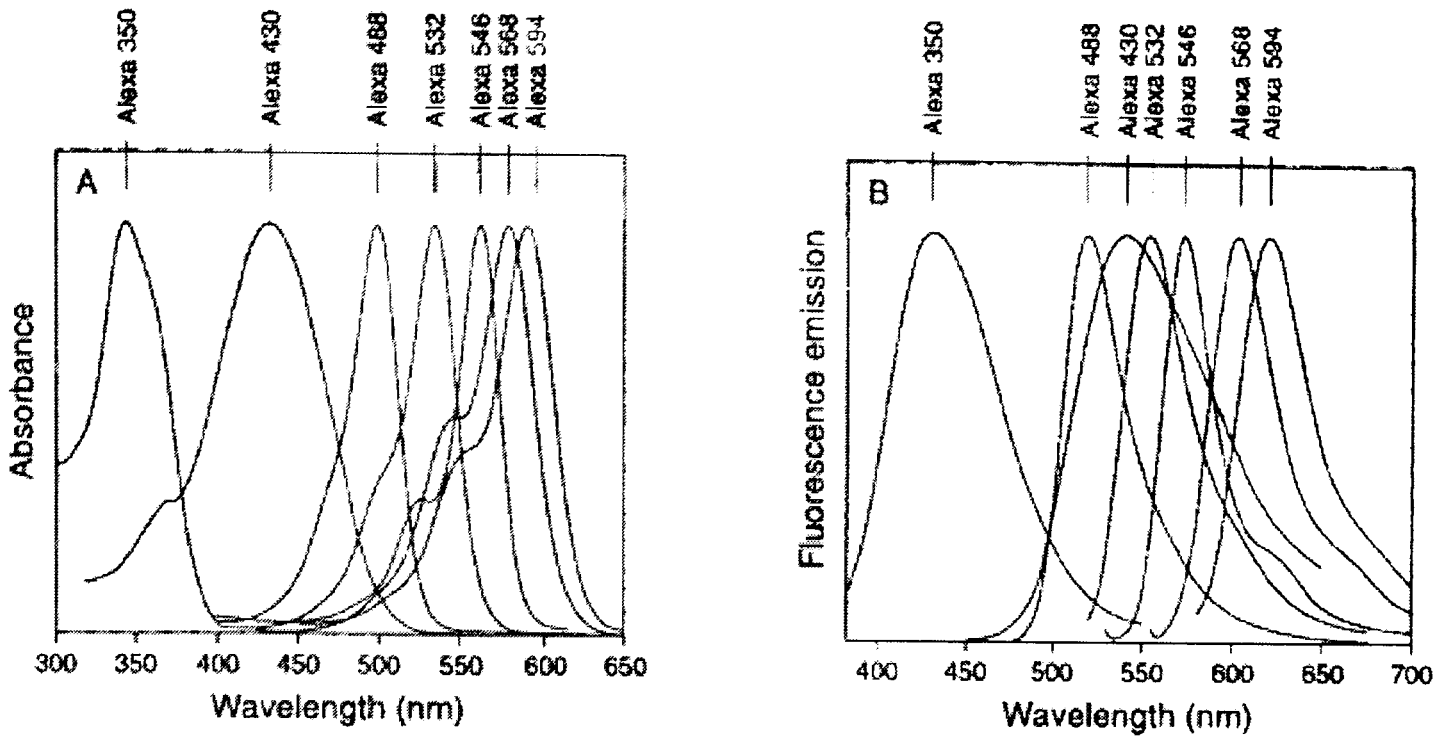

Figure 1. 18 Absorption and emission profiles for the range of Alexa Fluor dyes

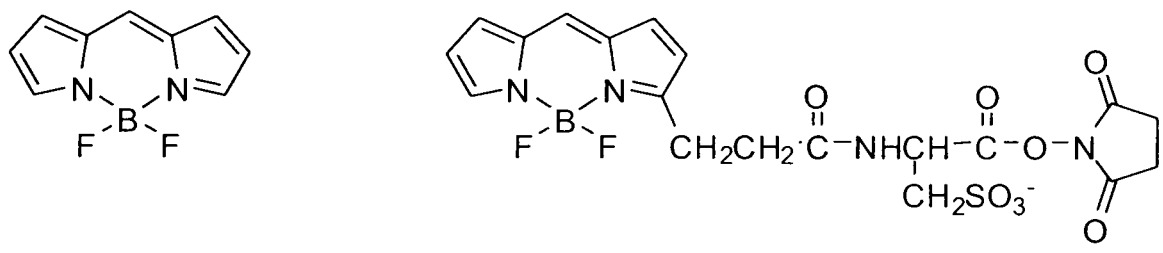

Figure 1. 19 Examples of BODIPY dyes, Left: BODIPY Fluorophore Right: BODIPY FL, CASE

Both Alexa Fluor® and BODIPY® dyes are available with a wide range of excitation and emission wavelengths and can span most of the visible spectrum (Figure 1.18). Alexa Fluor® dyes are similar in structure to fluorescein and rhodamine. BODIPY® dyes are based on 4,4-difluoro-4-bora-3a,4a-diaaza-5-indacene they are unusual in that they are relatively non-polar and the chromophore is charge neutral. It is interesting to note that their low molecular weight conjugates are also more permeable in live cells than those of charged fluorophores. They also possess multiphoton absorption cross sections.[49]

However, all organic dyes have certain limitations, as a result of their short emissive lifetimes (of the order of nanoseconds) and small Stokes' shift. In fluorescence and confocal microscopy this can lead to noisy images due to light scattering, and also to interference from the natural fluorescence from certain biomolecules. Metal complexes and quantum dots have received increasing interest over recent years for

their potential to act in these roles for a number of reasons relating to their photophysical properties (which shall be discussed further in the following sections) but particularly because they display a long-lived emission that allows the possibility of time-resolved detection.

1.4.3 Quantum Dots as Fluorescent Labels in the Analysis of Living Systems

Quantum dots are fluorescent semiconducting nanocrystals; they are generally made from either group II and VI (e.g. CdSe and CdTe) or group III and V elements (*e.g.* InP and InAs). They have recently received interest for applications in *in vivo* (and *in cellulo*) imaging and in diagnostics, due to their unique photophysical properties. In particular, they have attracted attention because of their very high molar absorption coefficients ($0.5 - 5 \times 10^6$ M^{-1} cm^{-1}) and emissive quantum yields (values up to 80 – 90 % have been reported), their broad absorption bands and narrow emission profiles, their relatively long emissive lifetimes (~ 20 – 50 ns) and their large Stokes' shift (up to 300 – 400 nm). In addition, the optical and electronic properties of the quantum dots can be modulated through varying the composition and size of the crystal.[51] In terms of imaging applications, this allows the emissive wavelength to be tuned continuously from 400 to 2000 nm. An interesting recent article by Alivisatos[52] explains in simple terms, how the changes in band structure upon moving from single molecule to bulk semiconductor materials lead to this sensitivity.

Semiconducting nanocrystals are synthesised in high-boiling point, non-polar organic solvents such as tri-octylphosphine oxide (TOPO) and hexadecylamine. These coordinate to unsaturated metal atoms on the surface and prevent the formation of a bulk semiconductor. However, as a result the nanocrystals are coated with a monolayer of the organic solvent that renders them soluble only in other non-polar, hydrophobic solvents (*e.g.* chloroform). In order for them to be used in an aqueous biological medium some form of solubilisation strategy must be employed. An extensive list of these strategies has recently been compiled.[53] The general methodologies usual involve either ligand exchange; layering of appropriate

molecules onto the surface; or encapsulation, for example by an amphiphilic polymer. This final method is perhaps the most useful, since it allows easy functionalisation of the quantum dot. This allows the possibility of linking, so that it can be used as a tag or as a component in a biological assay, if it is attached to an appropriate recognition element (bioconjugation).

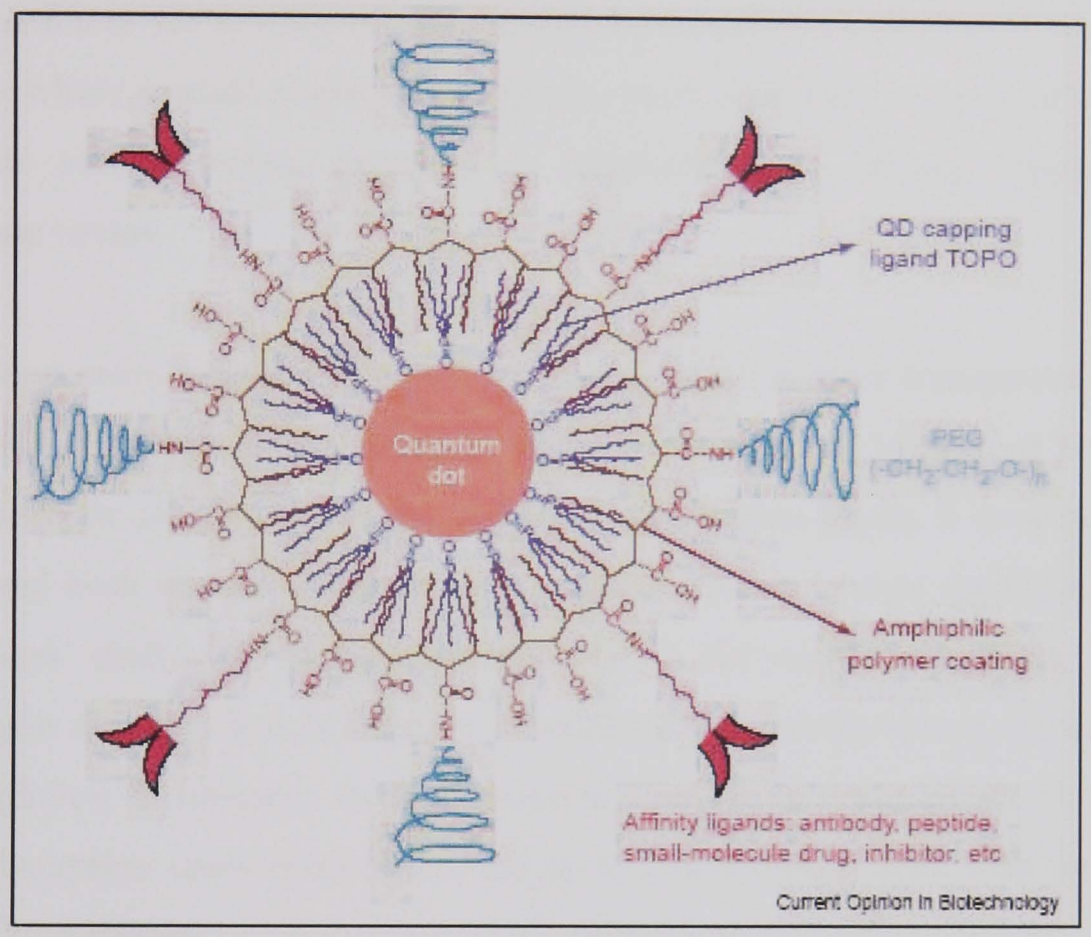

Figure 1. 20 – The structure of a multifunctional quantum dot probe showing the capping ligand TOPO, an encapsulating copolymer layer, tumor targeting ligands (such as peptides, antibodies or small molecule inhibitors, and polyethylene glycol (PEG)[51]

Quantum dots have dimensions in the range of 2 – 8 nm, of a similar order to that of the fluorescent proteins discussed above (4 – 6 nm). They also show resistance to photobleaching. Both of these properties mean that single quantum dots can be observed or tracked over long periods of time (minutes to hours) without significant degradation of the signal by microscopic techniques such as confocal microscopy, total internal reflection microscopy or basic wide-field epifluorescence microscopy. Single molecule fluorescence microscopy is a powerful technique that is providing a significant contribution towards the understanding of processes that occur within organisms and living cells; the use of single molecule FRET can provide further information about interactions between individual pairs of molecules.

A number of reviews have been published in the last two or three years detailing examples where quantum dots have been used for both *in cellulo* and *in vivo* imaging.[51, 52] Whilst photophysically they have clear advantages over the organic dyes more commonly used for cellular imaging, they suffer from difficulties associated with their intracellular delivery. This is usually done either through microinjection or *via* an endocytosis pathway (although there are one or two reported examples where peptide coated nanoparticles have been able to enter cells).[54] Once inside the cell, however, targeting is relatively facile through linking to an appropriate vector.

As has been previously mentioned,[24] biological tissue is most transparent to visible and near-IR radiation. If luminescence-based techniques are to be used for imaging *in vivo*, then in order to achieve a sufficient penetration depth, it is necessary that they should both absorb and emit in this region. Quantum dots typically display a large Stokes' shift, and, whilst they may emit in the visible or near-IR, excitation wavelengths are often less favourable. A method to overcome this is through the use of multiphoton techniques; in fact quantum dots have been shown to have two photon absorption cross-sections that are up to 2 or 3 times higher than for common organic fluorophores.

A further requirement of any compound that is to be used *in vivo* or *in cellulo* is that it should have a high stability with respect to dissociation and that it should display low cytotoxicity. Encapsulated quantum dots are relatively stable with respect to dissociation, although this stability is due in large to the stability of the shell protecting the core. Both Weiss[53] and Nie[51] report that quantum dots do not appear to adversely affect cell viability *in cellulo*. However, they conclude that there is a need to examine more thoroughly both their toxicity in cells and inside animals and to understand if there is a mechanism by which they can be excreted from the body. Quantum dots constitute an important new tool to complement the techniques currently available, but they are limited by the fact that they can act only as fluorescent tags, they cannot act as responsive probes or provide information about

their local environment. This is perhaps one area where metal complexes could extend the range of analyses possible in live cells.

1.4.4 Transition Metal Complexes

Complexes of transition metal ions, and in particular those belonging to the platinum group (i.e. ruthenium, rhodium, palladium, osmium, iridium and platinum) have received much attention for applications relating to their use as luminescent sensors or probes. The majority are designed to provide quantitative information about the presence of certain analytes in solution either indirectly *via* the attachment of a pendant group, or by direct coordination to the metal.[55] The response is generally observed as a change in the emission profile of the complex, often as a result of a charge (MLCT/LMCT/ILCT) or energy transfer interaction (Förster). There are a number of examples of complexes that are designed for DNA intercalation (such as the well known ruthenium dppz complexes - Figure 1.21), [56-58] membrane binding and micelle encapsulation.[59] However, as yet there are very few examples where this has been extended to *in cellulo* or *in vivo* use; fluorescence imaging of pO_2 in liver tissue has been reported using a ruthenium tris-1,10-phenanthroline complex.[60] The successful application of both ruthenium and rhenium in immunological assays has also been demonstrated.[61, 62] The emission lifetimes of these and similar transition metal complexes are of the order of microseconds, allowing the use of time-resolved techniques, similar to those already being commercially used in lanthanide based assays.[63]

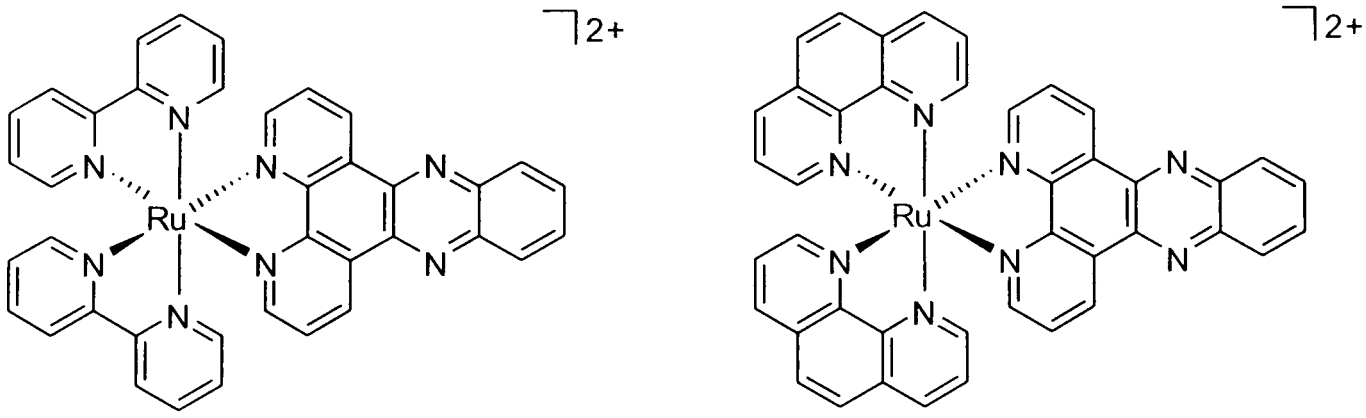

Figure 1. 21 – Structures of $Ru(bpy)_2dppz^{2+}$ and $Ru(phen)_2dppz^{2+}$

1.4.5 Luminescent Lanthanide Complexes

Luminescent lanthanide complexes combine almost all of the beneficial properties that are associated with the fluorescent proteins and organic dyes that are commercially available for live-cell imaging, in addition to those of the rapidly developing quantum-dot luminescent tags. To reiterate, the span of emission wavelengths is broad, ranging from the near-IR for complexes of Yb(III), Er(III) and Nd(III) to the visible for Eu(III), Tb(III), Sm(III) and Dy(III). They possess sharper line-like emission spectra than quantum dots. Their large Stokes' shifts, and long emissive lifetimes ranging from microseconds *e.g.* Yb(III), Er(III), Nd(III) to milliseconds *e.g.* Eu(III), Tb(III), allow the use of time-gated detection methods. Through the use of appropriate ligands, complexes are water soluble, have high quantum yields of emission and can incorporate a linking functionality, allowing the possibility of bioconjugation (perhaps to be used as a component in a FRET based assay) or attachment to a targeting vector.

Despite these very favourable properties, there are relatively few examples in the literature where lanthanide complexes have been used for the imaging of live cells. However, recent work has shown that following the incubation of certain complexes in the presence of a range of eukaryotic cell lines, they are able to cross the cell membrane and localise within the cell. Microinjection and induced endocytosis can be used where compounds are non-cell permeable, as has been demonstrated in recent work using quantum dots (see 1.4.3). This is not desirable, if they are to achieve widespread application.

A useful perspective on the engineering of emissive lanthanide complexes for molecular imaging and sensing was published earlier this year and provides a review of the *status quo* in using lanthanide complexes for *in cellulo* imaging.[24] The mechanism by which the complexes are able to penetrate the plasma membrane is not well understood and a number of different compartmentalisation profiles has been observed. Given the small number of studies that have been undertaken, it is possible only to draw very tentative conclusions as to which structural features may be responsible for mediating the uptake, transport and localisation of the complexes.

Representative examples are presented below (Figures 1.22 – 1.24); in each case, a series of images confirming the localisation of the complexes are provided.

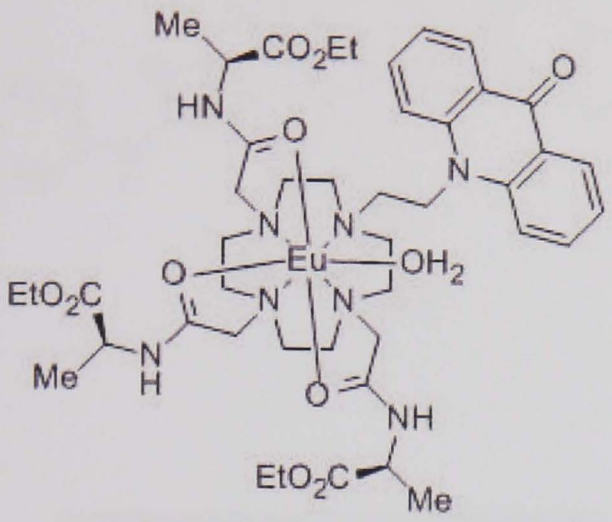

a

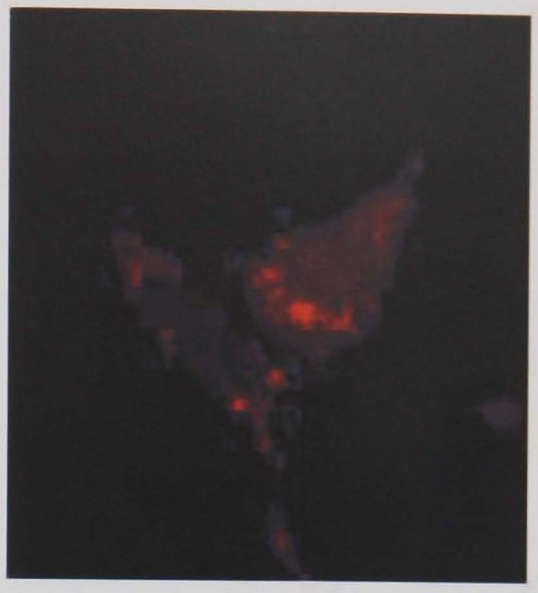

Eu Complex

Lysotracker Green

Merged Image

Figure 1. 22 – Confocal microscopy images of europium complex 'a' co-localised with Lysotracker green in NIH 3T3 cells. Orange regions of the merged image correspond to areas where the complex and stain are coincident and indicate that localisation is concentrated in lysosomes.

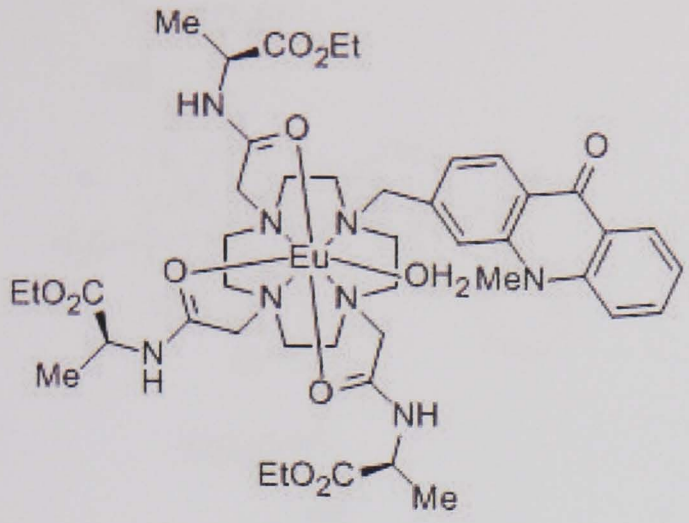

b

Eu Complex

Brefeldin-A

Merged Image

Figure 1. 23 – Confocal microscopy images of europium complex 'b' co-localised with Brefeldin-A in NIH 3T3 cells. Brefeldin-A is commonly used as a stain for the endoplasmic reticulum. The merged image indicates that specific localisation is observed in the ER, but a more diffuse background is also apparent, corresponding to distribution throughout the cytosol.

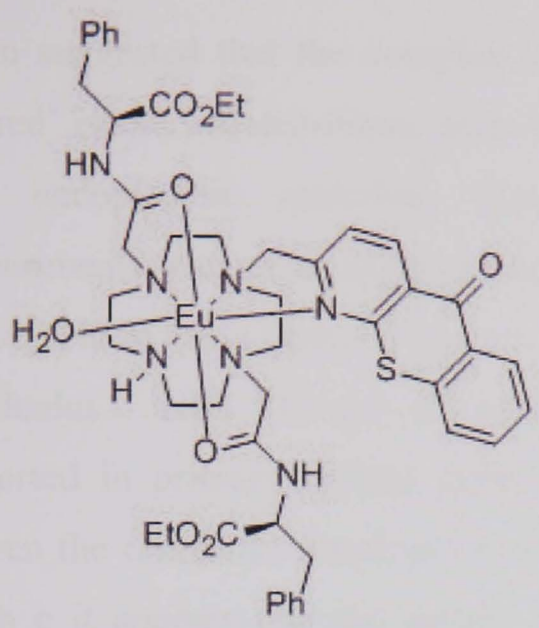

c

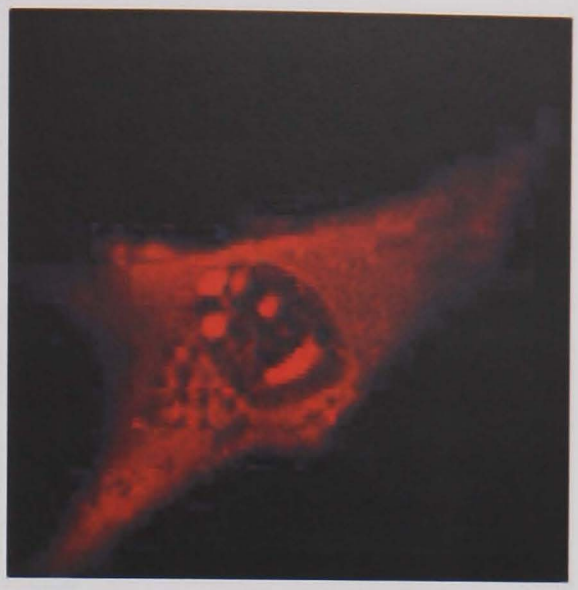

Eu Complex

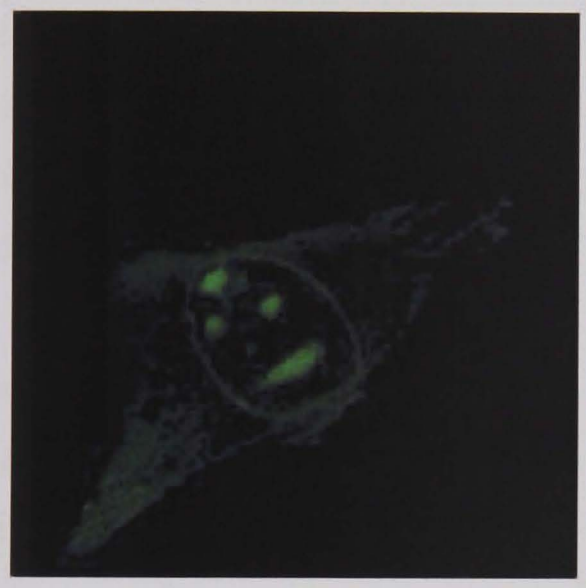

Syto-RNASelect

Merged Image

Figure 1. 24 – Confocal microscopy images of europium complex 'c' co-loaded with Syto-RNASelect in NIH 3T3 cells, showing the cellular localisation and revealing the staining of the nucleolus inside the cell nucleus.

Each of the complexes shown in Figures 1.22 – 1.24 share many common structural features. In each case they have a cationic charge, are relatively lipophilic, are based on the cyclen macrocycle, have amide-based pendent arms and incorporate a planar aromatic sensitising group. In particular, complexes **a** and **b** are constitutional isomers differing only in the position through which the chromophore has been linked to the cyclen ring. Each of the complexes is clearly taken up by the cell line (NIH 3T3), but display markedly different localisations. In co-localisation studies with Lysotracker-green, the 'N-linked' isomer, **a**, shows good correspondence with the organic dye, that is known to localise in acidic lysosomal compartments. It has

been suggested that the complex is taken up by an endosomal pathway. The 'C-linked' isomer, **b**, distributes quite well in the cytosol and shows a tendency to stain the endoplasmic reticulum (localisation strongly suggested in co-staining experiments with a conjugate of Brefeldin-A).[24, 70, 71] Complex **c**, in contrast, appears to be able to cross both the plasma and nuclear membranes and localises within the nucleolus.[73] NIH 3T3 are a transformed cell line; similar localisation has been reported in primary human dermal fibroblast (HDF) and HeLa carcinoma cells. Given the otherwise identical structures of complexes **a** and **b**, and their similarity with **c** it appears that the nature and orientation of the chromophore are able to influence the uptake profile of the complex. This could be due to either the operation of different uptake mechanisms or redistribution of the complex once it has been taken up by the cell. This can only be confirmed through the systematic variation and imaging of series of structurally related complexes. Incorporation of a suitable vector into the ligand structure that is already known to target specific locations could provide a useful alternative route.

The majority of complexes that have so far been shown to be cell-permeable are relatively lipophilic and positively charged. However, single examples of neutral and anionic complexes related to complex **a** (again based on the cyclen macrocycle, bearing pendent amide arms and incorporating an acridone chromophore) have also been imaged *in cellulo*. The complexes are shown in Figure 1.25.

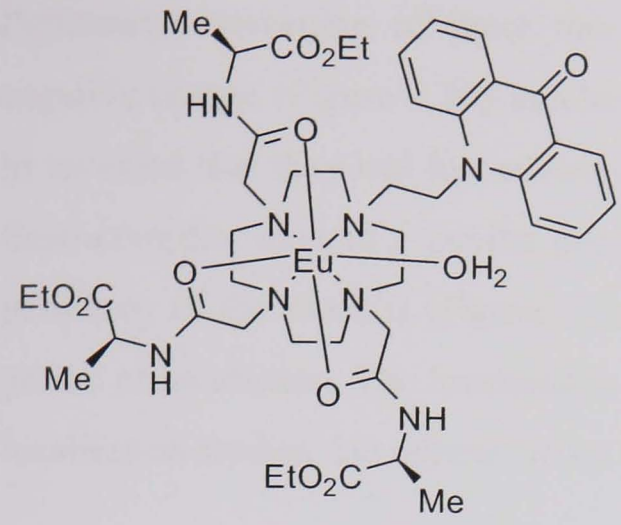

a

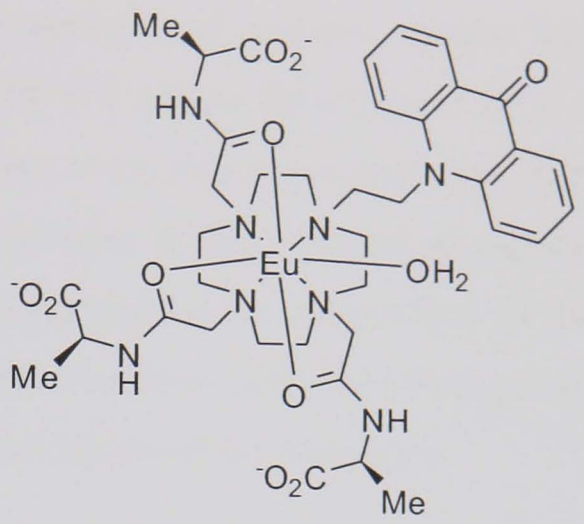

d

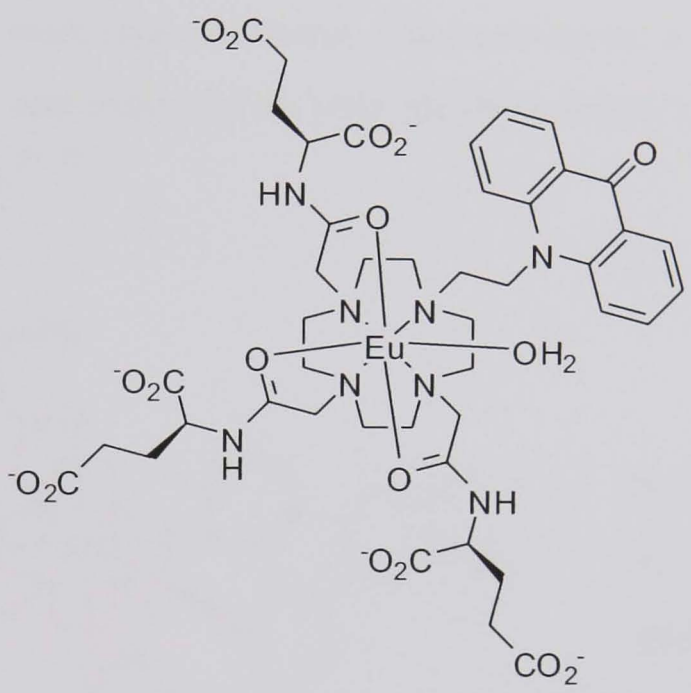

e

Figure 1. 25 – A series of europium complexes incorporating an acridone chromophore with positive, neutral and anionic charge respectively

Figure 1. 26 – Fluorescence microscopy images of 'a' (centre), 'd' and 'e' (left), showing each complex inside NIH 3T3 cells

Preliminary screening of these three related complexes of cationic, neutral and negative charge (Figure 1.25) incubated with NIH-3T3 mouse fibroblasts (1 mM, 3 h) revealed that they had low toxicity and that they were able to penetrate the cells. Each complex showed a similar punctuated localisation profile, centred around the periphery of the nucleus (Figure 1.26); staining appeared to be independent of the period of incubation. The localisation of **d** and **e** has not been confirmed through co-localisation studies, but appears to be similar to that observed for complex **a**.

This amphipathic and cationic group of complexes (Figure 1.27) provide the starting point for much of the work reported herein. The enantiopure Λ and Δ isomers were originally synthesised and examined *in vitro* for there ability to bind to helical B-DNA stereoselectively.[25, 72]

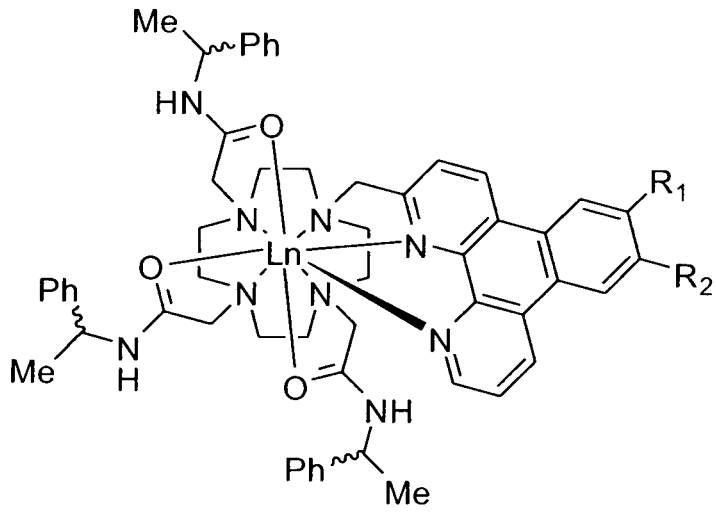

R_1	R_2	
H	H	**f**
-$(CH_2)_4$-		**g**

Figure 1. 27

Preliminary experiments were carried out which showed that **f** is taken up by NIH 3T3 mouse fibroblast cells (1 mM loading concentration);[72] localisation has not been confirmed. Time course analysis indicated that uptake of the europium complex appears faster than for the terbium analogue and that migration occurred over a period of hours through the cytosol, across the nuclear membrane and into the nucleus (Figure 1.28); in the absence of a positive concentration of complex in the external medium the images show a transfer of luminescence from the nucleus back to the cytoplasm (Figure 1.29).

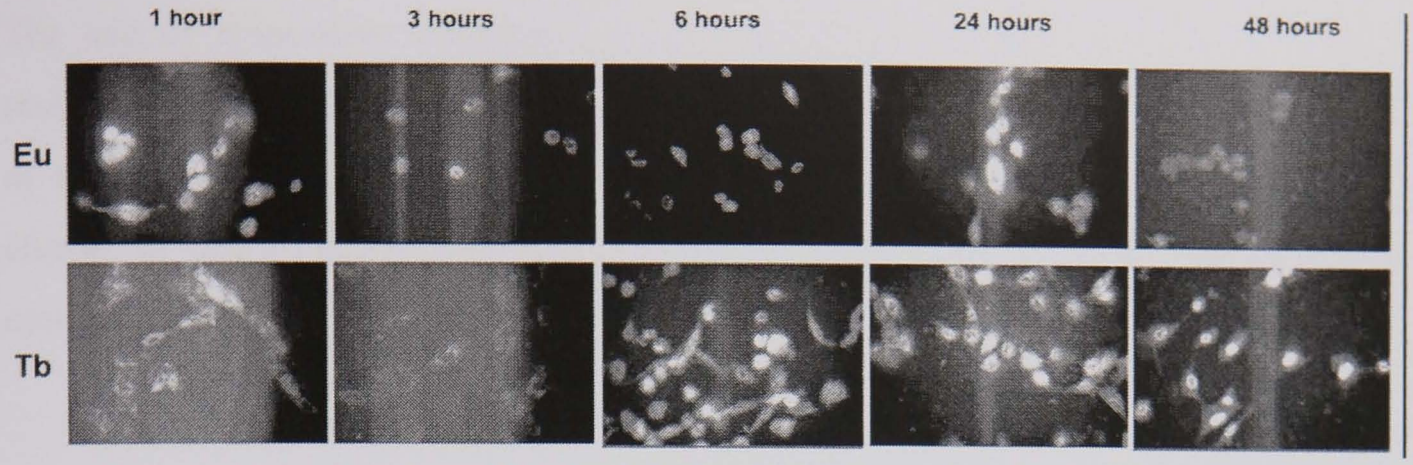

Figure 1. 28 – Microscopy images for the internalisation of the [Ln.1] Eu and Tb probes at different times. (1 mM loading concentration in DMEM supplemented with 50 mg ml^{-1} penecillin/streptomycin and 10 % NCS)

Figure 1. 29 – Microscopy images for the transit of Eu probe after 3 hours incubation and washing of unbound complex.

These images constituted some of the first examples where a lanthanide complex had been shown to be taken up by cells. Discussion and further analyses are presented in Chapter 4 of this thesis.

The following section (1.4.5.1) provides examples of lanthanide-based sensors and probes; if the application of these or similar complexes could be extended to intracellular use, they could perhaps constitute a new class of responsive sensor or probe. Their spectral emission profile, lifetime or circular polarisation may vary as a function of the local concentration of a targeted analyte, and also could provide information about the binding environment of the complex.[24] For example, complexes **a** and **b** were developed to report on local concentrations of HCO_3^- by monitoring changes in the ratio of two (or more) europium emission bands. Bicarbonate is an important intracellular species as it binds reversibly to the enzyme adenylcyclase, thereby regulating release of the key secondary messenger cyclic-AMP.[24] If the anion could be bound with a high enough selectivity in an intracellular medium, it could be used to provide information on these processes inside live cells.

The use of responsive complexes would also introduce the possibility of using multidimensional acquisition. For example, a labelled cell could be analysed in terms of the spatial localisation of the complex by intensity and at the same time, the change in concentration of a local analyte could be monitored by measuring the emission profile or lifetime at specific points within the image.

1.4.5.1 Responsive Lanthanide-Based Sensors

There are a number of examples of responsive lanthanide sensors that provide information about the presence of particular analytes in solution by modulations in their photophysical properties, usually through either a change in their emission intensity or in the form of their emission spectra.

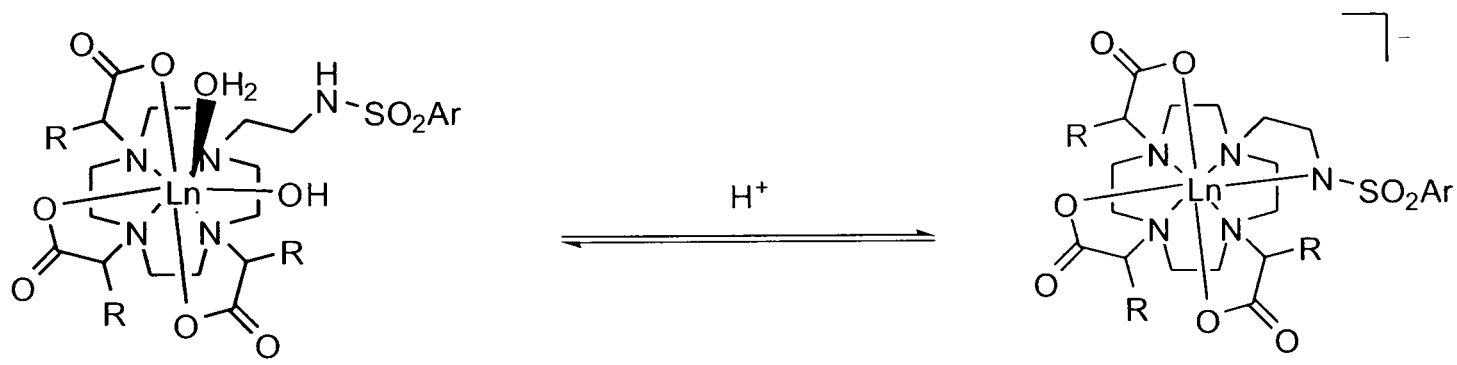

Figure 1. 30

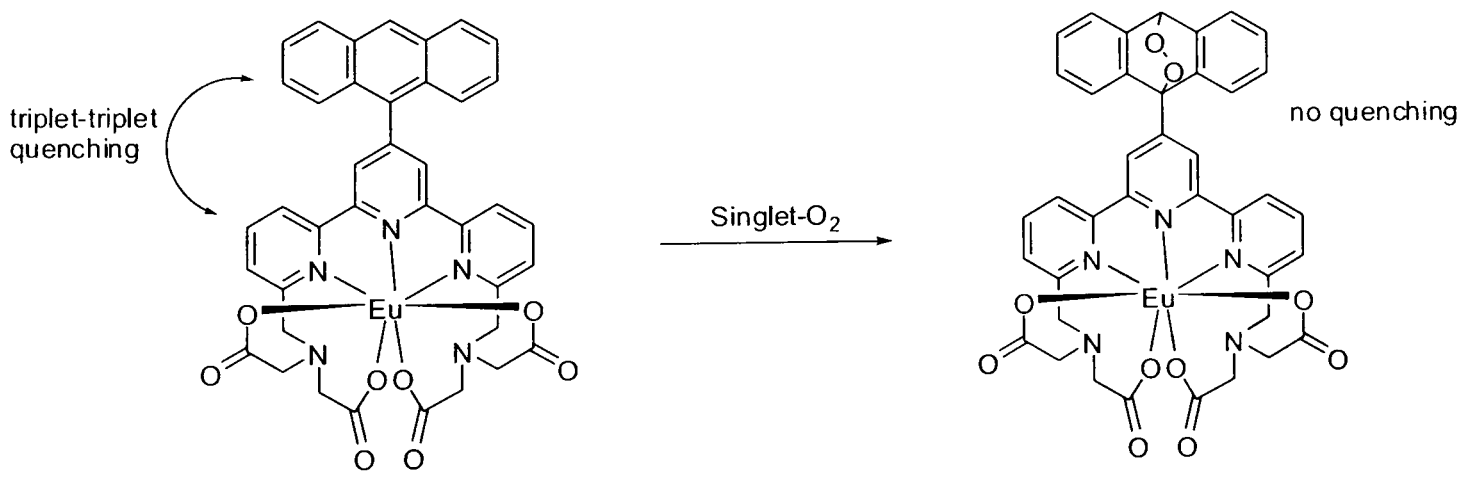

Figure 1. 31

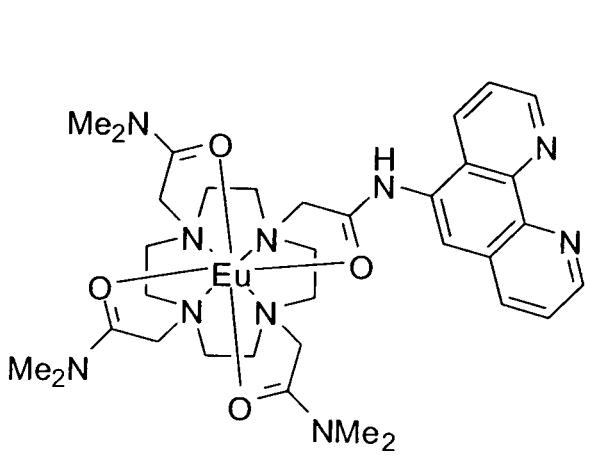

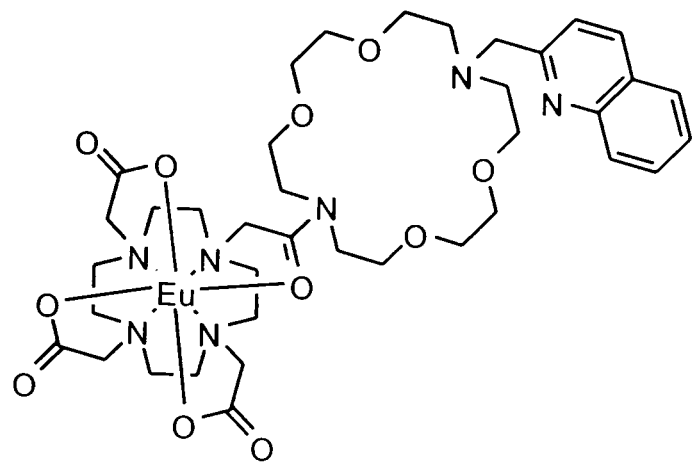

Figure 1. 32

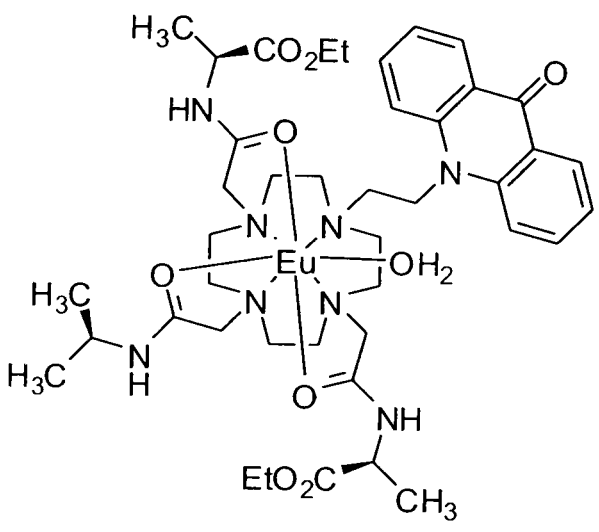

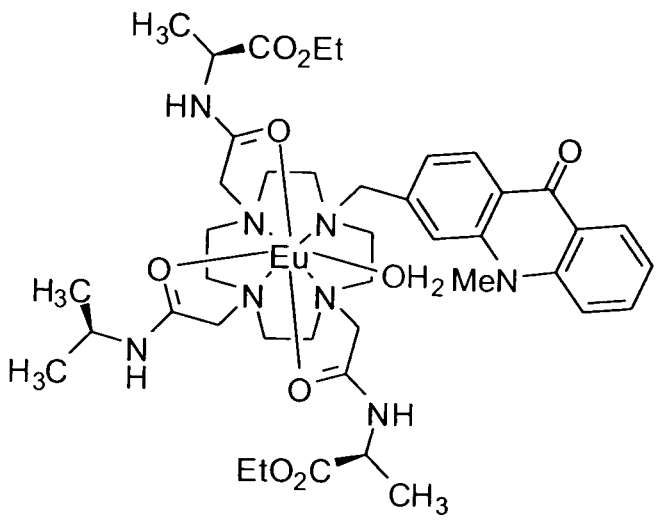

Figure 1. 33

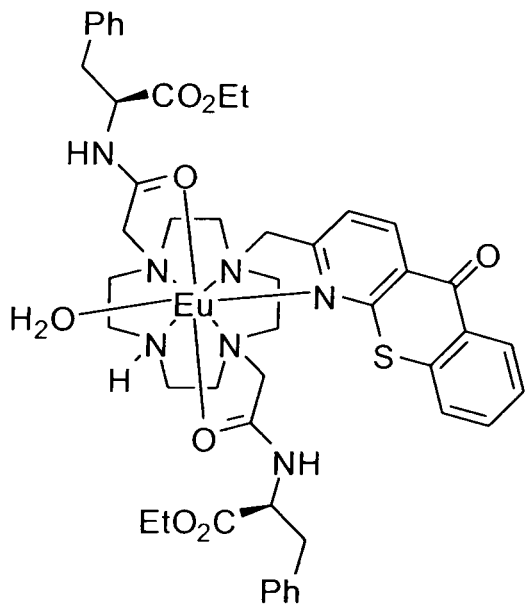

Figure 1. 34

Selected examples include complexes that are sensitive to pH (Figure 1.30),[64-66] can report on the concentration of singlet oxygen in solution (Figure 1.31),[67] can bind cations (Figure 1.32),[68,69] can reversibly bind bicarbonate in intracellular media

(Figure 1.33);[70,71] and can selectively bind citrate in a competitive medium (Figure 1.34).[27]

References

1. J–C. G. Bünzli, C. Piguet, *Chem. Soc. Rev.*, 2005, **34**, 1048.
2. R. S. Dickins, D. Parker, A. S. de Sousa, J. A. G. Williams, *Chem. Commun.*, 1996, 697.
3. I. Hemmilä, V.M. Mukkala, *Crit. Rev. Clin. Lab. Sci.*, 2001, **38**, 441.
4. A. Døssing, *Eur. J. Inorg. Chem.*, 2005, 1425
5. S. Faulkner, S. J. A. Pope, B. P. Burton-Pye, *App. Spec. Rev.*, 2005, **40**(1), 1.
6. I. M. Clarkson, *Energy Transfer in Lanthanide Complexes*, PhD Thesis, University of Durham, 1999.
7. G. F. de Sá, O. L. Malta, C. de M. Donegá, A. M. Simas, R. L. Longo, P. A. Santa-Cruz, E. F. da Silva Jr., *Coord. Chem. Rev.*, 2000, **196**, 165.
8. O. L. Malta, *J. Lumin.*, 1997, **71**, 229.
9. G. E. Buono-Core, H. Li, *Coord. Chem, Rev.*, 1990, **90**, 55.
10. D. Imbert, M. Cantuel, J–C. G. Bünzli, G. Bernardinelli, C. Piguet, *J. Am. Chem. Soc.*, 2003, **125**, 15698.
11. N. M. Shavaleev, G. Accorsi, D. Virgili, Z. R. Bell, T. Lazarides, G. Calogero, N. Armaroli, M. D. Ward, *Inorg. Chem.*, 2005, **44**, 61.
12. S. J. Pope, B. J. Coe, S. Faulkner, R. H. Laye, *Dalton Trans.*, 2005, 1482.
13. N. M. Shavaleev, L. P. Moorcraft, S. J. A. Pope, Z. R. Bell, S. Faulkner, M. D. Ward, *Chem. Eur. J.*, 2003, **9**, 5283.
14. S. Faulkner, S. J. A. Pope, *J. Am. Chem. Soc.*, 2003, **125**, 10526.
15. G. E. Buono-Core, H. Li, *Coord. Chem. Rev.*, 1990, **99**, 55.
16. J. L. Cropp, M. W. Windsor, *J. Chem. Phys.*, 1965, **42**, 1599.
17. Y. Haas, G. Stein, *J. Chem. Phys.*, 1972, **76**, 1093.
18. R. S. Dickins, D. Parker, A. S. de Sousa, J. A. G. Williams, *Chem. Commun.*, 1996, 697.
19. A. Beeby, I. M. Clarkson, R. S. Dickins, S. Faulkner, D. Parker, L. Royle, A. S. de Sousa, J. A. G. Williams, M. Woods, *J. Chem. Soc., Perkin Trans. 2*, 1999, 493.
20. S. Faulkner, A. Beeby, M. –C. Carrié, A. Dadabhoy, A. M. Kenwright, P. G. Sammes, *Inorg. Chem. Commun.*, 2001, **4**, 187.

21. R. M. Supkowski, W. D. Horrocks, Jr., *Inorg. Chem. Acta*, 2002, **340**, 44.

22. D. Parker, J. A. G. Williams, *J. Chem. Soc., Perkin Trans. 2*, 1995, 1305.

23. D. Parker, J. A. G. Williams, *Metal Ions in Biological Systems*, Marcel Dekker, Inc., New York, Volume 40, 233.

24. S. Pandya, J. Yu, D. Parker, *Dalton Trans.*, 2006, 2757.

25. G. Bobba, J.–C. Frias, D. Parker, *Chem. Commun.*, 2002, 890.

26. R. A. Poole, G. Bobba, M. J. Cann, J. –C. Frias, D. Parker, R. D. Peacock, *Org. Biomol. Chem.*, 2005, **3**, 1013.

27. D. Parker, J. Yu, *Chem. Commun.*, 2005, 3141.

28. P. Atkinson, K. S. Findlay, F. Kielar, R. Pal, D. Parker, R. A. Poole, H. Puschmann, S. L. Richardson, P. A. Stenson, A. L. Thompson, J. Yu, *Org. Biomol. Chem.*, 2006, **4**, 1707.

29. N. Weibel, L. J. Charbonnière, M. Guardigli, A. Roda, R. Zeissel, *J. Am. Chem. Soc.*, 2004, **126**, 4888.

30. (*a*) G. Mathis, *Clin. Chem. (Washington D. C.)*, 1993, **39**, 1953; (*b*) G. Mathis, *Clin. Chem. (Washington D. C.)*, 1995, **41**, 1391; (*c*) H. Bazin, M. Préaudat, E. Trinquet, G. Mathis, *Spectrochim. Acta.*, 2001, **A57**, 2197; (*d*) D. Maurel, J. Kriazeff, G. Mathis, E. Trinquet, J. P. Pin, H. Ansanay, *Anal. Biochem.*, 2004, **329**, 253; (*e*) M. Gabourdes, V. Bourgine, G. Mathis, H. Bazin, B. Alpha-Bazin, *Anal. Biochem.*, 2004, **333**, 105.

31. (*a*) I. Hemmila, V. –M. Mukkala, *Crit. Rev. Clin. Lab. Sci.*, 2001, **38**, 441; (*b*) V. W. W. Yam, K. K. Lo, *Coord. Chem. Rev.*, 1999, **184**, 157; (*c*) H. Sitari, I. Hemmila, K. Pettersson, T. Lovgren, *Nature (London)*, 1983, **301**, 258.

31a E. B. van der Tol, H. J. van Ramesdonk, J. W. Verhoeven, F. J. Steemers, E. G. Kerver, W. Verboom, D. N. Reinhoudt, *Chem. Eur. J.*, 1998, **4**(11), 2315.

31b B. H. Bakker, M. Goes, N. Hoebe, H. J. van Ramesdonk, J. W. Verhoeven, M. H. V. Werts, J. W. Hofstraat, *Coord. Chem. Rev.*, 2000, **208**, 3.

31c D. Parker, R. S. Dickens, H. Puschmann, C. Crossland, J. A. K. Howard, *Chem. Rev.*, 2002, **102**, 1977.

31d R. S. Dickins, J. A. K. Howard, C. W. Lehmann, J. Moloney, D. Parker, R. D. Peacock, *Angew. Chem., Int. Ed. Engl.*, 1997, **36**, 521.

31e M. Elbanowski, B. Makowska, *J. Photochem. Photobiol. A: Chem.*, 1996, 85.

32. D. Parker, *Coord. Chem. Rev.*, 2000, **205**, 109.

33. S. Blair, R. Kataky, D. Parker, *New. J. Chem.*, 2002, **26**, 530.

34. S. Blair, M. P. Lowe, C. E. Mathieu, D. Parker, P. K. Senanayake, *Inorg. Chem.*, 2001, **40**, 5860.

35. X. Michalet, A. N. Kapanidis, T. Laurence, F. Pinaud, S. Doose, M. Pfulghoefft, S. Weiss, *Annu. Rev. Biophys. Biomol. Struct.*, 2003, **32**, 161.

36. K. Suhling, P. M. W. French, D. Philips, *Photochem. Photobiol. Sci.*, 2005, **4**, 13.

37. N. J. Emptage, *Curr. Opn. Pharm.*, 2001, **1**, 521.

38. J. R. Lakowicz, *Principles of Fluorescence Spectroscopy*, Kluwer Academic/Plenum Publishers, New York, 1999.

39. R. D. Goldman, D. L. Spector, *Live Cell Imaging – A Laboratory Manual*, Cold Spring Harbor Laboratory Press, New York, 2005.

40. G. W. Gordon, G. Berry, X. H. Liang, B. Levine, B. Herman, *Biophys. J.*, 1998, **74**, 2702.

41. J. Zhang, R. E. Campbell, A. Y. Ting, R. Y. Tsien. *Nat. Rev.*, 2002, **3**, 906.

42. M. Zimmer, *Chem. Rev.*, 2002, **102**, 759.

43. R. Pepperkok, A. Squire, S. Geley, P. I. H. Bastiaens, *Curr. Biol.*, 1999, **9**, 269.

44. J. Zhang, R. E. Campbell, A. Y. Ting, R. Y. Tsien, *Nat. Rev. Mol C. Biol.*, 2002, **3**, 906.

45. M. Zimmer, *Chem. Rev.*, 2002, **102**, 759.

46. M. H. V. Werts, N. Nerambourg, D. Pélégry, Y. Le Grand, M. Blanchard-Desce, *Photochem. Photobiol. Sci.*, 2005, **4**, 531.

47. T. Ueno, Y. Urano, K. Setsukinai, H. Takakusa, H. Kojima, K. Kikuchi, K. Ohkubo, S. Fukuzumi, T. Nagano, *J. Am. Chem. Soc.*, 2005, **126**, 14079.

48. Y. Urano, M. Kamiya, K. Kanda, T. Ueno, K. Hirose, T. Nagano, *J. Am. Chem. Soc.*, 2005, **127**, 4888.

49. R. P. Haugland, *A Guide to Fluorescent Probes and Labelling Technologies*, Molecular Probes, Eugene, Oregon, 10th edn, 2005.

50. T. Yogo, Y. Urano, Y. Ishitsuka, F. Maniwa, T. Nagano, *J. Am. Chem. Soc.*, 2005, **127**, 12162.

51. X. Gao, L. Yang, J. A. Petros, F. F. Marshall, J. W. Simons, S. Nie, *Curr. Op. Biotech.*, 2005, **16**, 63.

52. A. P. Alivisatos, *Science*, 1996, **271**, 933.

53. X. Michalet, F. F. Pinaud, L. A. Bentolila, J. M. Tsay, S. Doose, J. J. Li, G. Sundaresan, A. M. Wu, S. S. Gambhir, S. Weiss, *Science*, 2005, **307**, 538.

54. A. G. Tkachenko et al., *Bioconjug. Chem.*, 2004, **15**, 482.

55. M. H. Keefe, K. D. Benkstein, J. T. Hupp, *Coord. Chem. Rev.*, 2000, **205**, 201.

56. R. Poole, *Highly Emissive Tetraazatriphenylene Complexes*, First Year Report, University of Durham, 2004.

57. A. E. Friedman, J. C. Chambron, J. P. Sauvage, N. J. Turro, J. K. Barton, *J. Am. Chem. Soc.*, 1990, **112**, 4960.

58. C. Hiort, P. Lincoln, B. Nordén, *J. Am. Chem. Soc.*, 1993, **115**, 3448.

59. L. Li, F. N. Castellano, I Gryczynski, J. R. Lakowicz, *Chem. Phys. Lip.*, 1999, **99**, 1.

60. M. Paxian, S. A. Kellar, B. Cross, T. T. Huynh, M. G. Clemens, *Am. J. Physiol.: Gastrointest. Liver Physiol.*, 2004, **286**, 637.

61. H.J. Youn, E. Terpetschnig, H. Szmacinski, J.R. Lakowicz, *Anal. Biochem.*, 1995, **232**, 24.

62. X.-Q. Guo, G.N. Catellano, L. Li, J.R. Lakowicz, *Anal. Chem.*, 1998, **70**, 632.

63. J. N. Demas, B. A. DeGraff, *Coord. Chem. Rev.*, 2001, **211**, 317.

64. M. P. Lowe, D. Parker, O. Reany, S. Aime, M. Botta, G. Castellano, E. Gianolio, R. Pagliarin, *J. Am. Chem. Soc.*, 2001, **123**, 7601.

65. M. P. Lowe, D. Parker, *Inorg. Chim. Acta.*, 2001, **317**, 163.

66. M. P. Lowe, D. Parker, *Chem. Commun.*, 2000, 707.

67. G. Song, G. Wang, J. Yuan, *Chem. Commun.*, 2005, 3553.

68. T. Gunnlaugsson, J. P. Leonard, K. Senechal, A. J. Harte, *Chem. Commun.*, 2004, 782.

69. C. Li, E. –L. Law, W. –T. Wang, *Org. Lett.*, 2004, **6**, 4841.

70. Y. Bretonniere, M. J. Cann, D. Parker, R. Slater, *Chem. Commun.*, 2002, 1930.

71. Y. Bretonniere, M. J. Cann, D. Parker, R. Slater, *Chem. Commun.*, 2004. 1624.

72. J. –C. Frias, G. Bobba, M. J. Cann, C. J. Hutchison, D. Parker, *Org. Biomol. Chem.*, 2003, **1**, 905.

73. J. Yu, D. Parker, R. Pal, R. A. Poole, M. J. Cann, *J. Am. Chem. Soc.*, 2006, **128**, 2294.

CHAPTER 2

Ligand and Complex Synthesis

2 Ligand and Complex Synthesis

A series of europium(III) and terbium(III) complexes has been synthesised that is based on the cyclen macrocycle and incorporates a common antenna group. The cyclen macocycle has four ring nitrogens that may readily be alkylated; through the use of an appropriate protecting strategy, up to four different pendent arms can be attached. These arms should bear a functional group in the correct position and with an orientation that allows them to coordinate to the metal centre in order to give a complex with high kinetic and thermodynamic stability with respect to metal ion dissociation. Common examples include: amides (in particular those obtained through the use of amino acids), carboxylic acids (DOTA and DTPA complexes of gadolinium are perhaps the most widely used lanthanide complexes – in common use as MRI contrast agents) and phosphinates. Through the presence of two or more arms of the same chirality, a degree of control is possible over the overall chirality of the complex. Where three or four of the arms have the same chirality, the chirality of the complex can be predicted with some certainty (see Chapter 1.2.5). In the present work, the pendent arms are varied in order to provide a series of complexes of varying overall charge and lipophilicity.[1]

2.1 Synthesis of a Series of Cyclen Based Complexes with a Tetraazatriphenylene Sensitising Moiety Incorporating Amide or Carboxylic Acid Pendent Arms

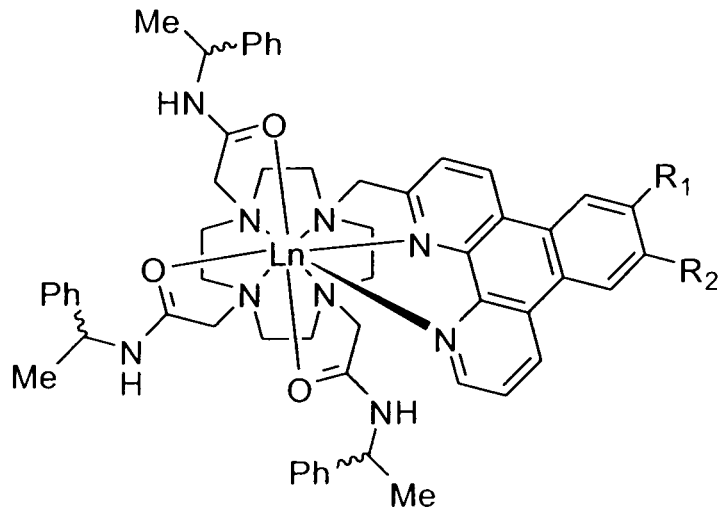

R_1	R_2
H	H
$-(CH_2)_4-$	

Figure 2. 1 – LnPh3dpq/dpqC (Ln = Eu(III), Tb(III))

The favourable photophysical properties of the Δ-SSS and Λ-RRR enantiomeric europium and terbium complexes depicted in Figure 2.1 have been previously reported.[2,3] Complexes [Ln.**1**-**4**] constitute a series of structurally related compounds, each with an appended tetraazatriphenylene sensitising chromophore (Figure 2.2). Due to the contracted nature of lanthanide 4f orbitals and the mostly electrostatic nature of the metal-ligand interaction, the pendent arms can be varied without greatly affecting the photophysical properties of the complex.[4]

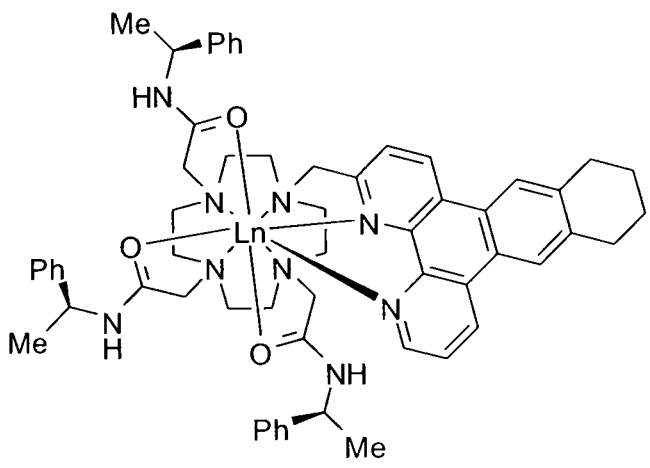

[Ln.**1**]$^{3+}$

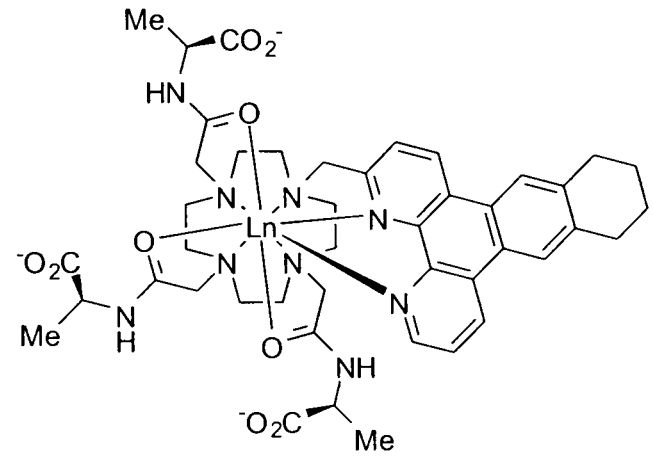

[Ln.**2**]

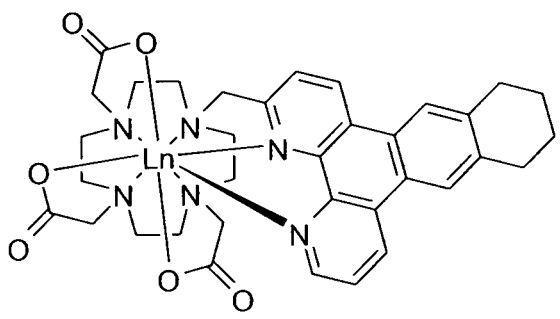

[Ln.**3**]

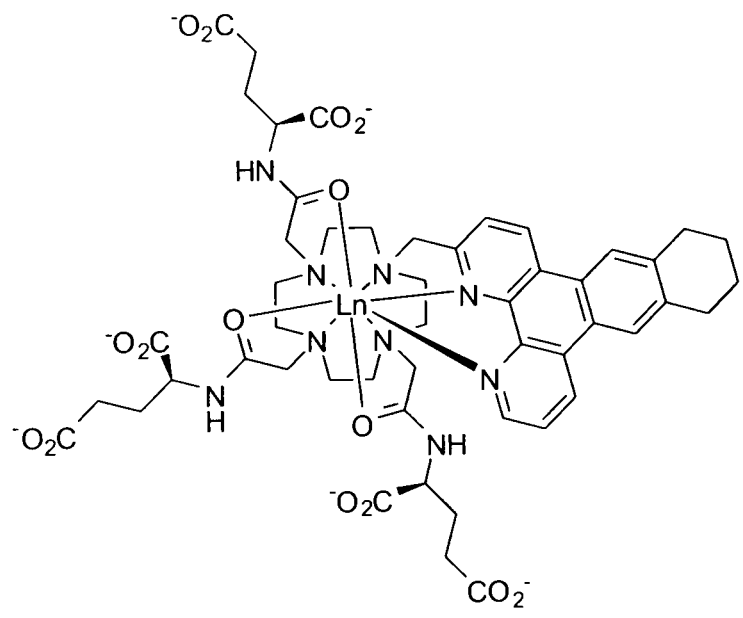

[Ln.**4**]$^{3-}$

Figure 2. 2 – A series of structurally related lanthanide complexes (Ln = Eu(III), Tb(III)) of differing charge and lipophilicity

2.1.1 10,11,12,13-Tetrahydrodipyrido-[3,2a:2',3'-c]-phenazine (dpqC)

10,11,12,13-Tetrahydrodipyrido-[3,2a:2',3'-c]-phenazine (dpqC) has been shown to be an excellent antenna chromophore for both europium(III) and terbium(III). It has a reasonably high molar absorption coefficient (~ 6440 cm^{-1}); it possesses a high quantum yield of triplet formation ($\phi_T \sim 1$) as a result of its fast rate of intersystem crossing. It displays virtually no fluorescence either as the free chromophore or when coordinated to a metal centre and has a suitably high triplet energy (23400 cm^{-1}) such that it can excite both europium(III) and terbium(III) and is sufficiently higher in energy such that it is not excited by thermally activated back energy transfer from the lanthanide. It can also coordinate through the two pyridyl nitrogens to the lanthanide, minimising the donor-acceptor distance for energy transfer and enabling the ligand to be nonadentate, thus excluding water or other possible ligands from the coordination sphere of the metal.[5, 6]

Although the number of steps (Scheme 2.1) required to synthesise the chloro derivative of the tetraazatriphenylene chromophore is rather high, the synthesis may be accomplished in reasonable yield, utilises low cost starting materials and the product is stable to storage in air. It has been demonstrated that the synthesis is amenable to scale-up to a multigram scale. The procedure used follows a similar route to that previously used for the synthesis of the related tetraazatriphenylene chromophore 'dpq'.[7]

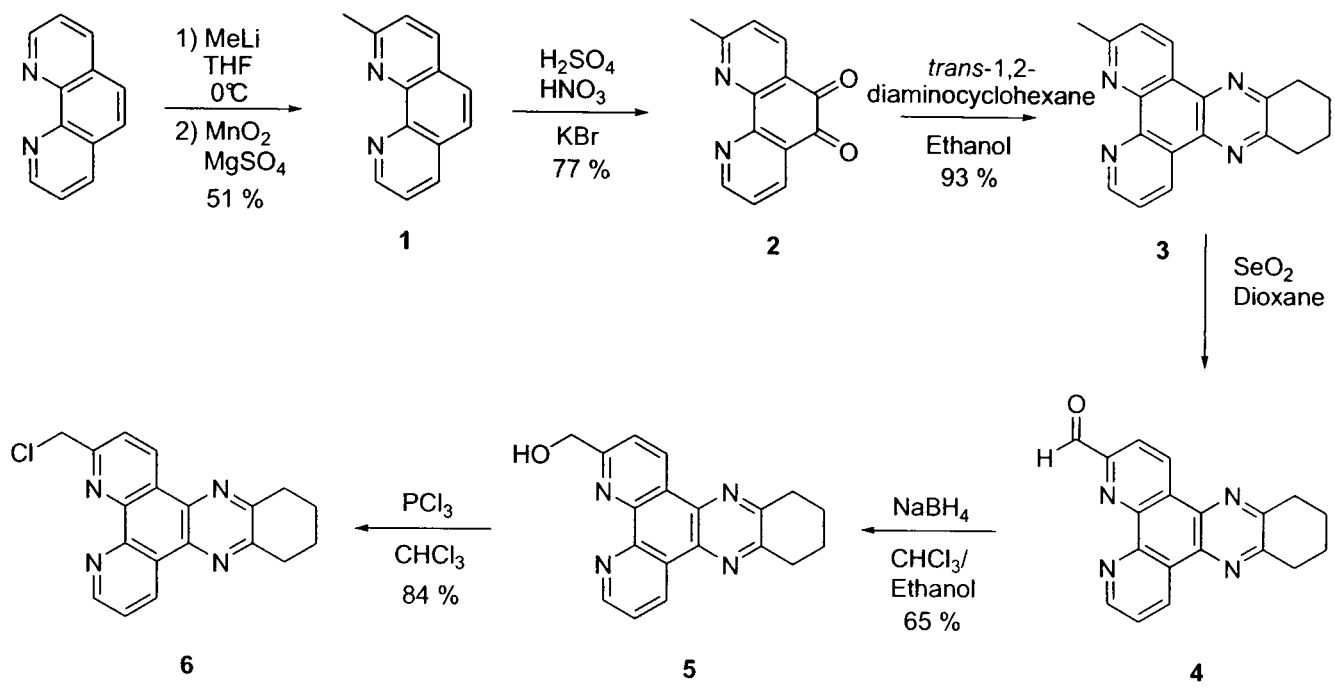

Scheme 2. 1 – Reaction scheme for the synthesis of the chloromethyl derivative of the 10,11,12,13-tetrahydrodipyrido-[3,2a:2',3'-c]-phenazine (dpqC) chromophore

1,10-Phenanthroline was first alkylated in order to provide a position that can be functionalised and from which the chromophore can be attached to 1,4,7,10-tetraazacyclododecane. The methylation step involved a nucleophilic aromatic substitution reaction using MeLi at 0°C in THF to form a Meisenheimer intermediate, which was subsequently re-aromatised by oxidation with manganese oxide. The established procedure[7] used a small excess of MeLi leading to some 2,9-dimethyl-1,10-phenanthroline that persisted in small quantities after purification both by chromatography and recrystallisation. The problem was overcome by using the reagents in stoichiometric amounts. 2-Methyl-1,10-phenanthroline, **1**, was purified by recrystallisation from an ethyl acetate/hexane mixture. The relatively low yield was ascribed to an inefficient extraction of the anionic intermediate into diethyl ether from water.

Oxidation of 2-methyl-1,10-phenanthroline to the 5,6-quinone, **2**, used molecular bromine (generated in situ from KBr and H_2SO_4) and HNO_3, according to a literature procedure[8]. Care was taken in neutralising the strongly acidic mixture due to the base sensitivity of the quinone. Under basic conditions, decarboxylation can occur to give 4,5-diazafluoren-9-one.[9]

Condensation of 2-methyl-1,10-phenanthroline-5,6-quinone, **2**, with 1,2-diaminocyclohexane gave the corresponding Schiff base which, upon oxidation by oxygen from the air, yielded the 10,11,12,13-tetrahydrodipyrido-[3,2a:2',3'-c]-phenazine chromophore with a methyl substituent at the 3-position, **3**. Early attempts at the reaction were carried out using THF as a solvent under high dilution as previously carried out within the group. However this procedure led to low yields of about 40 %. The yield was greatly improved by changing the solvent to ethanol, in accordance with a synthesis for 3,6-dimethyl-10,11,12,13-tetrahydrodipyrido[3,2-a:2',3'-c]-phenazine[10]. Purification was successfully achieved by recrystallisation from hot ethanol.

The final stages in the synthesis are associated with generation of the benzylic chloride of dpqC, **6**. It has been shown[7] that direct halogenation with one equivalent of N-chlorosuccinimide is not successful and that the use of an excess leads to the trichloromethyl derivative. Therefore, a three step strategy was used involving mild oxidation with selenium(IV) oxide to yield the aldehyde, **4**, which was subsequently reduced with sodium borohydride. The alcohol, **5**, was then chlorinated with phosphorus trichloride.

2.1.2 Amide Based Ligands and Complexes

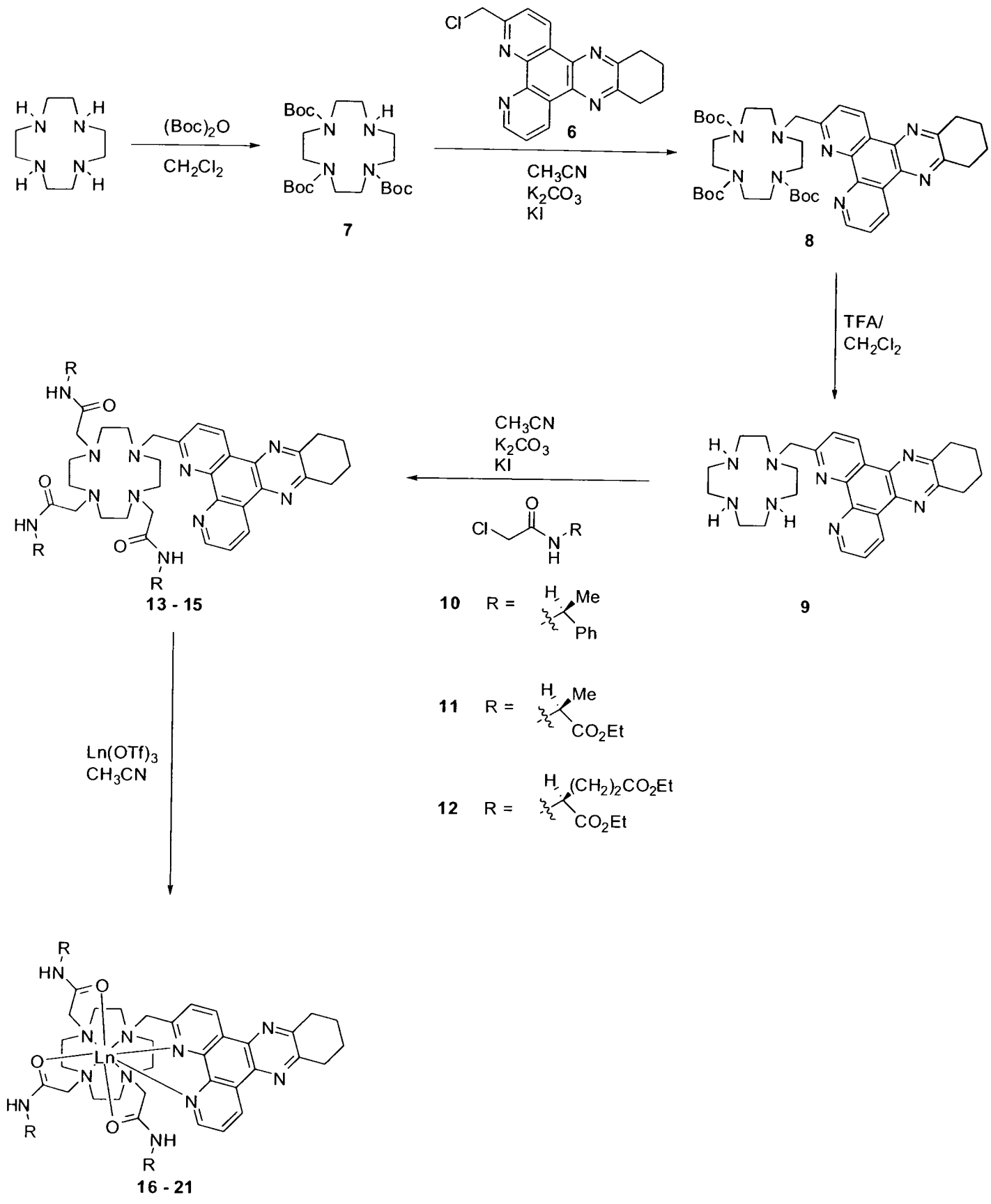

Scheme 2. 2 – Synthesis of the series of complexes bearing pendent amide arms

A procedure analogous to that used previously within the group[7] was followed to obtain the desired α-methyl-benzyl, alanine and glutamic acid based amide ligands, **13**, **14**, **15** respectively (Scheme 2.2). In order to monofunctionalise cyclen with the

dpqC chromophore, cyclen was first triprotected using 2.4 equivalents of $(Boc)_2O$. Alkylation with the chloromethyl derivative was followed by removal of the protecting groups with trifluoroacetic acid in dichloromethane.

N-Chloroacetyl-L-glutamic acid diethyl ester, **10**, *N*-chloroacetyl-L-alanine ethyl ester, **11**, and (S)-N-chloroethanoyl-2-phenylethylamine, **12**, were each synthesised by addition of chloroacetyl chloride to the appropriate chiral amino acid ethyl ester hydrochloride or amine, in the presence of triethylamine, in THF at low temperature. Compounds **10** – **12** were then added to the macrocycle by an alkylation reaction in acetonitrile, with a catalytic amount of potassium iodide added. Each of the ligands was purified by chromatography on alumina using a dichloromethane/methanol solvent system.

The europium and terbium complexes of each of the ligands were prepared in anhydrous acetonitrile by reaction of the ligands with the appropriate trifluoromethanesulphonate salt. Initial purification involved repeated precipitation onto dry diethyl ethyl. The final stage in the synthesis of the $LnAla_3dpqC$, [Ln.**2**] and $LnGlu_3dpqC^{3-}$ [Ln.**4**] ligands was to hydrolyse the esters to the corresponding carboxylic acid using dilute potassium hydroxide.

HPLC provides a useful tool for the analysis of lanthanide complexes, in particular in terms of monitoring the progress of the complexation reaction and confirming the presence or absence of uncomplexed ligand that may otherwise affect the validity of photophysical measurements made on the complex. Complexes [Ln.**1-4**] were each analysed using a Phenomenex C18 column using water/acetonitrile gradient elution. The amide based complexes each required the presence of 0.1 % trifluoroacetic acid to prevent sticking to the column. In each case, a single major product was observed in > 90 % purity. Semi-preparative HPLC allowed further prurification of small quantities of the complexes where necessary for quantitative measurements and in particular for the quantum yield determinations.

2.1.3 Tris(Carboxymethyl) Ligands and Their Lanthanide Complexes

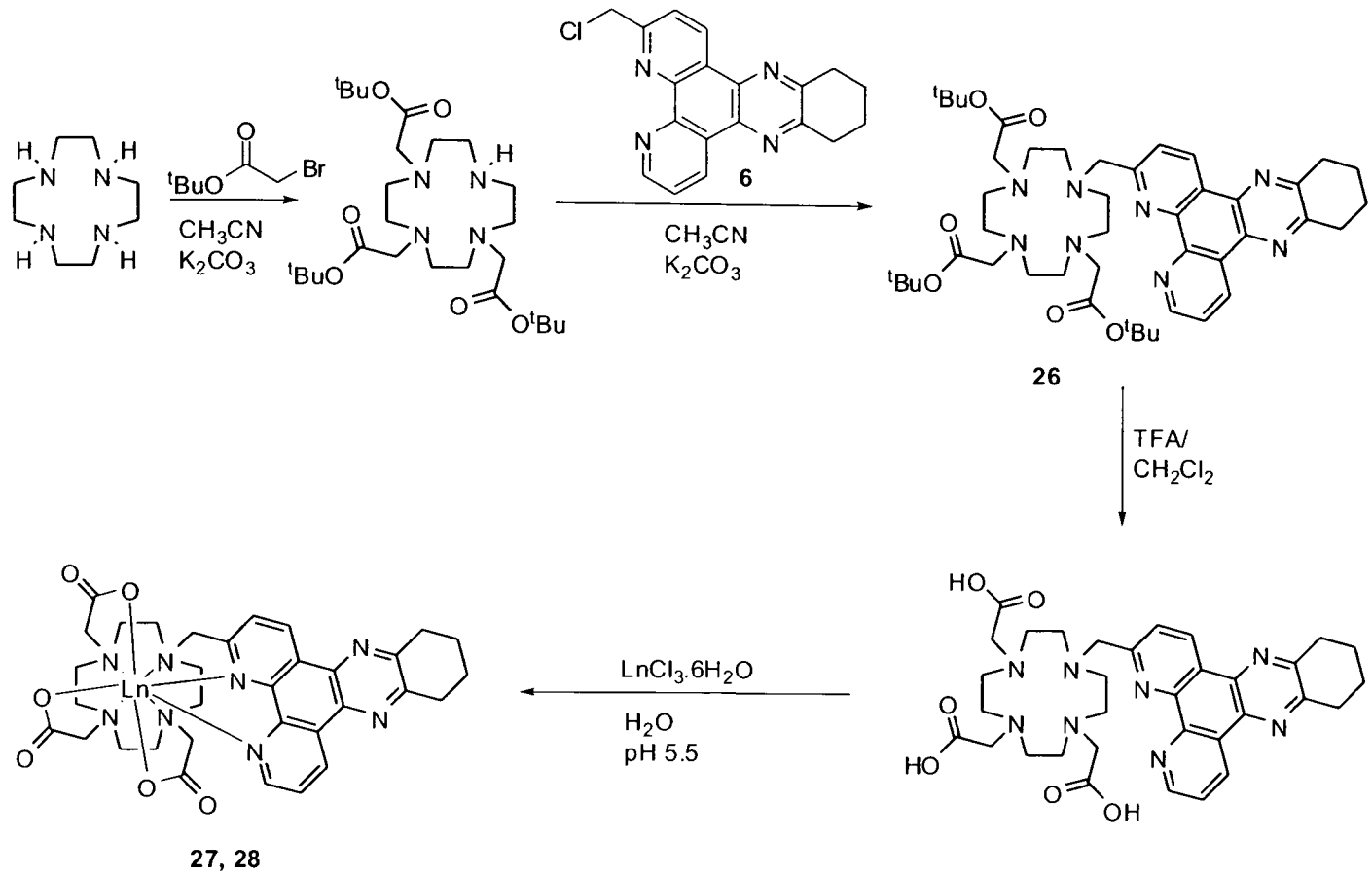

Scheme 2. 3 – Synthesis of the tris(carboxymethyl) ligands and their lanthanide complexes

Tris(carboxymethyl) ligands constitute one of the simplest and most studied group of ligands used for lanthanide chelation; appropriate synthetic strategies are well established. Alkylation of the *tert*-butyl ester of DO3A with the chloromethyl dpqC derivative, **6**, afforded **26** in good yield. The ester was hydrolysed with trifluoroacetic acid and the product analysed by ^{1}H NMR to ensure complete removal of the tert-butyl groups. The crude ligand was immediately complexed with the appropriate lanthanide(III) chloride in a synthetic procedure that involved the adjustment of pH both prior to reaction (to pH 5.5) and after 18 hours (to pH 10) to allow removal of free lanthanide as the hydroxide salt.

2.1.4 Characterisation of The Series of Amide and Carboxylic Acid Based Complexes

2.1.4.1 Solution NMR studies

The majority of lanthanide(III) ions are paramagnetic. As a result, the NMR resonances of atoms that are either directly coordinated, or are in close proximity to the metal exhibit both a broadening and a shift; the extent to which they are affected is dependent upon the lanthanide under study. These effects have been exploited in the development of shift reagents and MRI contrast agents.[11,12] Where the coordination environment around the metal ion is well defined, and in particular when the lanthanide is coordinatively saturated, solution NMR can provide structural information about the complex. Lanthanide induced shifts fall off rapidly as the distance of the nucleus under study from the metal increases.[11] For cyclen based complexes, the most shifted ^{1}H resonances are those of the macrocyclic ring protons.

The spectrum of the europium(III) complex, [Ln.**1**]$^{3+}$, in D_2O closely resembled that of the previously synthesised Δ- and Λ-EuPh3dpq and of the related triamide europium complexes[7, 13, 14] The most paramagnetically shifted 'pseudo-axial' cyclen ring protons resonated as one set of four broadened singlets in the range 32-20 ppm. This is consistent with the presence of a major species, adopting a square antiprismatic geometry. An additional peak was evident in the region above 20 ppm and was assigned as the proton α- to the nitrogen of the dpqC chromophore. The large chemical shift is accounted for since it falls within the McConnell cone and so experiences a large positive paramagnetic shift effect. Again, assignment was made through comparison with spectra that had previously been assigned for the EuPh3dpq complexes and confirmed by COSY ^{1}H NMR spectroscopy. The less rigid complexes [Ln.**2** and **4**] displayed broader spectra. Spectral resolution of each of the chiral complexes improved in CD_3OD at low temperatures (< 0 °C). Arm rotation is inhibited by the chiral groups introduced δ to the ring nitrogen atoms, therefore the sharpening of signals is assigned to freezing out of cyclen ring 'wobble' or inversion, previously noted for a multitude of related complexes.[1, 15]

A number of different stereoisomers are possible for [Ln.**3**] and other DO3A/DOTA based complexes as was explained in Chapter 1.[1] It was therefore unsurprising that the spectra of europium and terbium [Ln.**3**] were broad and poorly resolved. However, the ytterbium complex [Yb.3] has also been synthesised and at room temperature displayed a single set of resonances corresponding to the 'pseudo-axial'-ring protons confirming that a preferred geometry was adopted. Such behaviour can perhaps be accounted for by the smaller size of ytterbium compared to europium and terbium, enhancing steric interactions between the ligand arms.

2.1.4.2 Absorption and Emission Spectra

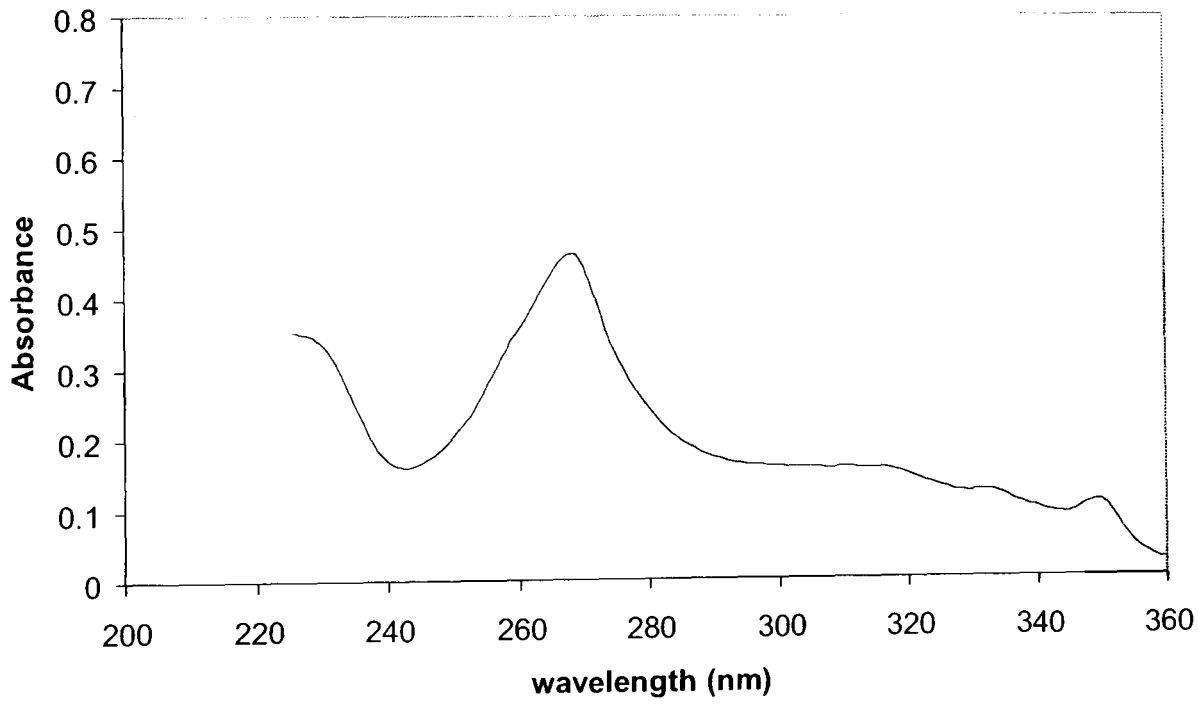

Figure 2. 3 – Absorption spectrum of [Eu.1] recorded in H_2O at 295 K

The absorption spectra for each of the complexes [Ln.**1-4**] in H_2O were identical, with major bands at 224 (ε = 23 100 M^{-1} cm^{-1}), 267 (ε = 30 200 M^{-1} cm^{-1}), 308 (ε = 10 200 M^{-1} cm^{-1}), 332 (ε = 7 700 M^{-1} cm^{-1}) and 348 nm (ε = 6 440 M^{-1} cm^{-1}). The spectral form is similar to that observed for the free chromophore and is indicative of the small electronic interaction between the tetraazatriphenylene antenna and the metal acceptor.

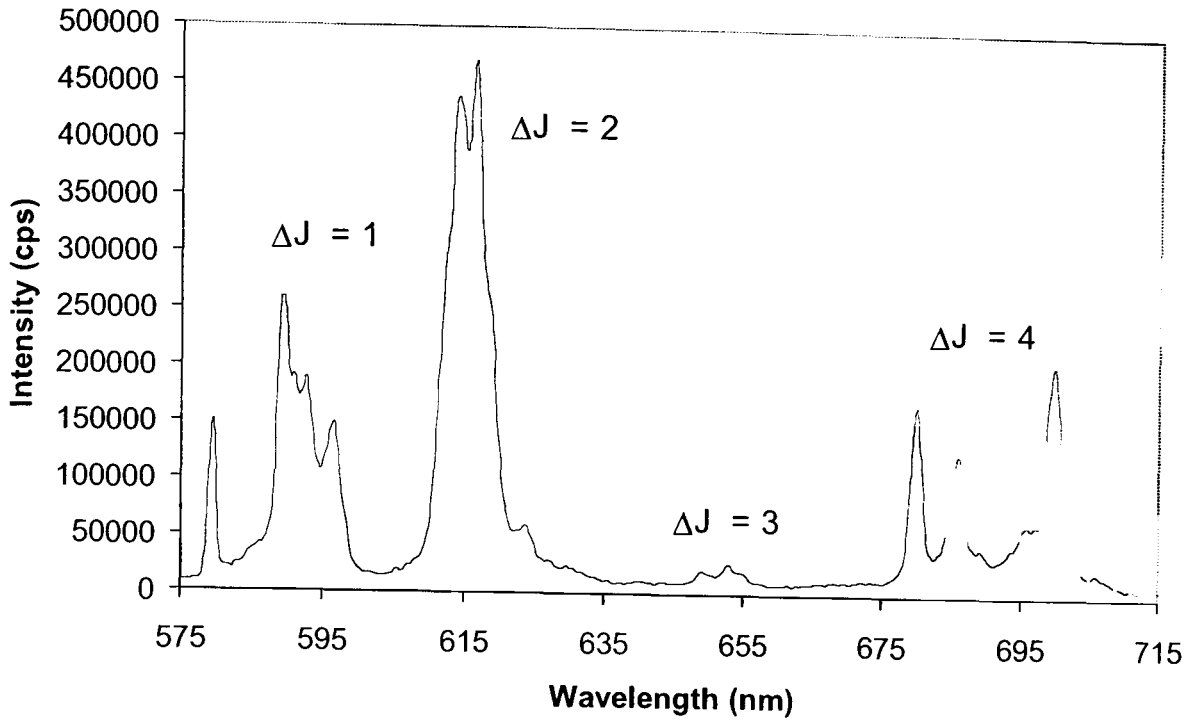

Figure 2. 4 – Emission spectrum of [Eu.1] recorded in H_2O at 295 K

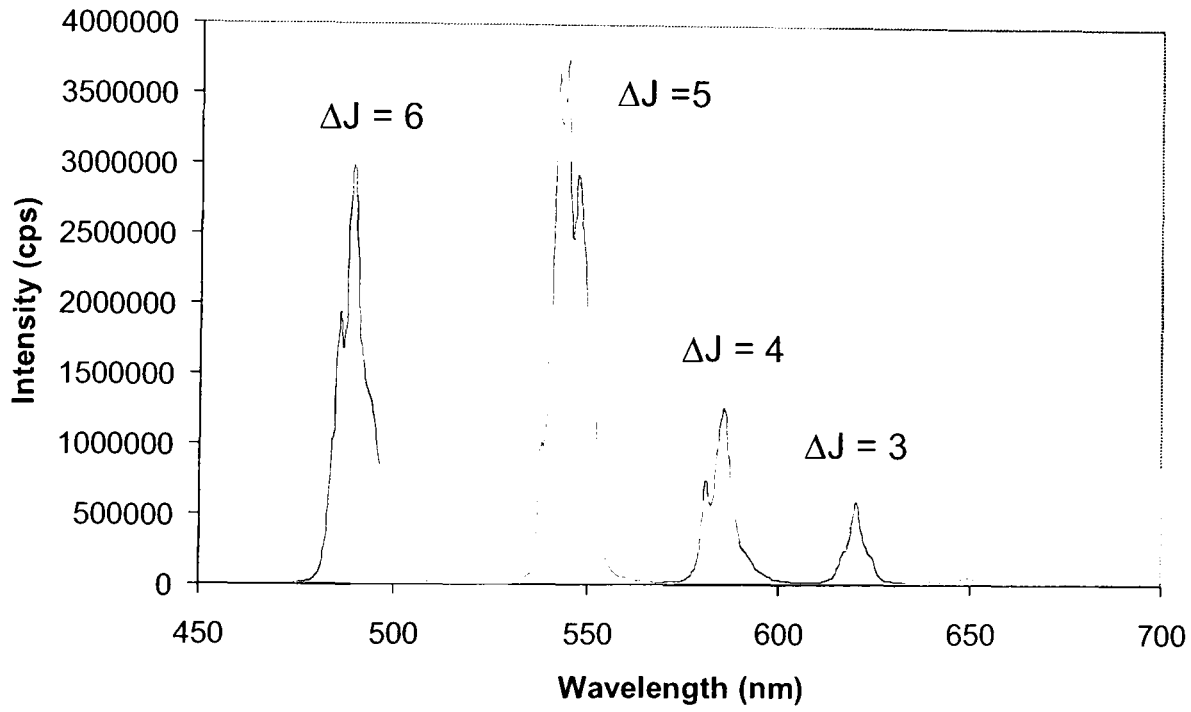

Figure 2. 5 – Emission spectrum of [Tb.1] recorded in H_2O at 295 K

The emission spectra of the lanthanide(III) complexes were recorded at 295 K in H_2O. Spectra shown are for the europium(III) and terbium(III) $[Ln.\mathbf{1}]^{3+}$ complexes but are analogous to those obtained for each of the other pairs of complexes [Ln.**2-4**]. This is as would be predicted from the well defined and common coordination geometry around the metal centre, comprising four tertiary amine donors, three amide C=O donors and two pyridyl nitrogen donors. No fluorescence was observed from the tetraazatriphenylene chromophore, consistent with the expected high

efficiency of the intersystem crossing process, as has been reported previously in studies involving this chromophore.[2, 3, 7]

The fine-splitting of the europium $\Delta J = 1$ band can be interpreted to provide confirmation as to whether there are one, or multiple structural isomers that exist in solution. Three transitions would be expected for a complex lacking a C_n element of symmetry. A fourth transition is apparent for the series of complexes [Ln.**1**-**4**] suggesting the presence of a minor isomer. HPLC and ^{1}H NMR confirm that the complexes adopt one major conformation; however previous low temperature ^{1}H NMR of complex EuPh3dpq (Figure 2.1) in CD_3OD have revealed the presence of a second isomer.[7] This is likely also to be the case for the closely related complexes [Ln.**1**-**4**].

2.1.4.3 Circularly Polarised Luminescence Studies (CPL)

The complexes [Ln.**1**], [Ln.**2**] and [Ln.**4**] are chiral and as such are amenable to study by chiroptical spectroscopy i.e. to circular dichroism and circularly polarized luminescence. Circular dichroism measures the differential absorption of left and right circularly polarised light;[16, 17] in order to probe the ground state structure of the complex we must be able to observe the absorption spectrum of the lanthanide (not the chromophore). The forbidden nature of 4f-4f transitions, and hence their low molar absorption coefficients mean that high sample concentrations would be required; this limits the utility of circular dichroism studies to such lanthanide(III) complex. Circularly polarized luminescence, in contrast, probes the excited state structure of the complex and measures the differential emission of left and right circularly polarized light.[16] Since excitation is indirect, being *via* an antenna chromophore, it does not suffer from the same limitation. Thus, CPL can provide information about both the helicity about the metal centre and the structure of the complex, in addition to some information regarding the electronic and magnetic environment of the lanthanide(III) ion.[18]

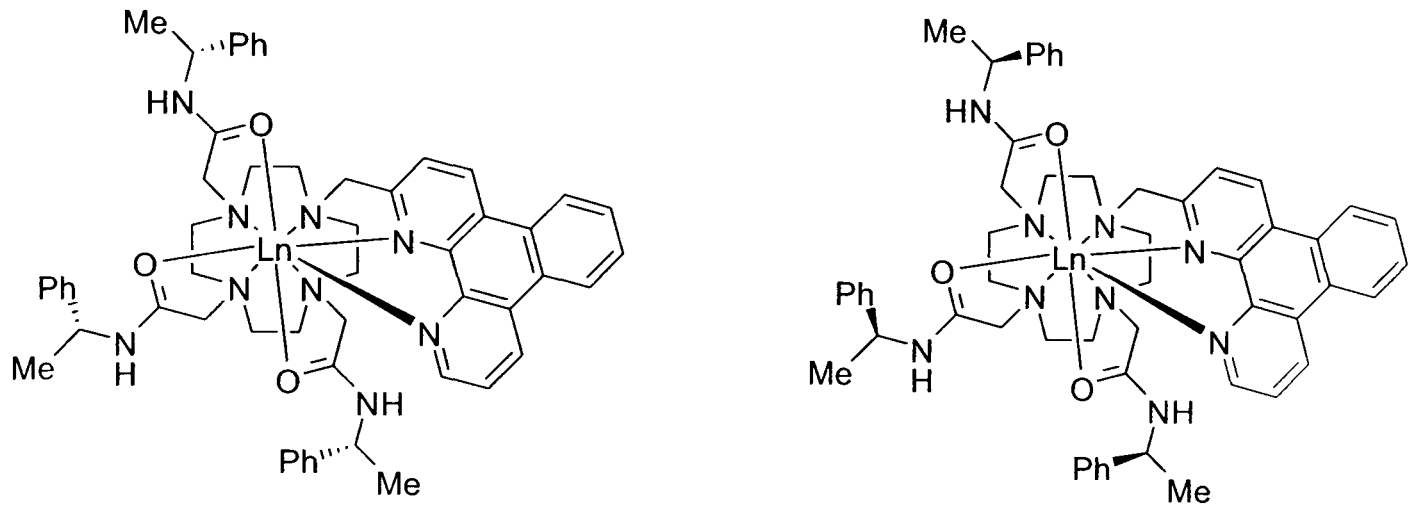

RRR-Λ-$LnPh_3dpq^{3+}$ SSS-Δ-$LnPh_3dpq^{3+}$

Figure 2. 6 – Structures of an enantiomeric pair of $LnPh3dpq^{3+}$ complexes

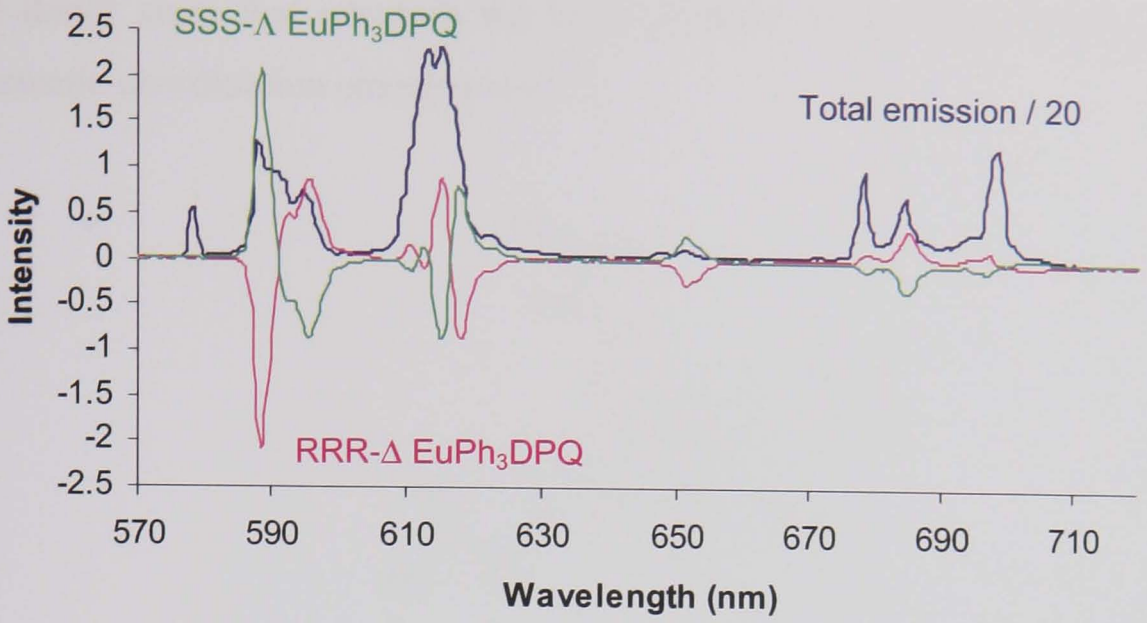

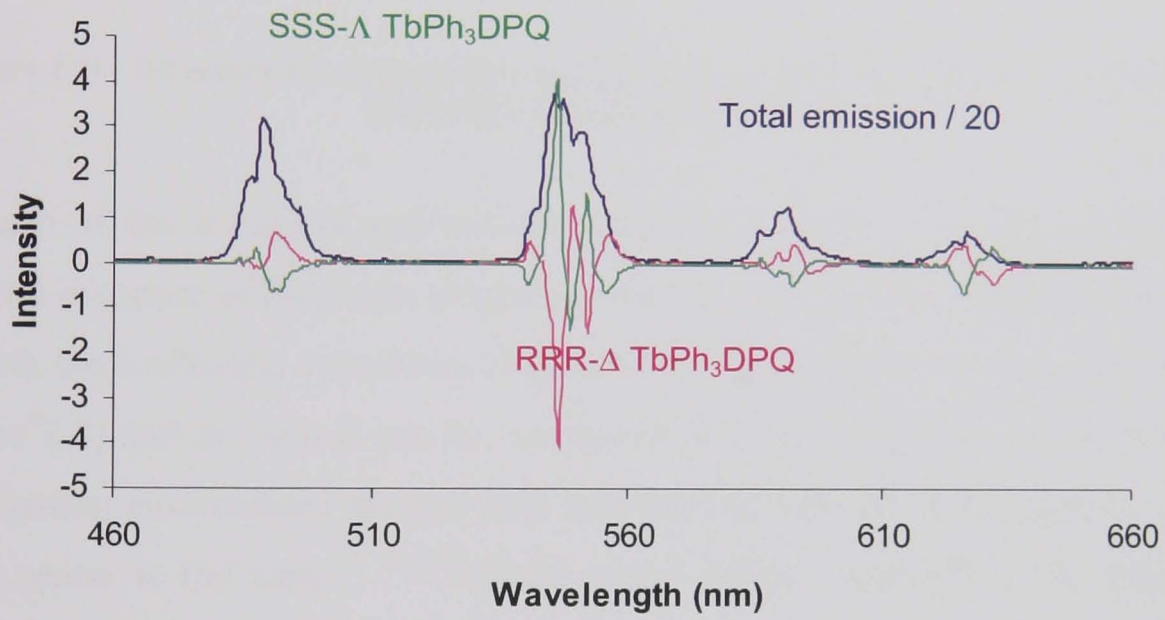

Figure 2. 7 Mirror image CPL spectra for (SSS)-Δ (green) and (RRR)-Λ (purple) europium and terbium complexes of the structure shown above. The blue trace represents the total emission spectrum (λ_{ex} = 340 nm, pH 7.4, 100mM HEPES, 10 mM NaCl)

Mirror image CPL spectra (Figure 2.7) have previously been reported for the enantiomeric lanthanide(III) complexes of the dpq ligand (Figure 2.6).[7] The sign and sequence of the transitions observed for these complexes is the same as for the parent C-4 symmetric tetra-amide Eu(III) and Tb(III) analogues (Figure 2.8), whose absolute configuration has been verified by X-ray crystallography.[19] Only one exception was noted for the europium complex, where a reversal in the sign of one transition in the $\Delta J = 2$ manifold was observed. This was attributed to the high sensitivity of this electric-dipole-allowed transition to the nature and polarisability of

the donor atom that occupies the axial position in the mono-capped square anti-prismatic coordination environment.[18]

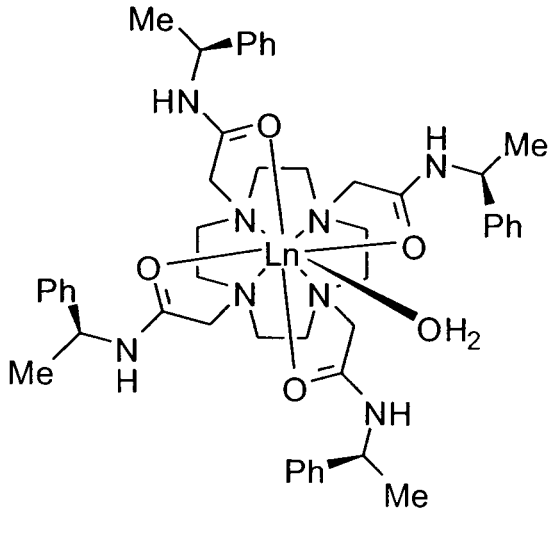

S-Δ

Figure 2. 8 – Structure of a tetraamide complex that is structurally similar to [Ln.1] and the LnPh3dpq complexes (Figure 2.4)

For each of the europium and terbium complexes $[Ln.\mathbf{1}]^{3+}$, [Ln.**2**] and [Ln.**4**], the sign and sequence of the peaks (Figures 2.9 and 2.10) was observed to be the same as for both the $LnPh_3dpq$ complexes (Figure 2.6) and the parent tetraamide complexes (Figure 2.8) and as such it can be concluded that the lanthanide ion is in the same coordination environment in each case and that the helicity of the ligand around the metal centre is the same.[7, 18, 19] Each of the (SSS)– complexes can therefore be assigned a Δ helicity.

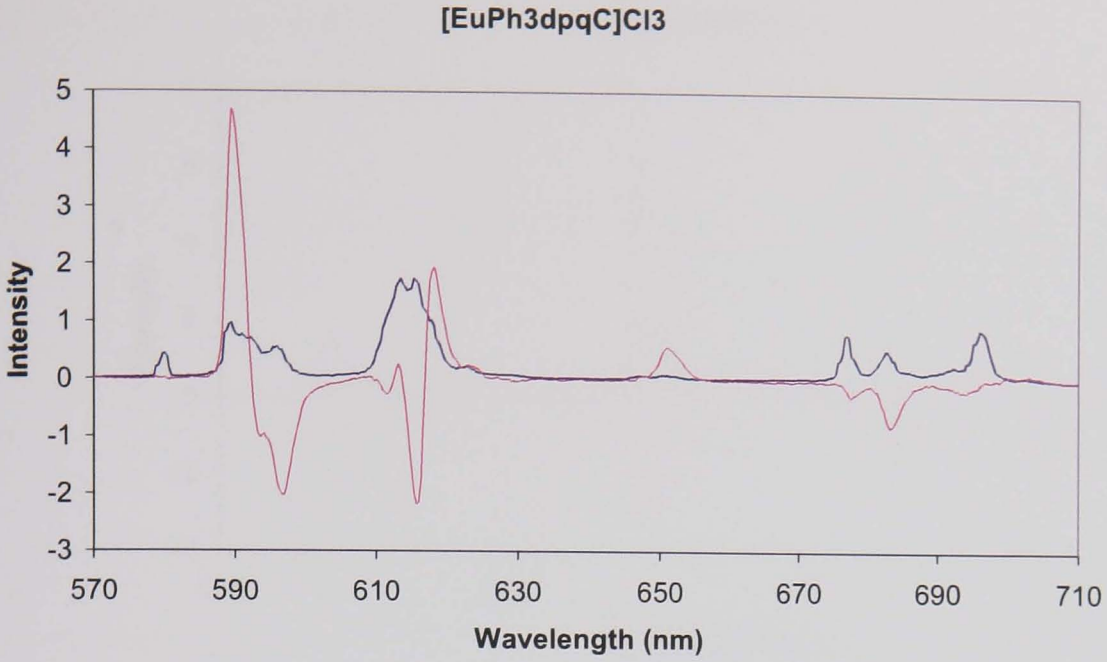

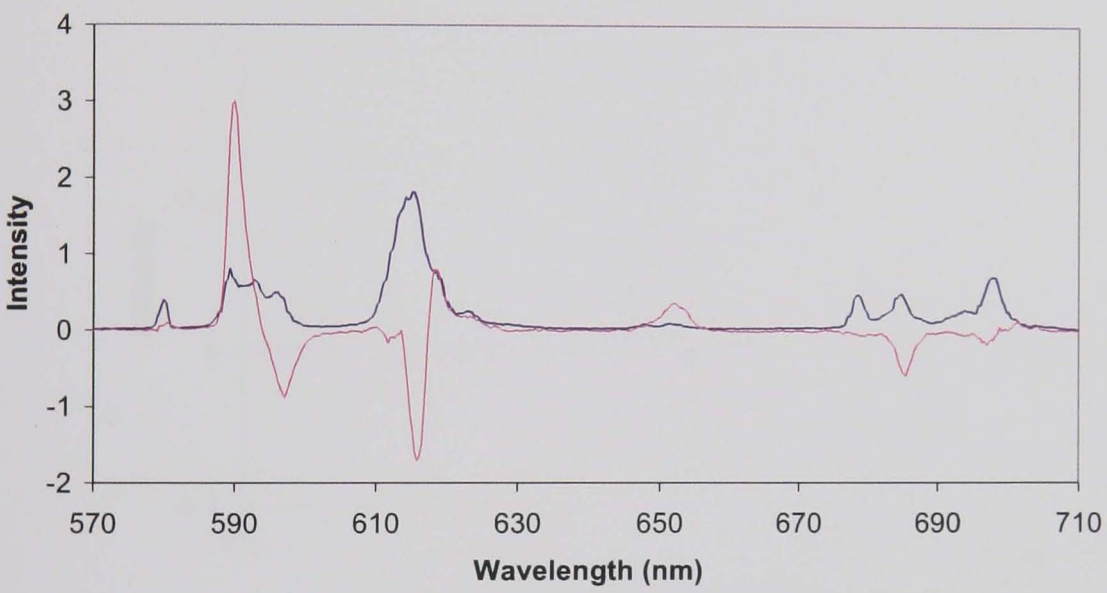

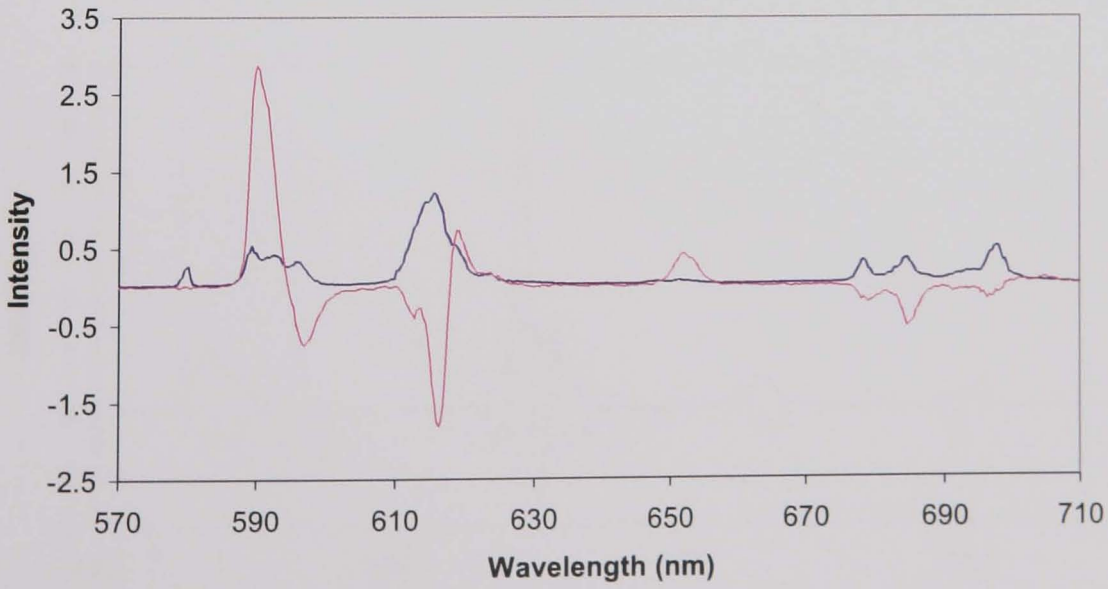

Figure 2. 9 – CPL spectra of [EuPh3dpqC]Cl3, [Eu.1] (top); EuAla3dpqC, [Eu.2] and EuGlu3dpqC, [Eu.4] (bottom). Recorded in H_2O at 298 K, λ_{ex} = 348 nm.

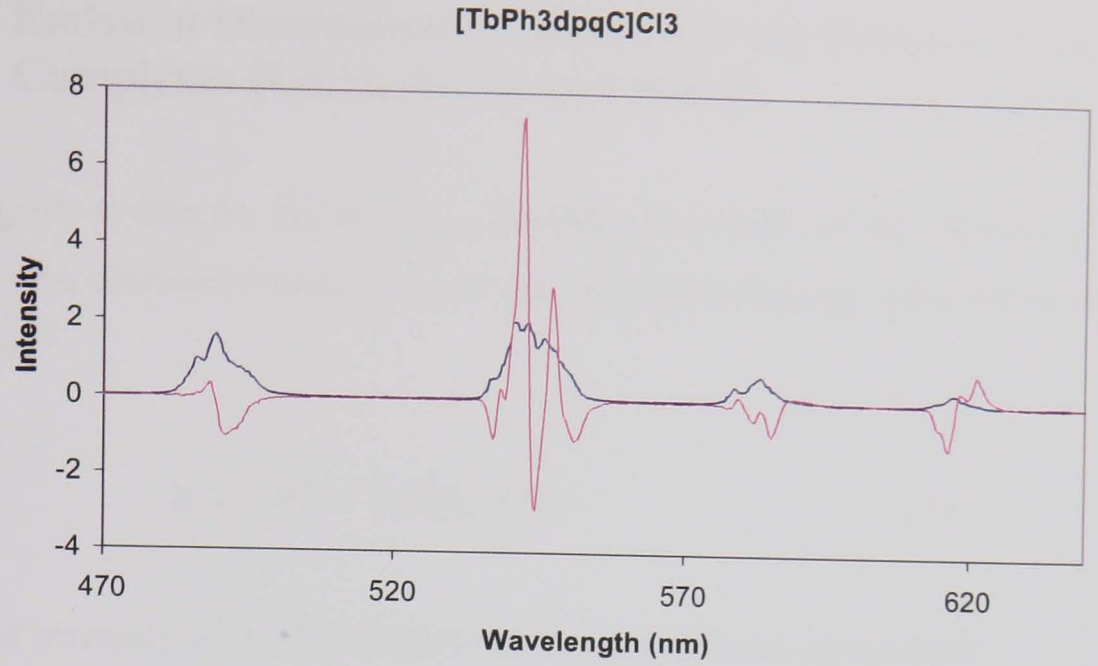

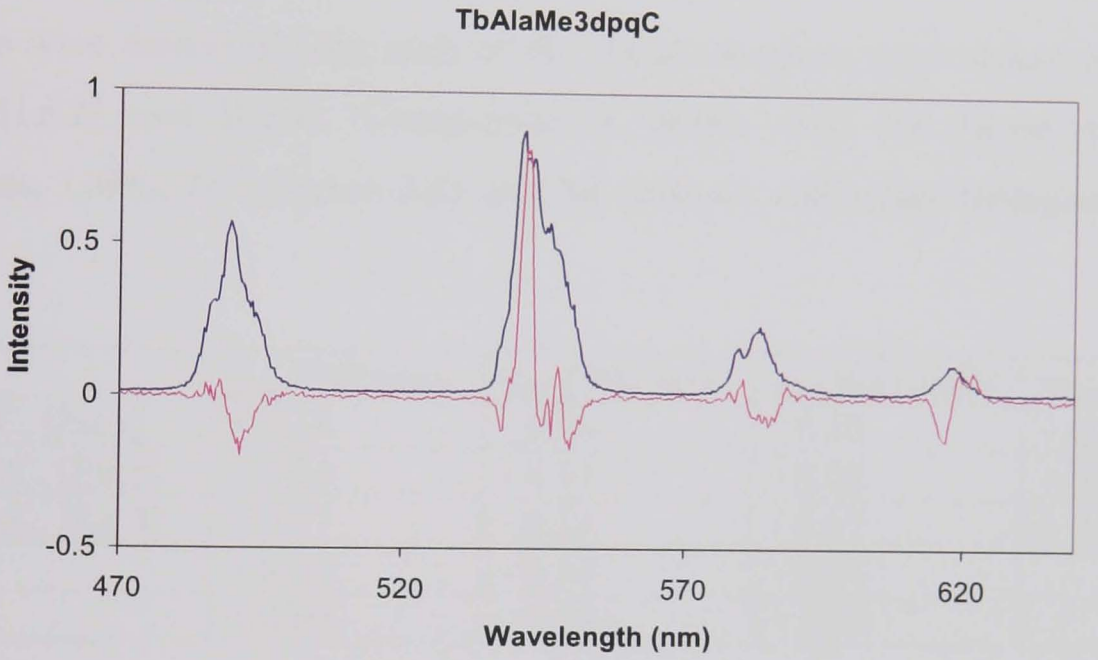

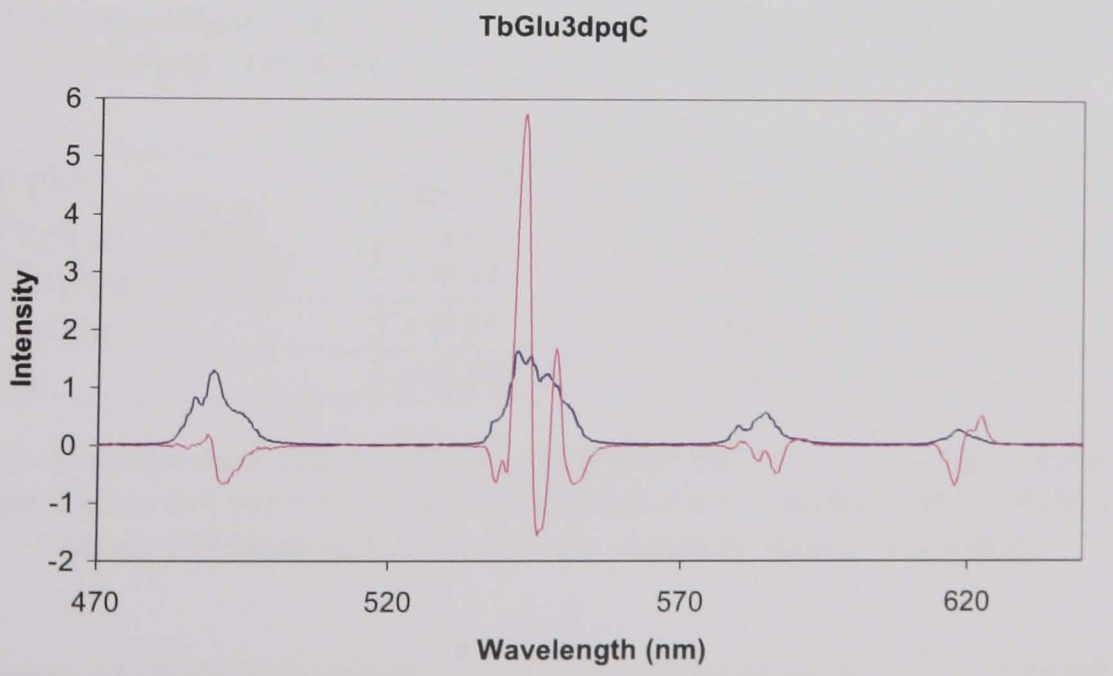

Figure 2. 10 - CPL spectra of [TbPh3dpqC]Cl3, [Tb.1] (top); TbAla3dpqC, [Tb.2] and EuGlu3dpqC, [Tb.4] (bottom). Recorded in H_2O at 298 K, λ_{ex} = 348 nm.

2.1.4.4 Emission Dissymmetry Factors For the Series of Lanthanide Complexes [Ln.1], [Ln.2] and [Ln.4]

Emission dis-symmetry factors, g_{em}, provide a measure of the 'degree of chirality' sensed by an electronic transition and are calculated through application of Equation (1) below.[18]

$$g_{em} = 2(I_L - I_R)/(I_L + I_R) \qquad (1)$$

$I_{L(R)}$ is the intensity of the left (right) circularly polarised component.

g-Factors were determined for each of the chiral europium and terbium complexes [Ln.**1**], [Ln.**2**] and [Ln.**4**]. Comparison is drawn with the parent tetraamide complexes, $LnPh_4$, (see Figure 2.8) and the triamide $LnPh_3dpq$ analogues (Figure 2.6).[7, 19]

Complex	g_{em} (589 nm)	g_{em} (595 nm)	g_{em} (615 nm)	g_{em} (617 nm)
$EuPh_3dpqC$, [Eu.**1**]	+ 0.18	- 0.16	- 0.10	+ 0.08
$EuAla_3dpqC$, [Eu.**2**]	+ 0.25	- 0.13	- 0.08	+ 0.06
$EuGlu_3dpqC$, [Eu.**4**]	+ 0.17	- 0.13	- 0.07	+ 0.04
$EuPh_3dpq$	+ 0.18	- 0.16	- 0.04	
$EuPh_4$	+ 0.09	- 0.09	+ 0.08	

Table 2. 1 – Emission dissymmetry factors (± 10 %) for [Eu.1], [Eu.2], [Eu.4] and the related triamide $EuPh_3dpq$ (Figure 2.6) and tetra-amide $EuPh_4$ (Figure 2.8) complexes (H_2O, 295 K, λ_{ex} = 340 (dpq) / 348 (dpqC)). In each case, the complexes have S-Δ helicity.

Complex	g_{em} (541 nm)	g_{em} (544 nm)	g_{em} (547 nm)
$TbPh_3dpqC$, [Tb.**1**]	+ 0.15	- 0.08	+ 0.08
$TbGlu_3dpqC$, [Tb.**4**]	+ 0.15	- 0.06	+ 0.07
$TbPh_3dpq$	+ 0.15	- 0.09	+ 0.12
$TbPh_4$	+ 0.14	- 0.10	+ 0.17

Table 2. 2 – Emission dissymmetry factors (± 10 %) for [Tb.1], [Tb.4] and the related triamide $TbPh_3dpq$ (Figure 2.6) and tetra-amide $TbPh_4$ (Figure 2.8) complexes (H_2O, 295 K, λ_{ex} = 340 (dpq) / 348 (dpqC)). In each case, the complexes possess S-Δ helicity.

For the series of europium complexes, g factors found for the $\Delta J = 1$ band have the same sign in each case, although the magnitude of the values for the triamide dpq

and dpqC complexes are up to twice those for the tetraamide parent. This may reflect the more sterically constrained coordination environment and correspondingly reduced motional freedom. A change in sign is observed at 615 nm compared to the C_4 symmetric tetraamide complex; this has previously been related to its high sensitivity to the polarisability of the axial donor.[7]

Transitions for the terbium complexes again have the same sign in each case and the magnitudes are similar for both [Ln.**1**] and [Ln.**4**]. At 547 nm, the g factors are > 30 % lower than for $TbPh_4$, perhaps again reflecting the sensitivity of the transition to the nature, of the axial donor atom.

2.1.4.5 Determination of Luminescent Quantum Yield and Lifetime of Emission

Luminescent lifetimes and absolute quantum yields were recorded in H_2O at ambient temperature.

Complex	Lifetime (ms)	Luminescent Quantum Yield
$[Eu.\mathbf{1}]^{3+}$	1.04 (1.59 in D_2O)	16 % (20 % in D_2O)
[Eu.**2**]	0.96	18 %
[Eu.**3**]	1.08	18 %
$[Eu.\mathbf{4}]^{3-}$	1.00	15 %
$[Tb.\mathbf{1}]^{3+}$	1.56 (1.72 in D_2O)	40 % (48 % in D_2O)
[Tb.**2**]	1.49	36 %
[Tb.**3**]	1.46	33 %
$[Tb.\mathbf{4}]^{3-}$	1.59	34 %

Table 2. 3 – Emissive lifetimes and luminescent quantum yields for the series of comples [Ln.1-4] (Ln = Eu, Tb)

These values are some of the highest recorded in aqueous media (Table 2.3). The high values may be ascribed to: the high quantum yield of triplet formation of the tetraazatriphenylene chromophore; the absence of directly coordinated water

molecules; the efficiency of energy transfer from the sensitizer to the lanthanide, in part accounted for by the bidentate nature of the chromophore and the correspondingly short donor acceptor distance; a suitably large energy gap between the lowest lying excited state of the lanthanide and the triplet level of the chromophore such that thermally activate back energy transfer is not feasible. Additionally, the luminescent properties of this series of complexes remain virtually unchanged following deoxygenation of the sample.

2.1.4.6 Analysis of Complex Hydration State

The excited states of europium and terbium are particularly sensitive to quenching by OH and NH vibrational oscillators. The extent to which they are quenched is different in H_2O and D_2O, as has been previously explained (1.2.1.1). This difference has been used to derive expressions that allow determination of the number of water molecules that are directly coordinated to the lanthanide centre. Practically, this is achieved through a comparison of the rates of depopulation of the lanthanide excited state in both H_2O and D_2O. Care must be taken to ensure that H/D exchange is complete through repeated exchange cycles in D_2O. The appropriate expressions for europium and terbium are respectively:[20]

$$q_{Eu} = 1.2(k_{H2O} - k_{D2O} - 0.25 - 3(0.075)) \quad (2)$$

$$q_{Tb} = 5(k_{H2O} - k_{D2O} - 0.06) \quad (3)$$

where the 0.25 term (0.06 for Tb) refers to quenching by second sphere water molecules, and the 0.075 factor is ascribed to quenching by each NH amide oscillator.

Example: Determination of the number of water molecules coordinated to the europium and terbium complexes [Ln.**1**].

Complex	τ_{H2O}	k_{H2O} (= $1/\tau_{H2O}$)	τ_{D2O}	k_{D2O} (= $1/\tau_{D2O}$)
$EuPh_3dpqC$, [Eu.**1**]	1.04	0.96	1.59	0.63
$TbPh_3dpqC$, [Tb.**1**]	1.56	0.64	1.72	0.58

Table 2. 4 – Emission lifetimes and rate constants for depopulation of the lanthanide emissive states of europium and terbium complexes [Ln.1] in H_2O and D_2O

Therefore:

$$q_{Eu} = 1.2(k_{H2O} - k_{D2O} - 0.25 - 3(0.075))$$
$$= 1.2(0.96 - 0.93 - 0.25 - 3(0.075))$$
$$= 0$$

$$q_{Tb} = 5(k_{H2O} - k_{D2O} - 0.06)$$
$$= 5(0.64 - 0.58 - 0.06)$$
$$= 0$$

In every other case, the lanthanide was shown to possess no directly bound water molecules.

2.2 Development of a Complex Suitable for Protein Conjugation

The excellent photophysical properties of the series of complexes [Ln.**1-4**], in particular in terms of their high luminescent quantum yields, long emissive lifetimes and well defined coordination environment make them of potential interest for use in FRET based biological assays. The complex $[Ln.\mathbf{1}]^{3+}$ was thought to be the most appropriate candidate to assess as it shows a relatively low susceptibility to quenching, in particular by uric acid (which quenches the neutral and anionic complexes much more strongly – Chapter 3) and has been shown to be readily taken up by cells, opening up the possibility of developing '*in cellulo*' FRET studies.

In order for the complex to be of use, it is necessary to have some point of attachment through which the complex can be linked, for example, to an antibody or enzyme, or other component, depending on the system under study. For this series of complexes there are two ways in which this can be readily achieved: firstly through

functionalisation of the chromophore; or secondly by modifying one (or more) of the cyclen pendent arms to incorporate an additional functionality. Within the Parker group both approaches have been adopted (unpublished work 2005/6), although linking *via* the pendant arm(s) is perhaps synthetically less challenging and offers more scope for incorporating a range of linkers, without adversely affecting the photophysical properties of the complex. The method that was adopted was to exchange the amide arm *trans* to the chromophore (synthetically simpler than *cis* modification) to incorporate a hydrocarbon spacer and a free amine, whilst maintaining the same coordination environment for the metal, *i.e.* 3 amide C=O donors. The structure of the target complex is shown below.

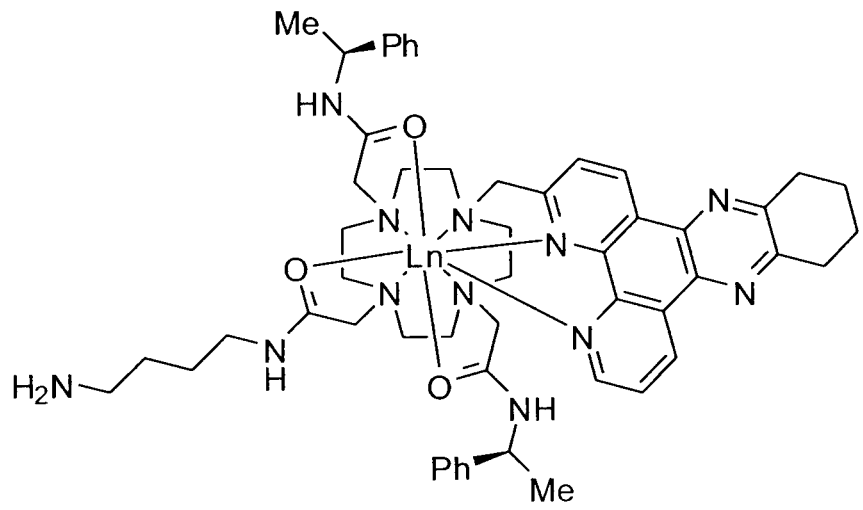

$[Ln.5]^{3+}$

Figure 2. 11 – Structure of $LnPh_2dpqC\_NH2$, [Ln.5]

2.2.1 Synthetic Route to [Ln.5]

The major advantage to the use of cyclen as a core, around which macrocyclic ligands can be built-up, is the ease with which up to four different pendent arms can be attached. This allows simple modification of a parent complex, whose properties are well understood, in order to meet the needs of a specific application. The synthetic procedure that was adopted for the synthesis of [Ln.**5**] could be adapted to allow a range of different linking groups and functionalities to be used.

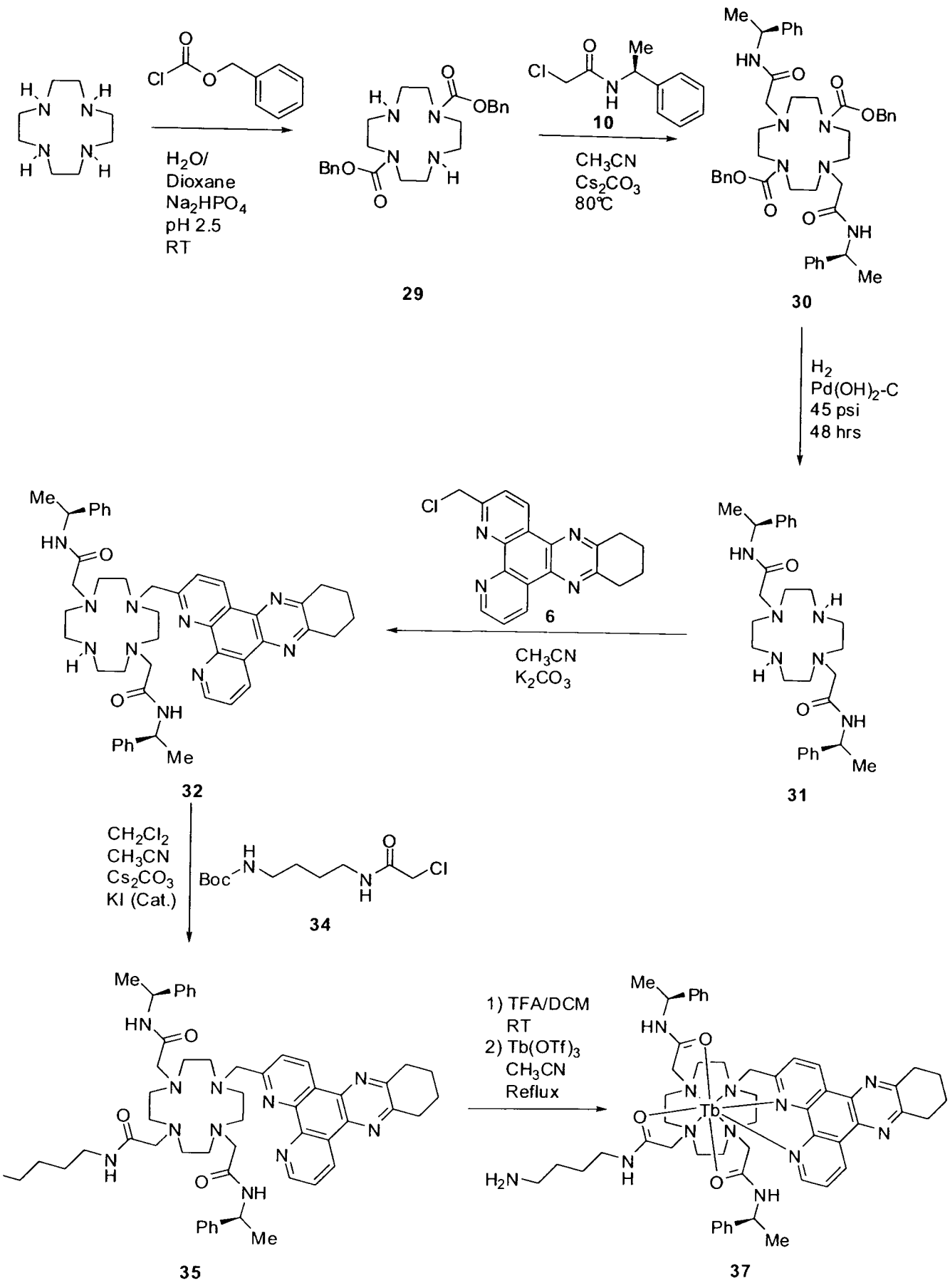

Scheme 2. 4 – Synthetic scheme leading to the synthesis of an amide-based lanthanide chelate for protein conjugation.

In order to synthesise the di-functionalised cyclen species, **31**, it is possible to carry out a direct alkylation reaction with two equivalents of 2-chloro-N-[(S)-1-phenylethyl]ethanamide. However, this usually leads to a mixture of mono, tri and tetra alkylated products, in addition to the required di-substituted compound. Column

chromatography of mixtures of cyclen complexes, in particular where the desired product has free amine NH groups, is commonly difficult and low yielding. An alternative approach, and the one that was adopted for this synthesis, was to use a protecting group strategy whereby cyclen is first di-protected as a trans-bis(benzyl carbamate). The reaction is carried out in phosphate buffer, with the pH adjusted to 2.5. Under these conditions, in the presence of excess benzyl chloroformate, the major product of the reaction is the di-protected cyclen. Purification takes advantages of the differing solubilities of the 'over' and 'under-alkylated' compounds at high and low pH, allowing the desired product to be obtained in high yield by extraction into diethyl ether, without the need for column chromatography. The reaction can be carried out on a multigram scale. Previous approaches involved the careful maintenance of pH during addition of benzyl chloroformate; the use of a buffer obviates the need to do this.

Alkylation of 1,7-bis(benzyloxycarbonyl)-1,4,7,10-tetraazacyclododecane, **29**, using a small excess of 2-chloro-N-[(S)-1-phenylethyl]ethanamide proceeded to give mostly the desired product, **30**, which was readily purified by column chromatography on silica in reasonable yield. The protecting groups were removed by hydrogenation over a palladium hydroxide on carbon catalyst (Pearlman's catalyst) in ethanol.

The two N-4 and N-10 substituted arms, i.e. the chloromethyl derivative of the chromophore and the linking group, could be added in different sequence. The difficulty associated with this first step is that monofuctionalisation is required. It was decided to functionalise firstly with the tetraazatriphenylene derivative, since it was thought in the case of over-alkylation, that there was likely to be a larger R_f difference between the two products, facilitating separation by column chromatography.

Alkylation with the chloromethyl derivative of the tetraazatriphenylene chromophore, **6**, was undertaken in acetonitrile, with one equivalent of base. The product **32** was obtained, with no sign of over-alkylation, perhaps due to its steric

bulk making the cyclen ring too crowded for a second functionalisation to occur rapidly under the reaction conditions. The final alkylation step required the use of Cs_2CO_3 as a base and a catalytic amount of KI before any reaction was observed, in-line with the observation of low reactivity in the previous step. It should be noted that purification of both **32** and **35** required column chromatography on alumina as a result of the basic nature of the ligand; unfortunately this results in a 50 % loss of product per purification. By NMR analysis, the crude product was > 90 % pure; if the synthesis were to be scaled up it would be desirable to improve the purification procedures for these final two products.

2.2.2 Characterisation

2.2.2.1 HPLC Analysis

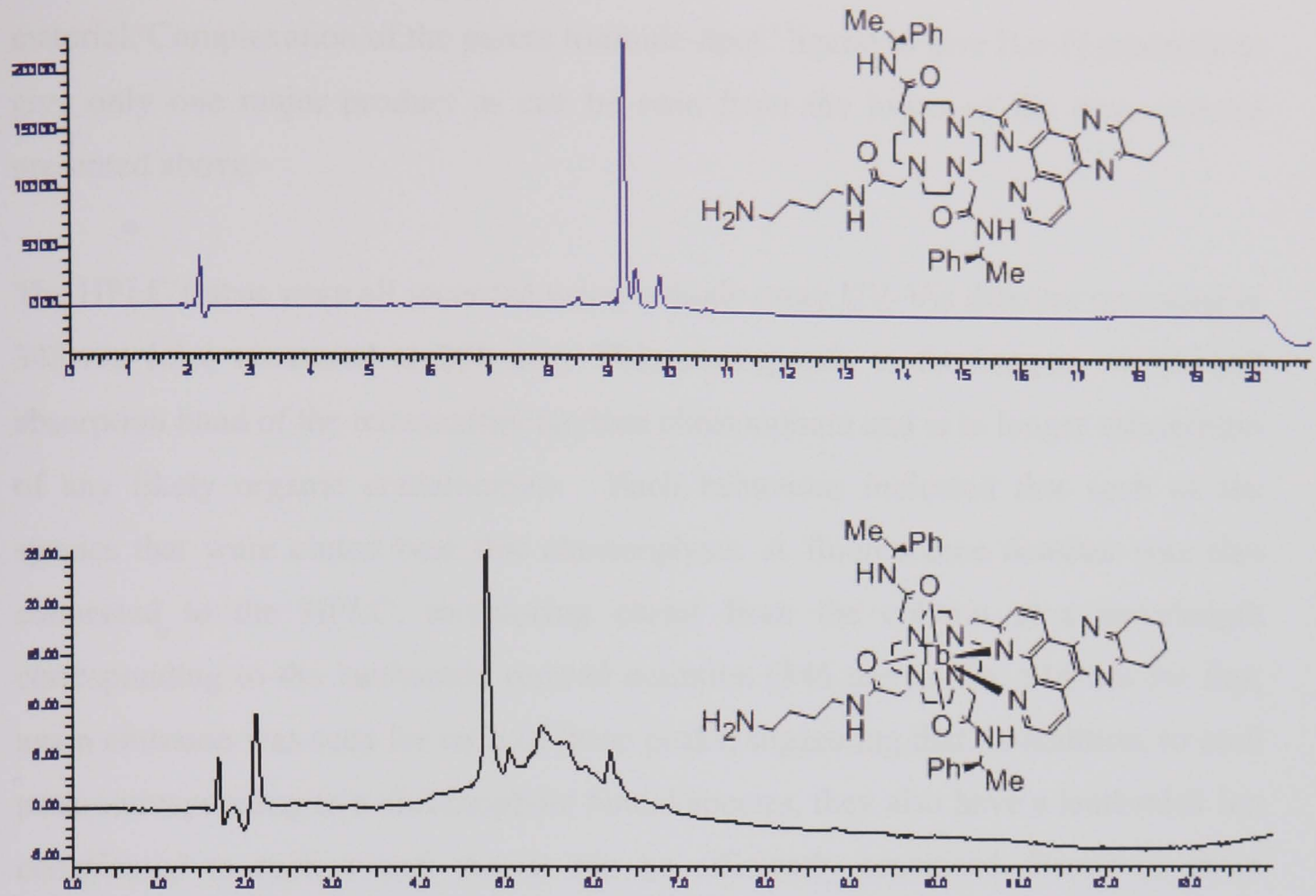

Figure 2. 12 – Comparative HPLC traces of LnPh2dpqC ligand (top), [Tb.5] and [Tb.1] (bottom) (λ_{abs} = 348 nm), For gradient see general experimental Chapter 5.

The above HPLC traces (Figure 2.12) were recorded for the Ph2dpqC_NH2 ligand, its complex [Ln.**5**] and for comparison, the parent complex [Ln.**1**]. The free ligand was shown to be one major species in solution; NMR and ESMS characterisation confirmed its assignment and purity. Upon complexation to give [Ln.**5**], a major species was observed, but also a number of new peaks that eluted over several minutes following the major peak and constitute a significant percentage of the total

material. Complexation of the parent triamide-dpqC ligand to give [Ln.**1**] proceeds to give only one major product as can be seen from the lower of the three spectra presented above.

The HPLC traces were all recorded using a diode array UV-Vis detector operating at 348 nm (also measured at 280 nm). This corresponds to the longest wavelength absorption band of the tetraazatriphenylene chromophore and is to longer wavelength of any likely organic contaminants. Such behaviour indicated that each of the species that were eluted bear this chromophore. A fluorescence detector was also connected to the HPLC, monitoring eluent from the column at a wavelength corresponding to the lanthanide centred emission (546 nm for Tb, 616 nm for Eu); again emission was seen for each of these peaks, suggesting that, in addition, to each peak corresponding to a chromophore bound species, they also have a lanthanide ion coordinated in such a way that it can be efficiently sensitised. Based on these observations, it was tentatively suggested that they may be a result of different stereoisomers that are retained to different extents by the C18 column. Separation of the major peak was possible by preparative HPLC, and the ESMS spectrum and luminescence spectral data (excitation/emission profiles) were in agreement with the proposed structure.

The most notable difference between the complexes [Ln.**5**] and [Ln.**1**] is the number of chiral centres δ to the cyclen ring nitrogen atoms. It is known that these impart rigidity on the complex and as a result restrict the number of isomers that the complex may adopt.[18] This effect decreases as the number of stereocentres is reduced and may, in part, account for the number of species observed by HPLC.

2.2.2.2 Variable Temperature Solution ^{1}H NMR Analyses

In D_2O, the room temperature ^{1}H NMR spectrum of $[Ln.\mathbf{5}]^{3+}$ is exchange broadened (200 – 500 MHz) and does not provide any definitive structural information about the complex. To overcome this problem, low temperature spectra were recorded in CD_3OD. Below 0 °C the same features can be discerned as for the parent complex

[Ln.**1**] i.e. the observation of resonance ascribed to 'pseudo-axial' ring protons in the range 20-32 ppm in addition to a fifth peak corresponding to the chromophore proton taking up a position close to the principal axis of the complex. The peaks become increasingly sharp as the temperature decreases (reaching a limit as the viscosity of the solvent increases) and one major species was discernible.

2.2.2.3 Absorption and Emission Spectral Properties of [Ln.5] (Ln = Tb, Eu)

The absorption and emission spectra had the same form as for the parent amide complexes, consistent with their well defined coordination environments. The emission lifetimes for the europium(III) and terbium(III) complexes were measured to be 1.0 ms and 1.5 ms respectively.

2.2.2.4 CPL Analysis

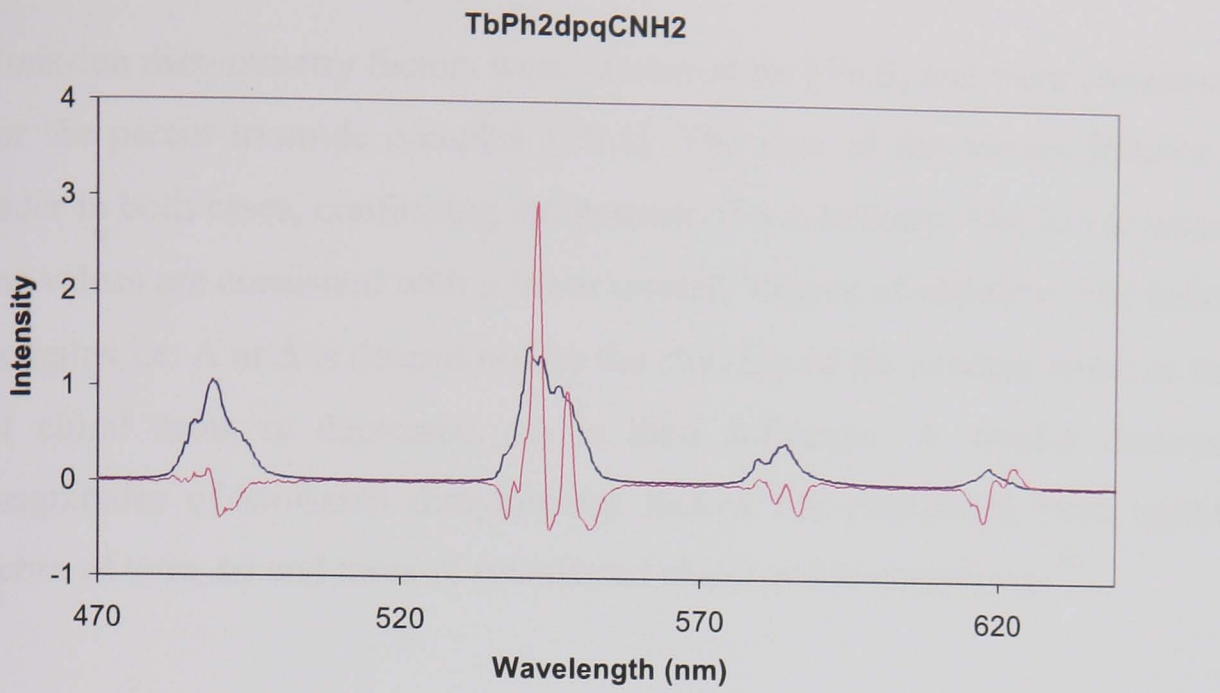

Figure 2. 13 – CPL spectra for SS-Δ [Ln.5] (top) and for comparison the parent triamide species SSS-Δ [Ln.1] (bottom). The blue trace represents the total emission spectrum/50 (H_2O, 298 K, λ_{ex} = 348) nm,

The CPL spectrum of [Tb.**5**] was recorded in H_2O at ambient temperature, comparison is drawn with [Tb.**1**]. The form and sign of the spectra are similar in each case. The overall chirality of the complex can again be assigned as Δ-SS.

Complex	g_{em} (541 nm)	g_{em} (544 nm)	g_{em} (547 nm)
$TbPh_3$dpqC, [Tb.**1**]	+ 0.15	- 0.06	+ 0.07
TbPh2dpqC_NH2, [Tb.**5**]	+ 0.09	- 0.02	+ 0.02

Table 2. 5 – Emission dissymmetry factors (± 10 %) for [Tb.1] and [Tb.5] (H_2O, 295 K, λ_{ex} = 348 (dpqC)). In each case the complexes have all-S-Δ helicity.

Emission dissymmetry factors were measured for [Tb.**5**] and were compared to those for the parent triamide complex [Tb.**1**]. The sign of the factors follows the same order in both cases, confirming assignment of a Δ-helicity. The lower magnitudes of the values are consistent with a lower overall 'degree of chirality': the helicity of the complex i.e. Λ or Δ is determined by the chirality of the pendent arms; as the number of chiral arms is decreased, so is their influence. A similar decrease in the magnitudes of emission dissymmetry factors has previously been reported for a series of tetra, tri and trans-di substituted chiral amide complexes.[18]

2.2.2.5 Homogeneous Time Resolved Fluorescence Assay (HTRF)

A model HTRF assay was undertaken in order to assess the potential application of $[Tb.\mathbf{5}]^{3+}$ in a FRET experiment. The majority of commercially available HTRF assays use europium chelates[21] (although examples of terbium complexes are available from Wallac/Perkin Elmer; their application has been demonstrated using rhodamine as an acceptor by Hemmila *et al*)[22]. The ligands used typically incorporate chromophores with a triplet energy that is too low to excite terbium. The use of both terbium and europium complexes in combination would allow for the possibility of undertaking multicolour/multicomponent assays.

The assay was undertaken at Cisbio International in collaboration with Drs Hervé Bazin and Nathalie Gregor. Comparison was made to a europium tris-bipyridine cryptate labelled in the same way, as will be described below for $[Tb.\mathbf{5}]^{3+}$. It is important to note that the experimental setup was optimized for a europium complex using nitrogen laser excitation at 337 nm. Emission filter sets were considered to be appropriate for both complexes.

The assay involved monitoring the interaction between the antibody labeled chelate Anti-GST-$[Tb.\mathbf{5}]^{3+}$ (Tb-Ab) and a streptavidin-XL665 conjugate (SA-XL) as a function of added GST-biotin conjugate (GST-biot). (Figure 2.14)

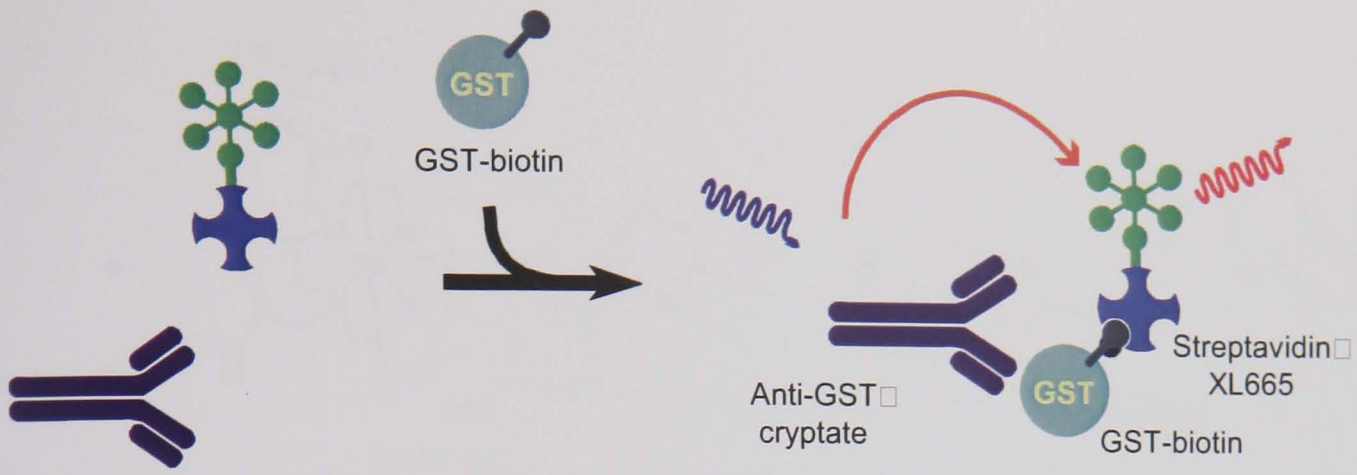

Figure 2. 14 – A diagram to illustrate the principle of the HTRF assay monitoring the interaction of Tb-Ab and SA-XL as a fuction of added SA-XL

In the absence of GST-biot, emission is seen only from the terbium chelate. The XL fluorescent protein is not excited by the 337 nm laser line used as an excitation source. Upon addition of GST-biot, it can interact with its antibody, and biotin with streptavidin; this brings the terbium chelate into the proximity of the XL665 fluorescent protein and energy transfer can then occur from the terbium donor to the XL665 acceptor; emission was observed at 665 nm, corresponding to the protein based emission.

2.2.2.5.1 Chelate Activation

It is necessary that the chelate should react cleanly and at temperatures of 37° C or lower with the free thiol groups on the antibody; in order to do this, it is activated as a maleimide.

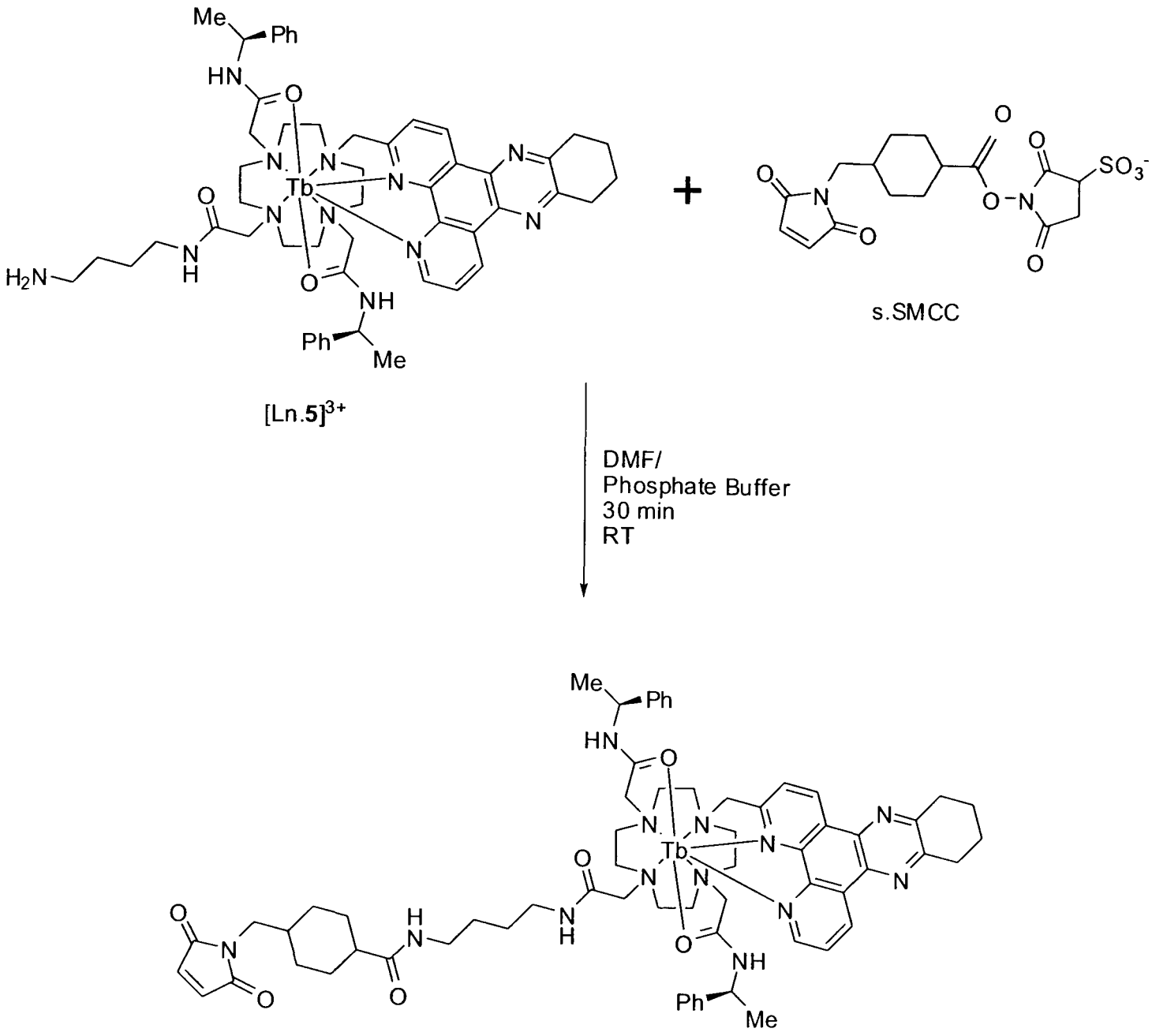

Scheme 2. 5 – Activation of the terbium chelate using a sulphonated maleimide bifunctional linker

$[Ln.\mathbf{5}]^{3+}$ was reacted with an excess of the sulphonated maleimide bifunctional linker s.SMCC for 30 mins at room temperature. The linker s.SMCC is poorly soluble in water and the reagents and product are sensitive to hydrolysis, therefore the reaction was carried out in a mixture of DMF and phosphate buffer, maintained at pH 6 – 7. After this period the reaction mixture was quenched with water and purified using size exclusion chromatography. Unfortunately unreacted chelate could not be recovered cleanly from the column, requiring elution with a high-salt buffer (1M NaCl, 10 % DMF, 10 mM Phosphate); under these conditions some coelution of 'free maleimide' with the sulfo-NHS species resulted.

'Activation' was carried out on both a purified fraction of the complex (corresponding to the major peak in its HPLC spectrum) and on the complex prior to preparative HPLC. HPLC was also used to confirm that the activation had been successful. It is interesting to note that it appeared that each of the peaks that was evident in the HPLC trace of the unpurified complex also appeared to shift by the same amount corresponding to activation of the complex. This perhaps indicates that each of the species also contain the linking functionality and support the propostion that the peaks can be explained as stereoisomers, with differing λ/δ configurations in the NCCN chelates.

2.2.2.5.2 Antibody Activation and Labelling

Anti-GST is activated by partial reduction of disulfide bridges using DTT (dithiothreitol – Cleland's reagent) the reaction proceeds in 10 minutes at 20°C and the product is again readily purified using size exclusion chromatography with phosphate buffer as the eluent.

The maleimide-activated chelate was added to the reduced Anti-GST in phosphate buffer (pH 7) to obtain an initial chelate to antibody ratio of 15:1. The reaction mixture was either kept at 37 °C for 2 hours (GSS11-chelate Tb (1)) or at 4 °C overnight (GSS11-chelate Tb (2)). It was found that, under both sets of conditions, conjugates were obtained that gave similar results in the FRET assay. The reaction mixture was purified using size exclusion chromatography.

2.2.2.5.3 Determination of the Average Label/Antibody Ratio

The number of exposed functions available for labelling on Anti-GST is not accurately known for a given experiment; also, the maleimide function on the activated complex is slowly hydrolysed in buffer pH 7 (more slowly at pH 6 or below). The true number of chelates per antibody is therefore lower than the initial ratio and must be determined experimentally in order to make a useful comparison between procedures and different complexes. Within a population of labelled

antibodies there is a distribution of complex/antibody ratios: it has been proposed that a Poisson distribution is approximated;[23] therefore, what is actually measured is the average number of complexes per antibody.

Since the extinction coefficients are known for both the antibody and the complex, the ratio can be determined by absorbance based techniques. As an example, consider labelling with the terbium complex $[Tb.\mathbf{5}]^{3+}$:

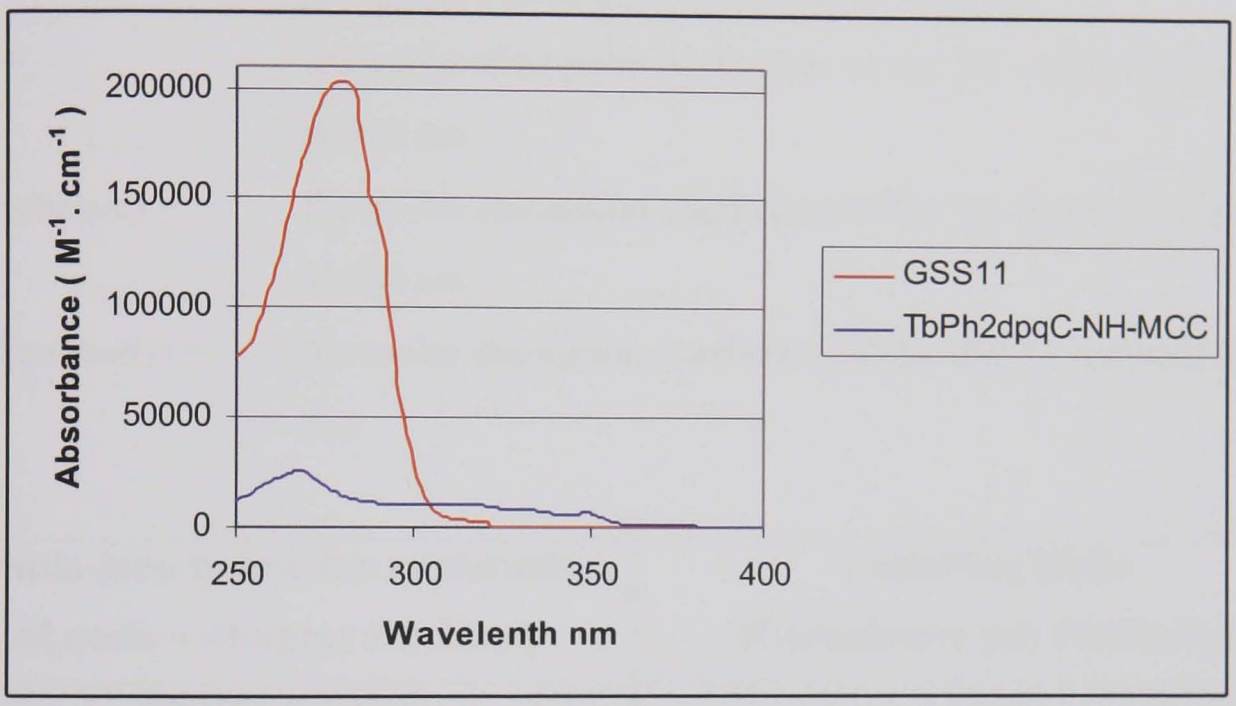

Figure 2. 15 – Absorbance spectra of the GSS11 antibody and the terbium chelate [Tb.6]

ε_{348} (complex) = 6440 M^{-1} cm^{-1}

ε_{280} (complex) = 14480 M^{-1} cm^{-1}

ε_{280} (Antibody) = 202500 M^{-1} cm^{-1}

If we assume that the spectrum of the conjugate is a combination of the antibody and the complex, the average number of complexes per antibody can be calculated by measuring the absorbances at 280 and 348 nm and substituting their values into equations (4) – (6). From the plot, it is clear that the contribution of the antibody in the estimation of the complex concentration (at 348 nm) is negligible, but the estimation of the antibody concentration must be corrected due to the substantial contribution of the complex absorption at 280 nm.

$$[\text{Complex}] = A_{348} / \varepsilon_{348} \quad (4)$$

$$[\text{Antibody}] = A_{280} - (\varepsilon_{280}(\text{chelate}) \times [\text{chelate}]) / \varepsilon_{280}(\text{antibody}) \quad (5)$$

$$\text{Therefore, labelling ratio} = [\text{chelate}] / [\text{antibody}] \quad (6)$$

$A_{280(348)}$ = the absorbance of a solution of the chelate labelled antibody in phosphate buffer (pH = 6.5) at 280 (348) nm

ε_{348} = the molar absorption coefficient of the Tb chelate (i.e. [Ln.**6**]) at 348 nm

ε_{280} (chelate) = the molar absorption coefficient of the Tb chelate (i.e. [Ln.**6**]) at 280 nm

ε_{280} (antibody) = the molar absorption coefficient of the GSS11 antibody at 280 nm

Sample (see below for explanation of code – chapter 2.2.2.5.4)	Labelling Ratio (Complexes per Antibody)
GSS11-K Prod	3.9
GSS11-K	7.0
GSS11-chelate Tb (1)	2.5
GSS11-chelate Tb (2)	3.2

Table 2. 6 – Labelling ratios for the GSS11 antibody. GSS11-K Prod = The commercial EuTBP-antibody labelled conjugate as supplied by Cisbio; GSS11-K = A EuTBP-antibody conjugate synthesised at the same time and using the same procedure as described for the terbium chelate $[Ln.5]^{3+}$; GSS11-chelate Tb (1) = The $[Tb.5]^{3+}$ Tb chelate labelled over 2h at 37°C with the antibody; GSS11-chelate Tb (2) = The $[Tb.5]^{3+}$ Tb chelate labelled overnight at 4°C with the antibody

2.2.2.5.4 HTRF Assay – The Experiment

EuTBP (europium tris-bipyridine cryptate) is a commercially available label used in HTRF assays (Cisbio) and was therefore used as a reference in order to make a comparative assessment of the potential of $[Tb.\mathbf{5}]^{3+}$ in similar applications.

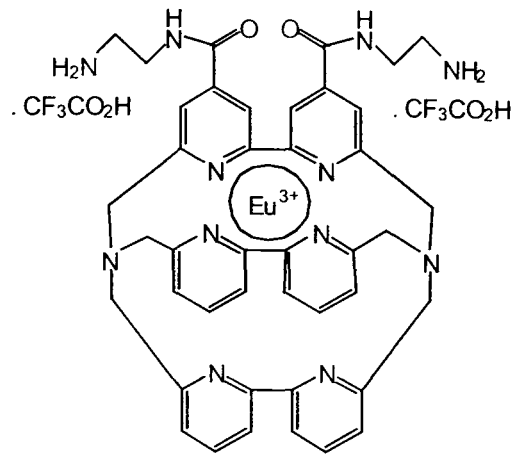

Figure 2. 16 – Tris-bipyridyl based europium cryptate (EuTBP) used as a reference compound

Six different labelled antibodies were prepared to allow a full comparison between the two different labelling methods and the effect of adding potassium fluoride to the assays. The emissive properties of the europium cryptate complex are sensitive its local environment in solution and the presence of a large excess of fluoride (a very hard ligand) is necessary to overcome this. The preparations were as follows:

1) The commercial EuTBP-antibody labelled conjugate as supplied by Cisbio with potassium fluoride (GSS11-K Prod + KF)

2) A EuTBP-antibody conjugate synthesised at the same time and using the same procedure as described for the terbium chelate $[Ln.\mathbf{5}]^{3+}$ with KF (GSS11-K + KF)

3) The $[Tb.\mathbf{5}]^{3+}$ Tb chelate labelled over 2 hours at 37°C with the antibody, without KF (GSS11-Tb (1) – KF)

4) The $[Tb.\mathbf{5}]^{3+}$ Tb chelate labelled over 2 hours at 37°C with the antibody, with KF (GSS11-Tb (1) + KF)

5) The $[Tb.\mathbf{5}]^{3+}$ Tb chelate labelled overnight at 4°C with the antibody, without KF (GSS11-Tb (2) – KF)

6) The $[Tb.\mathbf{5}]^{3+}$ Tb chelate labelled overnight at 4°C with the antibody, with KF (GSS11-Tb (2) + KF)

The assay was carried out as follows:

Where no potassium fluoride was used, the complex labelled antibodies prepared as above were diluted to 8 nM in phosphate buffer (0.1M phosphate pH 7 containing 0.1% BSA). Streptavidin-XL665 conjugate (SA-XL) was diluted to 20 nM in

phosphate buffer. GST-biotin conjugate (GST-biot) serial dilutions (5nM , 2.5 nM , 1.25 nM , 0.62 nM and 0.31 nM) were prepared in phosphate buffer.

To the wells of a black microtiter plate (Costar 96 wells) were added 50 µl each of the complex-antibody solution, GST-biotin dilution, SA-XL solution and 50 µl of phosphate buffer. Negative wells were prepared by replacing GST-biotin dilution by phosphate buffer.

Where potassium fluoride was used, the same protocol as described above was used (8 nM in phosphate buffer), but in this case 50 µl each of the EuTBP-Ab solution, GST-biotin dilution, SA-XL solution and 50 µl of 1.6 M potassium fluoride in phosphate buffer were added to the wells.

The fluorescence was measured after incubation (overnight 20°C) on a RubyStar two channel (665 nm and 620 nm filters) time-resolved fluorimeter (BMG Labtechnologies) and an Analyst spectrofluorometer (LJL BioSystems, 665 nm, 620 nm and 546 nm filters) set in time-resolved mode (t_d = 50 µs , t_g = 400 µs).

The concentration for labelled antibody refers to the antibody concentration and not to the label concentration since the number of label / antibody can change from one conjugate to another.

2.2.2.5.5 Results and Discussion of the Pilot HTRF Assay

A summary of the results is presented in Table 2.7 below. Both instruments were used in time-resolved mode; the intensities reported are the total intensity recorded during a gate time of 400 µs; a delay time of 50 µs was introduced in order that background fluorescent levels would have decayed to zero and scattered light would not reach the detector. Each measurement was made in duplicate and the intensities recorded in the Table as Ruby 620, Ana 620 and Ana 546 are an average of the two measurements. 'Ruby 620' refers to a measurement made on the 'Rubystar' using a 620 nm emission filter, 'Ana 620' and ' Ana 546' refer to measurements made on the

'Analyst' using 620 nm and 546 nm emission filters respectively. A comparison between the two machines is interesting since they use different excitation sources; the 'Rubystar' uses a nitrogen laser (337 nm) and the 'Analytic' a pulsed xenon lamp source. The 'Rubystar' has been developed by BMG Labtech in collaboration with Cisbio International for use specifically with their europium cryptate based HTRF technologies. The Analyst is comparable to the multiwell plate readers more commonly used in analytical laboratories and is more easily modified for applications using labels requiring different excitation wavelengths and emission filters. The 620 nm wavelength corresponds to the strongest Eu $\Delta J = 2$ emission band and also the Tb $\Delta J = 3$ band. The 546 nm band is the most intense terbium $\Delta J = 5$ emissive manifold. Emission from the XL665 fluorescent protein is monitored at 665 nm.

Fluorescent intensity measurements can be used to monitor directly the particular interaction under study, in this case by monitoring the decrease in intensity of the donor and/or the appearance of fluorescence from the acceptor. However, this method suffers from problems associated with the 'inner-filter' effect and the variability of the optical properties of the media. To overcome this, a ratiometric approach can be used. When the acceptor signal at 665 nm is taken as a ratio compared to the donor signal (chelate or cryptate), the data obtained is then independent of the optical characteristics of the media at the excitation wavelength i.e. the emissive intensities of both the donor and acceptor are proportional to the optical properties of the medium, such as its transmission.

Results are normally reported in terms of their $\Delta F\%$ values defined as:

$$\mathbf{\Delta F\% = ((Calibrator\ or\ Sample\ Ratio - Ratio_{neg}) / Ratio_{neg}) \times 100} \quad (7)$$

($Ratio_{neg}$ = negative control)

$$\mathbf{Ratio = (I_{665\ nm} / I_{620\ or\ 546\ nm}) \times 10^4} \quad (8)$$

Values of ΔF% for a series of complex labelled antibodies provide not only a comparison between FRET efficiencies, but also between the labelling and the immunoreactivity of the labelled antibody. For instance, for a given antibody, the ΔF% term increases with an increase in the number of complex/antibody, but may also decrease as a result of "over labelling" if the complex binds to functionality involved in the antibody-antigen recognition.

		Ruby 620 Average	I /chelate	Ana 620 Average	I/chelate	Ana 546 Average	I/chelate	Ruby 665/620 DF %	Ana 665/620 DF %	Ana 665/546 DF %
	Blank Buffer - KF	455		227		417				
	Blank Buffer + KF	301		196		394				
	Sa-XL 5 nM - KF	378		200		411				
	Sa-XL 5 nM + KF	300		175		363				
	GSS11-K prod 30 2 nM - KF	202181	51841	53123	13621	421	108			
	GSS11-K prod 30 2 nM + KF	42096	10794	18754	4809	393	101			
	GSS11-K TBP 23 05 2005 2 nM - KF	285773	41000	65843	9447	428	61			
	GSS11-K TBP 23 05 2005 2 nM + KF	76088	10916	31629	4538	386	55			
	GSS11-Chelate Tb (1) 23 05 2005 2 nM - KF	41873	16550	7574	2993	37871	14969			
	GSS11-Chelate Tb (1) 23 05 2005 2 nM + KF	33851	13380	6170	2439	37636	14876			
	GSS11-Chelate Tb (2) 23 05 2005 2nM - KF	40830	12563	7434	2287	38029	11701			
	GSS11-Chelate Tb (2) 23 05 2005 2nM + KF	31966	9836	6195	1906	37509	11541			
GSS11-K Prod + KF	std 0 = 0 nM GST-Biot	42921	11005	19109	4900	401	103			
	std 1 = 0.07 nM GST-Biot	43181	11072	18934	4855	393	101	97%	113%	116%
	std 2 = 0.15 nM GST-Biot	43185	11073	19225	4929	372	95	189%	225%	250%
	std 3 = 0.31 nM GST-Biot	42792	10972	18761	4811	350	90	360%	405%	466%
	std 4 = 0.61 nM GST-Biot	41585	10663	18282	4688	349	89	669%	734%	831%
	std 5 = 1.25 nM GST-Biot	40165	10299	17894	4588	361	92	1241%	1309%	1367%
GSS11-K 23 05 2005 + KF	std 0 = 0 nM GST-Biot	76368	10957	31554	4527	397	57			
	std 1 = 0.07 nM GST-Biot	76660	10998	30976	4444	379	54	74%	89%	100%
	std 2 = 0.15 nM GST-Biot	76641	10996	30837	4424	380	55	148%	170%	169%
	std 3 = 0.31 nM GST-Biot	75904	10890	30598	4390	345	49	307%	334%	384%
	std 4 = 0.61 nM GST-Biot	72913	10461	29782	4273	331	47	586%	604%	686%
	std 5 = 1.25 nM GST-Biot	70334	10091	29103	4175	375	54	1207%	1105%	1081%
GSS11-Chelate Tb (1) 23 05 2005 - KF	std 0 = 0 nM GST-Biot	41285	16318	7567	2991	37340	14759			
	std 1 = 0.07 nM GST-Biot	41718	16489	7562	2989	37642	14878	27%	27%	30%
	std 2 = 0.15 nM GST-Biot	40485	16002	7383	2918	38167	15086	52%	53%	54%
	std 3 = 0.31 nM GST-Biot	39275	15524	7276	2876	37854	14962	108%	107%	107%
	std 4 = 0.61 nM GST-Biot	38199	15098	7035	2780	37326	14753	209%	222%	199%
	std 5 = 1.25 nM GST-Biot	35240	13929	6516	2575	35454	14013	432%	402%	398%
GSS11-Chelate Tb (1) 23 05 2005 + KF	std 0 = 0 nM GST-Biot	32950	13024	6093	2408	36143	14286			
	std 1 = 0.07 nM GST-Biot	34369	13585	6141	2427	36935	14559	27%	33%	22%
	std 2 = 0.15 nM GST-Biot	34258	13541	6199	2450	37428	14794	54%	55%	53%
	std 3 = 0.31 nM GST-Biot	34160	13502	6218	2458	37153	14685	104%	116%	99%
	std 4 = 0.61 nM GST-Biot	34338	13572	6224	2460	36879	14577	197%	203%	189%
	std 5 = 1.25 nM GST-Biot	32049	12667	5918	2339	35035	13848	395%	411%	365%
GSS11-Chelate Tb (2) 23 05 2005 - KF	std 0 = 0 nM GST-Biot	40517	12467	7503	2308	37429	11517			
	std 1 = 0.07 nM GST-Biot	40999	12615	7231	2225	38449	11830	27%	42%	14%
	std 2 = 0.15 nM GST-Biot	40772	12545	7345	2260	38478	11839	50%	73%	45%
	std 3 = 0.31 nM GST-Biot	40300	12400	7206	2217	38417	11821	106%	136%	95%
	std 4 = 0.61 nM GST-Biot	37927	11670	6812	2096	37775	11623	210%	256%	179%
	std 5 = 1.25 nM GST-Biot	36572	11253	6700	2062	37373	11499	423%	483%	349%
GSS11-Chelate Tb (2) 23 05 2005 + KF	std 0 = 0 nM GST-Biot	34571	10637	6311	1942	37697	11599			
	std 1 = 0.07 nM GST-Biot	32851	10108	6143	1890	36656	11279	28%	27%	27%
	std 2 = 0.15 nM GST-Biot	34591	10643	6239	1920	37937	11673	50%	53%	61%
	std 3 = 0.31 nM GST-Biot	34737	10688	6216	1912	37797	11630	100%	98%	105%
	std 4 = 0.61 nM GST-Biot	33473	10299	6068	1867	36685	11288	193%	198%	212%
	std 5 = 1.25 nM GST-Biot	32677	10054	5985	1841	35786	11011	396%	377%	414%

Table 2. 7 – Summary of the results obtained from the pilot HTRF assay

A number of conclusions can be drawn from a comparison of the ΔF% values reported in Table 2.7.

1) For each of the experimental setups (i.e. the instrument used, the excitation source and the use of different emission filters) a similar set of results was obtained; this confirms the validity of the method. The ratiometric nature of the analysis eliminates many of the 'sample to sample' and 'instrument to instrument' effects that otherwise make comparisons difficult. The advantage of the use of a 546 nm instead of a 620 nm emission filter for terbium complexes is that it provides a larger signal to noise ratio. This permits the use of a lower concentration of label.

2) Each of the complexes participates in FRET. The terbium complexes each give a similar series of ΔF% values regardless of whether the antibodies were labelled overnight at 4 degrees or in 2 hours at 37 degrees, despite having different numbers of antibodies per chelate (3.2 versus 2.5).

3) The presence or absence of fluoride ions has no effect on the ΔF% values observed for the terbium complexes. In contrast the reference chelate has a very strong dependence on added fluoride *NB*. The emissive lifetimes of the terbium chelate in the presence of fluoride increased somewhat although the observed decay profile was biexponential and exact values were not estimated.

4) The terbium labelled chelates have ΔF% values that are approximately 25 % of those of the europium cryptate reference. Whilst, to a small extent this may be due to differences in the number of labels per antibody, it is most probably accounted for by a less favourable energy match between the donor and acceptor used in this 'proof of principle study'.

2.2.2.5.6 Summary and Conclusions

The potential of terbium complex, [Ln.**5**], as a FRET donor has clearly been demonstrated. However, in order to be commercially useful, it is necessary that the complex should adopt only one constitutional isomer in solution, similarly to the parent triamide dpqC complexes, [Ln.**1**]. This perhaps may be achieved through the use of a chiral amide linker whose structure is more similar to that of the other pendent arms. In order to achieve a high FRET efficiency, donor and acceptor pairs should be chosen such that their energies are well matched *i.e.* there should be good overlap between the emission spectrum of the donor and the absorption spectrum of the acceptor; in the current example, the choice of acceptor has been optimised for europium cryptates. Given the range of fluorescent proteins and organic fluorophores that are available (Chapters 1.4.1 and 1.4.2); systematic screening should provide a suitably matched pair. Finally, if terbium complexes are to be used as components in HTRF assays, it is necessary to carry out an extensive study to determine possible interferences. The higher sensitivity of this series of terbium complexes to quenching by a charge transfer process, compared to their europium analogues is covered in some detail in Chapter 3.

2.3 Longer Wavelength Excitation – Tetraazatriphenylene N-Oxides

The tetraazatriphenylene sensitising moiety dpqC has a longest wavelength excitation band centred at 348 nm. Biological tissue is poorly transparent to ultraviolet irradiation and, whilst 348 nm is on the borderline of what is acceptable, it is desirable to red shift the absorption spectrum of the chromophore such that light of longer wavelength could be used. However, a limiting value is defined by the energy of the lanthanide emissive state. In order to efficiently sensitise terbium, the chromophore should have a triplet energy that is more than 1500 – 2000 cm^{-1} above the terbium $^5D_4$ emissive state (20400 cm^{-1}). Inherently, the energy of the chromophore triplet state is lower than the lowest energy singlet excited state from which intersystem crossing occurs, and which corresponds to the longest wavelength 0-0 transition in the absorption spectrum. The N-oxide of dpqC was synthesised with the aim of shifting its longest wavelength absorbance to lower energy.

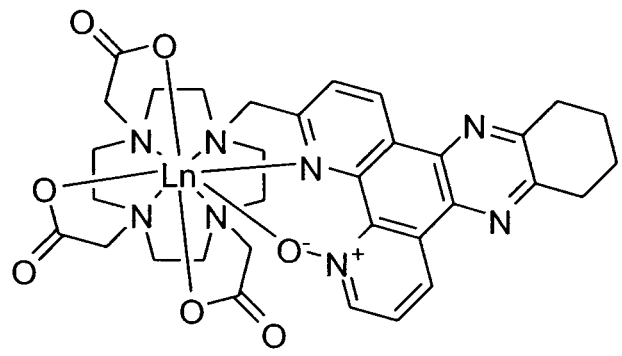

[Ln.7]

Figure 2. 17 – Structure of the tetraazatriphenylene-N oxide based lanthanide complex, [Ln.7]

2.3.1 N-Oxide of Chloromethyl-tetraazatriphenylene

The electronic interaction between a sensitising chromophore and the lanthanide to which it is coordinated is typically small and its photophysical properties are not expected to vary greatly upon binding (perhaps with the exception of ligands that undergo a conformational change upon coordination). Photophysical measurements that are made on the unbound chromophore generally provide a good means to assess its utility as a sensitiser.

2.3.1.1 Synthesis of the N-oxide

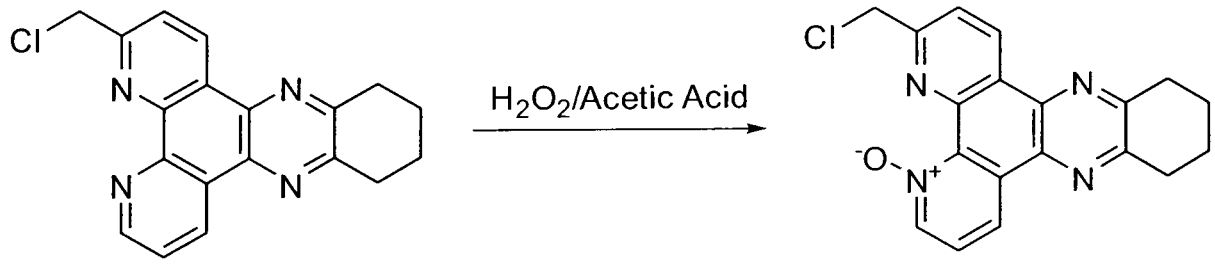

6 38

Scheme 2. 6 – Synthesis of dpqC-N Oxide, 38

The N-oxide of the chloromethyl derivative of dpqC, **6**, was prepared following a literature preparation for the synthesis of 2,9-dimethyl-1,10-phenanthroline-N-oxide.[24] The reaction was carried out using hydrogen peroxide in acetic acid; peroxy acetic acid was generated *in situ*, which reacted with **6** to form the mono-N-oxide, **38**. Phenanthroline-di-N-oxides do not form unless extremely forcing conditions are used. The product was purified by column chromatography on alumina using a dichloromethane/methanol solvent system. ^{1}H NMR characterisation demonstrated that oxidation occurred only on the least hindered nitrogen as shown (**38**).

2.3.1.2 Photophysical Properties of dpqC-N-oxide

2.3.1.2.1 Determination of the Longest Wavelength Absorbance

Figure 2.18 depicts the absorption spectra of the chloromethyl derivative of dpqC, **29**, and its N-oxide, **30**. The form of the spectrum is similar for both compounds, but each of the major peaks was shifted to lower energy for the N-oxide. The longest wavelength absorbance showed a red-shift of 27 nm from 348 nm to 375 nm. At 400 nm the absorbance remained significant, at approximately 25 % of its intensity at 375 nm.

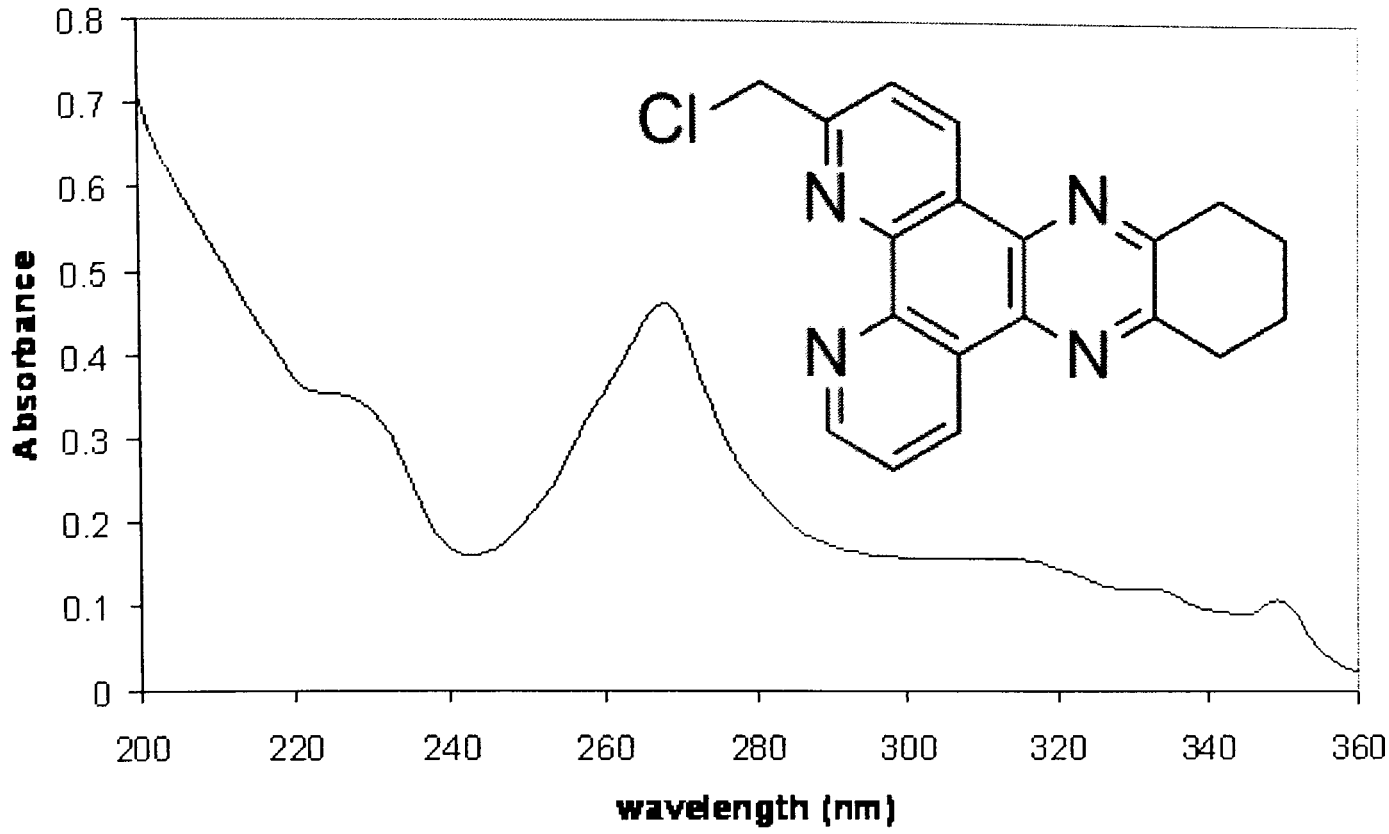

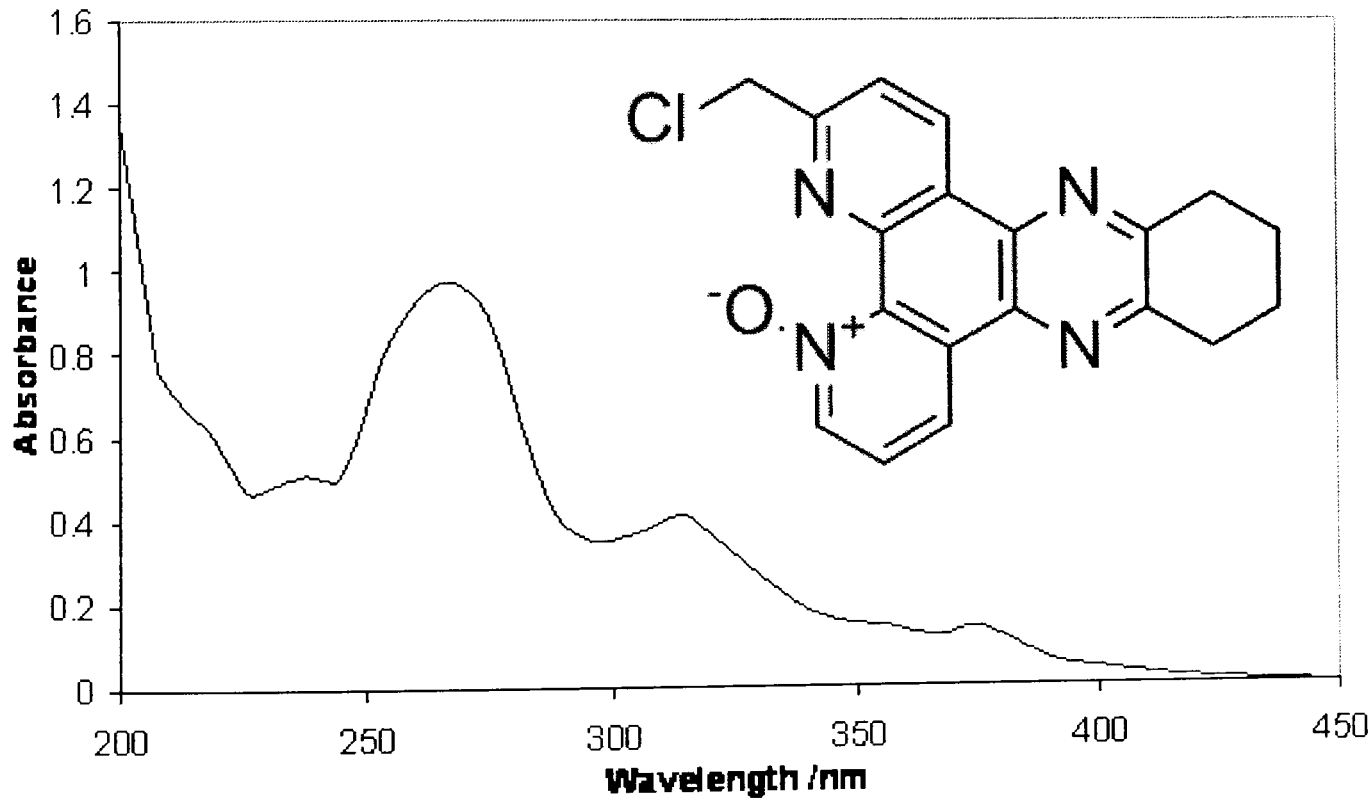

Figure 2. 18 – Absorption spectra for the chloromethyl derivative of dpqC, 29, and its N-Oxide, 30, in H_2O at 295 K

2.3.1.2.2 Measurement of the Triplet Energy

Methodology used to determine whether a particular chromophore has a sufficiently high triplet energy to sensitise europium and terbium traditionally involve synthesis of a gadolinium analogue of the target complex; gadolinium cannot be sensitised since

its first excited state lies at 32 150 cm^{-1}, well above the aryl triplet state of any useful chromophore.[25] However, for the reasons mentioned above (2.3.1), determination of the triplet energy of the unbound chromophore generally allows a good assessment to be made as to whether sensitisation of europium and terbium is feasible for a particular sensitiser.[26]

The phosphorescence spectrum of the chloromethyl dpqC-N-oxide, **30**, was recorded in an EPA glass at 77 K, its triplet energy was determined from the shortest-wavelength transition to be 23 200 cm^{-1}, significantly above the Eu (17,200 cm^{-1}) and Tb (20,400 cm^{-1}) emissive states. Consequently, synthesis of the complexes was undertaken.

2.3.2 N-Oxide Lanthanide Complexes

Degradation of the N-oxide of the chloromethyl-dpqC chromophore occurs on storage, therefore it was decided to undertake oxidation at the final stage, prior to deprotection of the ligand, and complexation.

2.3.2.1 Synthesis

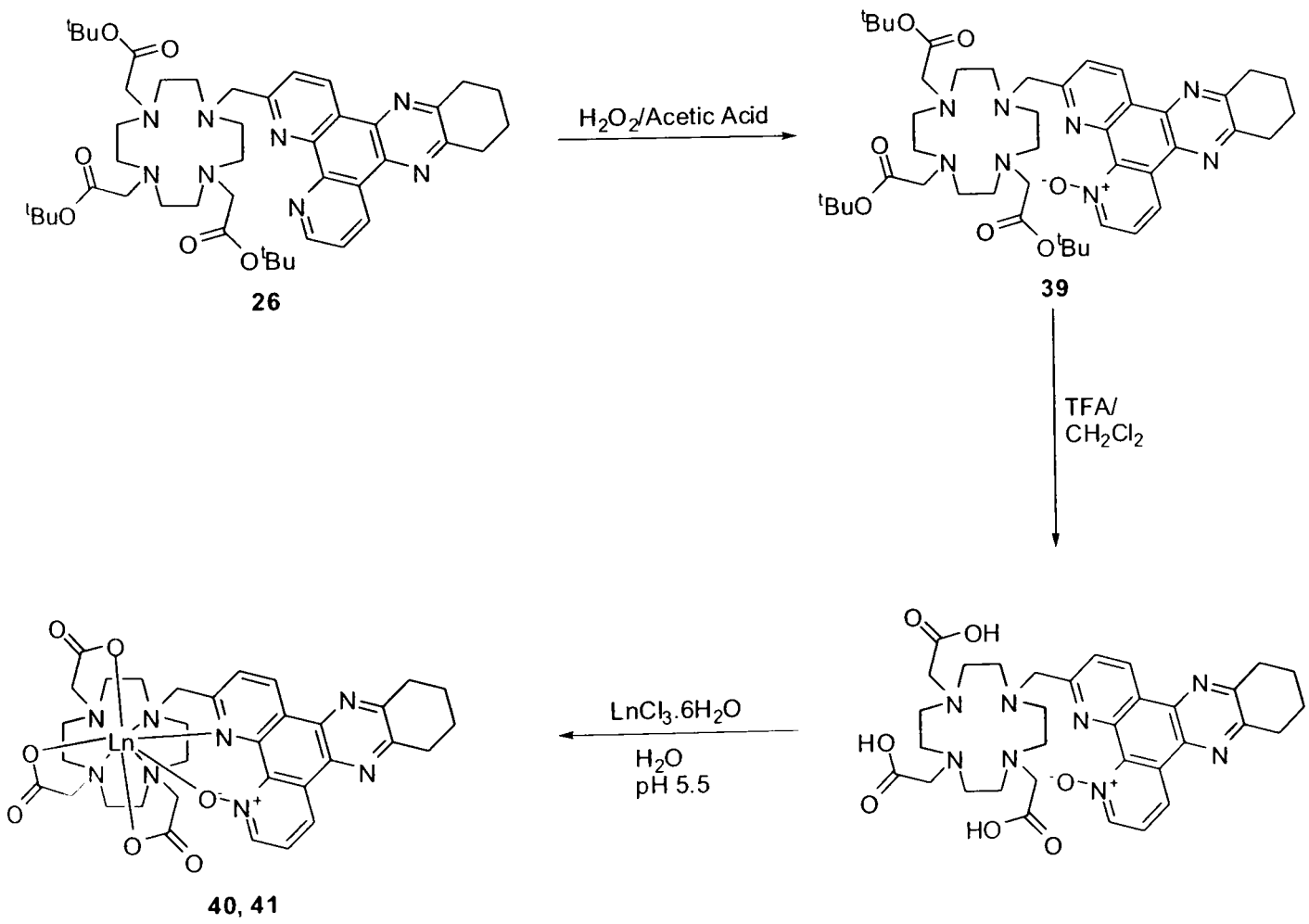

26 **39** **40, 41**

Scheme 2. 7 – Synthesis of the N-oxide derivative of LnDO3AdpqC, [Ln.3]

The ligand 1-dpqC-4,7,10-tris(tert-butyloxycarbonylmethyl)-1,4,7,10-tetraazacyclododecane, **26**, was reacted with hydrogen peroxide in acetic acid. Work-up for the reaction involved neutralisation with aqueous Na_2CO_3, and extraction into dichloromethane. Formation of the N-oxide was confirmed by electrospray mass spectrometry and ^1H NMR and given that only one product was observed using thin layer chromatography, **39**, was used without further purification. Deprotection of **39** was monitored by ^1H NMR and the ligand was used immediately for complexation with Eu(III) and Tb(III) salts.

2.3.2.2 Characterisation

Initial characterisation by electrospray mass spectrometry indicated that synthesis of the europium and terbium complexes, [Ln.**7**], had been successful; although peaks were also present with m/z values consistent with the corresponding complexes [Ln.**3**] i.e. LnDO3AdpqC, lacking the N-oxide functionality. Both metals appeared to be sensitised and the absorption spectrum of both complexes had the same form as for compound **38**, although the intensity of the 375 nm transition appeared to be weaker than for the free chloromethyl-dpqC-N-oxide. However, after several hours in solution, the absorption spectrum of the complex again resembled that of [Ln.**3**], i.e. the transition to longer wavelength was lost, indicating the degradation of the chromophore. Loss of the peak corresponding to europium and terbium [Ln.**7**] was also confirmed by mass spectrometry.

Unfortunately whilst the photophysical properties of the chromophore are very promising, the poor stability of their complexes with respect to reduction in solution limits their utility. The mechanism by which decomposition occurs is not well understood. The observation that both the europium and terbium complexes degrade suggests that reduction is not mediated by electron transfer involving the metal centre.

2.4 Phosphinic Acid Complexes

Through the coordination of three pendent phosphinic acid arms to cyclen, it is possible to synthesise a series of complexes of neutral charge. The overall lipophilicity of the complex can be modified through the use of different alkyl or aromatic phosphinate arms. Two ligands were synthesised bearing methyl phosphinate [Ln.**8**] and benzyl phosphinate [Ln.**9**] functionality; the reasons why these complexes were synthesised and details about their properties are explained further in Chapter 3.

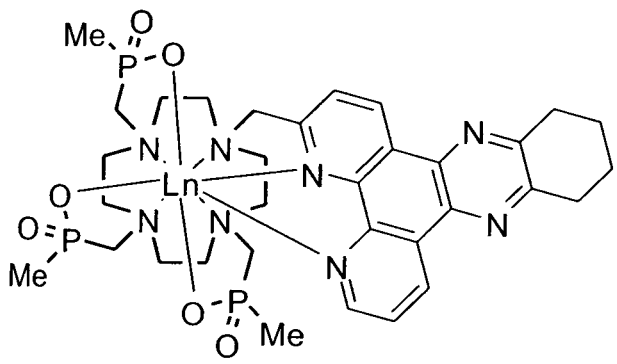

[Ln.**8**]

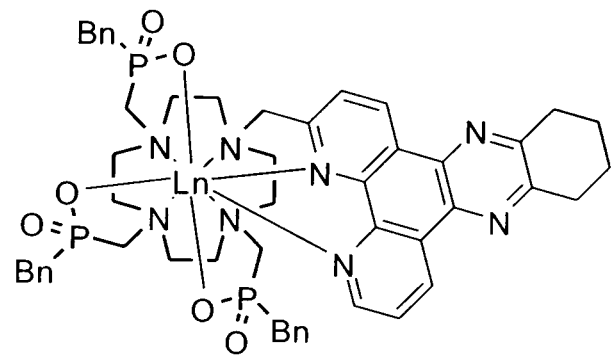

[Ln.**9**]

Figure 2. 19 – Structures of complexes $LnPMe_3dpqC$, [Ln.8] and $LnPBn_3dpqC$, [Ln.9]

2.4.1 Synthesis and Characterisation

There are two approaches that may be adopted for the synthesis of cyclen based complexes bearing three pendent phosphinic acid arms and a tetraazatriphenylene chromophore. The first involves tris-protection of cyclen, follow by alkylation with the chromophore, then deprotection of the remaining positions and functionalisation as the methyl or benzyl phosphinate. The second is the reverse of this process, whereby the pendent arms are attached first and the chromophore subsequently. This second method requires a more involved protection strategy, but less chromophore is used to achieve the same final yield, since its attachment is only at the final stages of the synthesis and, as a result, is not wasted in the intermediate purification steps. Both methods were adopted, the first in the preparation of [Ln.**8**] and the second for [Ln.**9**].

2.4.1.1 Methyl Phosphinic Acid Complexes

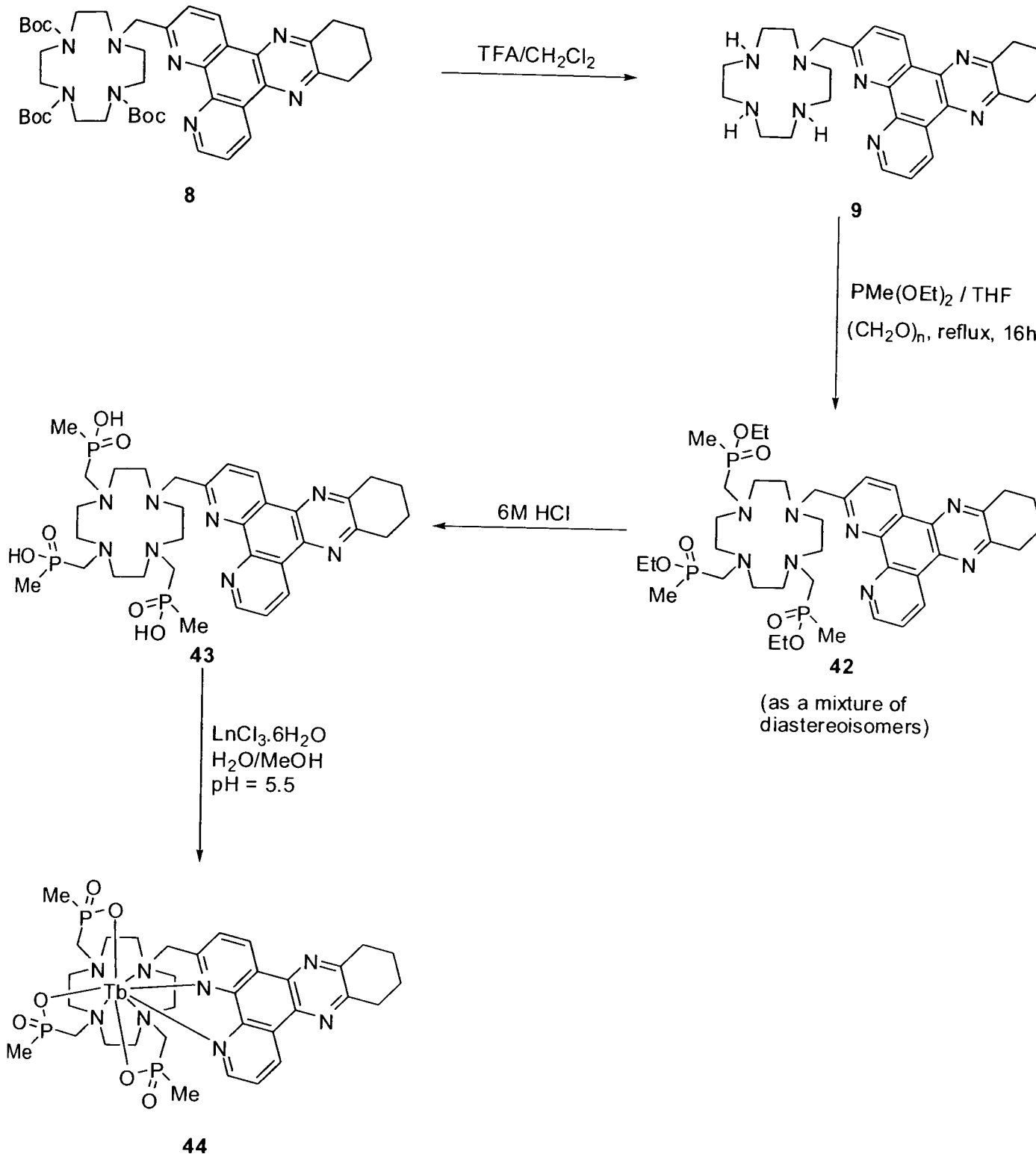

Scheme 2. 8 – Synthesis of LnPMe$_3$dpqC, [Ln.8]

Synthesis of the tri-Boc species **8** was described earlier for the amide based series of complexes [Ln.**1**, **2** and **4**]. Deprotection using TFA in dichloromethane proceeded cleanly to give the mono-alkylated cyclen species, **9**. Condensation with anhydrous paraformaldahyde in dry THF yielded an intermediate hydroxymethyl species which following dehydration was trapped with methyl diethoxyphosphine to give the corresponding methylphosphinate ester **42**. Methyl diethoxyphosphine is commercially available. Exclusion of moisture from the mixture was essential to prevent formation of hydroxymethylphosphinate esters; the reaction was carried out using a Soxhlet apparatus containing 4 Å molecular sieves to scavenge any water. The yield from the reaction was difficult to gauge due to the inefficiency of the

purification step. Thin layer chromatography revealed the product **42** to streak considerably on silica. Alumina appeared more promising using a mixture of methanol and dichloromethane to elute the product, but the recovered yield was less than 10 %. The following deprotection step progressed smoothly and the terbium(III) complex was synthesised without further purification. Characterisation of the free phosphinic acid ligand proved very difficult due to its low solubility in all but strong acid. Some success was met by carrying out the hydrolysis step in an NMR tube in order to monitor the characteristic change in the ^{31}P spectrum upon going from a phosphinate ester (δ_p 53.2 ppm) to a phosphinic acid (δ_p 37.7 ppm, pH 5).

2.4.1.1.1 Absorption and Emission Spectra

The absorption and emission spectra of the terbium complex are again consistent with those reported for the parent triamide and DO3A based complexes.

2.4.1.1.2 Quantum Yield and Lifetime

TbPMe3dpqC displays an exceptionally long emissive lifetime in water of 2.9 ms and has a luminescent quantum yield of 49 %. This is one of the highest values yet reported for a lanthanide chelate.

2.4.1.2 Benzyl Phosphinic Acid Complexes

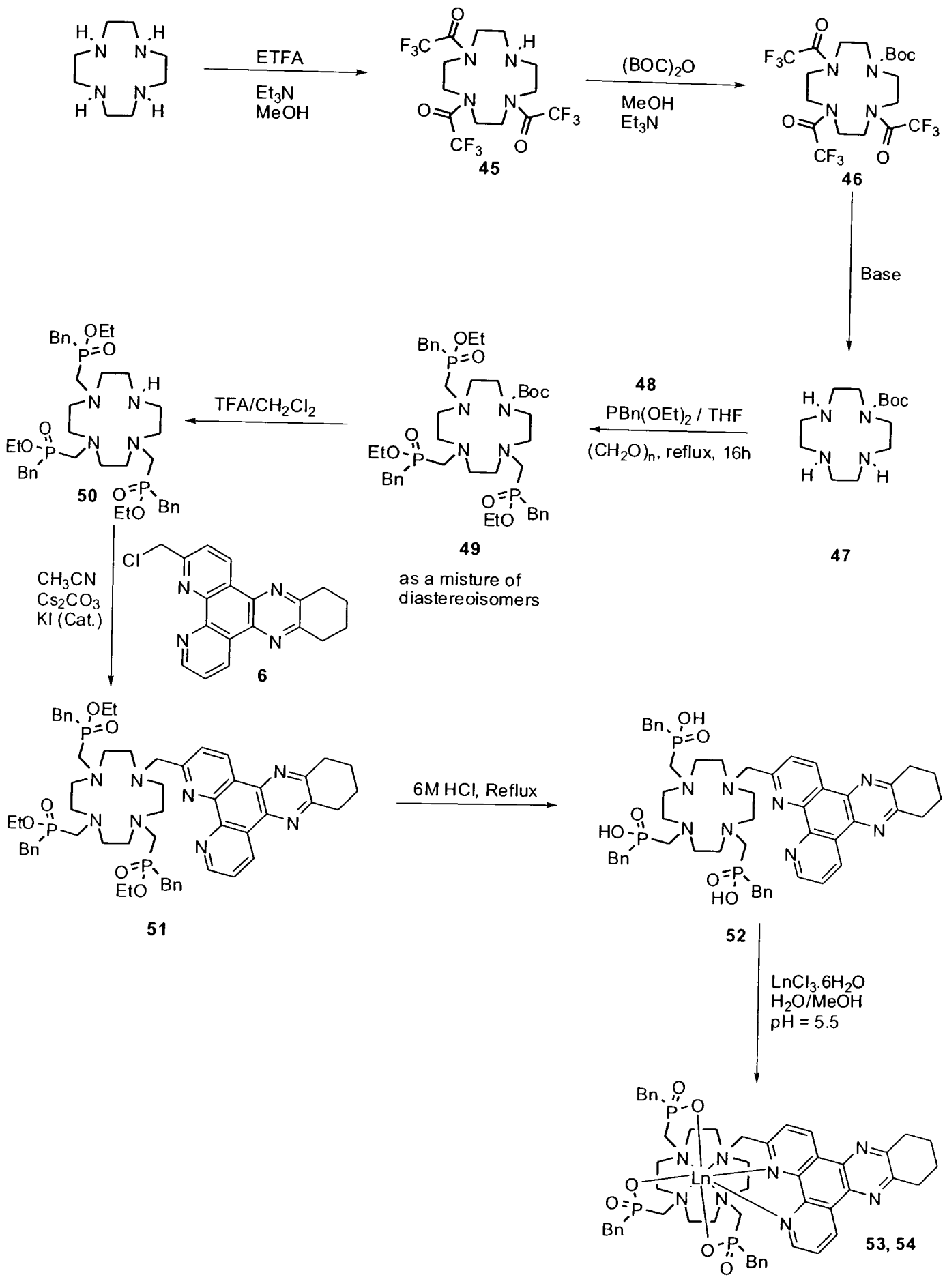

The methodology used for the synthesis of the tribenzyl phosphinic acid complexes, **53** and **54**, were similar to that used for their methyl analogues. However, in this case the first steps were targeted towards phosphinate functionalisation. Alkylation with

the chromophore was performed just prior to hydrolysis of the phosphinate ester and complexation.

Previous attempts within the group to directly synthesise the tris-phosphinate complex **50** using stoichiometric quantities of reagents have been met with only limited success; this is due to the formation of a distribution of mono, di, tri and the tetra substituted product. These could not be successfully separated by chromatography to give a good recovered yield. An alternative approach is to use a multi-step protecting strategy: the final aim is to obtain a mono-protected cyclen species in order that an excess of phosphine starting material can be used to 'drive' the reaction to completion; it should also allow easier chromatographic separation of the mixture.

The basis of the protection strategy was to functionalise cyclen with two different protecting groups, one of which is base labile and the other acid labile. Whilst a few methodologies are available to monofunctionalise cyclen in one reaction (such as through its prior coordination to a molybdenum tricarbonyl complex) it was thought that this multistep approach would be both higher yielding and more amenable to scale-up.

Synthesis of the tris-trifluoromethyl amide protected cyclen species was accomplished on a 10 g scale by dropwise addition of ethyl trifluoroacetate onto a mixture of cyclen and triethylamine in ethanol at 0 °C over 30 minutes. After being allowed to warm to room temperature with stirring overnight, the volatiles were removed *in vacuo* and the crude product purified through a plug of silica using 100 % ethyl acetate as the eluent. The pure product was obtained in 85 % yield. There was no evidence for over-alkylation leading to the tetra species.

Surprisingly, further alkylation of **45** did not proceed easily and required very long reaction times and the periodic addition of a large excess of $(Boc)_2O$. It is worth noting that $(Boc)_2O$ can also slowly react with methanol under the reaction conditions used. However the reaction did not proceed at all using the non-polar solvent dichloromethane. Following purification of **46** by column chromatography, the trifluoroacetamide protecting groups were removed cleanly with base to give **47**.

The benzyl phosphinate arms were introduced using the same procedure as described leading to the methyl phosphinic acid based complex **35** by condensation of the secondary cyclen amine groups with paraformaldehyde in the presence of benzyl diethoxyphosphine (synthesized by reaction of dimethoxychlorophosphite with a benzyl magnesium Grignard and purified by distillation). Following an Arbuzov rearrangement the ester **51** was obtained. Functionalisation with the tetraazatriphenylene chromophore following deprotection of **51** with TFA/CH_2Cl_2 was straightforward and followed the same procedure as has previously been described. Purification was achieved by column chromatography on alumina using dichloromethane and methanol as eluents. Unfortunately, once again recovery from the column was low. Hydrolysis of the phosphinate esters proceeded in 6 M hydrochloric acid and complexation was carried out in a mixture of methanol and water at pH 5.5. The complex precipitated out of solution upon formation.

2.4.1.2.1 Solubility

The high lipophilicity of the peripheral benzyl phosphinic acid arms unfortunately led to very poor solubility of the europium and terbium complexes [Ln.**9**]. The only solvent system that could be found in which the complexes had a reasonable solubility limit was a 1:1 mixture of methanol and dichloromethane leading to some problems associated with their characterization.

2.4.1.2.2 Emissive Lifetimes and Determination of the Number of Bound Water Molecules, q

Whilst the solubility limit of the complexes in water is very low, it was possible to obtain emissive lifetimes and from these, q-values could be determined. Due to the relatively poor signal to noise ratio it is estimated that the values are only accurate to within 20 %. The quoted lifetimes represent an average value obtained following three repeat measurements.

Complex	τ_{H2O}	τ_{D2O}	q
[Eu.**9**]	1.14	1.69	0.05
[Tb.**9**]	1.13	1.80	1.3

Table 2. 8 – Determination of the number of water molecules, q, coordinated to the lanthanide centre

The europium complex was found to have no bound water molecules and to have a relatively long lifetime, as predicted from an analysis of the parent benzylphosphinic acid species. The terbium complex in contrast had a non-zero q value and a lifetime in water that is considerably lower than would be predicted (the lifetime of the methyl phosphinic acid analogue is 2.9 ms). It is suggested that the steric bulk of the ligand leads to 'overcrowding' around the metal centre and whilst complete coordination is possible for the slightly larger europium centre, for terbium it is not. The two complexes were synthesized at the same time, under identical conditions using the same batch of ligand. The synthesis was also repeated to confirm the result.

References

1. D. Parker, R. S. Dickins, H. Puschmann, C. Crossland, J. A. K. Howard, *Chem. Rev.*, 2002, **102**, 1977.
2. G. Bobba, J. –C. Frias, D. Parker, *Chem. Commun.*, 2002, 890.
3. J. –C. Frias, G. Bobba, M. J. Cann, C. J. Hutchison, D. Parker, *Org. Biomol. Chem.*, 2003, **1**, 905.
4. D. Parker, J. A. G. Williams, *Metal Ions in Biological Systems*, Marcel Dekker, Inc., New York, Volume 40, 233.
5. E. B. Van der Tol, H. J. van Ramesdonk, J. W. Verhoeven, F. J. Steemers, E. G. Kerver, W. Verboom, D. N. Reinhout, *Chem. Eur. J.*, 1998, **4**(11), 2315.
6. B. H. Bakker, M. Goes, N. Hoebe, H. J. van Ramesdonk, J. W. Verhoeven, M. H. V. Werts, J. W. Hofstraat, *Coord. Chem. Rev.*, 2000, **208**, 3.
7. G.Bobba, *Interaction of chiral lanthanide complexes with nucleic* acids, PhD Thesis, University of Durham, 2002.
8. M. Yamanda, Y. Tanka, Y. Yoshimoto, S. Kuroda, I. Shimao, *Bull. Chem. Soc. Jpn.*, 1992, **65**, 1006.
9. G. A. Shabir, N. J. Forrow, *J. Pharm. Biomed. Anal.*, 2003, **33**, 219.
10. A. M. S. Garas, R. S. Vagg, *J. Heterocyclic. Chem.*, 2000, **37**, 151.
11. C. F. G. C. Geraldes, C. Luchinat, *Metal Ions in Biological Systems*, Marcel Dekker, Inc., New York, Volume 40, 513.
12. L. Helm, É. Tóth, A. E. Merbach, *Metal Ions in Biological Systems*, Marcel Dekker, Inc., New York, Volume 40, 589.
13. I. M. Clarkson, A. Beeby, J. I. Bruce, L. J. Govenlock, M. P. Lowe, C. E. Mathieu, D. Parker, K. Senanayake, *New J. Chem.*, 2000, **24**, 377.
14. J. I. Bruce, R. S. Dickins, L. J. Govenlock, T. Gunnlaugsson, S. Lopinski, M. P. Lowe, D. Parker, R. D. Peacock, J. J. B. Perry, S. Aime, M. Botta, *J. Am. Chem. Soc.*, 2000, **122**, 9674.
15. M. Woods, S. Aime, M. Botta, J. A. K. Howard, J. M. Moloney, M. Navet, D. Parker, M. Port, O. Rousseaux, *J. Am. Chem. Soc.*, 2000, **122**, 9781.
16. A. Rodger and B. Norden, *Circular Dichroism and Linear Dichroism*, Oxford University Press, 1997.

17. W. C. Johnson, M. Ardhammar, B. Norden and T. Kurucsev, *Circular Dichroism: Principles and Applications*, edited by N. Berova, K. Nakanishi, and R. W. Woody, John Wiley & Sons, 2000.
18. J. I. Bruce, D. Parker, S. Lopinski, R. D. Peacock, *Chirality*, 2002, **14**, 562.
19. R. S. Dickins, J. A. K. Howard, C. L. Maupin, J. M. Moloney, D. Parker, J. P. Riehl, G. Siligardi, J. A. G. Williams, *Chem. Eur. J.*, 1999, **5**, 1095.
20. A. Beeby, I. M. Clarkson, R. S. Dickins, S. Faulkner, D. Parker, L. Royle, A. S. de Sousa, J. A. G. Williams, M. Woods, *J. Chem. Soc., Perkin Trans. 2*, 1999, 493.
21. (*a*) G. Mathis, *Clin. Chem. (Washington D. C.)*, 1993, **39**, 1953; (*b*) G. Mathis, *Clin. Chem. (Washington D. C.)*, 1995, **41**, 1391; (*c*) H. Bazin, M. Préaudat, E. Trinquet, G. Mathis, *Spectrochim. Acta.*, 2001, **A57**, 2197; (*d*) D. Maurel, J. Kriazeff, G. Mathis, E. Trinquet, J. P. Pin, H. Ansanay, *Anal. Biochem.*, 2004, **329**, 253; (*e*) M. Gabourdes, V. Bourgine, G. Mathis, H. Bazin, B. Alpha-Bazin, *Anal. Biochem.*, 2004, **333**, 105.
22. K. Blomberg, P. Hurskainen, I. Himmilä, *Clin. Chem.*, 1999, **45**(6), 855.
23. G. Weber, E. Daniel, *Biochemistry*, 1966, **5**, 1900
24. G. R. Newkome, K. J. Theriot, V. K. Gupta, F. R. Fronczek, G. R. Baker, *J. Org. Chem.*, 1989, **54**(7), 1766.
25. J. I. Bruce, M. P. Lowe, D. Parker , *The Chemistry of Contrast Agents in Medical Magnetic Resonance Imaging*, edited by A. Merbach and E. Toth, Wiley, New York, 2001.
26. P. Atkinson, K. S. Findlay, F. Kielar, R. Pal, D. Parker, R. A. Poole, H. Puschmann, S. L. Richardson, P. A. Stenson, A. L. Thompson, J. Yu, *Org. Biomol. Chem.*, 2006, **4**, 1707.

CHAPTER 3

Quenching Studies

3 Quenching Studies

The susceptibility of a series of europium and terbium complexes to quenching of the lanthanide excited state *via* a charge-transfer interaction by common electron-rich donors is assessed herein. The aim of the analysis is to gain both an appreciation of the mechanism that is in operation and to allow the future synthesis of complexes that show a reduced sensitivity. Finally, differences between europium and terbium complexes of a common ligand to quenching by urate and ascorbate are exploited in the development of a ratiometric method for the determination of uric acid concentration in biological fluids.

3.1 Dynamic Quenching of the lanthanide excited state[1]

For the case of sensitised emission by an organic chromophore, there are three excited states that may be perturbed: the singlet and triplet excited states of the chromophore and the lanthanide emissive state. Two key features that make the ligand dpqC particularly interesting are the facility of S_1 to T_1 intersystem crossing (and hence also its lack of fluorescence) and the negligible sensitivity of the triplet state to quenching by mechanisms other than energy transfer to the lanthanide excited state.[1] In the absence of competitive chromophore localised deactivation processes, it is possible to probe the susceptibility of the lanthanide to dynamic quenching by a charge transfer mechanism. In addition, the nonadentate nature of the ligands used in the present investigation excludes water from their coordination sphere and hence quenching by vibrational energy transfer to OH oscillators is minimised.[2, 3]

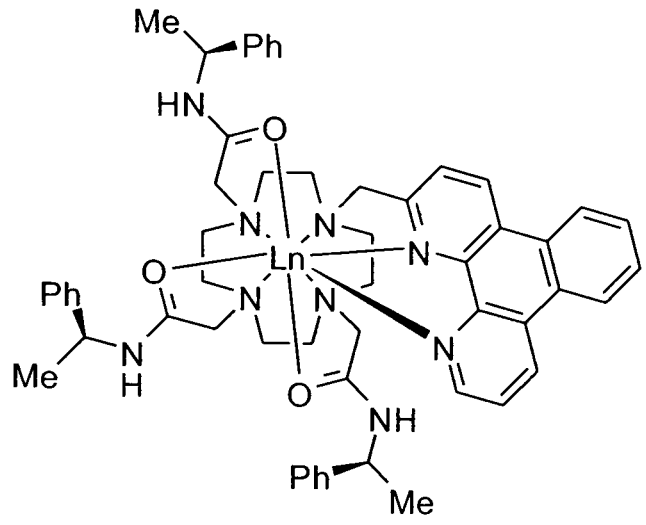

Figure 3. 1 $LnPh_3dpq^{3+}$

It has been reported in preliminary work,[4] that upon addition of iodide or $Fe(CN)_6^{4-}$ to the parent dpq triamide complex $EuPh3dpq^{3+}$ (Figure 3.1), a decrease in both the intensity and lifetime of the metal centred emission is observed. A change in lifetime leads implicitly to the conclusion that the lanthanide excited state is directly involved in the quenching process.

It is proposed that the free energy of the excited lanthanide ions (Tb and Eu excited states lie at 2.52 and 2.13 eV respectively) can be used to 'drive' the charge transfer process in quenching by electron rich species. The feasibility of this process can be assessed using the Weller equation (Equation 1):[5]

$$\Delta G_{ET} = nF[(E_{ox} - E_{red}) - E^{Ln*} - e^2/\varepsilon r] \text{ J mol}^{-1} \quad (1)$$

E_{ox} is the oxidation potential (*versus* NHE) of the electron donor (quencher, Q),
E_{red} is the reduction potential of the acceptor (ligand or metal based) in the complex,
E^{Ln*} is the energy of the lanthanide excited state,
$e^2/\varepsilon r$ is a Coulombic attraction correction term associated with the formation of a transient ion pair (or radical/ion) and is typically small (< 0.2 eV).

As an example of this approach, consider the quenching of $EuPh3dpq^{3+}$ by iodide in the first instance and, secondly, the plausibility of quenching with chloride.

Example 1: Given that the iodide oxidation potential is +0.54 V and that both the reduction of related cationic Eu(III) complexes[6-9] (metal-centred at -1.1 V) and of related $[Ru(bpy)_2dpqC]^{2+}$ complexes (ligand-centred at -1.07 V)[10] occur at a similar potential, then Equation 2 applies, giving a favourable free energy change of -65 kJ mol^{-1}.

$$\Delta G_{ET} = 96.5[(0.54 + 1.07) - 2.13 - 0.15] = -65 \text{ kJ mol}^{-1} \quad (2)$$

Example 2: The oxidation potential of a chloride ion is +1.36 V. All other values remain constant and application of the Weller equation leads to Equation 3 and gives an unfavourable free energy of +14 kJ mol^{-1}.

$$\Delta G_{ET} = 96.5[(1.36 + 1.07) - 2.13 - 0.15] = +14 \text{ kJ mol}^{-1} \quad (3)$$

This analysis is in line with the insensitivity of the europium emission intensity/lifetime (± 10 %) to added chloride ions (up to 100 mM). The magnitude of the second-order rate constant that defines the iodide quenching process is of the order of 10^5 M^{-1} s^{-1}. This is a rather low value compared to the values of $>10^9$ M^{-1} s^{-1} that characterise dynamic quenching of aryl triplet states by O_2. This probably reflects the inhibition to collisional encounter on diffusion (*i.e.* the longer range nature of the process), associated with the relative inaccessibility of the encapsulated lanthanide to the quenching species.

3.1.1 Susceptibility of a series of Cationic, Neutral and Anionic Complexes to Quenching by Electron Rich Species

The photophysical properties of lanthanide complexes in solution *(i.e.* their molar absorption coefficients, quantum yields and emissive lifetimes) can be optimised through the careful choice of a sensitising chromophore and its incorporation into a suitable macrocyclic ligand framework. Usually, it is these factors that are used to outline the potential of the complexes for fluorescence based applications. However, if the complex is to be used in biological media, it is important to have an

understanding of how other chemical species will affect these properties. Complexes such as $LnPh_3dpq$ (Figure 3.1) are highly emissive and, as has been previously described, are insensitive to the usual quenching mechanisms that would otherwise limit their utility, in particular in aerated aqueous media. This insensitivity is evident from their very high quantum yields that are observed under these conditions. However, electron-rich species that have an oxidation potential lower than that of iodide (e.g. ascorbate, urate, and polyhydroxyaromatics) are common in biological media and, as such, have the potential to quench the metal excited state similarly through a charge transfer mechanism.

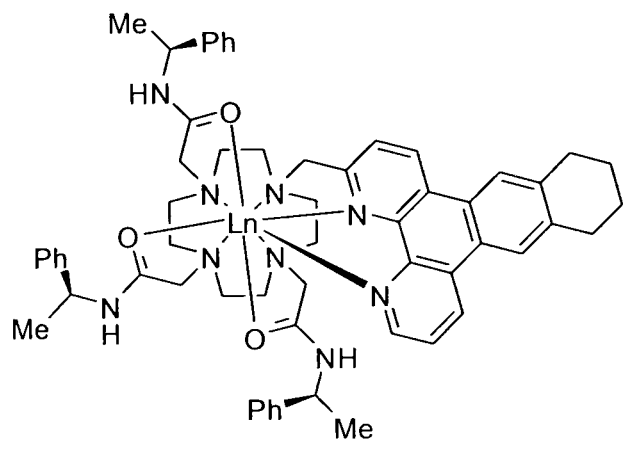

[Ln.**1**]$^{3+}$

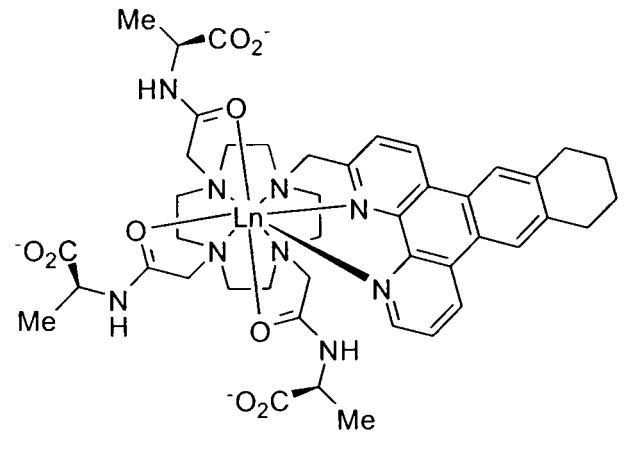

[Ln.**2**]

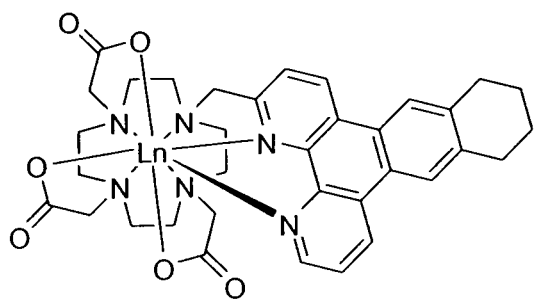

[Ln.**3**]

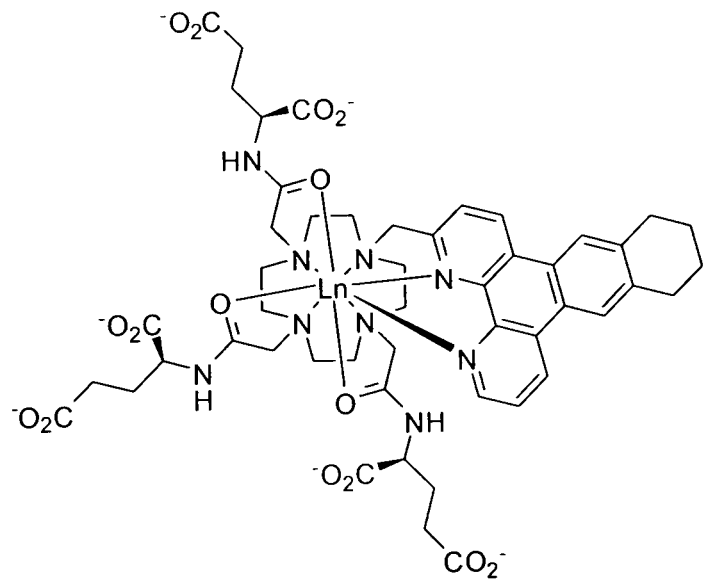

[Ln.**4**]$^{3-}$

Figure 3. 2 [Ln.**1**]$^{3+}$ = LnPh3dpqC, [Ln.**2**] = LnAla3dpqC, [Ln.**3**] = LnDO3AdpqC, [Ln.**4**] = LnGlu3dpqC

In order to understand better and minimise this quenching process, an analysis was undertaken of the structurally related series of complexes [Ln.**1**-**4**] with cationic,

neutral and anionic charge. Inherent in a charge-transfer mechanism is the need to form an encounter-complex between the electron donor and acceptor; it was thought that by varying the overall charge on the complex and in particular by increasing the electrostatic repulsion around the periphery that these factors may disfavour encounter-complex formation and, as a result, reduce the efficiency of the quenching process.

3.1.1.1 Stern-Volmer Quenching Constants

The differing sensitivities of complexes to collisional quenching can be described using the Stern-Volmer equation:

$$I_0/I = 1 + k_q\tau_0[Q] = 1 + K_{SV}[Q] \qquad (4)$$

where I_0 and I are the luminescent intensities in the absence and presence of quencher, k_q is the rate constant for a bimolecular quenching process, τ_0 is the emissive lifetime of the complex in the absence of quencher and [Q] is the concentration of the quenching species. The term K_{SV} is the Stern-Volmer quenching constant and has units of M^{-1}. For convenience we usually quote K_{SV}^{-1} and use units of mM. The term K_{SV}^{-1} defines the concentration of quencher needed to reduce the luminescent intensity to 50 % of its initial value.

For a dynamic quenching process, equation (5) applies revealing the concomitant emission lifetime variation.

$$\tau_0/\tau = I_0/I = k_q\tau_0[Q] = 1 + K_{SV}[Q] \qquad (5)$$

Stern-Volmer plots were obtained for each of the europium and terbium complexes [Ln.**2**-**5**] in pH buffered solution (HEPES, 100 mM, pH 7.4), in the presence of sodium chloride (10mM). The range of quenching species included, in addition to selected halide ions: urate (urine concentrations are usually 1 – 4 mM, serum concentration are typically 10 times lower), ascorbate (typically 0.2 mM) and

glutathione (well-established low molecular-weight anti-oxidants).[11-13] Representative plots are shown in Figures 3.3 and 3.4. The concentration of glutathione in serum or selected cells is typically much lower than that of ascorbate and averages 60 μM in human serum.[14] Ascorbate is found at much higher concentrations (0.8 to 2 mM typically) in oxygen-sensitive tissues such as the eyes, adrenal glands and in the heart, liver and brain.[15]

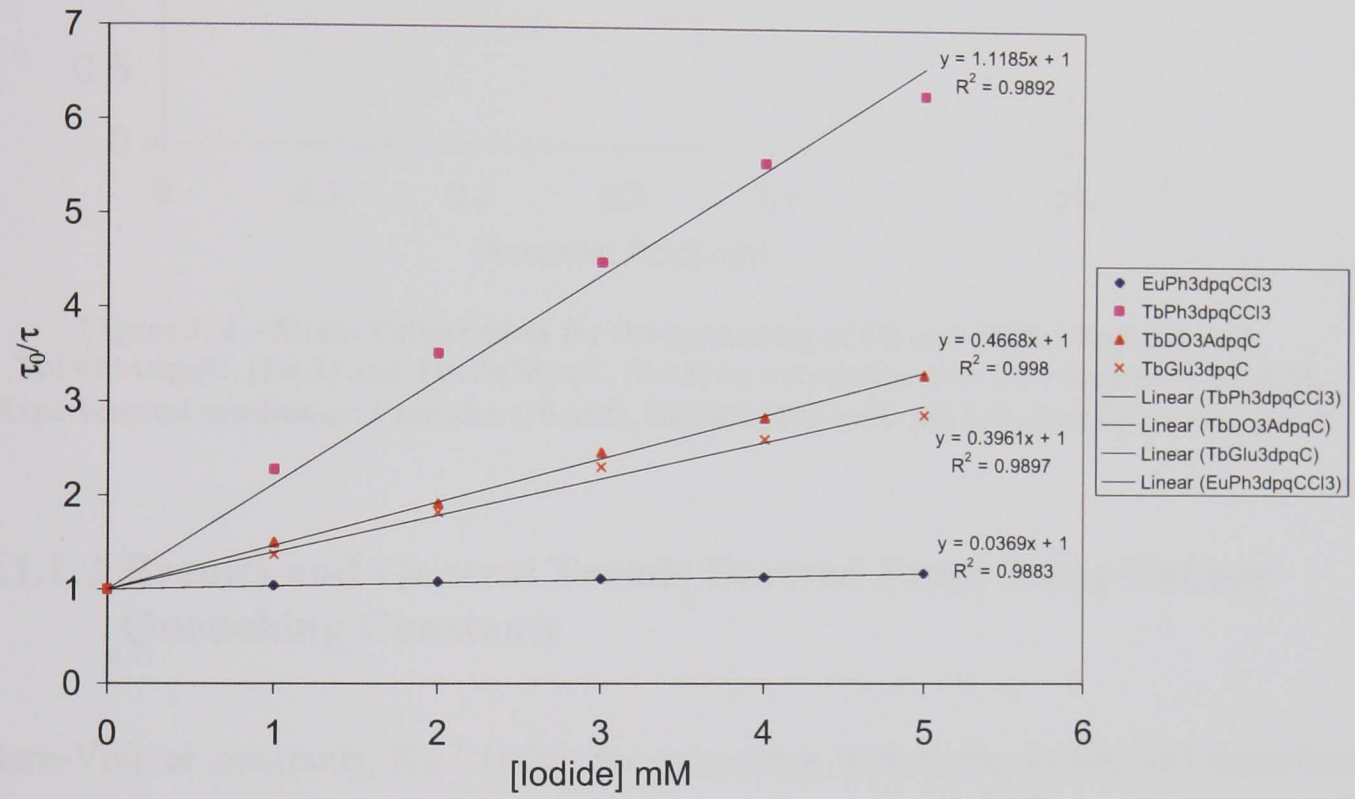

Figure 3. 3 – Stern-Volmer plots for the quenching of Eu and TbPh3dpqC, [Ln.1], TbDO3AdpqC, [Ln.2] and TbGlu3dpqC, [Ln.5] by iodide, over the range 0 – 5 mM. Experimental conditions: Complex (10 μM), HEPES (100 mM, pH 7.4), NaCl (10 mM), 298 K.

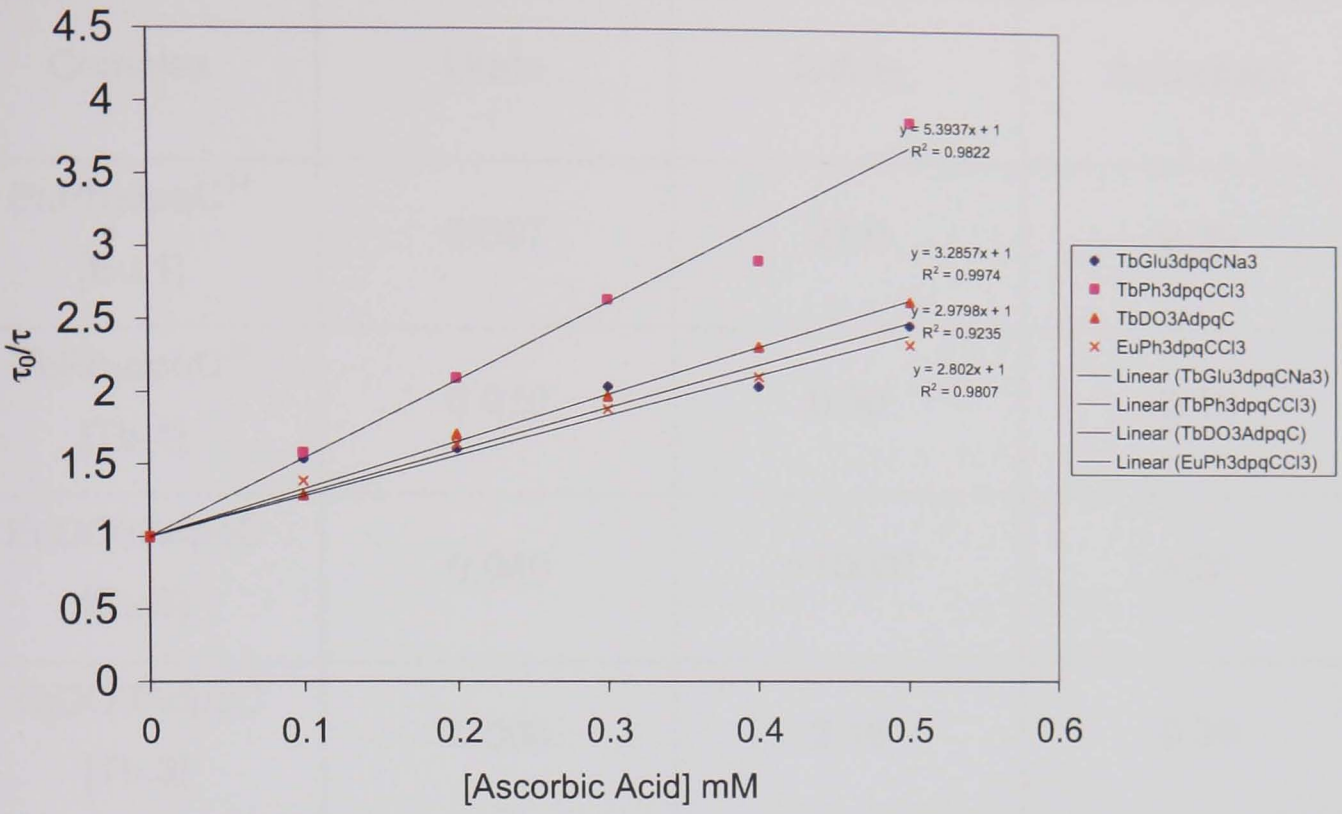

Figure 3. 4 – Stern-Volmer plots for the quenching of Eu and TbPh3dpqC, [Ln.1], TbDO3AdpqC, [Ln.2] and TbGlu3dpqC, [Ln.5] by ascorbate, over the range 0.1 – 0.5 mM. Experimental conditions: Complex (10 μM), HEPES (100 mM, pH 7.4), NaCl (10 mM), 298 K.

3.1.1.2 Results and General Trends Derived From Stern-Volmer Quenching Constants

Stern-Volmer constants, K_{sv}^{-1} (mM) for quenching with urate, iodide and ascorbate are presented in Table 3.1 for the series of complexes [Ln.**2**-**5**].

Complex	Urate	Iodide	Ascorbate
$EuPh_3dpqC^{3+}$ [Eu.**1**]	0.067	27.0	0.39
$TbPh_3dpqC^{3+}$ [Tb.**1**]	0.020	0.90	0.18
EuDO3AdpqC [Eu.**3**]	0.040	>1000[a]	4.31
TbDO3AdpqC [Tb.**3**]	0.006	2.10	0.30
$EuAla_3dpqC$ [Eu.**2**]	0.048	>1000[a]	1.13[c]
$TbAlaMe_3dpqC$ [Tb.**2a**]	0.008	4.97	0.42
$EuGlu3dpqC^{3-}$ [Eu.**4**]	0.084	>1000[a]	2.55[c]
$TbGlu_3dpqC^{3-}$ [Tb.**4**]	0.012	2.50	0.38[c]

Table 3. 1 – K_{SV}^{-1} (mM) values for the complexes [Ln.1-4] (10μM complex, 100 mM HEPES pH 7.4, 10mM NaCl). N.B. [Tb.2] was re-esterified to give the tris-methoxy ester, [Tb.2a], in order to provide a further example of a cationic complex. K_{SV}^{-1} values for glutathione were [Eu.1], 24 mM, [Tb.1], 20 mM. Quenching by bromide/chloride was only observed at very high concentrations (> 1 M).[a] No significant quenching was observed at iodide concentrations up to 1M. [c] Curvature was observed in the Stern-Volmer plots of these complexes above ~ 0.5 mM.

From an analysis of the K_{SV}^{-1} values presented in Table 3.1, a number of trends are evident:

- In each case, the terbium complexes are quenched considerably more strongly than their europium analogues; this is consistent with the proposed mechanism that it is the excited state energy of the lanthanide that is driving the quenching process (*i.e.* due to the higher energy of the terbium $^5D_4$ state).

- The sequence of sensitivity to quenching generally follows the ease of oxidation of the quenching anion, *i.e.* ascorbate >> I^- >>> Br^-/Cl^-. Glutathione does not readily fall into this sequence but is only partially ionised under the pH conditions used (thiol pK_a is 8.66). Given its one electron oxidation potential compared to ascorbate, urate is surprising in that for each of the complexes studied it quenches more strongly (Chapter 3.1.1.3).
- The anionic and neutral complexes are the least quenched by ascorbate and iodide as would be predicted using simple Coulombic considerations. Quenching by urate is again anomalous: the most sterically crowded complexes in this case are the least quenched; the neutral and least sterically shielded DO3A complexes are the most quenched.
- For the range of terbium complexes, the difference in sensitivity to quenching between ascorbate and iodide remains approximately constant with a relative factor of 5 to 10. (For europium it is not so clear since quenching by iodide is inefficient due to the lower excited state energy of the metal ion. At the high concentrations needed to observe a change in lifetime, static quenching becomes significant). With urate, there is considerably more variation from complex to complex. For example, complex TbPh3dpqC is approximately 10 times more quenched by urate than ascorbate, whereas for TbDO3AdpqC, the difference is of the order of 50 times.
- The Stern-Volmer plots have constant gradient (Figures 3.3 and 3.4), but the range of quencher concentrations had to be carefully chosen; above a certain value the rate of change of τ_0/τ versus concentration of quencher decreases and curvature is apparent in the Stern-Volmer plot. i.e. a limiting value is reached. (Chapter 3.1.1.5).

3.1.1.3 Accounting for the Enhanced Susceptibilities to Quenching by Urate compared to Ascorbate

The ability of a compound to donate an electron is usually affected by its protonation state; the pK_a values for ascorbate and urate are 4.2 and 5.4 respectively[16, 17] and both exist as the mono-anion in neutral aqueous solution. Under these conditions, their

one-electron redox potentials (vs NHE, 298 K) are 0.30 V and 0.59 V for ascorbate and urate respectively.[17] The simple argument that holds true for the halides and ascorbate that show enhanced quenching ability with decreasing oxidation potential would predict that ascorbate should quench more strongly than urate. However, this trend is reversed and indeed, the Stern-Volmer quenching constants that define the deactivation of the lanthanide excited state by urate are, in some cases, more than an order of magnitude lower than for quenching with ascorbate.

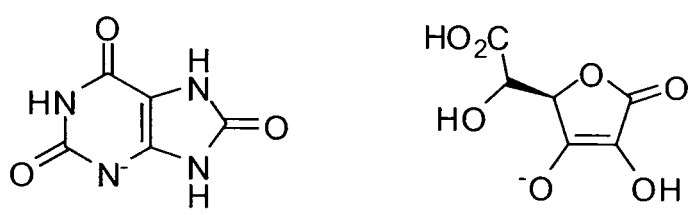

Figure 3. 5

Consideration of the structures of ascorbate and urate (Figure 3) and how they might interact with each of the complexes can perhaps help to provide some insight into the quenching mechanism. Urate has a 2-dimensional structure with an electron-rich π-system in which charge is delocalised.[17.1] Ascorbate, in contrast, has a less conjugated π-system and is significantly more hydrophilic.

Scheme 3.1 is a representation of the classic kinetic scheme proposed by Rehm and Weller for excited state electron transfer.[18. 19]

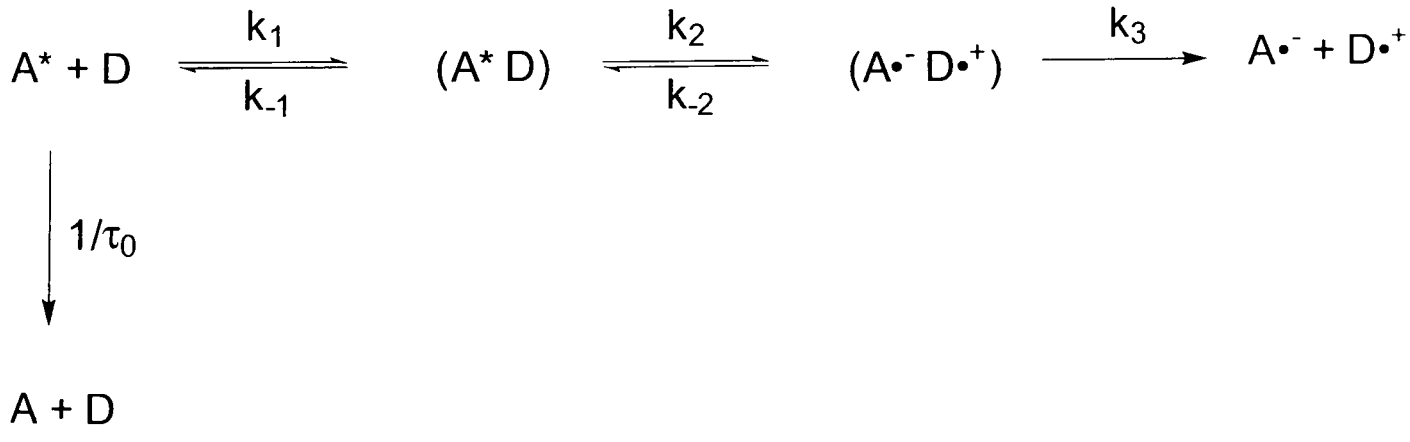

Scheme 3. 1 – Rehm and Weller kinetic scheme for quenching via excited state electron transfer

Integral to electron transfer, is the formation of an encounter complex between the excited acceptor and the donor.

It is tentatively suggested that quenching could be further enhanced by the presence of a weak, but favourable binding interaction, such as π-stacking involving the electron poor dpqC moiety. The neutral complexes LnDO3AdpqC, [Ln.**3**], have the least steric crowding and, as such, have the most accessible chromophore; they would therefore be expected to be the most strongly quenched where such interactions are possible. The cationic complexes LnPh3dpqC, [Ln.**2**], in contrast, have the most aromatic character and are sterically crowded; any π-stacking interaction with the chromophore would likely be inhibited or at least greatly reduced.

A π-type binding interaction may also introduce an additional quenching mechanism. It has been reported by several authors that for planar aromatic donor-acceptor pairs, quenching may be due to an exciplex quenching mechanism rather than through the formation of radical-ion pairs (Scheme 3.2). [19a, 19b]

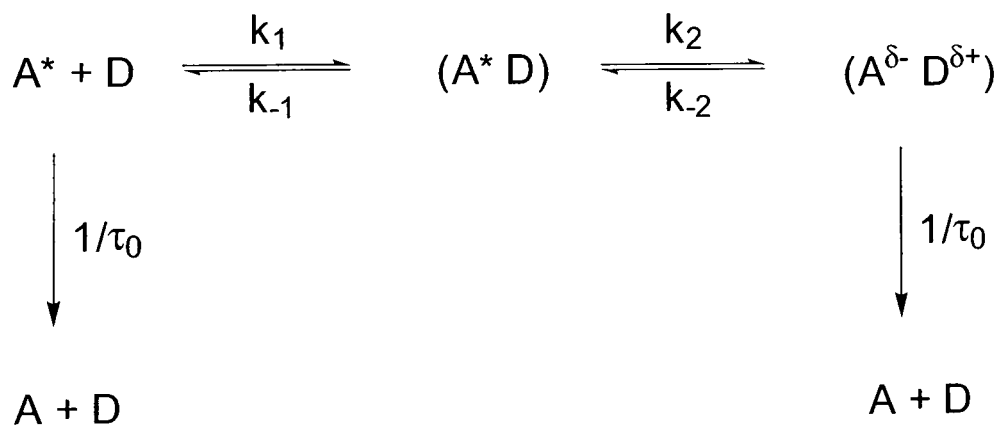

Scheme 3. 2 – Suggested kinetic scheme for quenching of pairs of planar aromatic compounds through an exciplex mechanism

3.1.1.4 Susceptibility to Quenching by Hydroxyaromatics

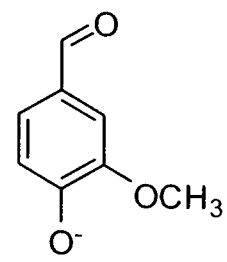

Vanillin

Figure 3. 6 – Structure of Vanillin, $pK_a = 7.4$

If the higher susceptibility to quenching of the complexes by urate when compared to ascorbate is due to the presence of a π-type binding interaction, then it would be predicted that other planar aromatic anions, with a suitable redox potential should show similar behaviour. A systematic analysis of a series of such compounds (for example Vanillin, $pK_a = 7.4$, $E_{ox} \sim 0.5$ V Figure 3.6) is currently underway at Durham. Preliminary results appear to be consistent with the proposed hypothesis.

3.1.1.5 Incomplete Quenching of the Lanthanide Emissive State

With each quenching species, it was noted that an upper limit may be reached, for a given complex, where the rate of change of τ_0/τ with increasing quencher concentration tends to zero; such behaviour leads to curvature in the Stern-Volmer plot. As a result, the range of concentrations of a given quencher had to be carefully chosen, in order for classic Stern-Volmer behaviour to be observed. The ranges used were: for iodide 1 – 5 mM, for ascorbate 0.1 – 0.5 mM and for urate 10 – 50 μM (the complex was used at a concentration of ~ 10 μM). However, the point at which this limit was reached with a given quenching species appears to be dependent upon the complex under study. For example, for quenching of the LnPh3dpqC complexes, [Ln.**1**], with urate, it was apparent that a limiting lifetime is reached at low urate concentration and, in fact, some curvature was apparent in their Stern-Volmer plots in the range 100 – 200 μM. For the neutral and anionic complexes [Ln.**2**-**4**] concentrations 5-10 times as high were required before their Stern-Volmer plots became non-linear. In contrast, the observed behaviour is reversed for quenching

with ascorbate; limiting values were only observed with the hydrophilic neutral and anionic complexes [Ln.**2**,**4**].

These observations appear to suggest that limits are reached at lower added quencher concentrations, where there is the possibility of some favourable association between the complex and the quenching species (not involving the chromophore). This could be, for example, through a hydrogen-bonding interaction with ascorbate, or for urate, by some hydrophobic attraction. Incomplete quenching of the lanthanide excited state is indicative of the inefficiency of the quenching mechanism. It is suggested that the point at which the Stern-Volmer plots become non-linear defines the point at which $k_q[q] = k_{em}$, i.e where the combined rate constant for deactivation of the lanthanide excited state is equal to the emissive lifetime of the complex. At very high quencher concentrations the emissive intensity decreases further, suggesting that static quenching or quenching of the chromophore excited states becomes significant.

The quenching behaviour of the complexes studied here is clearly complex and care should be taken in assessing complexes for a particular application based only on a comparison of their Stern-Volmer quenching constants.

3.1.2 Behaviour of Neutral Phosphinate Complexes Assessing the Importance of Lipophilicity

From the analysis of complexes [Ln.**2**-**5**], a number of features have been identified that appear to affect the susceptibility of the complexes to quenching by electron rich donors. In order to minimise quenching by urate, it should possess one or more of the following attributes: high lipophilicity, a positive charge, aromatic pendant arms on the cyclen ring or steric bulk. Quenching by simple anions and ascorbate is less efficient where the complex is either neutral or negatively charged, incorporates hydrophilic pendent arms or where the lanthanide ion is sterically shielded. It is only through the synthesis of further groups of complexes that the relative importance of each of these features can be more fully understood.

Complexes [Ln.**8**,**9**] were synthesised in an attempt to discern the relative importance of charge and lipophilicity/hydrophobicity.

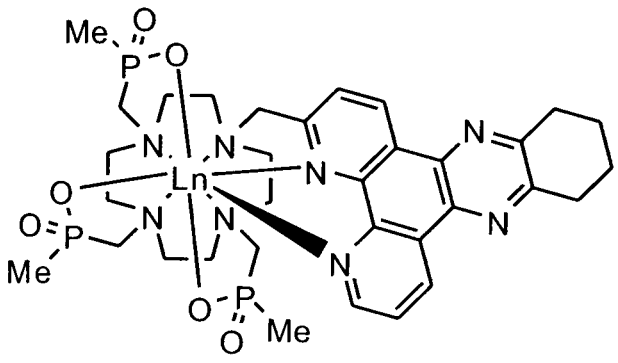

[Ln.**8**]

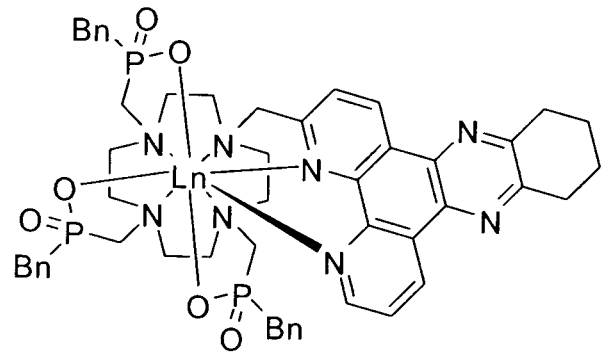

[Ln.**9**]

Figure 3. 7 – Structures of LnPMe$_3$dpqC, [Ln.8] and Ln,PBn$_3$dpqC, [Ln.9]

The parent mono-anionic tetraphosphinate complexes **8, 9** have been synthesised previously in Durham.

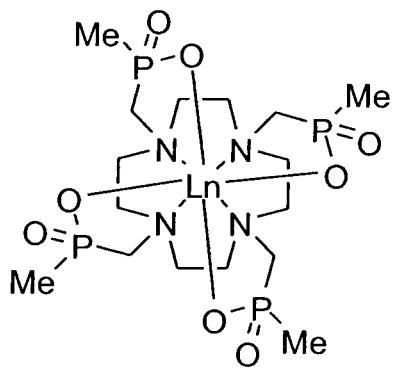

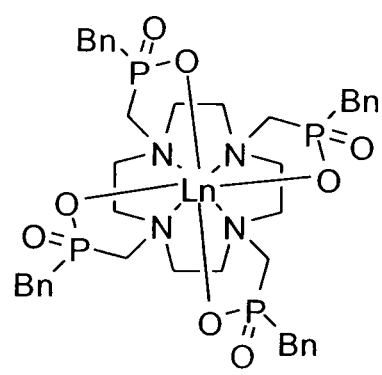

Figure 3. 8 – Structures of Tetra-phosphinate complexes LnPMe$_4$ (left) and LnPBn$_4$ (right)

	LnPMe$_4$	LnPBn$_4$
log P	-4.75	-0.66
$^{Tb}\phi_{em}$	0.01	0.44
$^{Eu}\phi_{em}$	0.6 x 10^{-3}	0.9 x 10^{-3}
$^{Tb}\tau_{H2O}$ /ms	2.96	4.13
$^{Eu}\tau_{H2O}$ /ms	1.25	1.59

Table 3. 2 – Partition coefficients, quantum yield and lifetime values for the complexes LnPMe$_4$ and LnPBn$_4$. Log P values were measured for the ^{153}Gd complexes in octanol/water.[3]

A partition coefficient (Log P) of -0.66 demonstrates the high lipophilicity of the tetrakis(benzylphosphinate) complexes.[3] It was therefore thought that the related complexes [Ln.**9**] with a dpqC sensitising moiety would provide examples of highly

lipophilic complexes, but which are charge neutral, for comparison with complexes [Ln.**1**-**4**]. The methyl analogue, [Tb.**8**] was also prepared as a control.

3.1.2.1 Stern-Volmer Quenching Constants and Discussion

A number of problems were unfortunately encountered in synthesising the benzyl phosphinate complexes, [Ln.**9**]. The ligand is sterically very demanding and through determination of the number of bound water molecules, it was found for the terbium complex that one of the metal coordination sites is occupied by a water molecule. The complex of the slightly larger europium ion, in contrast appeared to possess no bound water molecules. In addition, due to the high lipophilicity of the complexes, they showed very poor solubility in all but a 1:1 mixture of dichloromethane and methanol. (Sections 2.4.1.2.1 and 2.4.1.2.2). Solubility in water was sufficient to observe fluorescence, but the concentration of the complex could not be accurately determined. As a result, Stern-Volmer quenching constants are reported only for the europium complex, [Eu.**9**] and, for comparison, [Tb.**8**].

Complex	Urate	Iodide	Ascorbate
$TbPMe_3dpqC$, [Tb.**8**]	0.017	5.82	1.48
$EuPBn_3dpqC$, [Eu.**9**]	Insensitive	>1000	11.5

Table 3. 3 – Stern-Volmer quenching constants for the complexes [Tb.8] and [Eu.9]. For [Eu.9], the change in lifetime upon addition of urate was too small for a quenching constant to be accurately determined

Quenching constants, K_{SV}^{-1}, for complex [Tb.**8**] with each of urate, iodide and ascorbate are consistent with a reduced susceptibility to quenching relative to the neutral and anionic complexes [Ln.**2**-**4**] by a factor of 2-3. Complex [Eu.**9**] showed a marked improvement over all of the previously synthesised complexes and in fact showed virtually no susceptibility to quenching with urate.

Comparison between the phosphinate complexes [Ln.**8**] and [Ln.**9**], and the series of amide and carboxylate complexes [Ln.**1**-**4**] appears to demonstrate that the lipophilicity of the complexes has a significant influence on the susceptibility to

quenching by urate. The smaller improvements with respect to quenching by iodide and ascorbate are likely to be due to the increased steric bulk of the phosphinate arms, providing further shielding of the lanthanide and chromophore. Whilst these results indicate that the phosphinate complexes warrant further study, the air and moisture sensitivity of the phosphorus starting materials, difficulties associated with purification of the final macrocyclic ligands, and the poor solubility of the more lipophilic complexes will limit their utility.

3.1.3 Further Approaches Currently Underway in Durham in Order to Better Understand and Minimise Quenching of the Lanthanide Excited State by Electron-Rich Donors

Two further approaches have been adopted in Durham in an attempt to understand and minimise quenching by electron-rich donors. Firstly, since the mechanism is thought to involve electron transfer to the chromophore, complexes have been synthesised with chromophores that have more negative reduction potentials than dpqC (example 1). Secondly, the structure of dpqC has been modified to incorporate carboxylate functionality, in place of the terminal cyclohexyl group, in an attempt to increase electrostatic repulsion between the electron donor and acceptor and disrupt the formation of a π-type encounter complex (example 2). Examples are shown in Figure 3.9.

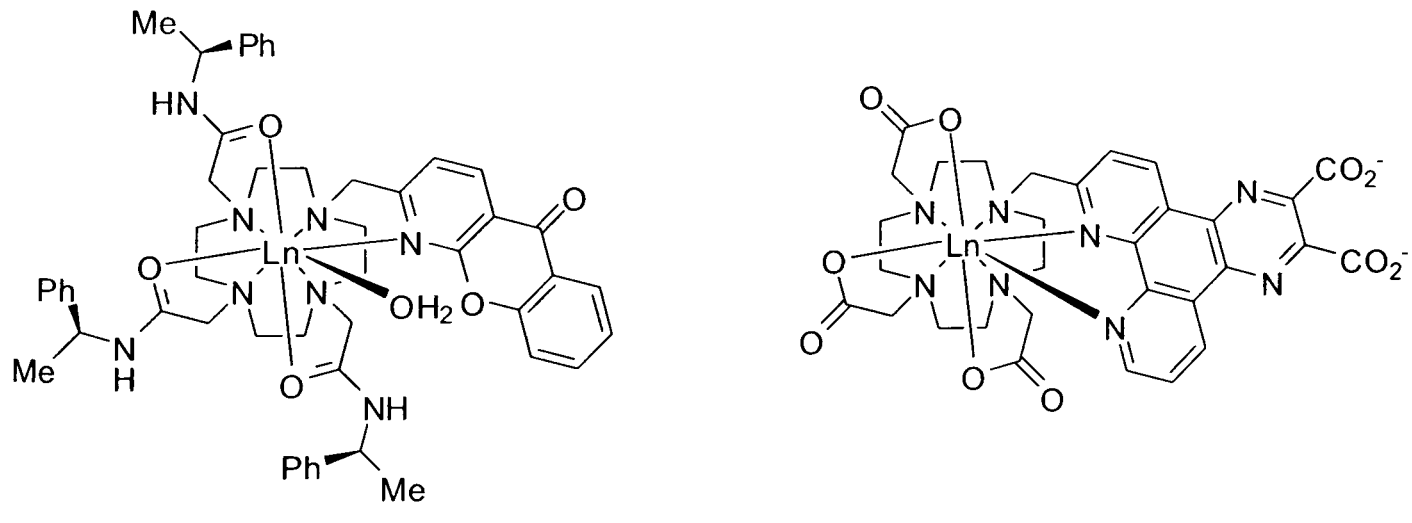

Figure 3. 9 – Structures of $LnPh_3AzaH$ (Synthesised in Durham by S Richardson) – left (Example 1) and $LnDO3Adpq\_diCO2^-$ (Synthesised in Durham by F Kielar) – right (Example 2)

Stern-Volmer quenching constants are provided for each of the complexes in Figure 3.9 in the presence of urate, iodide and ascorbate. Comparison is drawn in each case with the relevant structurally similar dpqC complex i.e. [Ln.**1**] and [Ln.**3**] respectively.

Example 1 – Comparative K_{SV}^{-1} values for $LnPh_3AzaH$ and [Ln.**1**]

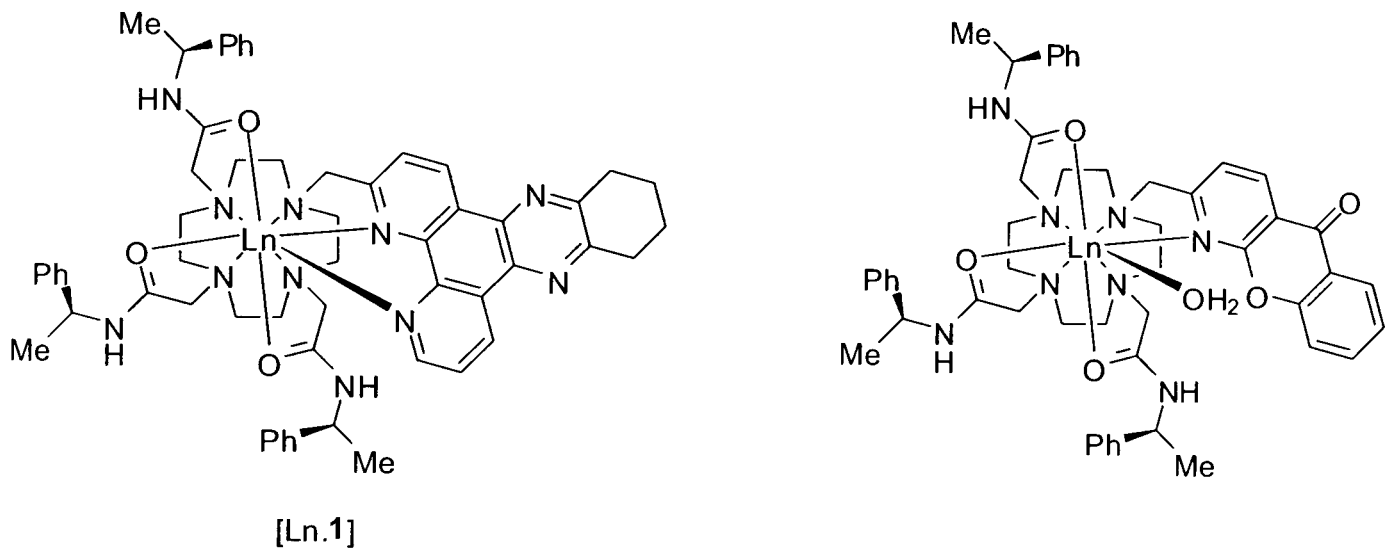

[Ln.**1**]

Figure 3. 10 – Structures of $LnPh_3dpqC$, [Ln.1] (left) and $LnPh_3AzaH$ (right)

Complex	Urate	Iodide	Ascorbate
$EuPh_3dpqC$, [Eu.**1**]	0.067	27	0.39
$EuPh_3AzaH$	0.60	278	1.5
$TbPh_3dpqC$, [Tb.**1**]	0.02	0.9	0.18
$TbPh_3AzaH$	0.04	9.2	0.37

Table 3. 4 - Comparative K_{SV}^{-1} values (mM) for $LnPh_3AzaH$ and [Ln.2]

The reduction potentials (298 K, NHE) for the tetraazatriphenylene (dpqC) and azaxanthone (AzaH) moieties are – 1.1 V and – 1.6 V respectively in CH_3CN. For quenching with each of iodide, ascorbate and urate, the europium and terbium LnPh3AzaH complexes are quenched less than their tetraazatriphenylene sensitised analogues (by a factor of approximately 10 with iodide and 3-4 with ascorbate).

Example 2 – Comparative K_{SV}^{-1} values for LnDO3AdpqC_diCO_2^- and [Ln.**3**]

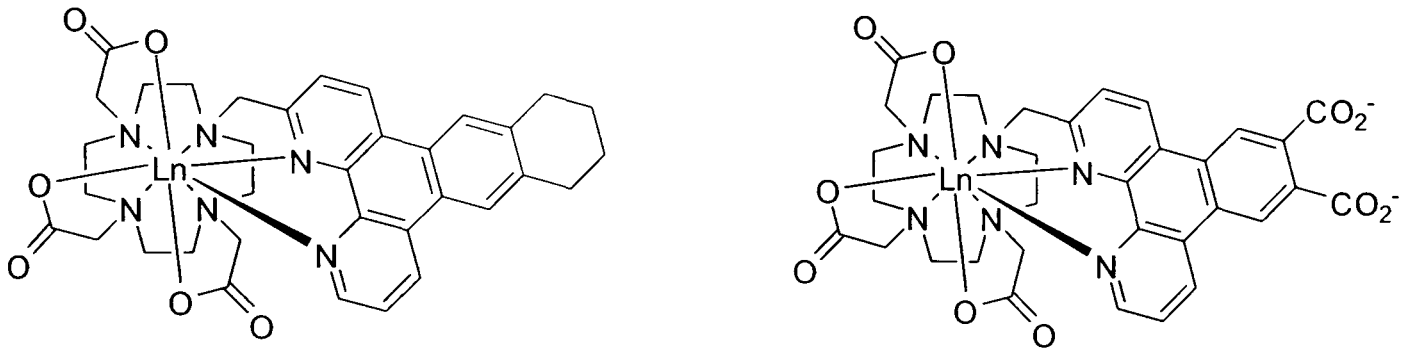

[Ln.**3**]

Figure 3. 11 – Structures of LnDO3AdpqC, [Ln.3] (right) and LnDO3Adpq_diCO$_2^-$

Complex	Urate	Iodide	Ascorbate
EuDO3AdpqC, [Eu.**3**]	0.048	>1000	4.31
EuDO3Adpq_diCO$_2^-$	0.16	1670	4.13
TbDO3AdpqC, [Tb.**3**]	0.006	2.1	0.3
TbDO3Adpq_diCO$_2^-$	0.010	6.9	0.75

Table 3. 5 – Comparative K_{SV}^{-1} values (mM) for LnDO3Adpq_CO$_2^-$ and [Ln.3]

The presence of peripheral carboxylate function on the chromophore appears to have a small, but favourable effect on the susceptibilities of the complexes to quenching by urate, iodide and ascorbate. In each case, the K_{SV}^{-1} values for the LnDO3Adpq_CO$_2^-$ complexes are slightly larger than for the analogous LnDO3AdpqC complex, [Ln.**3**].

A number of tentative conclusions can be drawn from the preliminary results exemplified by *examples 1* and *2*. The reduced susceptibility of complexes LnPh3AzaH to quenching by urate, ascorbate and iodide, when compared to the parent complexes [Ln.**1**], supports a mechanism that involves reduction of the chromophore (dpqC or AzaH). Finally, the slightly higher K_{SV}^{-1} values reported in *example 2* for the complex incorporating peripheral carboxylate groups indicates that the incorporation of such functionality onto new chromophores may have some affect in reducing the susceptibility of their complexes to quenching *via* a charge-transfer mechanism with electron-rich donors.

3.2 Ratiometric Luminescence Assay

Several of the complexes that have been described herein show a considerably higher sensitivity to quenching with urate than with ascorbate or other common electron-rich quenching species (in particular complexes [Ln.**3**,**4**]). In addition, differential susceptibility is observed in each case between the europium and terbium complexes of a common ligand. This combination of features allows the possibility of undertaking ratiometric analysis for the determination of uric acid concentration in biological fluids. A major advantage to the use of ratiometric methods is that it allows non-specific effects that may affect the observed emission intensity or lifetime of a given sample to be overcome. Examples of such effects include sample to sample variation of protein, light scattering due to particulates and surface adhesion. In addition, any static quenching component, operating *via* deactivation of the chromophore singlet excited state is very likely to occur to the same extent for each of the Tb and Eu complexes. Examples of halides deactivating chromophore singlet excited states are well known and have been studied as simple halide sensors in lanthanide complexes.[20]

3.2.1 Background

In humans, uric acid (pK_a 5.7, MW 168) is the final breakdown product of purine (e.g. adenine, guanine) metabolism. Purines from nucleic acid breakdown are converted to uric acid in the liver. The uric acid is transported to the kidney where it is filtered by the glomerulus; 98% is reabsorbed by the proximal tubules and secreted by the distal tubules, ultimately appearing in the urine. The body uric acid level is determined by the balance between synthesis and urinary elimination. Hyperuricaemia is divided into primary and secondary forms, involving either over-production or reduced elimination. Primary hyperuricaemia is usually due to reduced tubular secretion of urate and in 1% of these patients this condition is linked to an enzymatic defect in purine metabolism. These patients lack phosphoribosyl transferase, leading to Lesch-Nyhan syndrome, a sex-linked genetic disorder.

Elevated levels of uric acid (hyperuricaemia) are most commonly associated with gout, increased breakdown of cell nuclei and renal disease. Patients on chemotherapy for proliferative diseases such as lymphoma, leukaemia or myeloma often exhibit hyperuricaemia and levels must be monitored to avoid kidney damage. Treatment involves administration of allopurinol, an inhibitor of uric acid synthesis.[20a] In gout patients, precipitation of uric acid in the joints leads to pain and inflammation and in many examples, this is directly linked to over-production of uric acid. Plasma uric acid levels in such patients are usually high (above 60mg per litre [0.36 mM] *cf.* 1.5 to 4.5 mM in urine). Patients with gout are also susceptible to the formation of kidney stones (renal calculi).

Secondary hyperuricaemia may be caused by increased ingestion of foods rich in purines (shellfish/liver/kidney), leading to increased uric acid excretion. Secondary hyperuricaemia is linked to many conditions including excess alcohol consumption, haemolytic diseases, renal insufficiency, starvation/fasting, myeloproliferative diseases and lead intoxication. Hypouricaemia is much less common but may occur from under-production of uric acid, as in hereditary xanthinuria, toxemia in pregnancy, hereditary purine nucleoside phosphorylase deficiency and allopurinol therapy. Hypouricaemia (as measured in a urine analysis) may also result from a reduction in uric acid excretion, as may occur in AIDS, diabetes mellitus and various malignant diseases.

Measurement of uric acid excretion may assist in the treatment regime for hyperuricaemia, involving either use of uricosuric drugs, to enhance renal excretion or allopurinol to suppress purine synthesis.[20b]

3.2.2 Current Commercially Available Uric Acid/Urate Assays

Current *in vitro* clinical assays used to measure uric acid in urine and serum are predominantly based on the use of the uricase enzyme, which catalyses the hydrolysis of uric acid leading to formation of the more water-soluble compound, allantoin, and hydrogen peroxide.[21-24] The hydrogen peroxide is detected either

directly *via* oxidation of a phenolic dye to produce a strongly coloured compound, or indirectly by the action of a peroxidase enzyme, leading to formation of an intensely coloured chromogen or a strongly emissive fluorophore. These enzymatic methods are typically subject to interference from ascorbate (requiring co-administration of ascorbate oxidase) and bilirubin. Typically, clinical kits give a linear response for the range 0.09 to 1.8 mM for serum and plasma, and 0.12 to 6 mM for urine. Detection limits fall in the 5 μM range for serum analysis and 40 μM for urine. The analysis requires incubation for at least 30 minutes, careful control of the pH of the analyses, the enzymes must be stored carefully to avoid protein denaturation, and the organic dyes used are often light and temperature sensitive, requiring storage in the dark at low temperatures.

3.2.3 The Principle of the Ratiometric Analysis for the Determination of Urate Concentration in Biological Fluids[25,26]

The tetraazatriphenylene cyclen based complexes synthesised here are highly emissive with lifetimes in aqueous solution of the order of 1 ms. The chromophore has a reasonable molar absorption coefficient (6440 cm^{-1} M^{-1}); its triplet excited state is readily populated and is of suitable energy to efficiently sensitise both europium and terbium; it can also bind in a bidentate manner to the lanthanide, resulting in a short donor-acceptor distance and hence facilitates efficient energy transefer. The nonadentate coordination of the cyclen-based macrocyclic ligand provides a saturated and well-defined coordination sphere in addition to giving high kinetic and thermodynamic stability with respect to metal ion dissociation. These basic physical properties in combination with their high sensitivity to quenching by urate compared to other common biological oxidants (in particular ascorbate), and the differential sensitivities of the Eu and Tb complexes of a common ligand suggest an application for the direct analysis of urate concentration in aqueous samples.

Using a mixture of Eu and Tb complexes with a common ligand, measurement of the ratio of intensities of a Tb emission band (e.g. at 546 nm) versus a dominant Eu emission band (e.g. at 700 nm or 616 nm) is a direct function of the amount of urate

present in solution, providing that interfering species contribute little to the overall quenching effect. The only other requirement is that there should be no change in the form of the spectrum. Europium emission bands are sensitive to their coordination environment, in particular the strongest transition centred at 616 nm is sensitive to the polarisability of the donor in the axial position that can cause a change in ratio between the $\Delta J=1$ and $\Delta J=2$ bands by up to an order of magnitude. However, the class of cyclen based ligand that has been used here saturates the coordination sphere of the lanthanide and thus its coordination environment does not vary with different solvent or with different potential ligands in the solution under analysis.

3.2.4 Proof of Concept

In order to establish the concept, an analysis was undertaken to determine the concentration of uric acid in urine samples taken from healthy volunteers; determinations were made in duplicate, firstly using the commercially available Amplex Red uric acid/uricase kit and secondly using the ratiometric method defined here.

3.2.4.1 Amplex Red Uric Acid/Uricase Kit

The Amplex Red uric acid/uricase kit is an enzymatic kit, similar to that used routinely for the analysis of urine or serum in most hospitals. The basis of the method is the oxidation of uric acid to the more water soluble allantoin. The method can suffer from interference from the presence of ascorbic acid; this problem is often overcome through the application of a third enzyme – ascorbate oxidase.

3.2.4.2 A Ratiometric Determination of Urate in Urine Samples

A stock solution containing a 1:1 mixture of Eu and TbGlu3dpqC [Ln.**4**] was prepared in 100 mM HEPES (pH 7.4) to give a final absorbance of 0.1 at both 313 and 348 nm (equates to approximately 5 μM concentrations of each complex). This stock solution was used in each of the assays (it is important to note that the actual

concentration used is 50 % lower). The LnGlu3dpqC complexes were chosen since they show very little surface activity; even the most surface active complexes could be used if the stock solutions were modified to contain 10 – 20 % DMSO or DMF (this has been shown to give quantitative dilutions by monitoring absorbance changes).

A calibration must be carried out using a standard urate solution at a range of dilutions. A 1 mM solution was prepared, again in 100 mM HEPES (pH 7.4); the concentration was verified by measuring the absorbance at 292 nm ($\varepsilon = 1.22 \times 10^4$ M^{-1} cm^{-1}). Dilutions were made in the range 0 – 100 μM. Again it should be noted that the solutions are diluted by 50 % in the assay to give a working range of 0 – 50 μM. The calibration was performed by dispensing 100 μL of each of the complex stock solution and the appropriately diluted urate solution into the wells of a 96-well plate; each urate concentration was repeated in triplicate. In parallel, samples from healthy volunteers were diluted 10, 100 and 500-fold and again wells prepared in triplicate containing the complex solution.

For each well, 10 separate spectra were recorded over the range 450 – 720 nm (Analytik Flash Scan, λ_{ex} 313 nm) and averaged, and the ratio of the 546/616 and 546/700 nm bands was determined. For the range of calibration solutions, a plot was made of emission intensity ratio versus urate concentration; the curve was fitted iteratively to a bi-exponential model (Figure 3.12); less than 1 % variance was found in the measured intensity ratio for a given urate concentration. Such precision is an inherent feature of a ratiometric assay. Both of the complexes share a common ligand, therefore, non-specific effects that affect both of the complexes to the same extent will cancel each other out. This is particularly useful when using a multiwell plate reader since absolute fluorescent intensities are dependent on factors such as the presence of particulates in the sample, light scattering, surface effects, variations in the sample volume and the calibration of the plate reader. In addition, effects due to the presence of other components in the solution that may lead to variation in fluorescent intensities or lifetimes of emission, such as protein, will not reduce the accuracy of the method. Thus, the ratiometric method obviates any sample to sample

variation that compromises a method based on modulation of spectral emission using only one complex.

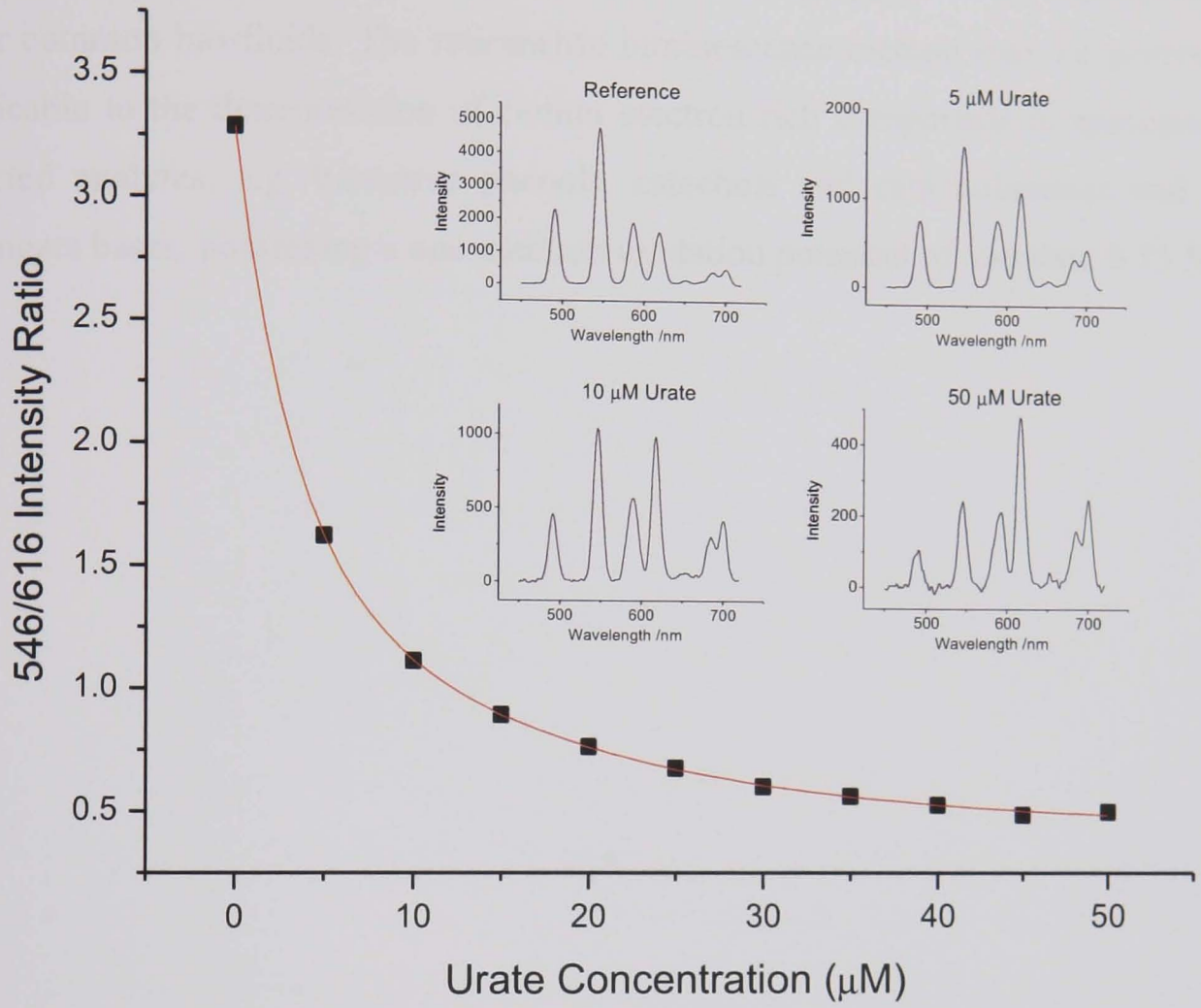

Figure 3. 12 – Variation of the Tb (546 nm) to Eu (616 nm) emission intensity ratio (pH 7.4, 0.1 M HEPES, 298 K) as a function of sodium urate concentration. The curve depicts the iterative fit to a double exponential decay and the inset shows selected spectra recorded (Analytik Flashscan 530F multiwell plate reader)

For the unknown samples, the urate concentration was readily computed, from the calibration curve or by applying the mathematical model. With the same samples the commercial uric aid kit was employed; agreement between the two methods was within 10 %, but it should be noted that the enzymatic assay gave values that were estimated to have a precision of no better than 10 % for the three replicates examined.

3.2.5 Other Potential Applications

The same methodology should also be applicable to diluted serum samples (preliminary results using reconstituted human serum appear encouraging) and to other common bio-fluids. The ratiometric luminescence method may be generically applicable to the determination of certain electron rich compounds in appropriately selected analytes, e.g. bioactive phenols, catechols and catecholamines and their conjugate bases, possessing a one-electron oxidation potential of less than 0.75 V.

References

1. R. A. Poole, G. Bobba, M. J. Cann, J. –C. Frias, D. Parker, R. D. Peacock, *Org. Biomol. Chem.*, 2005, **3**, 1013.
2. R. M. Supkowski, W. DeW. Horrocks, Jr., *Inorg. Chim. Acta*, 2002, **340**, 44.
3. A. Beeby, I. M. Clarkson, R. S. Dickins, S. Faulkner, D. Parker, L. Royle, A. S. de Sousa, J. A. G. Williams, M. Woods, *J. Chem. Soc., Perkin Trans. 2*, 1999, 493.
4. G. Bobba, J. –C. Frias, D. Parker, *Chem. Commun.*, 2002, 890.
5. A. Weller, *Pure Appl. Chem.*, 1968, **16**, 115.
6. D. Parker, *Coord. Chem. Rev.*, 2000, **205**, 109
7. S. Blair, R.Kataky, D.Parker, *New J. Chem.*, 2002, **26**, 530.
8. S. Blair, M. P. Lowe, C. E. Mathieu, D. Parker, P. K. Senanayake, *Inorg. Chem.*, 2001, **40**, 5860.
9. I. M. Clarkson, A. Beeby, J. I. Bruce, L. J. Govenlock, M. P. Lowe, C. E. Mathieu, D. Parker and K. Senanayake, *New. J. Chem.*, 2000, **24**, 377.
10. S. Delaney, M. Pascaly, P. K. Bhattacharya, K. Han, J. K. Barton, *Inorg. Chem.*, 2002, **41**(7), 1966.
11. S. Chevion, E. M. Berry, N. Kitrosky, R. Kohen, *Free Radical Biol. Med.*, 1997, **22**, 411.
12. J. M. Zen, C. T. Hsu, *Talanta*, 1998, **46**, 1363.
13. J. Chen, L. Gorton, B. Ahessan, *Anal. Chim. Acta*, 2002, **474**, 137.
14. H. Reiber, M. Ruff, M. Uhr, *Chin. Chim. Acta*, 1993, **217**, 163.
15. B. Frei, L. England, B. N. Ames, *Proc. Natl. Acad. Sci.*, 1989, **86**, 6377.
16. S. Steenken, P. Neta, *J. Phys. Chem.*, 1979, **83**(9), 1134.
17. M. G. Simic, S. V. Jovanovic, *J. Am. Chem. Soc.*, 1989, **111**, 5778.

17a J. P. Telo, *Org. Biomol. Chem.*, 2003, **1**, 588.

18. D. Rehm, A. Weller, *Ber. Bunsenges. Phys. Chem.*, 1969, **73**, 834.
19. D. Rehm, A. Weller, *Isr. J. Chem.*, 1970, **8**, 259.

19a M. G. Kuzmin, *Pure. Appl. Chem.*, 1993, **65**(8), 1653.

19b M. Dossot, D. Burget, X. Allonas, P. Jacques, *New. J. Chem.*, 2001, **25**, 194.

20. D. Parker, G. Bobba, J. A. G. Williams, *J. Chem. Soc., Perkin Trans. 2*, 1998, 2129.

20a M. L. Bishop, J. L. Duben-engelkirk. E. P. Fody, J. B. Lipincott, *Clinical Chemistry*, Philadelphia, 2nd Ed., 1992.

20b (a) N. B. Ames, *Science*, 1983, **221**, 1256; (b) N. Gochman, J. M. Schmitz, *Clin. Chem*, 1971, **17**, 1154.

21. P. Kabasakalian, S. Kalliney, A. Wescott, *Clin. Chem.*, 1993, **19**, 522.

22. P. H. Duncan, N. Grochman, T. Cooper, E. Smith, D. Bayse, *Clin. Chem.*, 1982, **28**, 284.

23. L. A. Pochla, P. T. Kissinger, *Clin. Chem.*, 1979, **15**, 1847.

24. M. Tanaka, M. Hama, *Clin. Chem.*, 1988, **34**, 2567.

25. R. A. Poole, F. Kielar, S. L. Richardson, P. A. Stenson, D. Parker, *Chem. Commun.*, 2006, 4084.

26. R. A. Poole, D. Parker, F. Kielar, *Brit. Pat. Appl., July 12, 2006.*

CHAPTER 4

Luminescent Europium and Terbium Complexes for in cellulo Applications

4 Luminescent Europium and Terbium Complexes for *in cellulo* Applications

Luminescent lanthanide complexes have been developed that are able to serve as 'tags' in bioconjugates for use in 'FRET' or tracking assays, or as responsive probes: information about their local coordination environment or the concentration of a specific analyte in solution can be gained through monitoring changes in their spectral emission profile, lifetime or circular polarisation.[1] Recently, lanthanide complexes have been reported that are taken up by live cells and can be observed by fluorescence based microscopy techniques.[1-8] Of significant interest would be the possibility of using lanthanide complexes as *in cellulo* probes. Their unique photophysical properties and the ease with which their structures can be modified to suit a particular application would both complement and extend the 'tool kit' currently available for the analysis of living cells and certain processes that occur within them.

The mechanism by which these complexes are able to cross the cell membrane and the factors that govern their localisation/compartmentalisation are not well understood. The structures below provide a cross-section of cyclen-based complexes that have been shown to be taken up by cells.

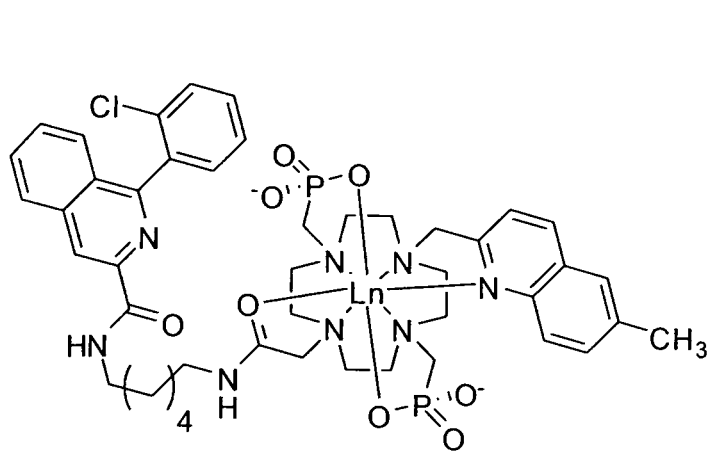

(a)

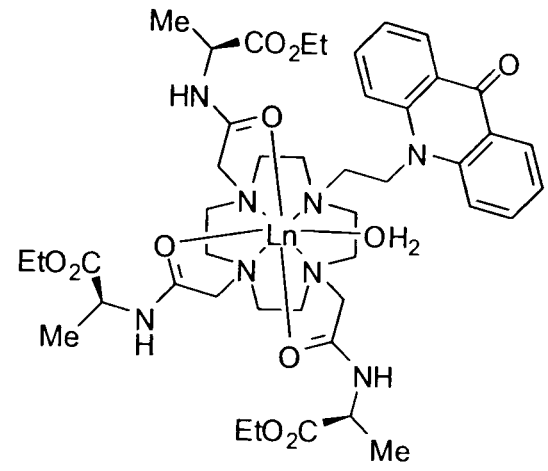

(b)

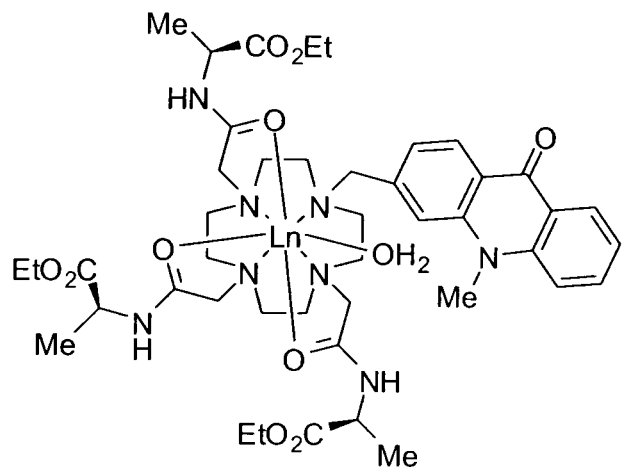

(c)

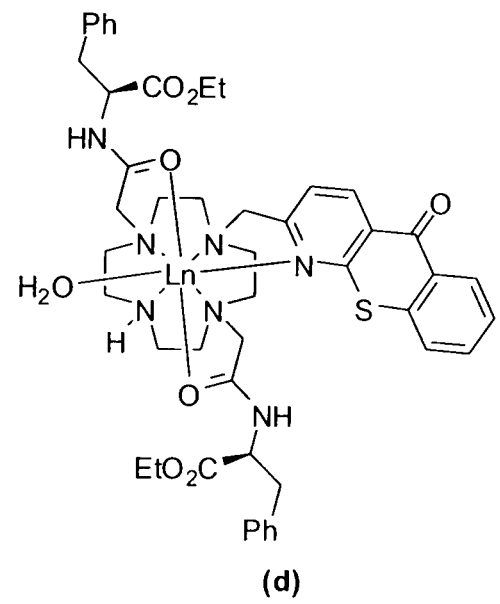

(d)

Figure 4. 1 – Representative structures of a series of complexes (a), (b) LnAlaOEt$_3$NAcr, (c) LnAlaOEt$_3$CAcr and (d) LnPheOEt$_2$ThiaH, that have been reported to be cell permeable

Each of the complexes **(a)** to **(d)** shown in Figure 4.1 is based on the cyclen macrocycle, has one or more planar aromatic heterocycles (usually the sensitising moiety), is relatively lipophilic and has an overall positive charge (1+ for **(a)** 3+ for **(b)-(d)**). These features appear to be common to almost all of the examples reported in the literature thus far that exhibit cellular uptake (with the exception of the neutral and anionic acridone complexes discussed in 1.4.5).

Whilst each of these examples is cell permeable, each displays a different localisation within the cell, as has been discussed in Chapter 1 (1.4.5): complex **(a)** has been suggested to localise in the outer mitochondrial membrane, where the target receptors are expressed; **(b)** has been shown to localise in lysosomal compartments by co-localisation studies with Lysotracker green; complex **(b)**, the isomer of **(a)**,

distributes quite well in the cytosol and stains the endoplasmic reticulum, again confirmed by localisation studies (using Brefeldin A); complex **(d)** is able to cross the nuclear membrane and stains the nucleoli of cells. Complexes **(a)** and **(b)** are thought to enter the cell via an endocytotic pathway. Molecules that enter cells via endocytosis are believed to be initially trapped in endocytotic vesicles and are subsequently transferred into endosomes. Endosomes age to become lysosomal compartments isolated from the rest of the cell. If complexes taken up by this mechanism are to localise in other regions or compartments inside of the cell then it is essential that they can escape from the endocytotic pathway.

4.1 Uptake of a Series of Complexes of Differing Charge and Lipophilicity

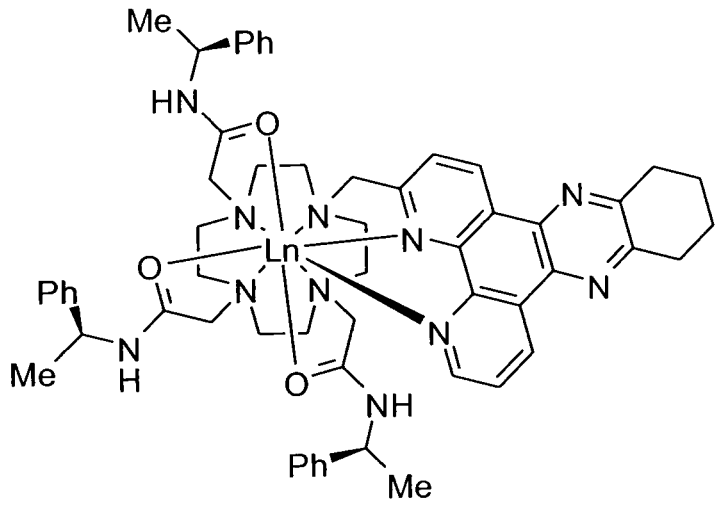

[Ln.1]

Figure 4. 2 – Structure of lanthanide complexes LnPh3dpqC, [Ln.1]

Preliminary experiments have previously been carried out which showed that [Ln.**1**] is taken up by NIH 3T3 mouse fibroblast cells (1 mM loading concentration). Time course analysis indicated that uptake of the europium complex appeared to be faster than for the terbium analogue and that migration occured over a period of hours through the cytosol, across the nuclear membrane and into the nucleus. In the absence of a positive concentration of complex in the external medium, the images showed a transfer of luminescence from the nucleus back to the cytoplasm.[2] It is difficult to explain why the europium and terbium complexes should exhibit different uptake times: both their structures and conformations are virtually identical. It has

been suggested that it could be due to the higher susceptibility of the terbium excited state to quenching by electron rich donors (urate[5], ascorbate and GC base pairs in DNA[8.1]) hence leading to a lower emissive intensity, perhaps with a higher concentration of complex being required before a signal can be observed.

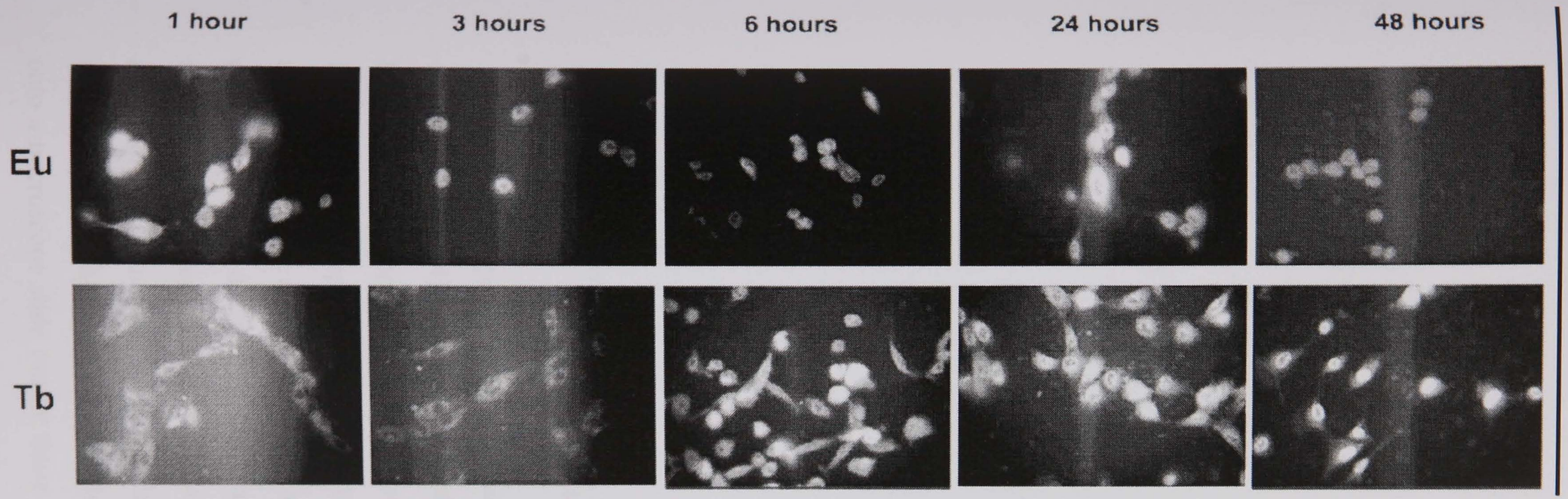

Figure 4. 3 – Microscopy images for the internalisation of the [Ln.1] Eu and Tb probes at different times. (1 mM loading concentration in DMEM supplemented with 50 mg ml^{-1} penecillin/streptomycin and 10 % NCS)

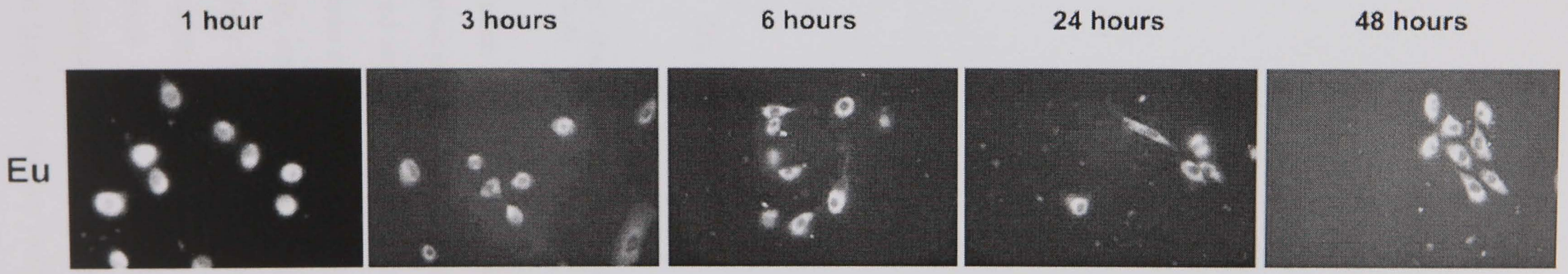

Figure 4. 4 – Microscopy images for the transit of Eu probe after 3 hours incubation and washing of unbound complex

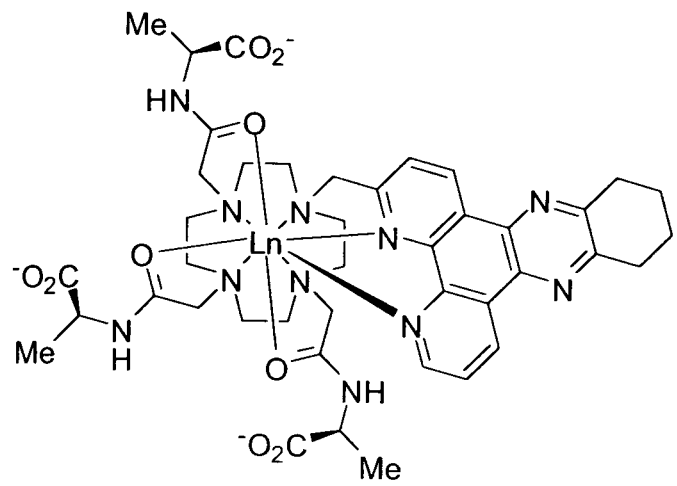

[Ln.**2**]

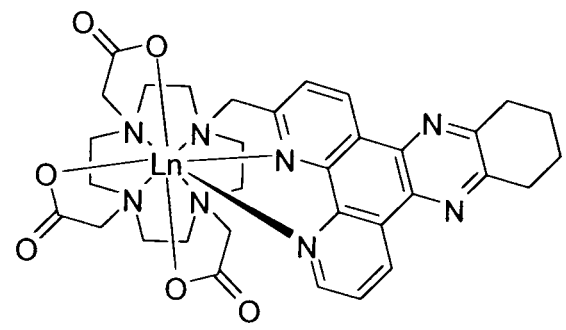

[Ln.**3**]

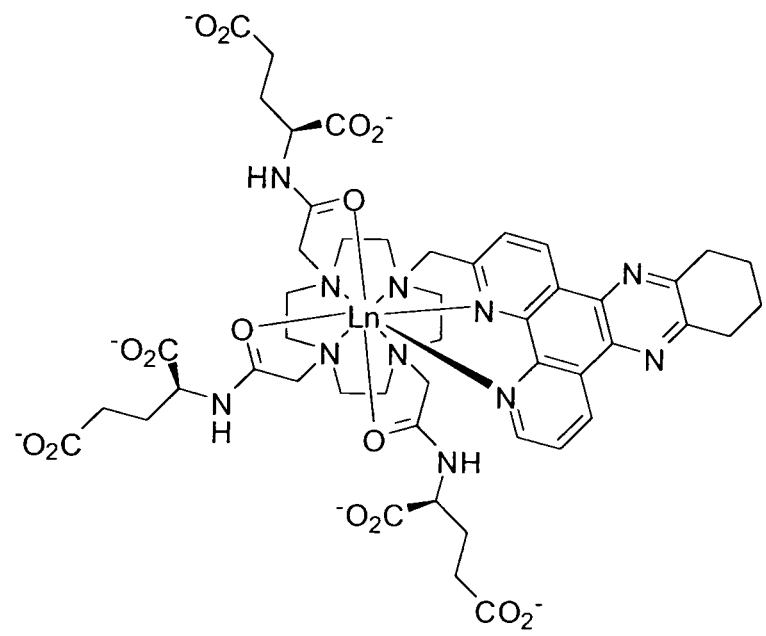

$[Ln.4]^{3-}$

Figure 4. 5 – Structures of complexes, LnAla3dpqC, [Ln.2], LnDO3AdpqC, [Ln.3] and LnGlu3dpqC, [Ln.4]

A series of comparative analyses was undertaken using the neutral and anionic complexes [Ln.**2-4**] to assess the relative importances of charge/lipophilicity on the uptake of the complexes. The cells were cultured in DMEM (Dulbecco's Modified Eagle Medium) supplemented with 10 % new-born calf serum, 50 μg ml^{-1} penicillin and streptomycin, and non-essential amino acids, on 10 mm cover slips. When the confluence on the cover slip reached approximately 70 %, the cells were loaded with an aqueous complex solution to give a final concentration in the growth medium of 1 mM. Following incubation for 24 hrs, the cover glass to which the cells were attached was washed repeatedly with PBS (phosphate buffered saline) and placed onto a microscope slide (under these conditions [Ln.**1**] is known to localise within

the cell nucleus). Each of the slides was imaged using a fluorescence microscope. Narrow excitation and emission filters were chosen (Excitation – 345 nm low pass or Zeiss G365; Emission – Eu 620 ± 25 nm or 575 – 625 nm band pass, Tb 546 ± 25 nm band pass) such that the chromophore was irradiated at wavelengths corresponding only to its longest wavelength absorbance (i.e. centred at 348 nm) and that the amount of scattered light reaching the CCD was minimised, to improve the signal to noise ratio.

In capturing the images, it was apparent that considerably longer exposure times (by a factor of 3-4) were required to image luminescence from cells containing any of complexes [Ln.**2**-**4**] when compared to cells loaded with [Ln.**1**] under identical conditions. Even under these conditions, the signal to noise ratio was low and was only slightly above the level of background and scattered fluorescence; specific localisation was difficult to discern and there did not appear to be any nuclear localisation.

In order to provide a further example of a cationic complex against which complexes [Ln.**2**-**4**] could be compared, [Tb.**2**] was re-esterified in dry (acidic) methanol to give the tri-positive methyl ester complex, [Tb.**2a**] as its chloride salt (Figure 4.6). In contrast to its neutral carboxylate analogue, it appeared to be taken up to a similar extent as [Ln.**1**] giving images that were considerably brighter than the unstained control sample.

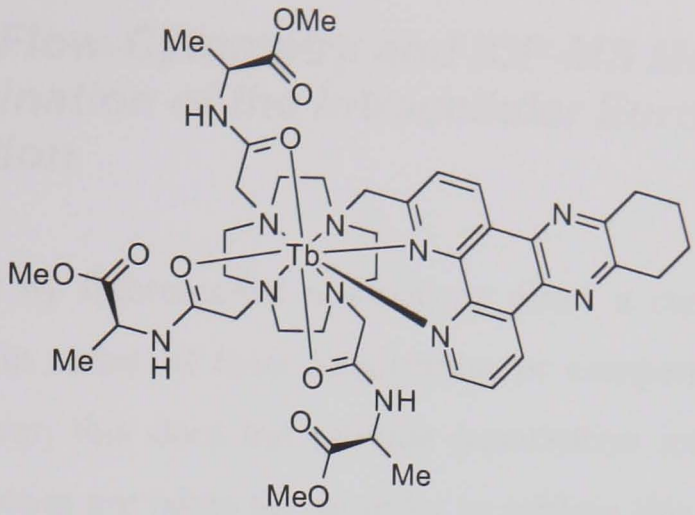

[Tb.**2a**]

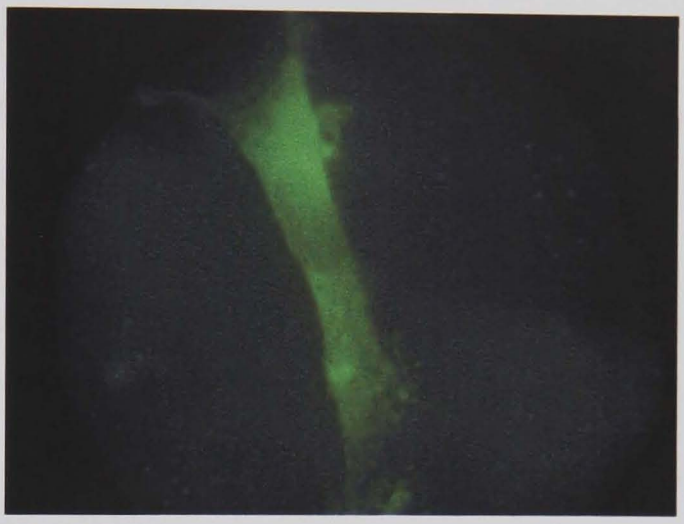

Figure 4. 6 – Structure of complex TbAlaMe3dpqC, [Tb.2a] (upper); Fluorescence microscope image (0.5 mM complex concentration, 4 hours post-incubation) (lower)

These results imply that either cellular uptake of the lipophilic and cationic complex [Ln.**1**] is favoured compared to that of the related neutral and anionic complexes [Ln.**2-4**], or that the complexes may be taken up to a similar extent but emission from complexes [Ln.**2-4**] is more strongly quenched '*in cellulo*' than for complex [Ln.**1**]. (Chapter 3 provides a full description of the differing sensitivities of the series of complexes to quenching by electron-rich donors). The coordination environment of the complex inside the cell is also not known, but if for example the complexes were bound to protein this too would affect their susceptibilities to quenching. In order to confirm to what extent the complexes were taken up by the cells, an experiment was undertaken to determine the intracellular lanthanide concentration.

4.2 Combined Flow-Cytometry and ICP-MS Methodology for the Determination of the Intracellular Europium Concentration

The images obtained by fluorescence microscopy allow a comparison to be made between complexes in terms of their localisation or compartmentalisation profile within a cell. However, this does not provide quantitative information about how effectively the complexes are taken up. In order to achieve this, the concentration of complex per cell was determined through a combination of flow-cytometry to determine the number of cells in a population, and ICP-MS (inductively coupled plasma – mass spectrometry) to determine the total lanthanide (europium) concentration. From knowledge of the number of cells, the total number of moles of europium in the sample and an approximate volume for a cell, the concentration per cell can be determined, also allowing a comparison to be drawn with the loading concentration. Alternatively, the number of moles of complex per cell can be quoted, eliminating the need to estimate the cell volume and allowing a comparison to be made between different cell lines.

4.2.1 Flow Cytometry

4.2.1.1 Instrumental Details: Background

Flow cytometry is a fluorescence based technique that allows the counting and sorting of a population of cells. The sample is introduced into the flow chamber and is hydrodynamically focused in a sheath of PBS. Hydrodynamic focusing allows the diameter of the flow to be narrowed to such an extent that single cells are forced down the centre of the stream. The cells are interrogated by a laser appropriate for the lumophore under study. Light that is emitted is directed to a series of detectors, usually focussed onto a photomultiplier tube, PMT. The range of wavelengths that are permitted to reach each of the detectors is controlled through the use of band-pass filters, allowing multi-colour analysis to be undertaken using two or more different luminescent stains.

4.2.1.2 Detection of Long-Lived Lanthanide Emission: Experimental Constraints

The speed of a cell as it passes through the flow chamber is of the order of 1 - 25 ms^{-1} (depending upon the operating pressure and nozzle diameter); the emissive lifetimes of the series of europium and terbium complexes are of the order of 1 – 2 ms. In conventional instruments, the laser intersection point is imaged to a pinhole located in front of the PMT; similarly to confocal microscopy, this is done to eliminate out of focus light and scattered laser light from reaching the detector. However, due to the long emissive lifetimes of the lanthanide ions, only a small fraction of the total emission reaches the detector. Unless very high complex concentrations are used, this unfortunately renders them impractical as lumophores for cell sorting and counting. Time-resolved flow cytometers have been developed earlier for the measurement of lanthanide chelate fluorescence.[9] Emission is collected from the cell as it covers a distance of several millimetres passing through the flow chamber, corresponding to a time of the same order as the emissive lifetime of the complexes. A pinhole arrangement is not needed to prevent scattered light from reaching the detector since the laser is effectively 'off' during the acquisition period.

4.2.1.3 Overcoming or Circumventing These Constraints

The combined flow-cytometry and ICP-MS method has previously been used to determine the intracellular europium concentration of complex $EuPheOEt_2ThiaH$ (Figure 4.7).

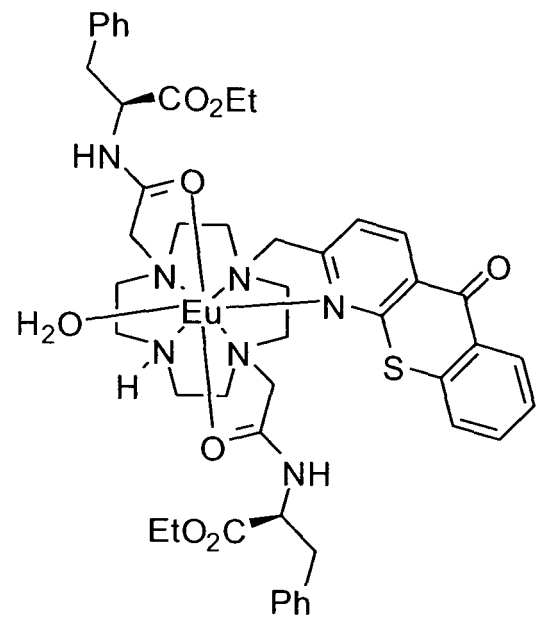

Figure 4. 7 – Structure of EuPheOEt$_2$ThiaH

The emission spectrum of complex EuPheOEt$_2$ThiaH consists of two components, short lived fluorescence from the sensitising chromophore and longer lived europium centred emission (Figure 4.8).

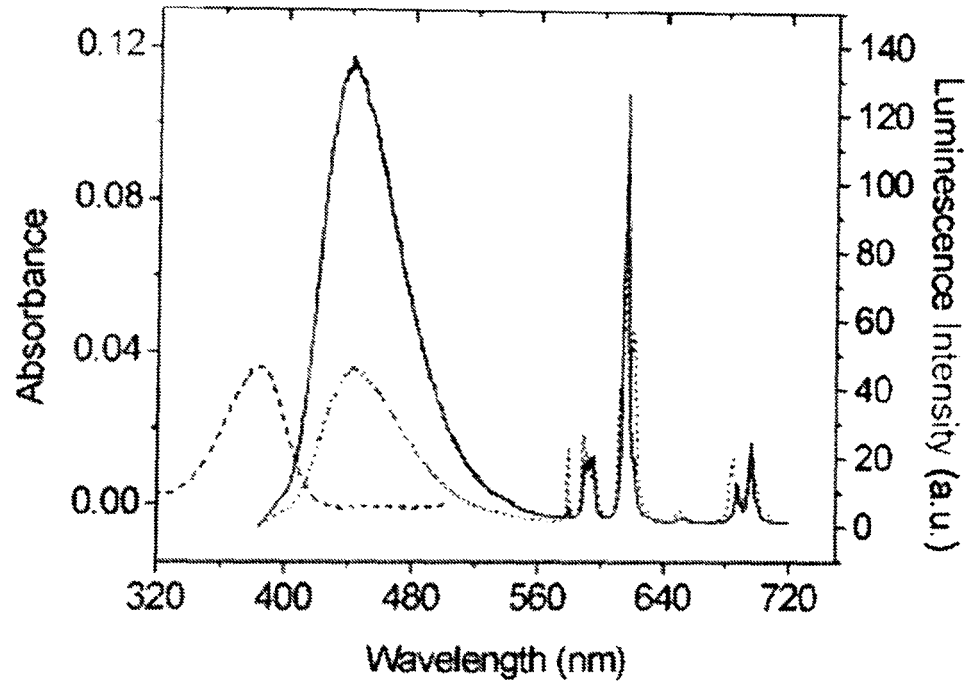

Figure 4. 8 - Absorption (dashed line) and total emission spectra of EuPheOEt$_2$ThiaH (5 μM) in water (dotted line) and in the presence of L-Asn (solid line, pH 7.3, 300 μM).

The dual emission indicates that the rate constants for deactivation of the singlet excited state by fluorescence and energy transfer to the triplet excited state are of a similar order. To obtain as high an emissive quantum yield as possible it is desirable to have a quantum yield of triplet formation that is close to unity, however in this case a degree of fluorescence provides a useful handle that allows cells that are

stained with the complex to be sorted by detection at wavelengths appropriate for the chromophore fluorescent emission.[9]

The series of complexes that are the subject of the current work all incorporate a tetraazatriphenylene sensitising moiety. Virtually no fluorescence is observed from this chromophore either as a free species, or when it is coordinated to a lanthanide centre. Consequentially, it was necessary to find an alternative means through which the sample of cells could be labelled. This was achieved by dual labelling with the complex of interest and the acetylmethoxy ester of calcein AM.

Calcein AM is a dye that is often used to assess cell viability in eukaryotic cells; in live cells, the non-fluorescent calcein AM is converted to green fluorescent calcein, following ester hydrolysis catalysed by intracellular esterases. It was therefore decided to co-localise CHO cells with both the lanthanide complex and calcein AM, allowing live cells containing the lanthanide complex to be selectively sorted and unviable cells discarded.

As a control experiment, it was necessary to confirm that for a population of cells co-loaded with both calcein AM and complex, in every case where green calcein emission could be observed, so too could lanthanide centred emission. CHO Cells loaded with either europium complex $EuPheOEt_2ThiaH$, or [Eu.**1**] (50 μM, 3 hours incubation - both previously shown to be taken up by cells and to be observable by fluorescence microscopy) and Calcein AM (2 μM, 30 min incubation) were analysed by fluorescence microscopy using appropriate excitation and emission filters so that the red europium and green calcein emission could be examined separately. An additional advantage to the experiment was that it allowed an assessment of the viability of the cells to be made: only live cells contain the active esterase enzymes necessary to catalyse hydrolysis of the acetylmethoxy ester. Using both complexes it was found that in >97 % of the cells examined, green and red emission could be observed, thus both validating the flow cytometry method and providing evidence of the viability of the populations of cells.

4.2.1.4 Experiment to Sort and Collect a Known Number of Cells Co-Labelled with Europium Complex and Calcein AM

Populations of CHO cells were cultured to approximately 70 % confluence in 75 cm^3 culture flasks in F-12 (Ham) growth medium supplemented with 10 % FBS (foetal bovine serum) and 50 $\mu g\ ml^{-1}$ penicillin and streptomycin. Additions of one or both of the europium complex and calcein AM were made as described below:

1) CHO cells only – a reference sample used to set up the flow cytometer;
2) CHO cells + Calcein AM (2 μM, 30 mins incubation) – a reference sample used to set up detection parameters;
3) CHO cells + complex (one of [Eu.**1**, **3** or **4**]) (~ 50 μM, 3 hours incubation) + Calcein AM (2 μM, 30 mins incubation).

Each of the cultures was washed 5 times with PBS to ensure that excess complex had been removed and was harvested using trypsin. The cells were collected by centrifugation and resuspended in buffer; again the process was repeated 3 times. Each of the populations was finally suspended in 1 ml of phosphate buffer for injection into the flow cytometer.

Following successful sorting and collection, populations of cells co-loaded with both calcein and complex [Eu.**1**, **3** or **4**] were recovered, containing a known number of cells. Typically, 10 000 – 100 000 cells were sorted and counted in this operation.

4.2.2 ICP-MS Analyses

In inductively coupled plasma mass spectrometry, ICP-MS, the accurate determination of the concentration of an element in a sample may be determined; detection limits are of the order of ppt – ppb. In the ICP-MS method, the sample is injected into an argon plasma, where the elements in the sample are atomised and ionised; these ions are then passed through a series of cones to a quadrupole mass spectrometer. Through calibration with elemental standards, accurate concentrations can be calculated since the observed ion signal is proportional to the concentration.

Prior to injection of the sample into the ICP-mass spectrometer, it was necessary to dilute quantitatively the samples using 3 % nitric acid solution. It has previously been noted within the group, that the ICP-MS or OES determination of gadolinium concentration in cyclen based MRI contrast agents did not always give accurate results following quantitative dilution in water. It is thought that this is due to adherence of the complex to the sample vial. Addition of nitric acid overcomes this problem.

4.2.3 Results and Discussion

Complex	Medium Concentration	Intracellular Concentration
$EuPh_3dpqC$, [Eu.**1**]	49 μM	26 μM
EuDO3AdpqC, [Eu.**3**]	31 μM	12 μM
$EuGlu_3dpqC$, [Eu.**4**]	33 μM	40 μM

Table 4. 1 – Eu concentrations determined by ICP-MS for CHO cells incubated in the presence of [Eu.1], [Eu.3] and [Eu.4] (3 h). In each case values reported represent the concentration of complex present in the external growth medium and the concentration per cell (a mean cell volume of 4000 μm^3 was assumed)

Values reported in Table 4.1 show that each of the complexes is taken up to a similar extent by the cells; intracellular and extracellular concentrations also appear to be of the same magnitude. These results indicate that it is the extent to which the complexes are quenched '*in cellulo*' that limits their utility as fluorescent probes, and not uptake preference. The intracellular concentration is an average across the whole cell and therefore it is suggested that the complex must be actively concentrated in certain compartments in accordance with the punctuate nature of localisation.

4.3 Concentration and Time Dependent Localisation of Complex [Ln.1]

The uptake of terbium complex [Tb.**1**] by mouse skin fibroblasts (NIH 3T3) was investigated further as a function of both loading concentration and incubation time. Cultured cells were exposed to DMEM growth medium (supplemented with 10 % NCS and 50 μg ml^{-1} penicillin and streptomycin) containing between 50 μM and 1 mM solution of the terbium complex. The living cells were imaged by fluorescence

microscopy at time intervals in the range of 30 minutes to 48 hours. In order to assess the effect on the localised complex of removing the external concentration gradient, a further analysis was undertaken by incubating the cells for up to 24 hours, then replacing the complex containing medium with fresh medium (after washing the cells several time with PBS). Representative images are shown in Figures 4.9 – 4.11.

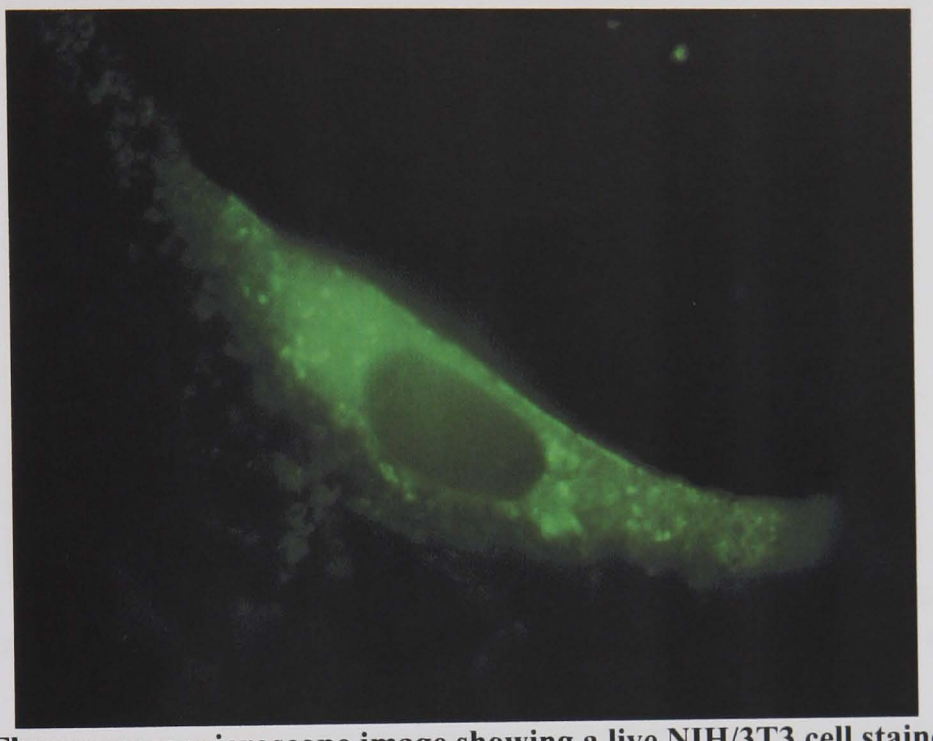

Figure 4. 9 – Fluroescence microscope image showing a live NIH/3T3 cell stained with [Tb.1] (0.3 mM in growth medium), 4 h post-incubation

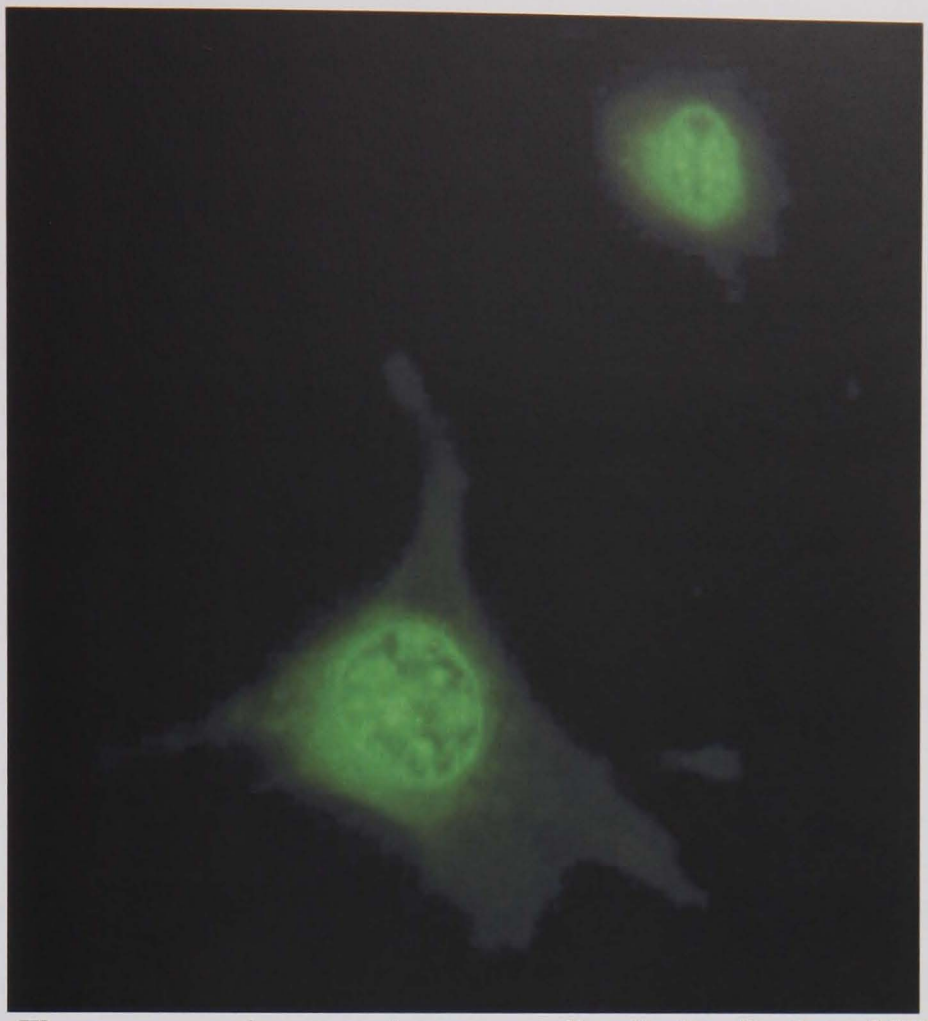

Figure 4. 10 – Fluorescence microscope image revealing the localisation of [Tb.1] (1 mM in medium, 24 h post-incubation) in the cell nucleus and defining the nuclear membrane

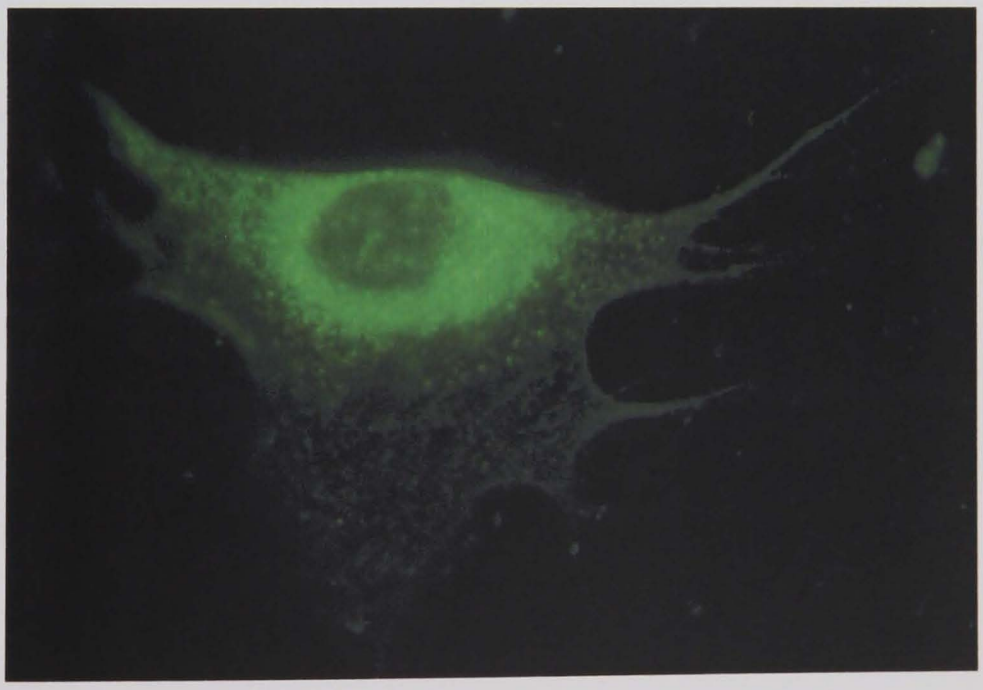

Figure 4. 11 – Fluorescence microscope image highlighting the egress of the [Tb.1] complex out of the cell nucleus and back into the extra-nuclear compartments, 24 h after removal of the external concentration gradient.

Figure 4.9, is taken of a cell that has been incubated in growth medium containing 0.3 mM terbium complex for a period of 4 h. The complex is distributed throughout the cytoplasm and shows a punctuate localisation that is more intense around the cell nucleus (although this remains dark). At higher concentrations and with longer

incubation periods, the complex is able to migrate across the nuclear membrane. In Figure 4.10 (1 mM, 24 h incubation) the luminescence highlights the nucleus and appears to be concentrated in certain compartments; the nuclear membrane is clearly delineated; diffuse localisation persists in the cytoplasm, but again appears to be concentrated around the nucleus. Following removal of the external concentration gradient, the complex migrates out of the nucleus. Figure 4.11 was captured 24 h after the complex had been removed from the external medium. Distribution is again in the cytosol; areas of the image also have a spotty appearance, suggesting localisation in a particular cell organelle. However, this localisation is different to that observed using a low external concentration of complex with short incubation times (*cf.* Figure 4.3).

These experiments provide confirmation that the complex is taken up by the cell and is able to cross the nuclear membrane in the presence of a sufficient external concentration gradient; the process reverses upon removal of the complex from the growth medium. At lower concentrations i.e. < 0.5 mM localisation is found only outside of the cell nucleus; the complex is taken up rapidly by the cell (15 – 30 mins). These conditions are the most relevant for practical applications *i.e.* low external concentration and short incubation times; Figures 4.12 – 4.13 show a field of view for cells labelled with [Tb.**1**] (100 μM loading concentration, 3 h incubation) and demonstrates the consistency of labelling across the sample.

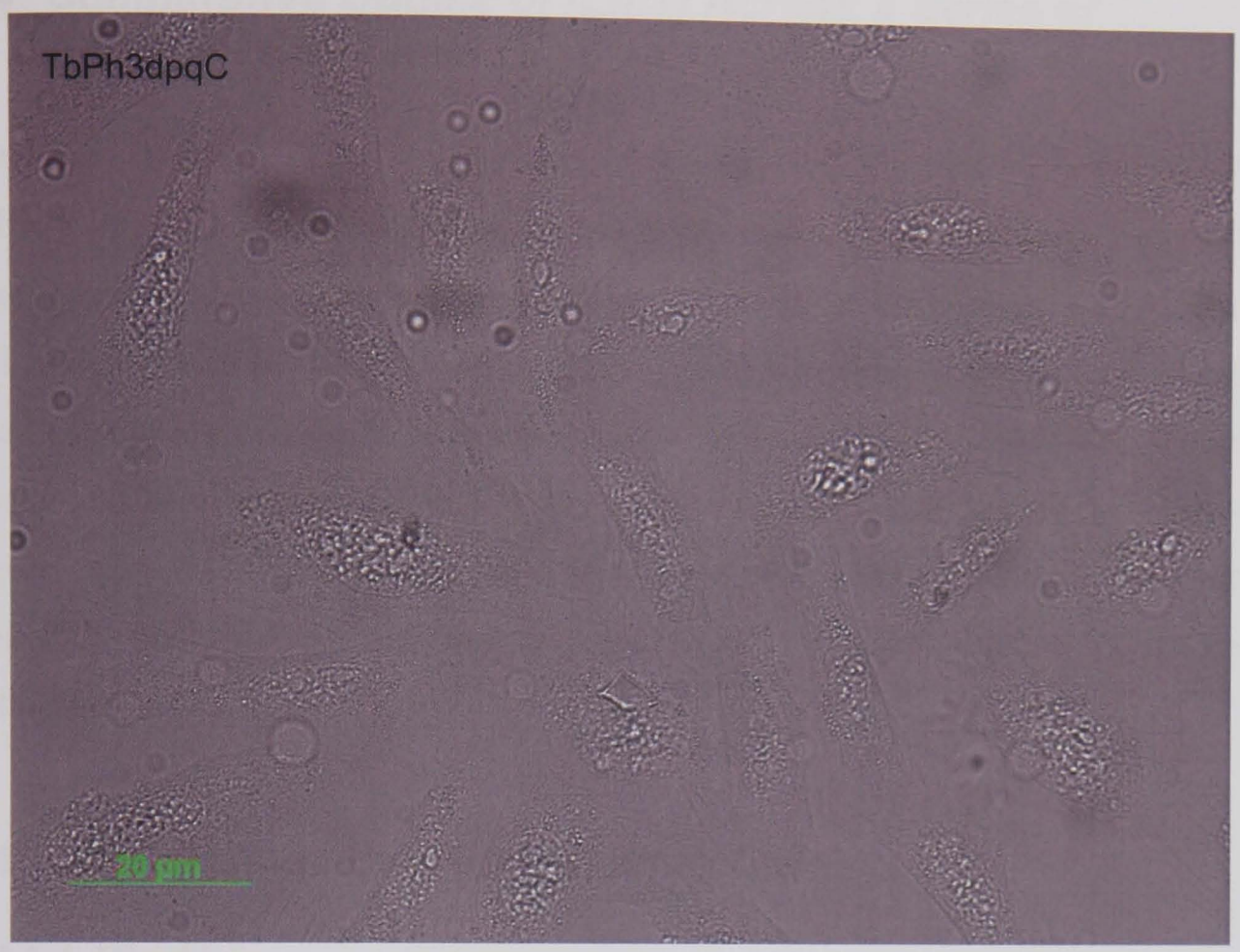

Figure 4. 12 – Transmitted microscope image of CHO cells loaded with [Tb.1] (100µM, 3 h post-incubation)

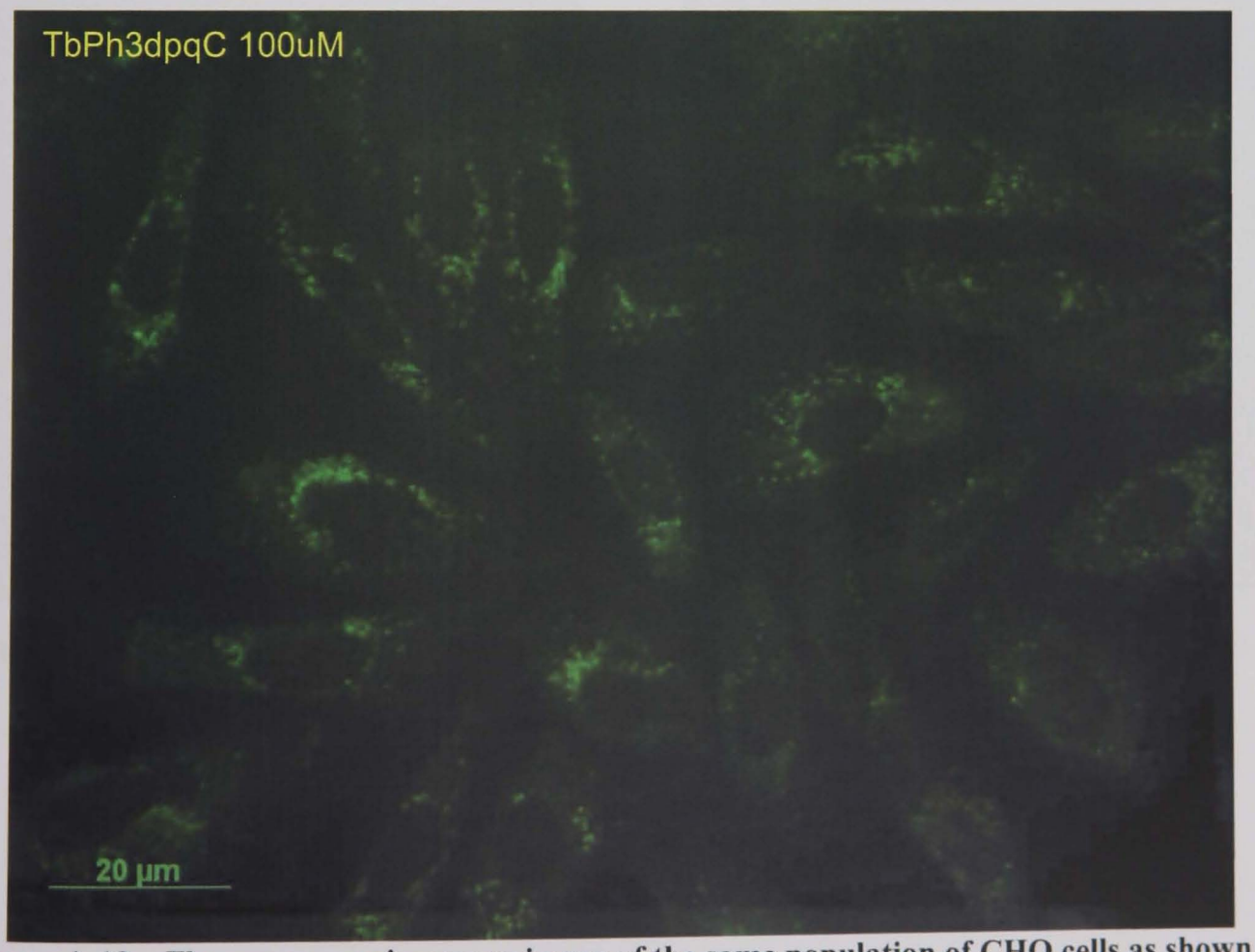

Figure 4. 13 – Fluorescence microscope image of the same population of CHO cells as shown in Figure 4.12 loaded with [Ln.1] (100 µM, 3 h post-incubation).

4.4 Comparative Uptake of [Ln.1] Across a Series of Adherent Cell Lines

Uptake of complex [Tb.**1**] by a range of primary (HDF), transformed (NIH 3T3, CHO, COS, HEK) and carcinoma (HeLa) cell lines has been examined. Images that were taken using a time resolved fluorescence microscope were carried out in collaboration with M. Laget, Cisbio, France, using 337 nm excitation, corresponding to a nitrogen laser line). In each case, under the same loading conditions, a similar uptake and localisation profile was observed. Representative images are shown in Figures 4.14 – 4.19; common features are a spotty compartmentalisation centred around the nucleus and a diffuse brightness in the cytosol extending to the periphery of the cell.

4.4.1 HEK (Human Embryonic Kidney Cells)

4.4.1.1 [Eu.1]

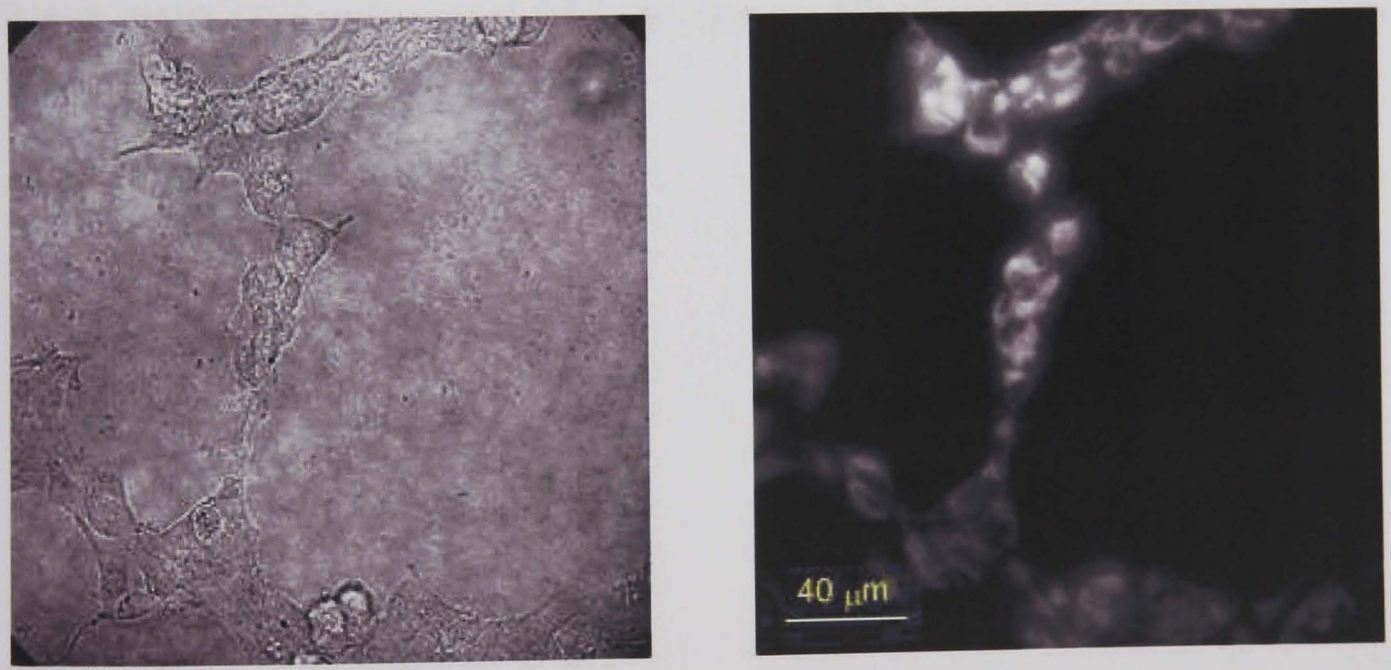

Figure 4. 14 – Transmission (left) and fluorescence microscope images (right) of HEK cells localised with EuPh3dpqC, [Eu.1] (50 µM, 24 h post-incubation)

4.4.1.2 [Tb.1]

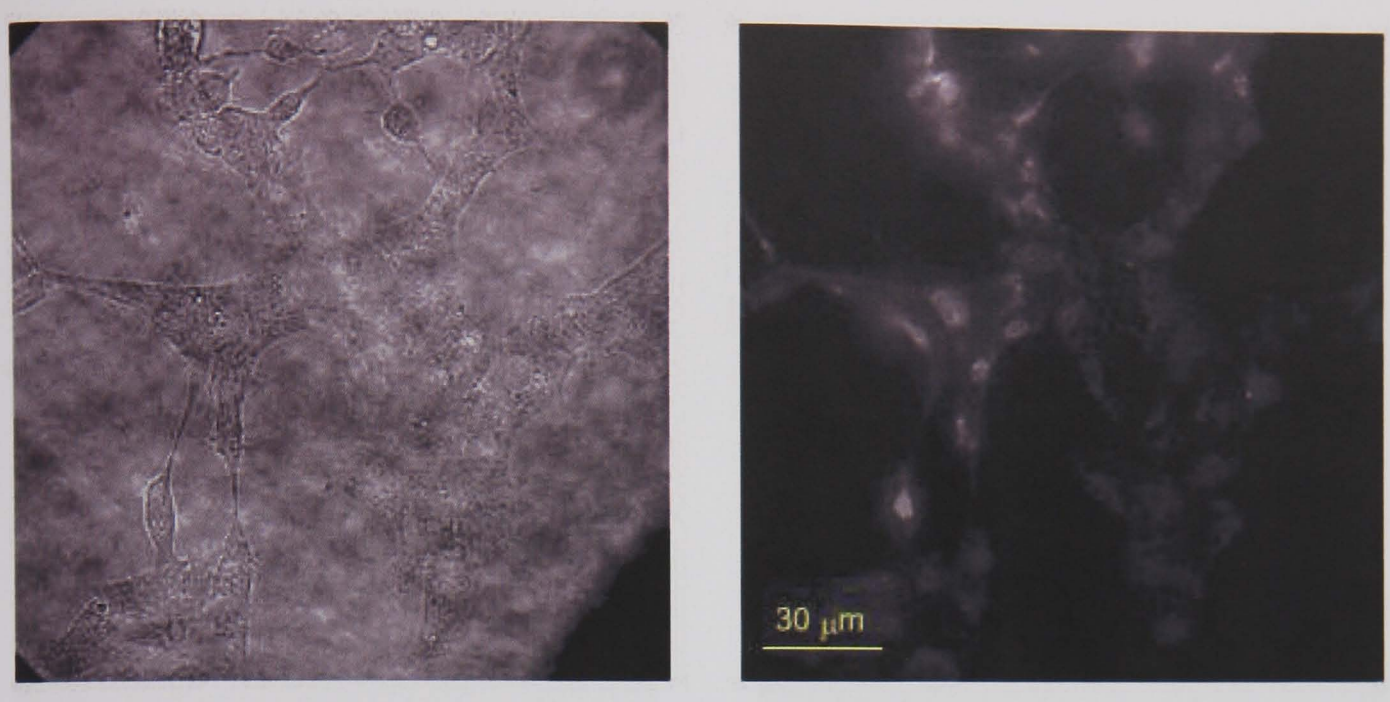

Figure 4. 15 – Transmission (left) and fluorescence microscope images (right) of HEK cells localised with TbPh3dpqC, [Tb.1] (50 μM, 24 h post-incubation)

4.4.2 COS (Transformed African Green Monkey Kidney Fibroblast Cells)

4.4.2.1 [Eu.1]

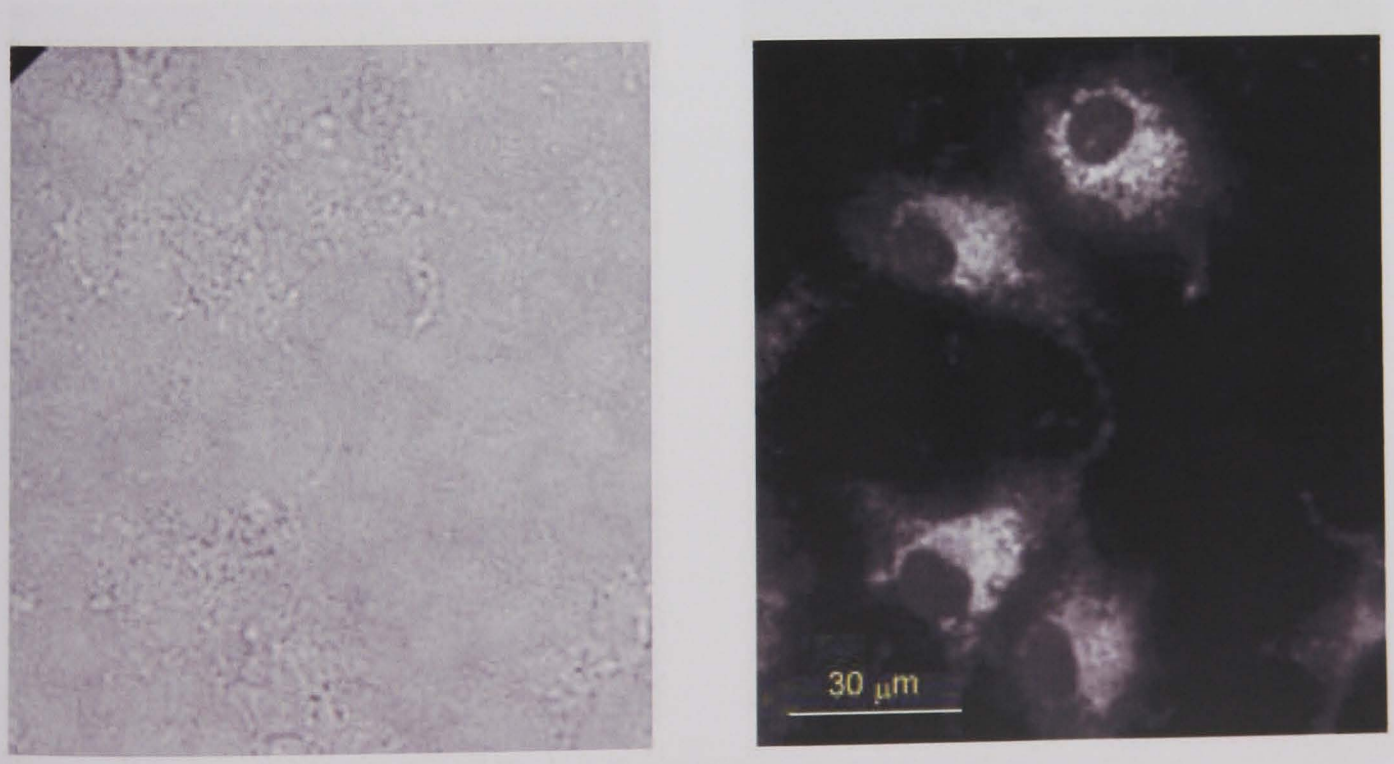

Figure 4. 16 – Transmission (left) and fluorescence microscope images (right) of COS cells localised with EuPh3dpqC, [Eu.1] (50 μM, 24 h post-incubation)

4.4.2.2 [Tb.1]

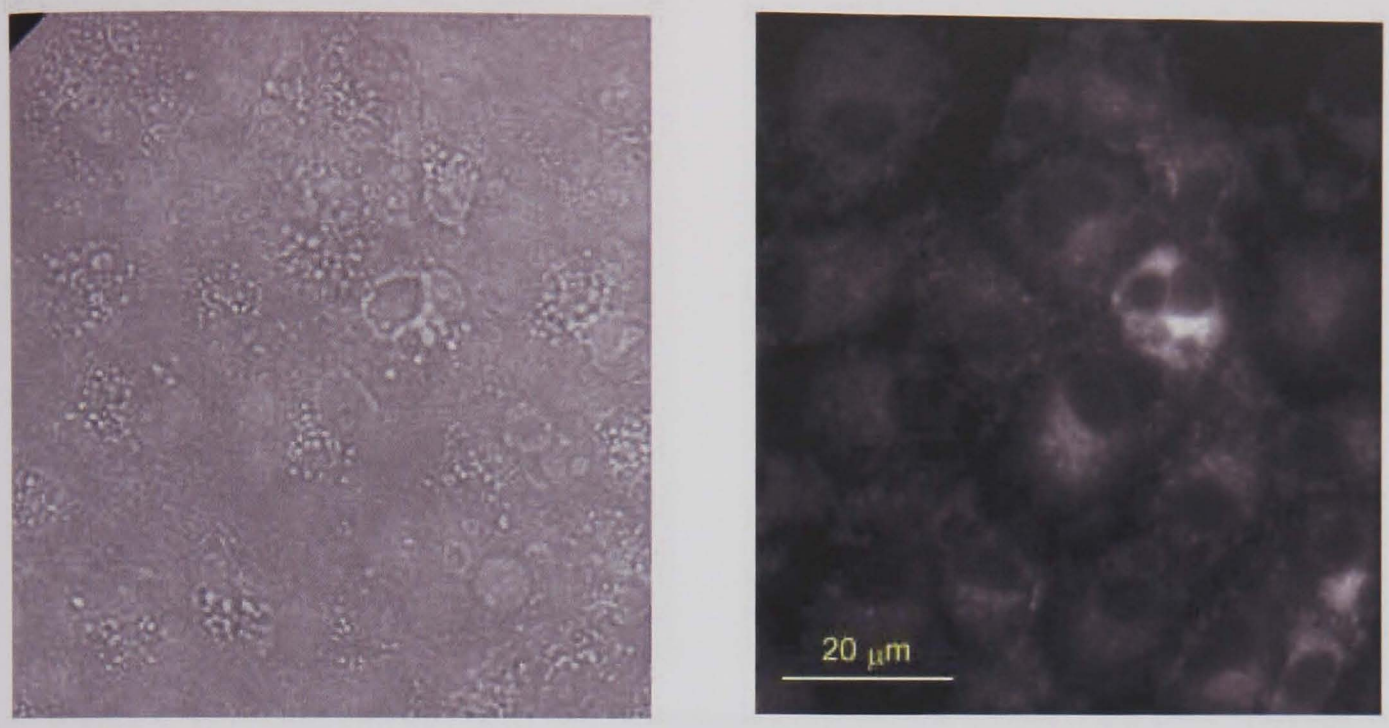

Figure 4. 17 – Transmission (left) and fluorescence microscope images (right) of COS cells localised with TbPh3dpqC, [Tb.1] (50 μM, 24 h post-incubation)

4.4.3 CHO (Chinese Hamster Ovary Cells)

4.4.3.1 [Eu.1]

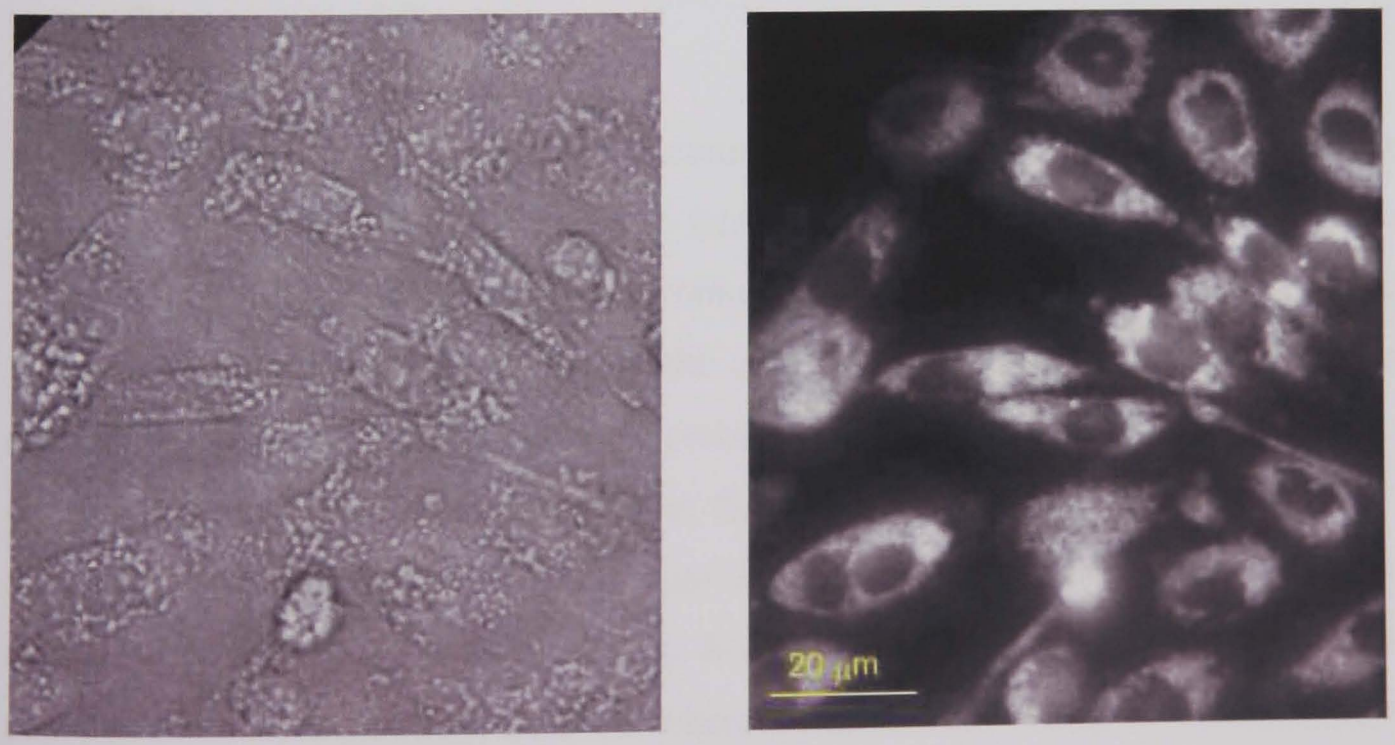

Figure 4. 18 – Transmission (left) and fluorescence microscope images (right) of CHO cells localised with EuPh3dpqC, [Eu.1] (50 μM, 24 h post-incubation)

4.4.3.2 [Tb.1]

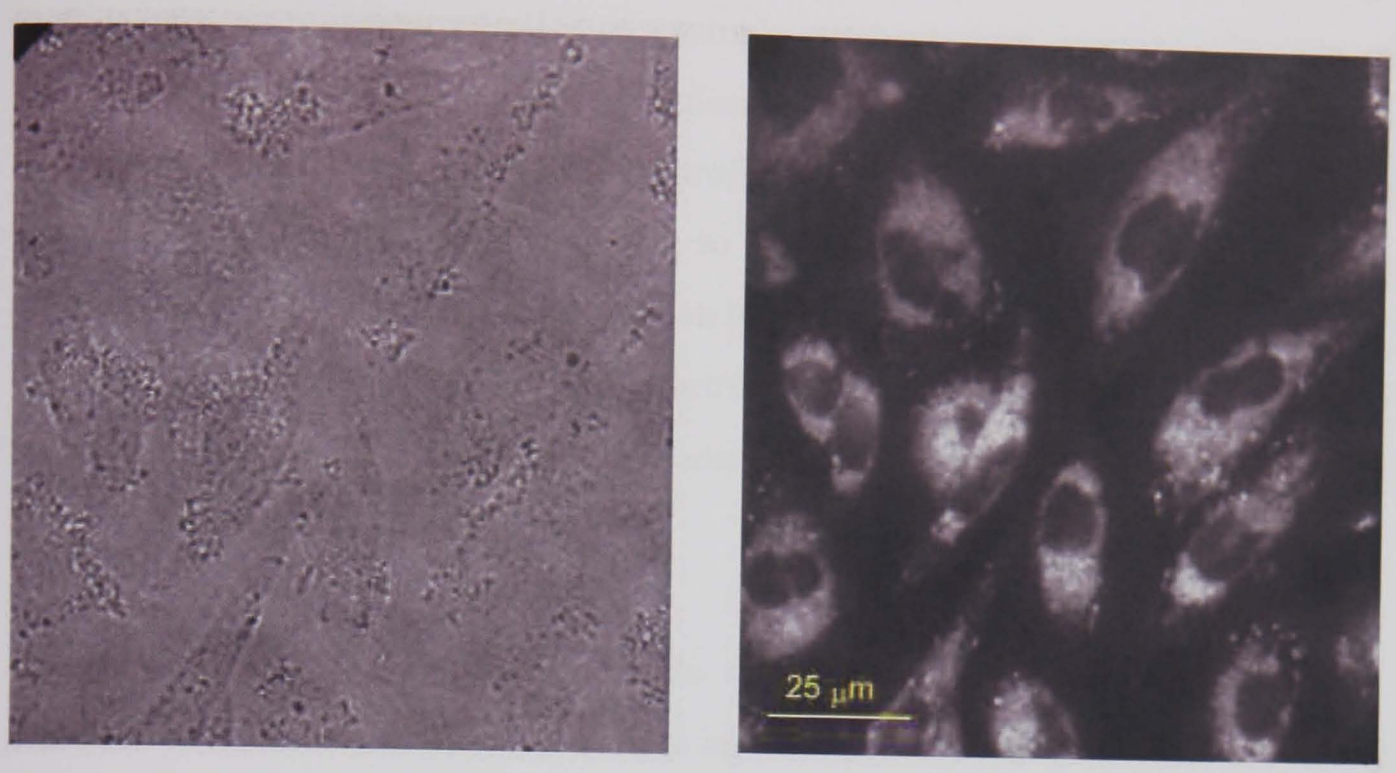

Figure 4. 19 – Transmission (left) and fluorescence microscope images (right) of CHO cells localised with TbPh3dpqC, [Tb.1] (50 μM, 24 h post-incubation)

4.5 Assessing the Protein Binding Affinity of [Gd.1]

4.5.1 Change in the Form of the NMRD Profile of [Gd.1] in the Presence of Protein

A series of lanthanide complexes of a common ligand would be expected to adopt similar structures. However, different lanthanide ions are amenable to specific analytical techniques. For example, europium is a useful fluorescence based probe since its fine structure is sensitive to the coordination environment of the ion; in contrast, gadolinium complexes can be probed using magnetic resonance techniques, in particular in terms of their affect on the relaxation times of bound or closely diffusing water molecules. The gadolinium complex [Ln.**1**] was synthesised in order to assess its affinity for protein binding. It was thought that uptake of the complex could be protein mediated; in addition, where complexes are protein bound, they may be expected to display a different sensitivity to a collisional quenching process.

NMRD (Nuclear Magnetic Resonance Dispersion) spectroscopy monitors the change in relaxivity per unit concentration of a sample relative to bulk water as a function of the magnetic field. A comprehensive explanation of relaxation theory and the factors that govern the form of an NMRD profile have been provided in reviews by Lauffer[17] and Caravan[18] It is sufficient to say in the current context, that protein binding would be predicted to give both an increase in relaxivity at all field strengths, and a change in the form of the spectrum at high field (where the rotational correlation term, τ_r associated with the reorientation of the metal ion-solvent nucleus vector, becomes dominant).

Figures 4.20 – 4.21 are NMRD profiles that were recorded for complex [Gd.**1**]. Figure 4.20 was measured for the sample in water at 25 °C, upon addition of a small excess of HSA (human serum albumin). The relaxivity increased by a factor of more than two in the range 0.01 – 10 MHz and exhibited a change in form and a much larger increase to higher field (Figure 4.21). In order to gain a more complete picture of the behaviour at high field, measurements were made (Ivrea, Italy) on a second instrument over the range 0.01 – 70 MHz. The profile (Figure 4.22) shows a narrow peak centred at ca. 30 MHz, indicating that a few second sphere water molecules are tightly bound to the complex. The form of the NMRD profile is typical of a complex that exhibits both a long τ_r and a relatively long water exchange lifetime, τ_m, for the second-sphere waters. In each case, this behaviour is indicative of a protein bound complex. It should be noted that the relaxivities are relatively high in the presence of protein, for a q = 0 system.[19]

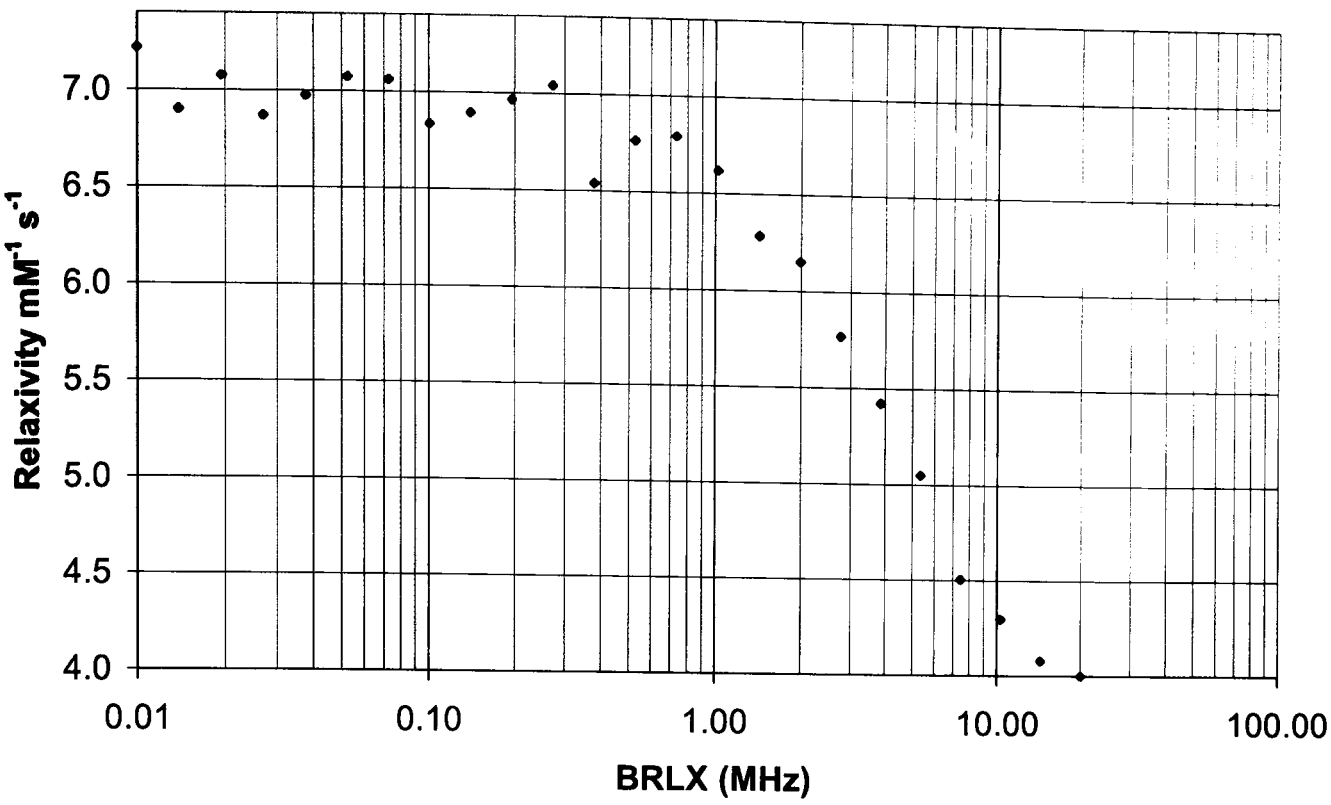

Figure 4. 20 – NMRD profile of [GdPh3dpqC]Cl_3, [Gd.1] (298 K, concentration = 0.2 mM, water T_1 correction = 0.38 s)

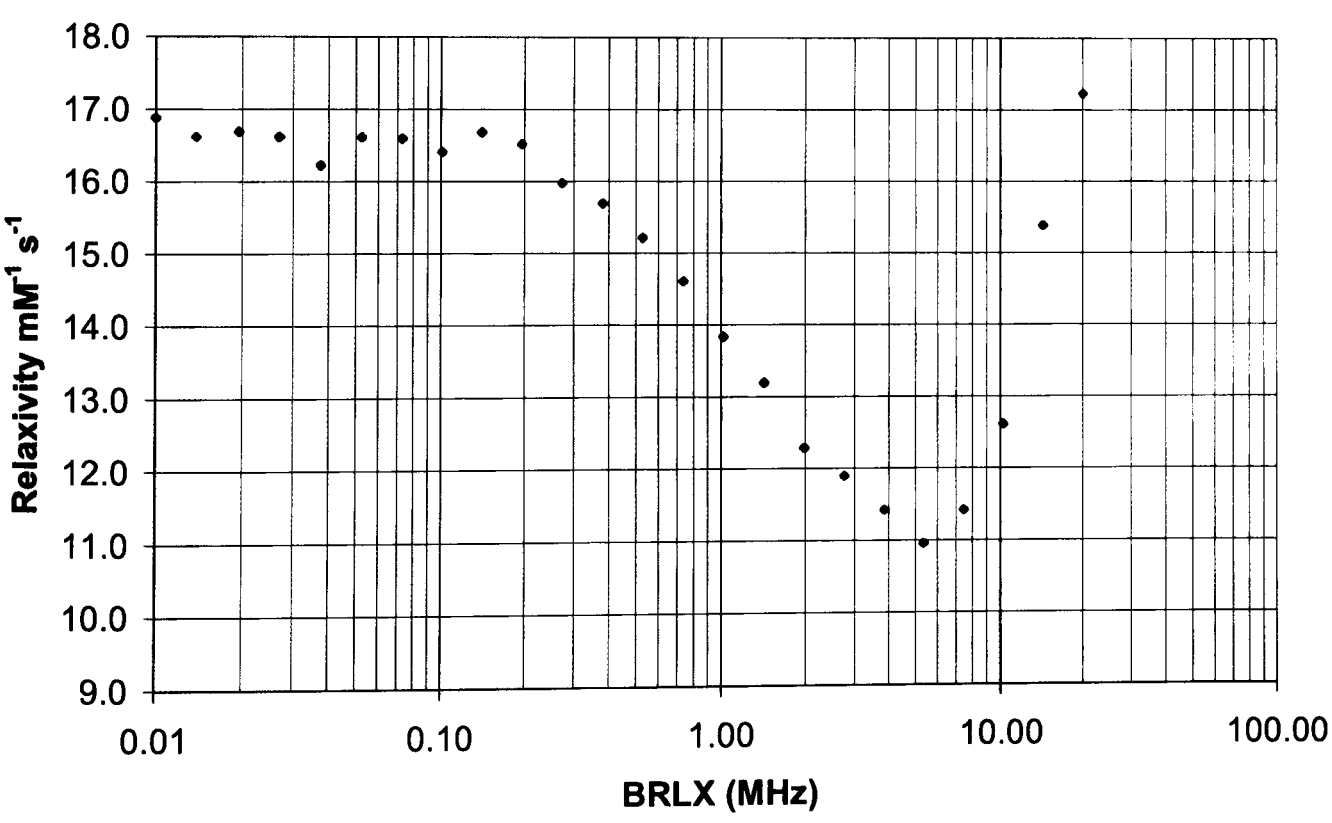

Figure 4. 21 – NMRD profile of [GdPh3dpqC]Cl_3, [Gd.1], with HSA (298 K, complex concentration = 0.2 mM, water T_1 correction = 0.38 s)

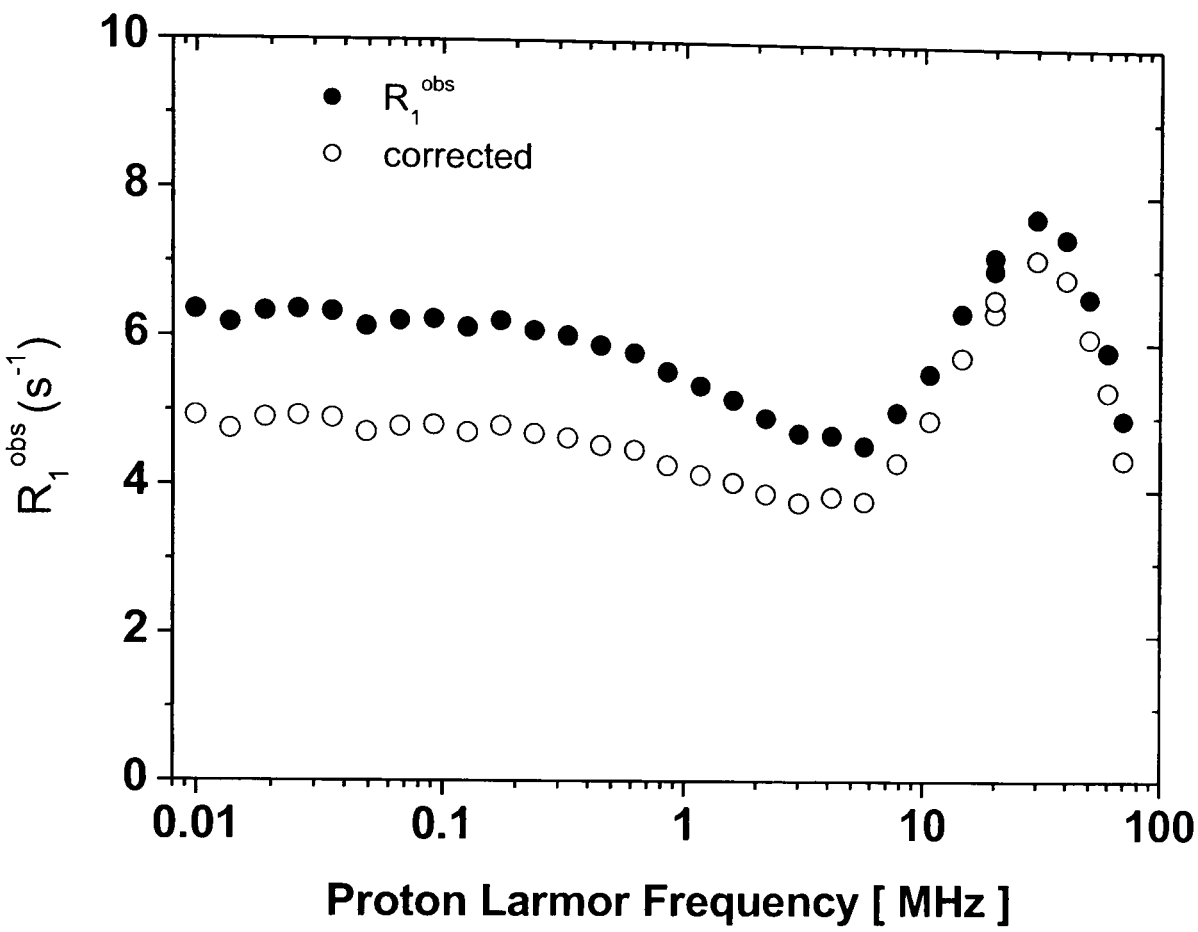

Figure 4. 22 NMRD profile of [Gd.1], The vertical axis is expressed as a relaxation rate rather than a relaxivity. The form of the spectrum is identical in each case. (298 K, complex concentration = 0.4 mM, 'corrected' refers to data, for which the protein contribution to relaxivity has been subtracted)

4.5.2 Assessment of the Binding Affinity of [Gd.1] to HSA

The relaxivity of [Gd.**1**] was measured as a function of added HSA at 37 °C using a Bruker Minispec at 60 MHz (Figure 4.23). The concentration of the complex was determined to be 1.69 mM for these analyses.

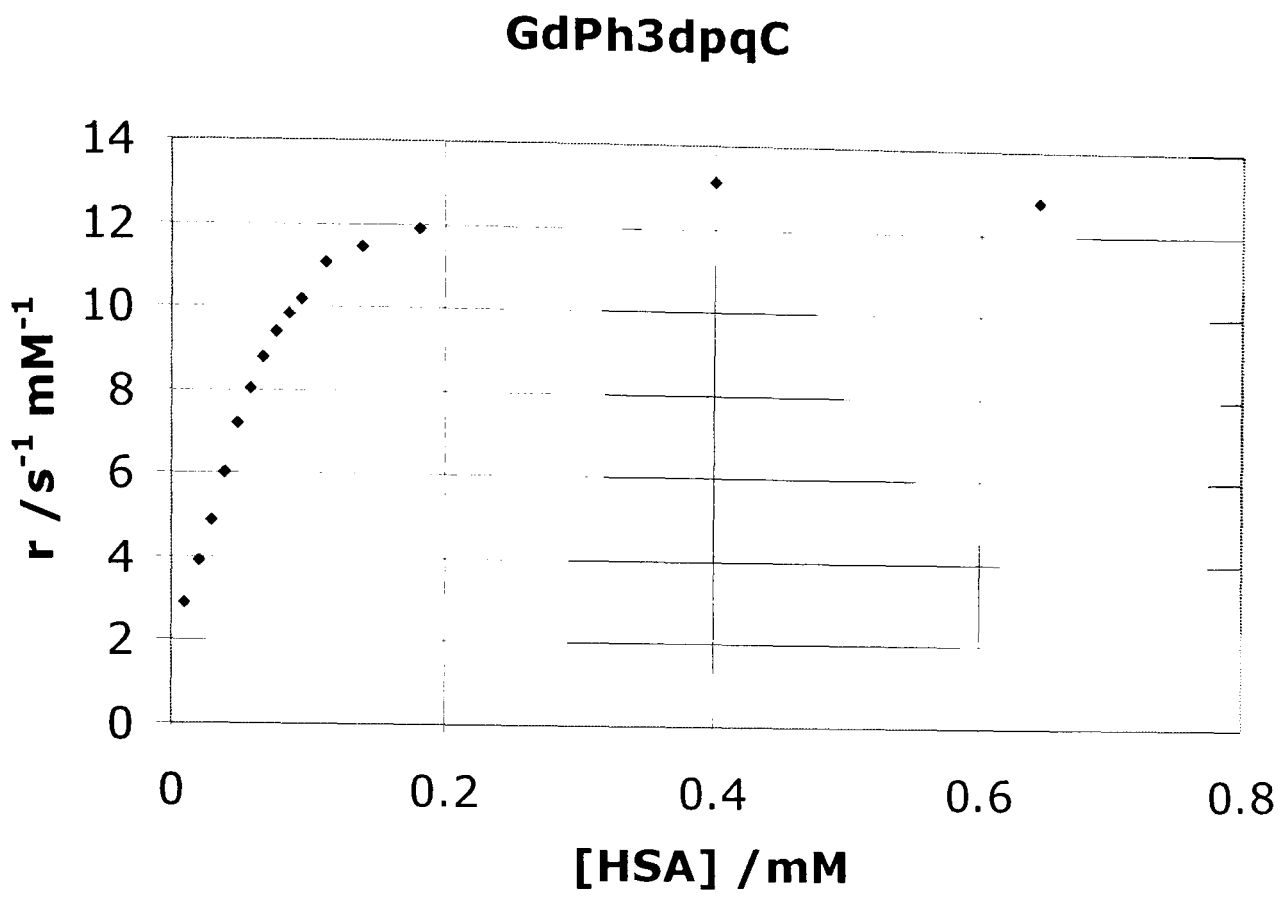

Figure 4. 23 – A plot of relaxivity versus concentration of human serum albumin in order to provide a measure of the binding affinity

The binding constant for coordination of the complex to HSA could not be determined since the data does not follow a simple exponential fit. However, the large increase in relaxivity of approximately 10 s^{-1} mM^{-1} confirms that the affinity towards binding is high. An upper limit is reached at a ratio of approximately 8 – 10 complex molecules per protein, precluding a binding mechanism involving incorporation of the complex into a specific HSA binding pocket that has been observed for a range of lipophilic anionic Gd complexes.[20, 21]

4.6 Towards an Understanding of How the Complexes are Able to Penetrate the Plasma Membrane

The mechanism by which complexes such as those described here are able to cross the plasma membrane is not well understood. The observation that uptake of [Ln.**1**] is fast and appears to be both concentration dependent and reversible can perhaps allow some tentative speculation.

The complexes are relatively large (MW ~ 1000) and although the uptake and localisation appears to be sensitive to the external concentration, they are unlikely to be able to cross the plasma membrane by either passive diffusion or through a transport protein. Each transport protein is considered to be specific for the narrow range of substance it translocates. However, recent work has demonstrated that the copper transporter CTR1 can also mediate the uptake of the anticancer drug Cisplatin [*cis*-diamminedichloroplatinum(II)] despite them being structurally unrelated, and hence, the mechanism by which the two substrates are transported is likely to be different.[15, 16]

Endocytosis is a process by which eukaryotic cells are able to internalise both small and large molecules through their incorporation into membrane vesicles at the plasma membrane.[10] It is generally classified as either phagocytosis (cell eating) or pinocytosis (cell drinking). The former refers to the internalisation of large particles (> 0.5 μm diameter) that must bind to specific plasma membrane receptors capable of triggering their own uptake. The latter refers to the formation of smaller (< 0.2 μm diameter) vesicles carrying extracellular fluid and macromolecules specifically or non-specifically bound to the plasma membrane; receptor mediated endocytosis can be included in this category.[11,12] The rate of these processes and the amount of membrane and extracellular fluid that can be internalised are such that it is estimated for cells such as macrophages and fibroblasts, that more than 200 % of their entire cell surface is turned over every hour. Pinocytosis can be divided into two further sub-categories: clathrin dependent endocytosis, and clathrin independent endocytosis.

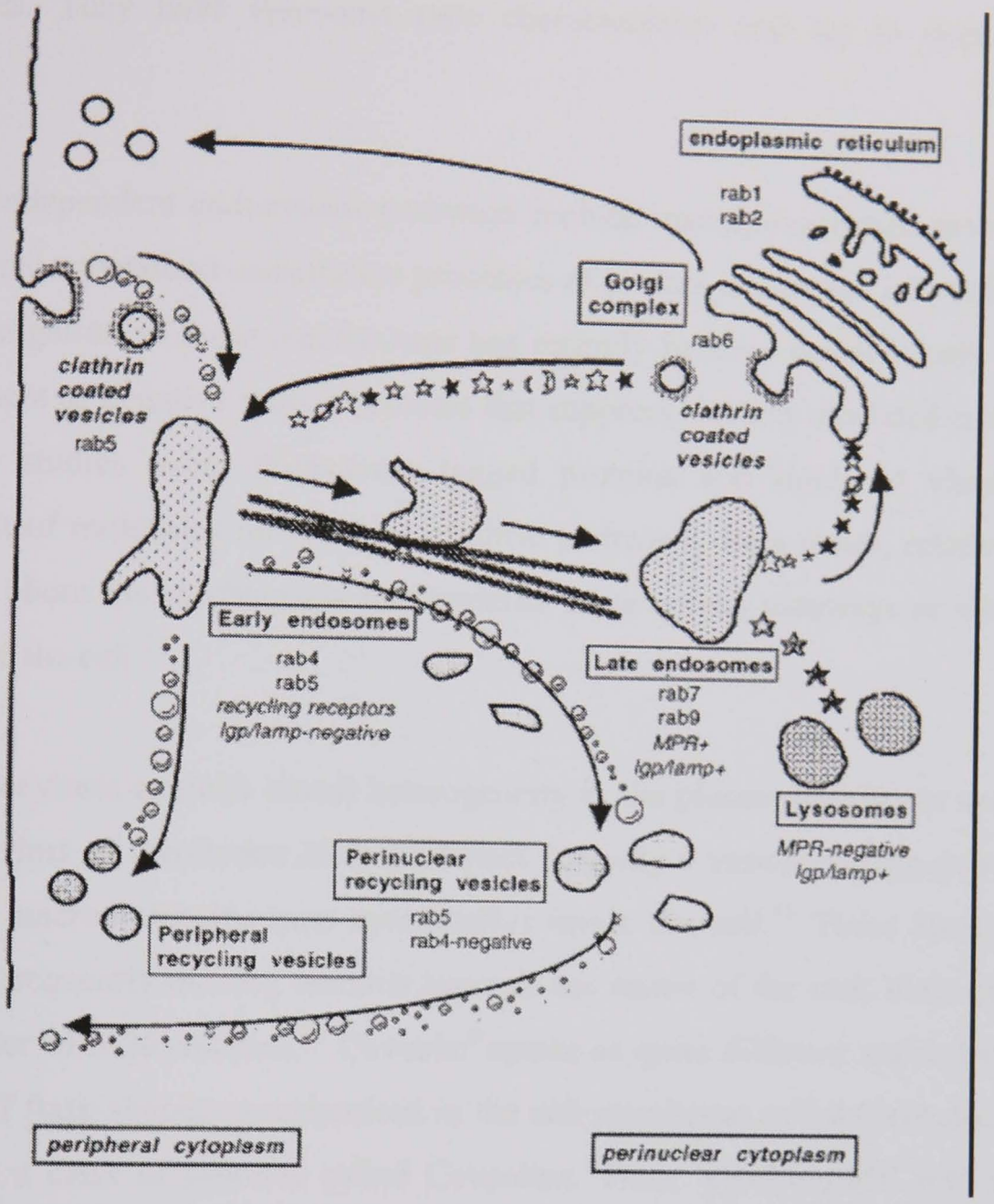

Figure 4. 24 – Representation of the endocytotic pathway for eukaryotic cells[11]

Clathrin is a large protein (180 kDa) and assists in the formation of coated pits on the inner surface of the plasma membrane. Within the pit are certain proteins and receptors (some of the best known are the LDL receptor which removes LDL cholesterol from the blood and the transferrin receptor). The pits invaginate (or form inward) and pinch off to form clathrin-coated vesicles; the lifetime of the pit is of the order of about a minute. Once inside the cell, the clathrin coat is quickly lost and the vesicle combines with an early endosome. The endosomes act as sorting stations: membrane and receptor molecules are returned to the cell surface by exocytosis or alternatively transferred to lysosomes to be degraded. Remaining material is transferred from early endosomes on microtubules to the perinuclear cytoplasm (i.e. around the cell nucleus) where they fuse with late endosomes. Late endosomes accumulate and concentrate internalised contents after their passage through early

endosomes. They have lysosome type characteristics and act to degrade their contents.

Clathrin-independent endocytosis pathways include macropinocytosis, caveolae and other poorly understood constitutive processes of plasma membrane internalisation.[13] The investigation of these mechanisms has recently become possible only with the development of negative mutant proteins that suppress clathrin-mediated endocytosis and with studies using fluorescent tagged proteins and lipids to visualise the movement of molecules through-non-clathrin pathways. As a result, relatively little is known about the mechanisms that underlie these uptake pathways or where they lead inside the cell.[13]

Macropinocytosis exploits lateral heterogeneity in the plasma membrane and occurs when the rims of membrane folds fuse back forming a vesicle, taking extracellular fluid and macromolecules (non-specifically) inside the cell.[11] These structures are dynamic, frequently moving inwards towards the centre of the cell; their lifetime is of the order of 5-20 minutes.[13] Caveolar uptake is quite different and relies on the presents of flask-shaped invaginations in the cell membrane called Caveolae that are coated by a class of proteins called Caveolins. Their 'pinching-off' into caveolin coated vesicles and uptake into the cell is ligand-triggered and allows routing of ligands to areas of the cell that are not easily accessible by other endocytotic mechanisms such as the endoplasmic reticulum (ER). This pathway also bypasses low pH and digestive compartments.[14]

Exocytosis is essentially the reverse of endocytosis: the cell excretes macromolecules by the fusion of vesicles with the plasma membrane. In order to account for the observed dependence on localisation inside the cell as a function of the external concentration, it is essential that transport of the complex between the inside and outside is dynamic and operates reversibly.

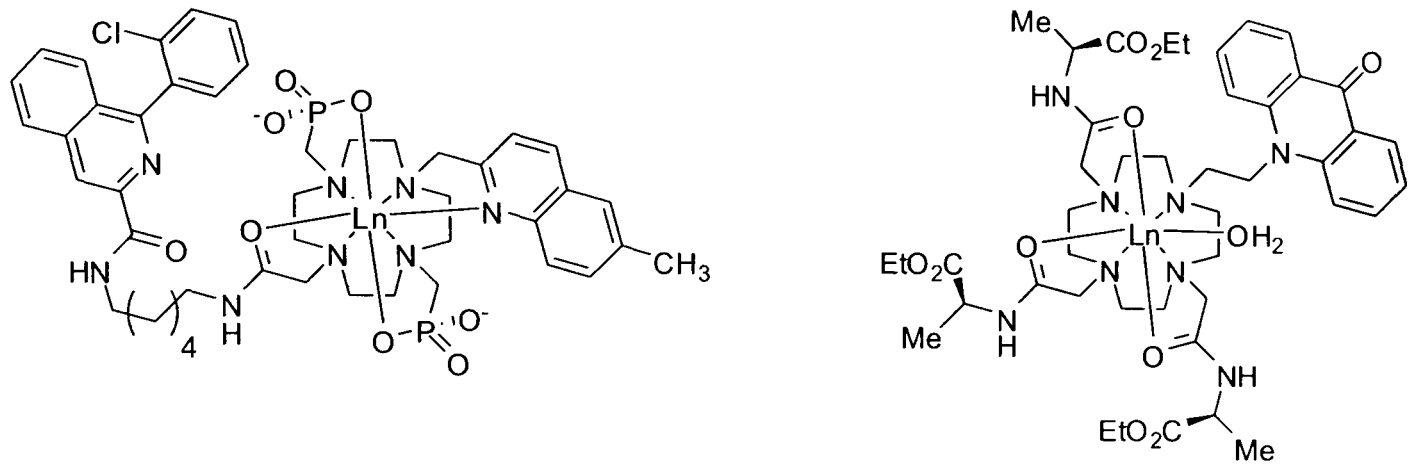

Figure 4. 25

It has been reported that complexes shown in Figure 4.25 are taken up by an endosomal pathway since the efficiency of their uptake is considerably reduced at 4 degrees (below this temperature endocytosis is generally considered to be 'switched off'). Incubation of NIH 3T3 cells in the presence of [Ln.**1**] at 4 °C did not significantly reduce uptake of the complex. However, it is suggested that due to the lipophilic nature of the complex and its high (but unspecific) affinity for protein, it could remain associated with the cell surface even after several washings with cold PBS. Since the cells are imaged live, as the slide returns to room temperature, endocytosis would again be 'switched on' and the associated complex could be taken inside the cell.

4.7 Which Structural Features Govern the Localisation of the Complex Within the Cell?

Whilst the mechanism that allows these complexes to cross the cell membrane and localise into specific compartments requires further investigation, a comparison between structurally similar complexes that show different compartmentalisation can help us to design new complexes to target (or prevent) uptake by a particular organelle. It is immediately apparent from the few examples of cell-permeable lanthanide complexes that have been published in the literature to date, that structurally fairly similar complexes can exhibit uptake to a different compartment. The isomeric complexes LnAlaOEt$_3$NAcr, **(b)** and LnAlaOEt$_3$CAcr, **(c)**, (Chapter 4, Figure 4.1) perhaps provide the best example; an obvious conclusion in this case is

that it is the structure and degree of conformational freedom of the planar aromatic chromophore that may be most important for controlling localisation.

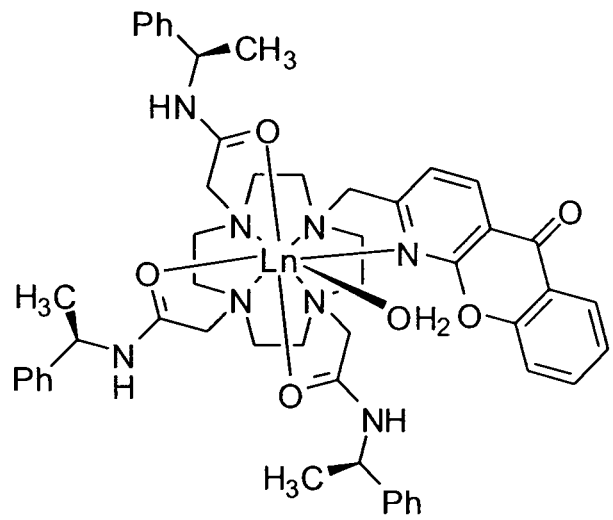

Figure 4. 26 LnPh3AzaH

The complex shown in Figure 4.26 has been synthesised during 2006 in the Parker lab and is similar in structure to complex [Ln.**1**], except it incorporates an azaxanthone chromophore in place of the tetraazatriphenylene moiety.[22]

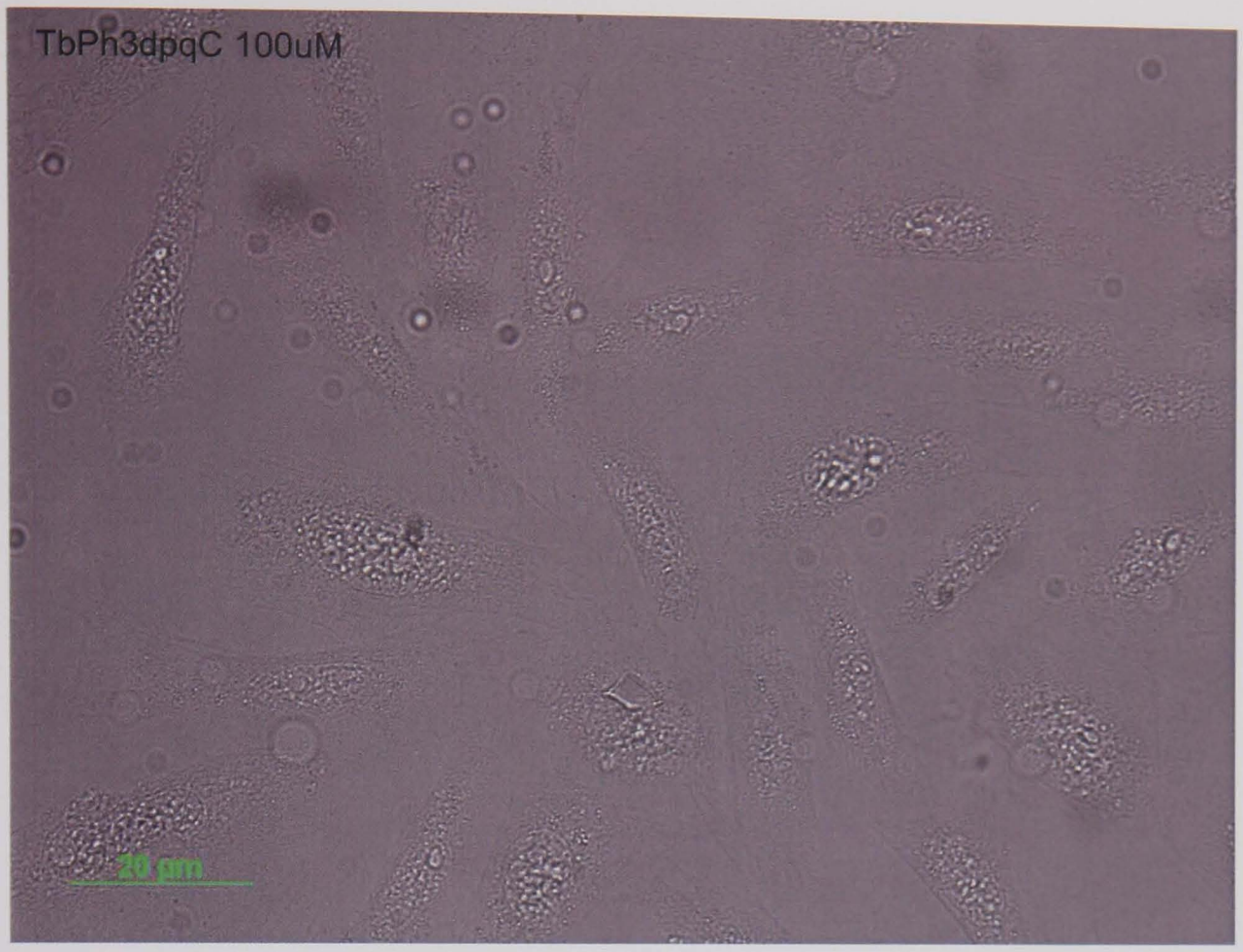

Figure 4. 27 – Transmitted microscope image of CHO cells loaded with [Tb.1] (100µM, 3 h post-incubation)

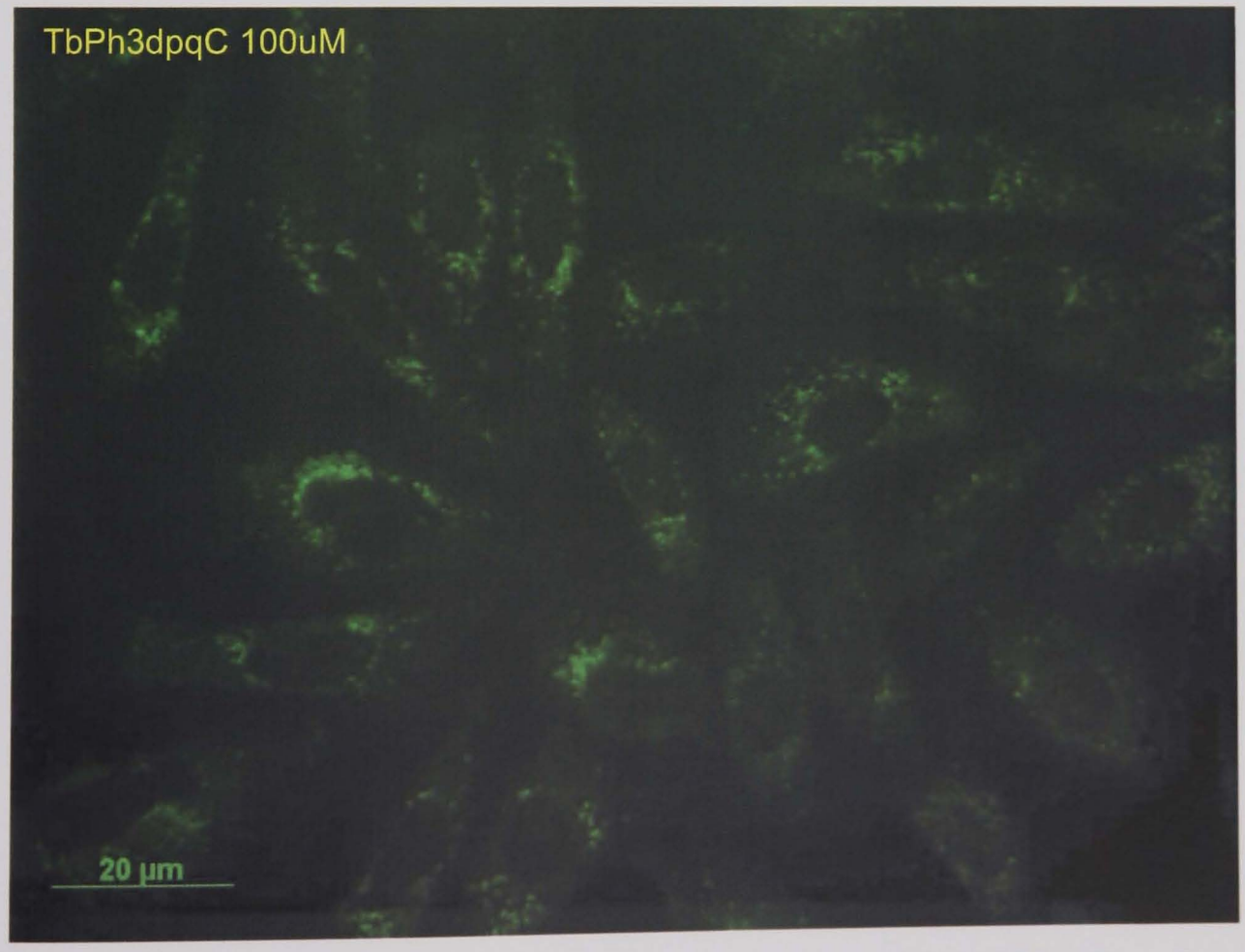

Figure 4. 28 – Fluorescence microscope image of the same population of CHO cells as shown in Figure 4.12 loaded with [Ln.1] (100 µM, 3 h post-incubation).

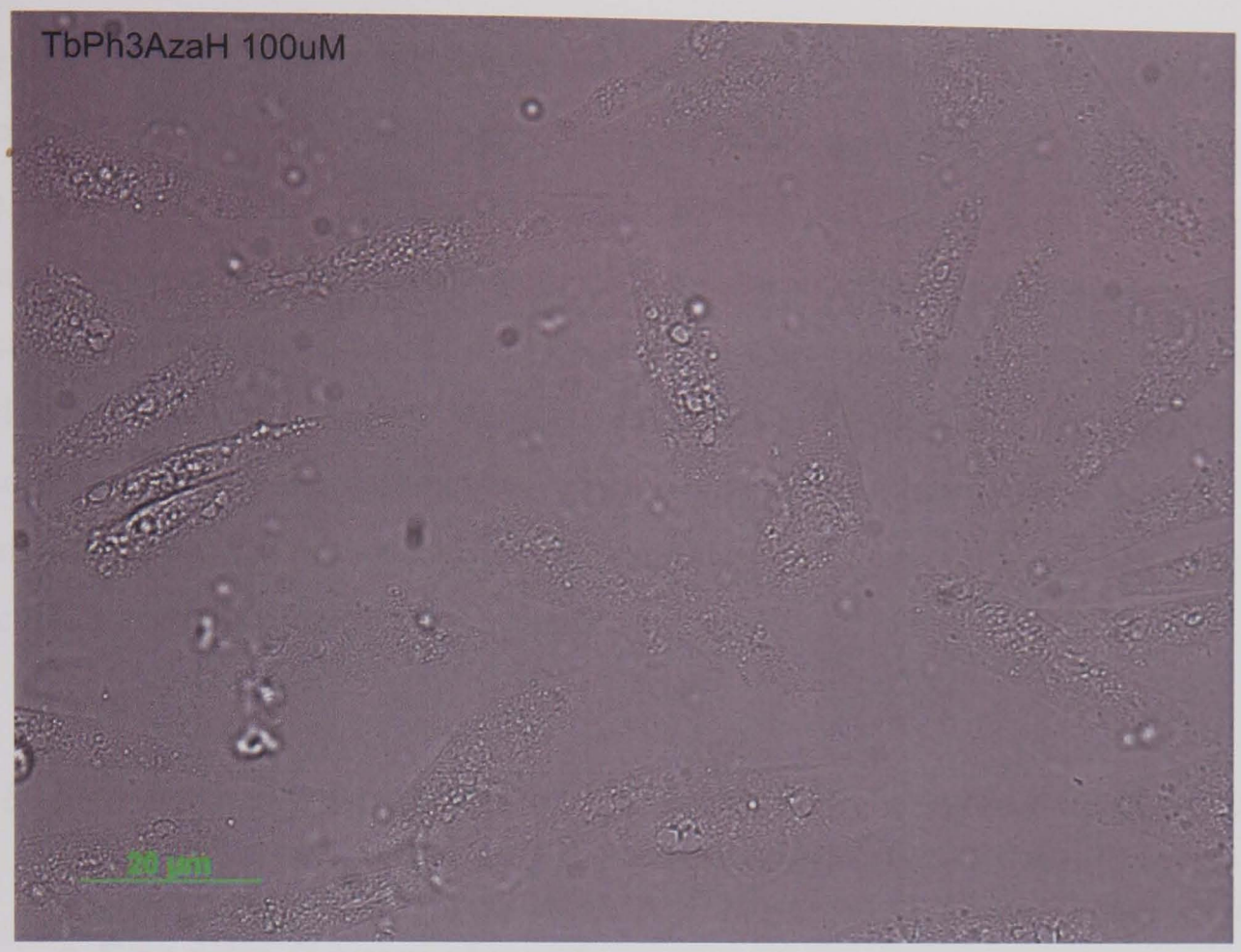

Figure 4. 29 – Transmitted microscope image of CHO cells loaded with TbPh3AzaH (100µM, 3 h post-incubation)

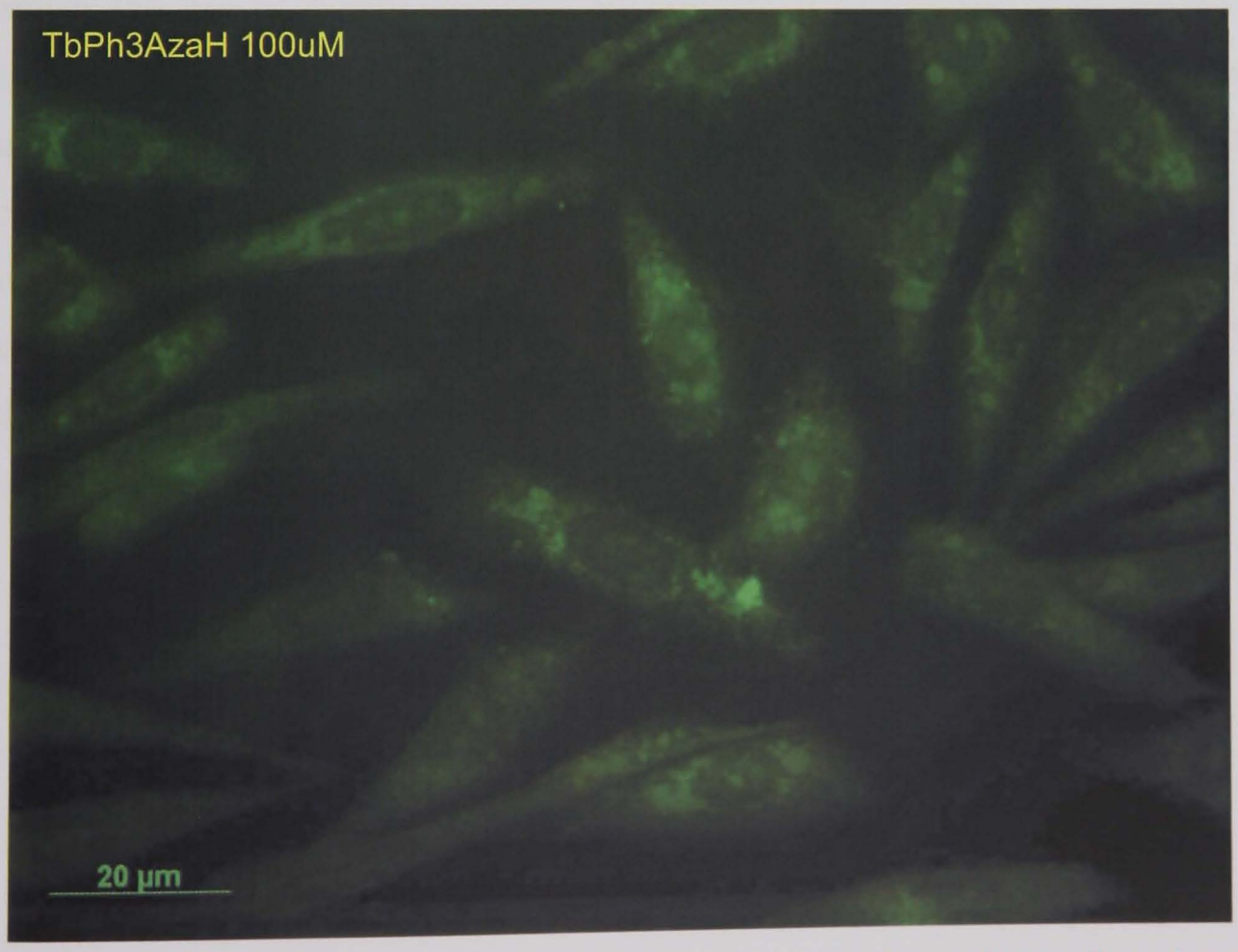

Figure 4. 30 – Fluorescence microscope image of the same population of CHO cells as shown in Figure 4.12 loaded with [Ln.1] (100 µM, 3 h post-incubation).

Figures 4.27 – 4.30 show CHO cells that have been cultured in F12 (Ham) medium supplemented with 50 μg ml^{-1} penicillin/streptomycin and 10 % foetal calf serum in the presence of either [Tb.**1**] or TbPh3AzaH (100 μM) for 3 hours. Despite their similar structures, they exhibit quite different localisation: [Ln.**1**] shows a spotty localisation centred around the nucleus as has previously been discussed: TbPh3AzaH appears to show plate-like structures in the cytosol. Compartments are also illuminated within the nucleus, which perhaps correspond to the nucleolus. The plate-like structures are also visible in transmission (Figure 4.24) and appear to be peculiar to cells loaded with this complex.

4.8 Preliminary Analysis of Intracellular Complex Emissive Lifetimes to Probe the Coordination Environment and Assess the Extent to Which Emission is Quenched within a Specific Compartment

Through the use of a time resolved microscope, it is possible to determine the lifetime at any point within an image; with appropriate treatment a lifetime 'density' map can be built up.[23] Quenching of the lanthanide excited state is characterised by a decrease in the metal centred emission lifetime (in addition to a decrease in the emissive intensity). This could prove a useful technique for probing the local environment of the complex. Figures 4.31 – 4.33 demonstrate the principle. CHO cells were incubated in the presence of a 1 mM solution containing $EuPh_3dpqC$, [Eu.**1**] for 4 hours (Figure 4.31).

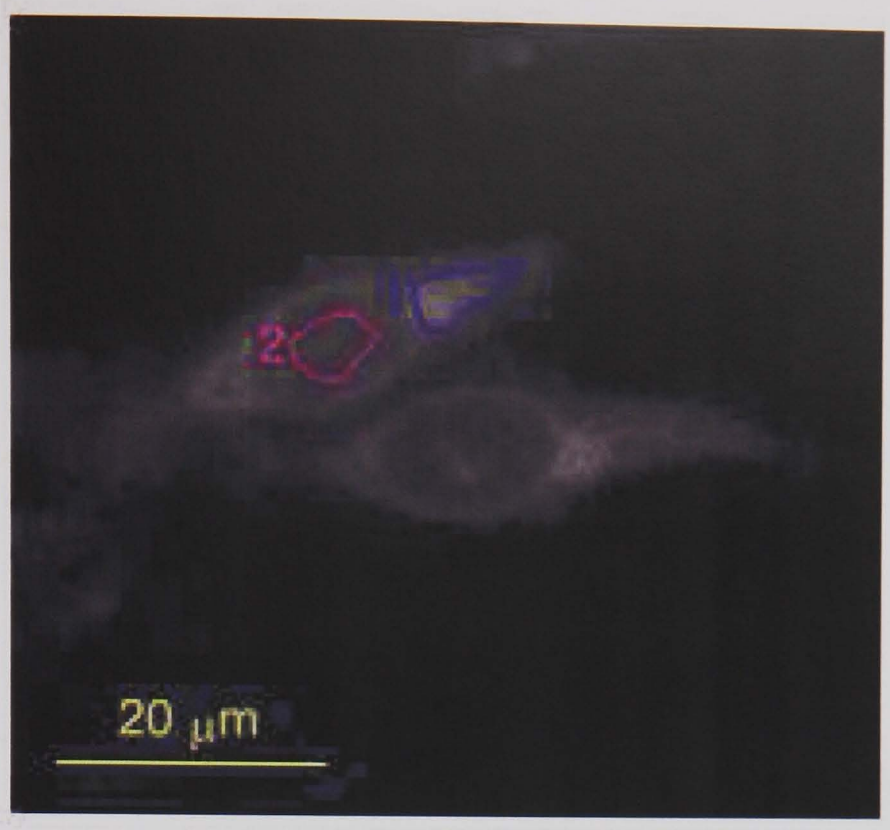

Figure 4. 31 – CHO cells labelled with EuPh3dpqC (1 mM, 4 hrs post-incubation). Two regions of interest are defined: ROI1 and ROI2

Images were then captured using gate times of between 0 and 2500 µs in 125 µs steps following excitation using a nitrogen laser at 337 nm. By plotting the change in emission intensity for individual pixels, or over a region of interest as a function of gate time, it is possible to estimate the lifetime of the complex over that area. This principle is depicted in Figures 4.32 and 4.33 for the regions of interest defined as ROI1 (centred on the punctate localisation around the periphery of the nucleus) and ROI2 (centred inside the nucleus).

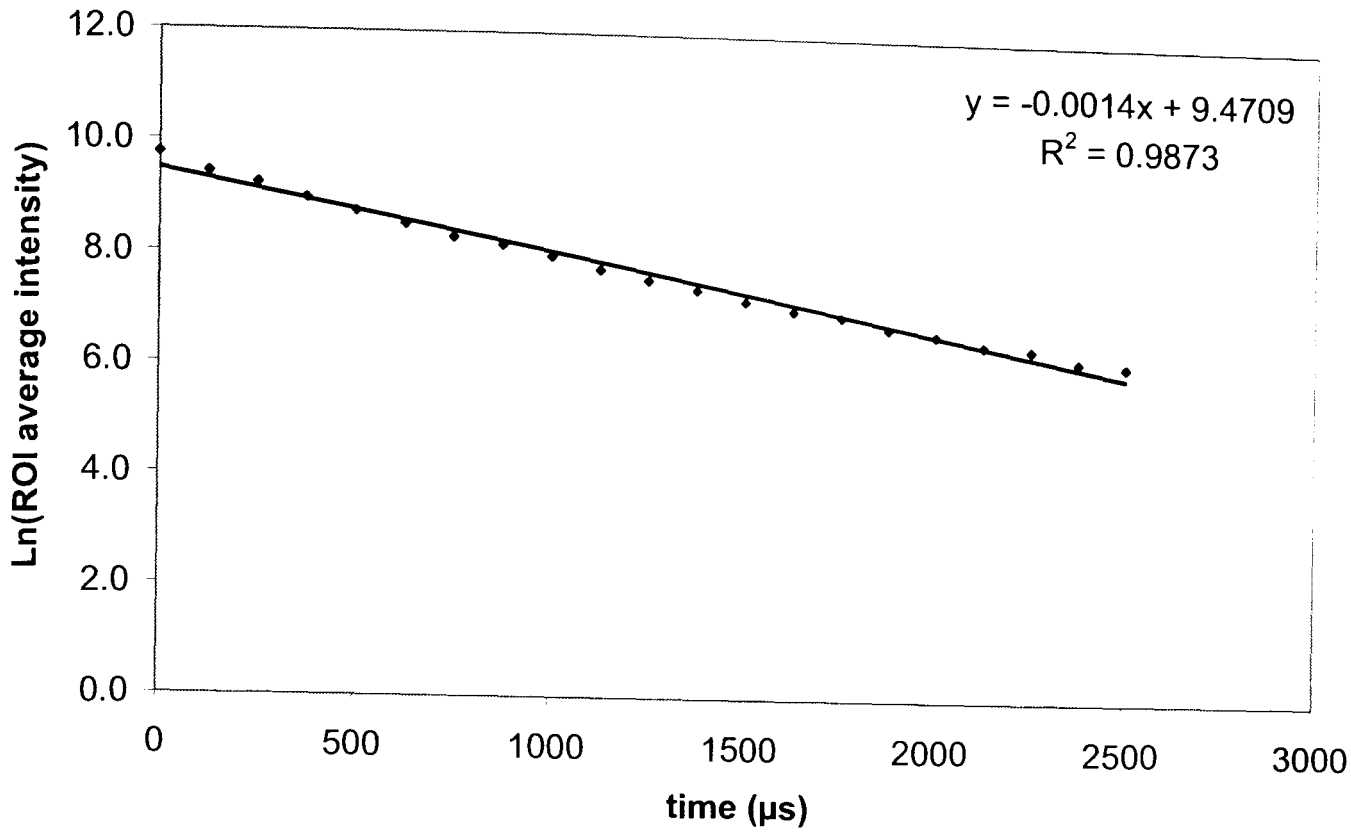

Figure 4. 32 – Decrease in emission intensity with increasing gate time for ROI1 (Lifetime = 714 ± 50 µs)

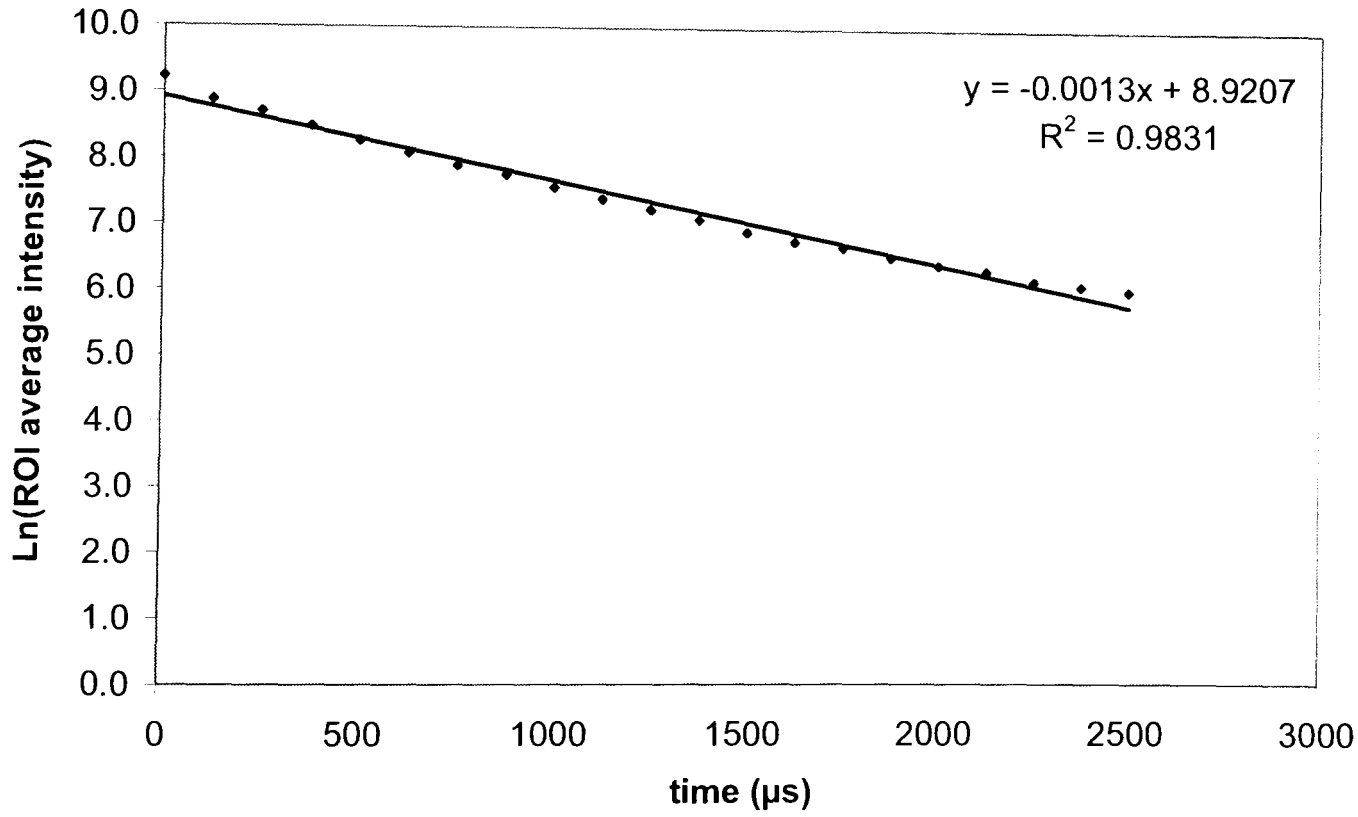

Figure 4. 33 – Decrease in emission intensity with increasing gate time for ROI2 (Lifetime = 769 ± 50 µs)

Lifetimes were found to be 716 µs and 769 µs over regions of interst ROI1 and ROI2 respectively. Whilst these are preliminary results, it is interesting to note that the lifetimes are relatively long (*c.f.* 1 ms for the complex in water), indicating that the complex is not strongly quenched within the cell. Following repetition of the results

and optimisation of the method, it would be interesting to now compare these results to those for the complexes that appear to give only very weak emission *in cellulo* (for example [Eu.**2**,**4**] in order to support the results reported in sections 4.1 and 4.2. I.e. that each of the complexes $EuPh_3dpqC$, [Eu.**1**], EuDO3AdpqC, [Eu.**2**] and $EuGlu_3dpqC$, [Eu.**4**] are taken up to a similar extent, but that [Eu.**1**] appears considerably more emissive and is assumed to be quenched to a lesser extent.

In Figure 4.31, the nucleus appears dark and localisation is apparent only around the periphery. However, pixel intensities are significant in the nucleus as is evident from the lifetime measurement, and are 2 – 3 times brighter than background luminescence. Using conventional fluorescence microscopy, where there are particularly bright regions in the image, other localisation can be difficult to discern, since the image is captured using exposure times such that no part of the image is over-exposed. Producing a false-colour lifetime map, may help provide a clearer comparison between complexes, in particular, where distribution is more diffuse.

References

1. S. Pandya, J. Yu, D. Parker, *Dalton. Trans.*, 2006, 2757.
2. J.–C. Frias, G. Bobba, M. J. Cann, D. Parker, C. J. Hutchison, *Org. Biomol. Chem.*, 2003, **1**, 905.
3. Y. Brettoniere, M. J. Cann, D. Parker, R. Slater, *Chem. Commun.*, 2002, 1930.
4. Y. Brettoniere, M. J. Cann, D. Parker, R. Slater, *Org. Biomol. Chem.*, 2004, 1624
5. R. A. Poole, G. Bobba, M. J. Cann, J.–C. Frias, D. Parker, R. D. Peacock, *Org. Biomol. Chem.*, 2005, **3**, 1013.
6. H. C. Manning, T. Goebel, R. C. Thompson, R. R. Price, H. Lee, D. J. Bornhop, *Bioconjugate Chem.*, 2004, **15**, 1488.
7. D. Parker, J. Yu, *Chem. Commun.*, 2005, 3141.
8. J. Yu, D. Parker, R. Pal, R. A. Poole, M. J. Cann, *J. Am. Chem. Soc.*, 2006, **128**, 2294.

8.1 G. Bobba, J. –C. Frias, D. Parker, *Chem. Commun.*, 2002, 890.

9. M. A. Condrau, R. A. Schwender, M. Zimmermann, M. H. Muser, U. Graf, P. Niederer, M. Anliker, *Cytometry*, 1994, **16**, 195.
10. N. A. Campbell, J. B. Reece, L. G. Mitchell, *Biology*, 5th ed., Addison Wesley Longman, 1999.
11. I. Mellman, *Annu. Rev. Cell Dev. Biol.*, 1996, **12**, 575.
12. C. Schnatwinkel, S. Chrisforidis, M. R. Lindsay, S. Uttenweiler-Joseph, M. Wilm, *Plos Biology*, 2004, **2**(9), 1249.
13. B. J. Nichols, J. Lippincott-Shwartz, *Trends in Cell Biol.*, 2001, **11**(10), 406.
14. L. Pelkmans, A. Helenius, *Traffic*, 2002, **3**, 311.
15. S. Ishida, J. Lee, D. J. Thiele, I. Hershkowitz, *Proc. Nat. Acad. Sci. U. S. A.*, 2002, **99**, 14298.
16. X. Lin, T. Okuda, A. Holzer, S. B. Howell, *Mol. Pharmacol.*, 2002, **62**, 1154.
17. R. B. Lauffer, *Chem. Rev.*, 1987, **87**, 901.
18. P. Caravan, J. J. Ellison, T. J. McMurry, R. B. Lauffer, *Chem. Rev.*, 1999, **99**, 2293.
19. S. Aime, A. S. Batsanov, M. Botta, J. A. K. Howard, D. Parker, P. K. Senanayake, J. A. G. Williams, *Inorg. Chem.*, 1994, **33**, 4696.

20. P. Caravan, N. J. Cloutier, M. T. Greenfield, S. A. McDermid, S. U. Dunham, J. W. M. Bulte, J. C. Amedio, Jr., R. J. Looby, R. P. Supkowski, W. deW. Horrocks, Jr., T. J. McMurry, R. B. Lauffer, *J. Am. Chem. Soc.*, 2002, **124**(12), 3152.
21. S. Aime, A. Barge, M. Botta, E. Terreno, *Metal Ions in Biological Systems*. Marcel Dekker, Inc., New York, Volume 40, 643.
22. R. A. Poole, F. Kielar, S. L. Richardson, P.A. Stenson, D. Parker, *Chem. Commun.*, 2006, 4084.
23. A. Beeby, S. Botchway, I. M. Clarkson, S. Faulkner, A. W. Parker, D. Parker, J. A. G. Williams, *Photchem. Photobiol. A*, 2000, **57**, 83.

Conclusions and Future Work

Structurally related complexes of europium(III) and terbium(III) have been synthesised, whose overall charge and lipophilicity have been modified through varying the pendent arms on cyclen; carboxylate, amide and phosphinate based systems have been investigated. The tetraazatriphenylene chromophore, dpqC, is common to each of the complexes and is an excellent sensitiser for both lanthanide(III) ions. It has a fast rate of S_1 to T_1 intersystem crossing, and a triplet state that is insensitive to quenching by molecular oxygen. These features, in combination with the well defined coordination environment of the lanthanide provided by the nonadentate ligand, lead to high luminescent quantum yields in aerated aqueous media of the order of 15 – 50 % and long luminescent lifetimes of the order of milliseconds. The metal-centred excited state has been shown to be susceptible to quenching by electron-rich donors, for example, urate, ascorbate and iodide. The favourable photophysical properties of the series of complexes reported herein has allowed an assessment to be made of deactivation though a dynamic charge-transfer mechanism, driven by the excited state energy of the lanthanide ion. It has been shown that the terbium(III) complexes are quenched more than their europium(III) analogues, and that the order of sensitivity to quenching generally follows the ease of oxidation of the quenching anion. However, urate quenches by an order of magnitude more than ascorbate, despite having a redox potential of 0.59 V, compared to 0.30 V for ascorbate. These differences have been exploited in the development of a ratiometric assay for the determination of uric acid concentration in biological samples. A number of mechanisms have been tentatively proposed to account for the quenching behaviour of these complexes in the presence of electron-rich donors and supporting evidence has been provided through comparison with examples of related complexes also synthesised in Durham.

The use of fast, time-resolved spectroscopies is essential if the mechanism is to be fully elucidated. It has been proposed that charge transfer occurs from the donor to the sensitising chromophore; this would be expected to manifest itself as a change in the excited state UV-Vis absorption spectrum of the complex. The work reported in

this thesis is aimed towards the design of lanthanide complexes for use '*in cellulo*'. In order to attain maximum efficiency using luminescence based detection techniques it is necessary that the susceptibility to quenching is reduced as much as is possible. Further systematic modification of complex structure, and careful determination of quenching behaviour currently provides the most effective method for achieving this.

The complexes have been shown to be taken up by a number of eukaryotic cell lines and are amenable to analysis by time resolved fluorescence microscopy. The cationic and lipophilic complexes generally give brighter images '*in cellulo*' than their neutral and anionic analogues. However, determination of the intracellular lanthanide concentration has revealed that the complexes are taken up to a similar extent. Further work should be aimed towards determining the factors that govern localisation of the complex; subsequently, conjugates of the complexes could be synthesised in order to target specific intracellular compartments. The ultimate aim, would be to be able to carry out time-resolved luminescence assays inside live cells. The use of lanthanide complexes as probes offers a unique advantage over current alternatives as information about their local coordination environment, or the concentration of a specific analyte in solution can be gained through monitoring changes in their spectral emission profile, lifetime or circular polarisation.

CHAPTER 5

General Experimental

5 General Experimental

All reagents were used as supplied by commercial sources unless otherwise stated. Solvents were dried over the appropriate drying agents when required (CH_3CN over CaH_2, CH_3OH over Mg/I_2 and THF over Na/benzophenone). Water and H_2O refer to high purity water with conductivity ≤ 0.04 μS cm^{-1}, obtained from the "PuriteSTILL Plus" purification system.

Thin layer chromatography was carried out using silica plates (Merck Art 5554) or neutral aluminium oxide plates (Merck Art 5550), both of which fluoresce under UV irradiation (254 nm). Preparative column chromatography was performed using neutral aluminium oxide (Merck Aluminium Oxide 90, activity II–III, 70–230 mesh), washed in ethyl acetate, or silica (Merck Silica Gel 60, 230–400 mesh).

^1H and ^{13}C NMR spectra were recorded on a Varian Mercury–200 (^1H at 199.975 MHz, ^{13}C at 50.289 MHz) on a Varian Unity–300 (^1H at 299.908 MHz, ^{13}C at 75.412 MHz) on a Bruker Avance spectrometer (^1H at 400.13 MHz, ^{13}C at 100.61 MHz) on a Varian Inova–500 (^1H at 499.78 MHz, ^{13}C at 125.67 MHz) or on a 1.53 T magnet connected to a Varian VXR400 console (^1H at 65.6 MHz). All spectra were referenced to solvent residual proton signals, except for complexes in D_2O, where tert–butanol was added as an internal reference ($\delta = 0$ ppm).[9] All chemical shifts are given in ppm and coupling constants in Hz.

Electrospray mass spectra were recorded on a VG Platform II instrument (Fisons) with methanol as the carrier solvent. Accurate masses were measured on a Thermo Finnigan LTQ or by the ESPRC Mass Spectroscopy Service at the University of Wales in Swansea.

Melting points were measured using a Reichart–Köfler block and are uncorrected.

All pH measurements were performed using a Jenway 3320 pH meter attached to an Aldrich Chemical Company micro–pH combination electrode, calibrated using pH 4, 7 and 10 buffer solutions.

UV/vis absorption spectra were recorded using a Perkin Elmer Lamda 900 UV/vis/IR spectrometer. Emission spectra were recorded at 295 K using an Instruments SA Fluorolog 3–11 spectrometer and DataMax v2.1 for Windows.

Luminescence spectra of the lanthanide(III) complexes were recorded at 295 K in aerated aqueous solution following indirect excitation of the lanthanide(III) ion via the tetraazatriphenylene chromophore, dpqC, at a wavelength of 348 nm.

Phosphorescence emission spectra were recorded at 77 K using an Oxford Instruments optical cryostat and LS 55B spectrometer, with EPA (diethyl ether, isopentane and ethanol, 5:5:2) as solvent.

Lifetime measurements were measured by excitation of the sample by a short pulse of light (348 nm) followed by monitoring the integrated intensity of light (545 nm for terbium, 620 nm for europium) emitted during a fixed gate time, t_g, a delay time, t_d, later. At least 20 delay times were used covering 3 or more lifetimes. A gate time of 0.1 ms was used, and the excitation and emission slits were set to 10 and 2.5 nm bandpass respectively. The obtained decay curves were fitted to the equation below using Microsoft Excel.

$$I = A_0 + A_1\exp(-kt)$$

where I = intensity at time t after the flash

A_0 = intensity after the decay has finished

A_1 = pre-exponential factor

k = rate constant for decay of the excited state.

The excited state lifetime, τ, is the inverse of the rate constant, k.

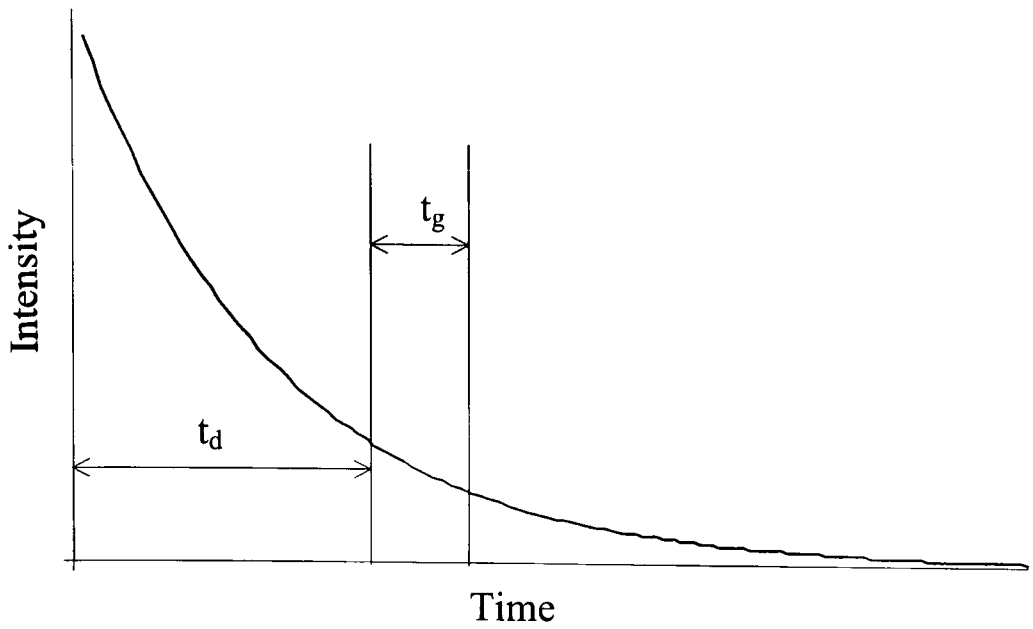

Measured parameters for lifetime measurements

The quantum yield for a given process is defined as the total number of photons emitted by that process divided by the total number of photons absorbed. The techniques and equipment necessary to make an absolute determination of quantum yields are not generally available. Therefore the usual method is to determine a relative quantum yield where the compound of unknown yield is compared to a compound of known yield. The unknown quantum yield can then be calculated using the following equation.

$$\Phi_x = \Phi_r \cdot \frac{A_r}{A_x} \cdot \frac{E_x}{E_r} \cdot \frac{I_r}{I_x} \cdot \frac{n_x^2}{n_r^2}$$

Where *r* and *x* refer to reference and unknown respectively

A = absorbance at λ_{cx}

E = corrected integrated emission intensity

I = corrected intensity of excitation light

(as all of the measurements were taken using identical excitation conditions this term can be ignored)

n = refractive index of solution.

The measurements were made relative to two known complexes. For europium this was $EuPh_3dpqC$ and for terbium $TbPh_3dpqC$. For each of the standards and the unknown, five solutions with absorbances between 0.02 and 0.1 were used. For each

of these solutions the absorbance at the excitation wavelength and the total integrated emission was determined. A plot of total integrated emission against absorbance gives a straight line with slope E/A. The unknown quantum yield can thus be calculated from the following equation. Since values for both the sample and reference compounds were recorded in water the refractive index term cancels out.

$$\Phi_x = \Phi_r \cdot \frac{slope_x}{slope_r} \cdot \left(\frac{n_x}{n_r}\right)^2$$

Errors in quantum yield determinations can arise due to the inner filter effect or errors in the amount of absorbed light. This effect can be minimised by only using samples with absorbances below 0.2. Errors in the amount of light absorbed by each sample can be minimised by choosing the excitation wavelength to be on a relatively flat area of the absorption curve and by using a small bandpass for excitation.

Epifluorescence images were taken on a Zeiss Axiovert 200M epifluorescence microscope with a digital camera, or a custom, time-resolved fluorescence microscope using nitrogen laser excitation at 337nm with the assistance of Michel Laget (Cisbio International, France); filters used were as stated in Chapter 4; confocal images were taken on a Zeiss LSM 500 META confocal microscope with 405 nm diode laser excitation and an LP 505 emission filter for europium complex luminescence and with 488 nm argon laser excitation and a BP 505-550 filter for SYTO dye fluorescence.

Flow cytometric analysis and sorting was conducted using a DakoCytomation Inc. MoFlo multi-laser flow cytometer (Fort Collins, CO, USA) operating at 60psi, 70 micron nozzle. Samples were interrogated with a 100 mW 488 nm solid state laser: (FSC, SSC). Fluorescence signals were detected through interference filters: (FL1 530/40, FL2 580/30, FL3 630/30, FL4 670/30). Fluorescence signals were collected in the logarithmic mode. The data were analyzed using Summit v4.0 (DakoCytomation) software.

CPL measurements were made using a home-built (Glasgow University) CPL spectrometer based on a Spex Fluoromax-2 spectofluorimeter with the assistance of Dr R. D. Peacock.

Inductively coupled plasma mass spectrometry determination of europium concentrations were made by Dr C. Ottley in the Department of Earth Sciences at Durham University.

Relaxivity measurements were made at 37 °C and 60 MHz on a Bruker Minispec mq60 instrument. The mean value of three separate measurements was recorded.

NMRD profiles were recorded in Durham on a Stelar Spinmaster, in the field range 0.001 – 20 MHz and in Ivrea, Italy on a similar instrument operating up to 90 MHz.

Reverse phase HPLC were performed at 298 K on a Perkin Elmer system using either a 4.6 x 20 mm 4μ Phenomenex Synergi Fusion RP analytical column or the equivalent 21.1 x 20 mm semi-semi preparitive column. In each case an H_2O + 0.1 % TFA / CH_3CN + 0.1 % TFA solvent system was used (gradient elution). Chapter 2.2.2.1, Figure 2.12, gradient programme:

Time (Mins)	H_2O + 0.1 % TFA (%)	CH_3CN + 0.1 % TFA
0	70	30
10	15	85
13	0	100
15	0	100
20	70	30

5.1 Synthetic Procedures

1. 2-Methyl-1,10-phenanthroline[1]

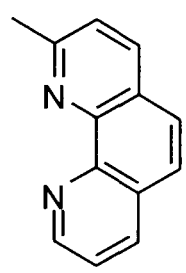

A solution of 1,10-phenanthroline (10 g, 55 mmol) in dry THF (100 ml) was added dropwise to a stirred solution of methyl lithium (1.6 mol dm^{-3} in Et_2O, 34.5 ml, 55 mmol) in dry THF (150 ml) at 0°C under argon. The mixture was stirred overnight at room temperature under argon to give a dark green solution. The reaction was quenched by careful addition of water (100 ml) at 0°C. THF was removed under reduced pressure using a rotary evaporator and the product extracted into diethyl ether (3 x 150 ml). Activated manganese dioxide (53 g, 0.61 mol) was added and the solution stirred for 1.5 hours; magnesium sulphate was added and the solution stirred for a further 2 hours. Filtration through a celite plug yielded a clear yellow solution. The solvent was evaporated to dryness to yield the crude product, which was purified by recrystallisation from ethyl acetate/hexane to give a white product (5.50 g, 28 mmol, 51 %). ^{1}H NMR (300 MHz, $CDCl_3$): 2.97 (3H, s, CH_3), 7.54 (1H, d, J = 8.1, H3), 7.63 (1H, dd, J = 8.1, 4.2, H8), 7.75 (1H, d, J = 8.7, H6), 7.79 (1H, d, J = 8.7, H5), 8.16 (1H, d, J = 8.4, H4), 8.26 (1H, dd, J = 8.1, 1.5, H7), 9.22 (1H, dd, J = 4.2, 1.2, H9). ^{13}C NMR (75 MHz, $CDCl_3$): 25.9 (CH_3), 122.8 (C8), 123.7 (C3), 125.5 (C6), 126.5 (C5), 126.7 (q Ar), 128.8 (q Ar), 136.1 (C7), 136.2 (C4), 145.7 (q Ar), 146.0 (q Ar), 150.3 (C9), 159.5 (C2). m/z (ES^+) 195 (MH^+), 217 (MNa^+), 411 (M_2Na^+); m.p. 75-76°C (lit. [33]78°C). Elemental analysis: found C 79.5, H 5.44, N 14.5%; $C_{13}H_{10}N_2.0.17H_2O$ requires C 79.2, H 5.23, N 14.2%.

2. 2-Methyl-1,10-phenanthroline-5,6-dione[1]

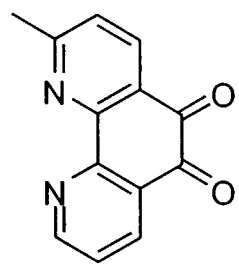

A mixture of 2-methyl-1,10-phenanthroline (2.00 g, 10.29 mmol) and potassium bromide (12.25 g, 102.9 mmol) was placed in an ice bath. Cold sulphuric acid (43 ml) was added carefully to the flask dropwise turning the solution to a dark reddish colour. Concentrated nitric acid (21.5 ml) was then added in a similar way and the solution boiled under reflux overnight. The mixture was cooled, poured into water (500 ml) and neutralised by addition of sodium hydroxide pellets. The product was extracted into dichloromethane (3 x 300 ml), which was dried over K_2CO_3 and removed under reduced pressure to yield a yellow solid. Purification was achieved by chromatography on silica (1.79 g, 7.98 mmol, 77 %) (gradient elution: CH_2Cl_2 to 1% CH_3OH/CH_2Cl_2, $R_f = 0.34$ [5% $MeOH/CH_2Cl_2$]). ^1H NMR (300 MHz, $CDCl_3$): 2.86 (3H, s, CH_3), 7.44 (1H, d, J = 7.8, H3), 7.58 (1H, dd, J = 7.8, 4.8, H8), 8.40 (1H, d, J = 8.1, H4), 8.50 (1H, dd, J = 7.8, 2.0, H7), 9.14 (1H, dd, J = 4.8, 2.0, H9). ^{13}C NMR (75 MHz, $CDCl_3$): 26.2 (CH_3), 125.6 (C8), 125.9 (C3), 126.2 (q Ar), 128.3 (q Ar), 137.5 (C7), 137.7 (C4), 152.7 (q Ar), 153.2 (q Ar), 156.6 (C9), 167.4 (C2), 178.7 (C5), 179.2 (C6). m/z (ES^+) 246 (MNa^+), 279 (MNa^+ + MeOH), 471 (M_2Na^+), 503 (M_2Na^+ + MeOH), 535 (M_2Na + 2MeOH). IR (KBr) 3074 (C-H Ar), 1681 (C=O), 1568, (py ring vibration) 1436 and 1301 (C=C py), 1216, 1123, 1013, 925, 829, 739 cm^{-1}; m.p. 98–100°C. Elemental analysis: found, C 66.3, H 3.46, N 12.2%; $C_{13}H_8N_2O_2.0.67H_2O$ requires C 66.1, H 3.94, N 11.9%.

3. 3-Methyl-10,11,12,13-tetrahydrodipyrido-[3,2a:2',3'-c]-phenazine

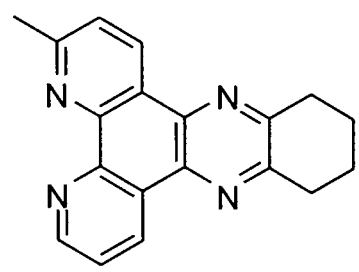

To a solution of 2-methyl-1,10-phenanthroline-5,6-dione (0.65 g, 2.90 mmol) in absolute ethanol (50 ml) was added trans-1,2-diaminocyclohexane (0.33 g, 2.90 mmol) and the resulting mixture boiled under reflux for 5 hours. The solution was allowed to cool and solvent removed under reduced pressure. The product was recrystallised from ethanol to give white crytals (0.81 g, 2.90 mmol, 93 %), m.p. >220°C (dec). ^{1}H NMR (300 MHz, $CDCl_3$): 2.09 (4H, m, H10, 13), 2.98 (3H, s, H15), 3.24 (4H, m, H11, 12), 7.63 (1H, d, J = 8.3, H2), 7.73 (1H, dd, J = 8.2, 4.4, H7), 9.26 (1H, dd, J = 4.4, 1.8, H6), 9.35 (1H, d, J = 8.3, H1), 9.47 (1H, dd, J = 8.2, 1.8, H8). ^{13}C NMR (75 MHz, $CDCl_3$): 22.7 (C11), 22.8 (C12), 25.7 (CH_3), 32.7 (C10), 32.8 (C13), 123.4 (C7), 124.2 9C2), 124.8 (q Ar), 151.5 (C6), 153.2 (q Ar), 153.6 (q Ar), 160.9 (q Ar). HRMS (+ m/z): $[M + H]^+$ calculated for $C_{19}H_{16}N_4Na$, 323.1273; found, 323.1269.

4. 3-Carboxaldehyde-10,11,12,13-tetrahydrodipyrido-[3,2a:2',3'-c]-phenazine

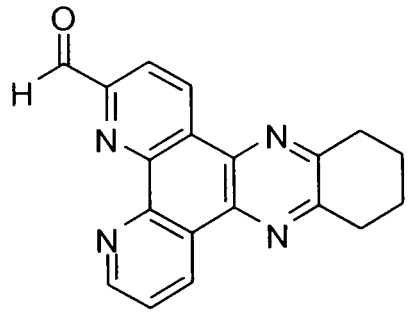

Selenium dioxide (0.96 g, 8.66 mmol) was added to a solution of 3-methyl-10,11,12,13-tetrahydrodipyrido-[3,2a:2',3'-c]-phenazine (1.30 g, 4.33 mmol) in dioxane (200 ml) and the mixture boiled under reflux for 4 hours. The solution was

cooled to room temperature and filtered through a celite plug to afford a crude product that was used directly in the next step. ^{1}H NMR (300 MHz, $CDCl_3$): 2.11 (4H, m, H10, 13), 3.28 (4H, m, H11, 12), 7.83 (1H, dd, J = 8.2, 4.5, H7), 8.41 (1H, d, J = 8.3, H1), 9.33 (1H, dd, J = 4.5, 1.8, H6), 9.53 (1H, dd, J = 8.2, 1.8, H8), 9.68 (1H, dd, J = 8.3), 0.9, H2), 10.60 (1H, d, J = 0.9, CHO). ^{13}C NMR (75 MHz, $CDCl_3$): 22.5 (C11), 22.6 (C12), 32.7 (C10), 32.8 (C13), 120.2 9C7), 124.1 (c1), 127.5 9q Ar), 130.0 (q Ar), 133.0 (c8), 134.1 (C2), 136.6 (q Ar), 138.3 9q Ar), 146.2 (q Ar), 146.7 9q Ar), 151.7 (C6), 153.1 (q Ar), 154.4 (q Ar), 155.1 (q Ar), 193.9 (CHO). EI (+): $[M^+]$ 314.

5. 3-Hydroxymethyl-10,11,12,13-tetrahydrodipyrido-[3,2a:2',3'-c]-phenazine

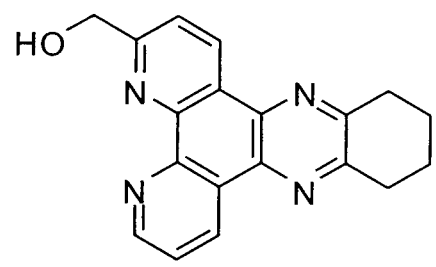

Sodium borohydride (164 mg, 4.33 mmol) was added to a solution of 3-carboxaldehyde-10,11,12,13-tetrahydrodipyrido-[3,2a:2',3'-c]-phenazine (1.36 g, 4.33 mmol) in $CHCl_3$/EtOH (200 ml). The mixture was heated under reflux for 2 hours. The solvent was evaporated and the orange solution taken into a saturated solution of Na_2CO_3 (200 ml) and extracted with CH_2Cl_2 (3 x 150 ml) then $CHCl_3$ (1 x 150 ml). The organic phase was dried over Na_2SO_4 filtered and the solvent removed under reduced pressure to afford a yellow solid (0.89 g, 2.81 mmol, 65 %), m.p. 210°C (dec). ^{1}H NMR (300 MHz, $CDCl_3$): 2.10 (4H, m, H10, 13), 3.25 (4H, m, H11, 12), 5.18 (2H, s, CH_2OH), 7.75 (1H, dd, J = 8.2, 4.4, H7), 7.80 (1H, d, J = 8.3, H2), 9.20 (1H, dd, J = 4.4, 1.7, H6), 9.47 (1H, d, J = 8.3, H1), 9.49 (1H, dd, J = 8.2, 1.7, H8). ^{13}C NMR (75 MHz, $CDCl_3$): 22.7 (C11, 12), 32.8 (C10, 13), 65.7 (CH_2), 121.0 (C7), 123.6 9C2), 125.9 (q Ar), 127.2 9q Ar), 132.9 (C8), 133.4 (C1), 137.4 (q Ar), 151.1 (C6), 153.5 (q Ar), 153.8 (q Ar), 162.3 (q Ar). HRMS (+ m/z): $[M + Na]^+$ calculated for $C_{19}H_{16}N_4ONa$, 339.1222; found, 339.1219.

6. 3-Chloromethyl-10,11,12,13-tetrahydrodipyrido-[3,2a:2',3'-c]-phenazine

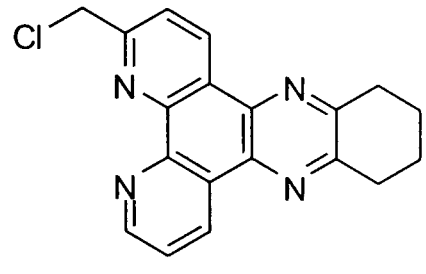

To a solution of 3-hydroxymethyl-10,11,12,13-tetrahydrodipyrido-[3,2a:2',3'-c]-phenazine (0.84 g, 2.66 mmol) in $CHCl_3$ (450 ml) was added phosphorus trichloride (1.46 g, 10.6 mmol). The mixture was heated under reflux for 4 hours. The solution was neutralized by addition of a saturated aqueous solution of Na_2CO_3 (500 ml). The organic layer was separated and the aqueous layer extracted with CH_2Cl_2 (2 x 400 ml) and $CHCl_3$ (1 x 400 ml). The combined organic layers were dried over K_2CO_3 and the solvent evaporated to afford a yellow solid. Purification by chromatography on silica (gradient elution: CH_2Cl_2 to 1 % CH_3OH/CH_2Cl_2) gave a pale yellow solid (R_f 0.38, 5%MeOH/CH_2Cl_2; 0.75 g, 2.25 mmol, 84 %), m.p. 207-8 °C. ^{1}H NMR (300 MHz, $CDCl_3$): 2.05 (4H, m, H10, 13), 3.17 (4H, m, H11, 12), 5.10 (2H, s, CH_2Cl), 7.70 (1H, dd, J = 8.2, 4.4, H7), 7.97 (1H, d, J = 8.3, H2), 9.23 (1H, dd, J = 4.4, 1.8, H6), 9.37 (1H, dd, J = 8.2, 1.8, H8), 9.40 (1H, d, J = 8.4, H1). ^{13}C NMR (75 MHz, $CDCl_3$): 22.7 (C11, 12), 32.2 (C10, 13), 47.0 (CH_2), 122.3 (C7), 123.2 (C2), 125.7 (q Ar), 126.7 (q Ar), 128.9 (q Ar), 130.1 (q Ar), 132.2 (C8), 133.4 (C1), 145.4 (q Ar), 145.9 (q Ar), 151.1 (q Ar), 153.3 (C6), 157.9 (q Ar). HRMS (+ m/z): $[M + Na]^+$ calculated for $C_{19}H_{15}N_4NaCl$, 357.0883; found, 357.0885.

7. 1,4,7-tris-*tert*-Butoxycarbonyl-1,4,7,10-tetraazacyclododecane

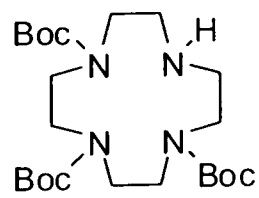

A solution of di-tert-butyl dicarbonate (3.05 g, 13.92 mmol) in CH_2Cl_2 (70 ml) was added dropwise to a stirred solution of 1,4,7,10-tetraazacyclododecane (1 g, 5.80 mmol) in CH_2Cl_2 (290 ml). The mixture was stirred at room temperature for 2 hours. Evaporation of the solvent afforded a transparent oil, which was purified by chromatography on silica (gradient elution: CH_2Cl_2 to 5 % CH_3OH/CH_2Cl_2, R_F = 0.29, 10 % CH_3OH/CH_2Cl_2) to give a colourless solid (1.71 g, 10.95 mmol, 56 %). ^1H NMR (300 MHz, $CDCl_3$): δ 1.42 (18H, s, CH_3), 1.44 (9H, s, CH_3), 2.81 (4H, br m, CH_2), 3.26-3.35 (8H, br m, CH_2), 3.60 (4H, m, CH_2). ^{13}C NMR (75 MHz, $CDCl_3$): δ 28.9 (CH_3), 29.0 (CH_3), 46.1 (CH_2), 49.9 (CH_2), 51.2 (CH_2), 79.4 (C), 79.6 (C), 155.8 (C=O), 156.0 (C=O). m/z (ES^+): 495 (MNa^+), 967 (M_2Na^+).

8. 1-(3-Methyl-10,11,12,13-tetrahydrodipyrido[3,2-a:2',3'-c]phenazine)-4,7,10-tris(*tert*-butoxycarbonyl)-1,4,7,10-tetraazacyclododecane

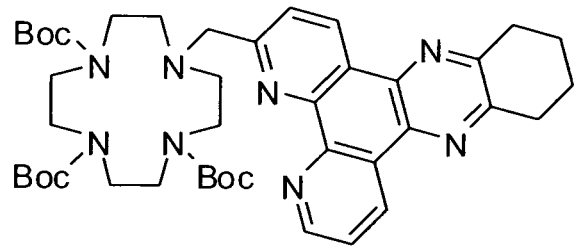

Potassium carbonate (124 mg, 0.716 mmol) and a catalytic amount (2 mg) of KI were added to a solution of 1,4,7-tris-*tert*-butoxycarbonyl-1,4,7,10-tetraazacyclododecane, **17**, (77 mg, 0.179 mmol) in CH_3CN (3 ml). The mixture was heated at 60°C and a solution of 3-chloromethyl-10,11,12,13-tetrahydrodipyrido-[3,2a:2',3'-c]-phenazine (60 mg, 0.179 mmol) in CH_2Cl_2 (3 ml) was added. The reaction mixture was boiled under reflux under argon overnight. The solution was filtered and the salts washed with CH_2Cl_2. The residue was purified by chromatography on silica gel (gradient elution: CH_2Cl_2 to 3 % CH_3OH/CH_2Cl_2, R_F = 0.44, 10 % CH_3OH/CH_2Cl_2) to yield a pale yellow solid (105 mg, 0.136 mmol, 76 %), m.p. 114-116°C. ^1H NMR (300 MHz, $CDCl_3$): 0.92-0.71 (27H, br m, CH_3), 2.04 (4H, m, H10, H13), 2.42-2.99 (4H, m, CH_2 ring), 3.07-3.87 (16H, br m, CH_2 ring + H11, H12), 4.24 (2H, s, CH_2-dpqC), 7.67 (1H, dd, J = 8.2, 4.4, H7), 7.72-7.97 (1H,

br s, H_2), 9.71 (1H, br s, H6), 9.26-9.44 (2H, br m, H8, H1). ^{13}C NMR (75 MHz, $CDCl_3$): 22.7 (C10, C13), 28.3 (CH_3), 28.5 (CH_3), 32.7 (C11, C12), 46.2-51.3 (C ring), 60.0-61.2 (CH_2-dpqC), 79.3 (CHN), 123.3 (C7), 123.8 (C Ar), 125.9 (c Ar), 127.0 (C2), 129.3 (C Ar), 130.4 (C Ar), 130.5 (C Ar), 137.6 (C Ar), 142.2 (C Ar), 146.4 (C Ar), 146.8 (C Ar), 151.3 (C Ar), 153.3 (C Ar), 154.7-157.0 (C=O). HRMS (+ m/z): $[M+Na]^+$ calculated for $C_{42}H_{58}N_8O_6Na$, 793.4377; found, 793.4379.

9. 1-(3-Methyl-10,11,12,13-tetrahydrodipyrido[3,2-a:2',3'-c]phenazine)-1,4,7,10-tetraazacyclododecane

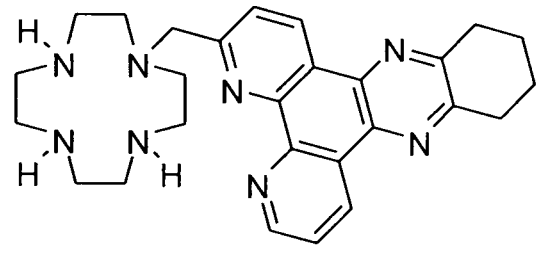

Trifluoroacetic acid (10 ml) was added to a solution of 1-(3-methyl-10,11,12,13-tetrahydrodipyrido[3,2-a:2',3'-c]phenazine)-4,7,10-tris(*tert*-butoxycarbonyl)-1,4,7,10-tetraazacyclododecane (104.7 mg, 0.136 mmol) in CH_2Cl_2 (3 ml). The mixture was stirred for 2 hours at room temperature. The solvent was evaporated and the residue redissolved for 3 times to facilitate elimination of excess acid and tert-butyl alcohol. The residue was taken into a 1 M KOH solution (5 ml) and the product extracted into CH_2Cl_2 (3 x 5 ml). The organic layer was dried over K_2CO_3. Removal of the solvent under reduced pressure yielded an orange solid (52.5 mg, 0.112 mmol, 82 %). m.p. >240 °C. ^1H NMR (300 MHz, $CDCl_3$): 2.09 (4H, m, H10, 13), 2.60-3.00 (16H, m, CH_2 ring), 3.24 (4H, m, H11, H12), 4.16 (2H, s, CH_2-dpqC), 7.69 (1H, d, J = 8.0, H2), 7.76 (1H, dd, J = 8.2, 4.4, H7), 9.26 (1H, dd, J = 4.4, 1.4, H6), 9.40 (1H, d, J = 8.0, H1), 9.46 (1H, dd, J = 8.2, 1.4, H8). ^{13}C NMR (75 MHz, $CDCl_3$): 22.6 (CH_2), 32.6 (CH_2), 45.2, 46.3, 47.1, 52.0 (CH_2 ring), 61.7 (CH_2), 122.8 (C7), 123.2 (C2), 125.9 (q Ar), 127.0 (q Ar), 132.7 (C8), 133.5 (C1), 137.1 (q Ar), 146.0 (q Ar), 146.8 (q Ar), 151.3 (C6), 153.3 (q Ar), 153.6 (q Ar), 162.3 (q Ar).

10. (S)-N-Chloroethanoyl-2-phenylethylamine[2, 3]

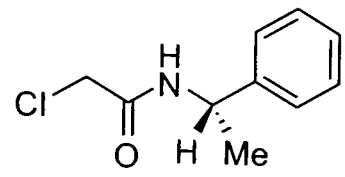

Chloroacetyl chloride (1.45 ml, 18.47 mmol) was added dropwise to a stirred solution of (S)-1-phenylethylamine (2 ml, 15.1 mmol) and triethylamine (2.45 ml, 18 mmol) in dry THF (75 ml) at -5°C under argon. The reaction mixture was allowed to return to room temperature and stirred for 1 hour. The product was extracted into diethyl ether, which was then washed with 0.1 M hydrochloric acid (15 ml), water (3 x 10 ml) and dried over K_2CO_3. Recrystallisation from diethyl ether yielded the product as white needles (1.17 g, 5.92 mmol, 39 %). M.p. 95-96°C. ^{1}H NMR (300 MHz, $CDCl_3$): δ 1.55 (3H, d, J = 6.9, CH_3), 4.08 (2H, m, CH_2), 5.15 (1H, q, J = 7.2, CH), 6.79 (1H, br s, NH), 7.35 (5H, m, Ph).

11. *N*-Chloroacetyl-L-alanine ethyl ester[4]

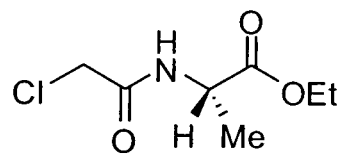

A solution of chloroacetyl chloride (0.81 g, 7.15 mmol) in THF (10 ml) was added dropwise to a stirred solution of L-alanine-ethyl-ester-hydrochloride (1 g, 6.5 mmol) and triethylamine (1.31 g, 13 mmol) in THF (25 ml) maintained at 0°C. The reaction was allowed to return to room temperature and stirred for approximately 90 minutes. The resulting suspension was filtered and washed with THF (2 x 25 ml) to give a slightly greenish solution. Upon reduction of the solvent volume and washing with slightly acidic water a greenish oily product was obtained (1.07 g, 5.53 mmol, 85 %). ^{1}H NMR (300 MHz, $CDCl_3$): δ 1.27 (3H, t, J = 7.2, $CH_2C\underline{H}_3$), 1.43 (3H, d, J = 7.2, $CHC\underline{H}_3$), 4.05 (2H, s, $C\underline{H}_2Cl$), 4.19 (2H, q, J = 7.2, $C\underline{H}_2CH_3$), 4.55 (1H, m, $C\underline{H}CH_3$), 7.18 (1H, br s, NH).

12. *N*-Chloroacetyl-L-glutamic acid diethyl ester[5]

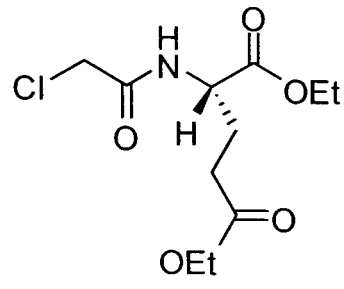

A solution of chloroacetyl chloride (0.78 g, 6.89 mmol) in THF (10 ml) was added dropwise to a stirred solution of L-glutamic acid-diethyl-ester-hydrochloride (1.5 g, 6.26 mmol) and triethylamine (1.26 g, 13.5 mmol) in THF (25 ml) maintained at 0°C. The reaction was allowed to return to room temperature and stirred for approximately 90 minutes. The resulting suspension was filtered and washed with THF (2 x 25 ml) to give a clear solution. Removal of the solvent under reduced pressure and washing with slightly acidic water yielded the product as a clear oil (1.66 g, 5.94 mmol, 95 %). ^{1}H NMR (300 MHz, $CDCl_3$): δ 1.27 (6H, m, $CH_2C\underline{H}_3$), 2.08 (4H, m, $C\underline{H}_2CH_3$), 4.07 (2H, s, CH_2Cl), 4.14 (2H, q, J = 15, $CHC\underline{H}_2CH_2$), 4.23 (2H, q, J = 15, $CHCH_2C\underline{H}_2$), 4.61 (1H, m, CH), 7.25 (1H, br s, NH).

13. 1-(3-Methyl-10,11,12,13-tetrahydrodipyrido[3,2-a:2',3'-c]phenazine)-4,7,10-tris[(S)-1-(1-phenyl)ethylcarbamoylmethyl]-1,4,7,10-tetraazacyclododecane

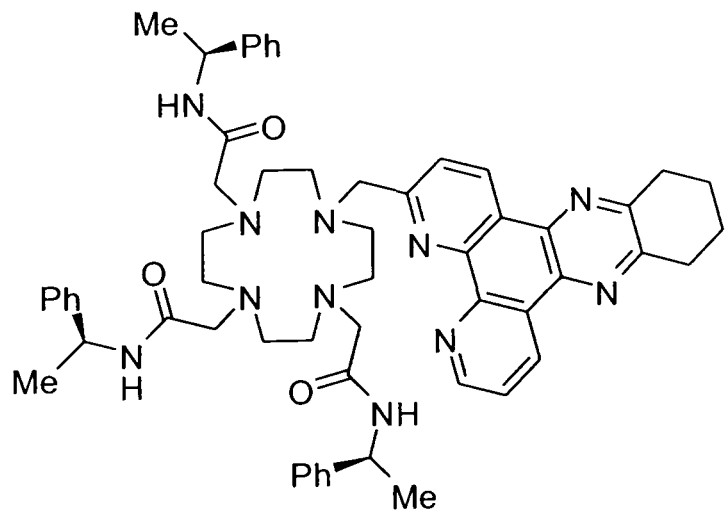

Potassium carbonate (138 mg, 0.995 mmol) and a catalytic amount of KI were added to a solution of 1-(3-methyl-10,11,12,13-tetrahydrodipyrido[3,2-a:2',3'-

c]phenazine)-1,4,7,10-tetraazacyclododecane (94.1 mg, 0.199 mmol) in CH_3CN (7 ml). The reaction mixture was heated at 60°C and a solution of (S)-N-(1-phenyleth-1-yl)chloroacetamide (118 mg, 0.597 mmol) in CH_2Cl_2 (7 ml) was added. The reaction mixture was boiled under reflux overnight, under argon. The solution was filtered and the salts washed with CH_2Cl_2. The product was purified by chromatography on neutral alumina to yield a yellow solid (gradient elution: CH_2Cl_2 to 1 % CH_3OH/CH_2Cl_2, R_F = 0.55, 7.5 % CH_3OH/CH_2Cl_2). (91 mg, 0.096 mmol, 48 %), m.p. 148-150°C. ^1H NMR (300 MHz, $CDCl_3$): 1.35 (6H, d, J = 6.7, CH_3), 1.56 (3H, d, J = 6.7, CH_3), 2.06 (4H, m, CH_2), 2.16-3.12 (16H, br m, CH_2 ring), 3.21 (4H, d, J = 4.0, CH_2), 3.42-4.45 (8H, br m, CH_2CO, CH_2-dpqC), 4.57 (1H, br m, CH), 4.75 (2H, br m, CH), 6.70-7.49 (18H, m , Ar, NH), 7.53 (1H, d, J = 8.3, H2), 7.96 (1H, br m, H7), 8.30 (1H, br m, H6), 9.37 (1H, d, J = 8.3, H1), 9.48 (1H, d, J = 8.2, H8). ^{13}C NMR (75 MHz, $CDCl_3$): 22.2 (CH_3), 22.7 (C10, C13), 22.8 (CH_3), 32.7 (C11, C12), 49.5 (CHN), 49.8-52.4 (CH_2 ring + CH_2CO), 60.4 (CH_2-dpqC), 123.4 (C2), 125.1 (C7), 126.3 (C Ar), 126.4 (C Ar), 126.8 (C Ar), 126.9 (C Ar), 127.4 (C Ar), 128.1 (C Ar), 128.2 (C Ar), 128.4 (C Ar), 133.2 (C8), 134.1 (C1), 137.0 (C Ar), 137.5 (C Ar), 143.5 (C Ar), 144.2 (C Ar), 145.6 (C Ar), 146.2 (C Ar), 153.6 (C Ar), 153.9 (C Ar), 154.1 (C Ar), 159.9 (C Ar), 169.1 (C=O), 170.7 (C=O). HRMS (+ m/z): $[M+H]^+$ calcd for $C_{57}H_{68}N_{11}O_3$, 954.5506; found, 954.5497.

14. 1-(3-Methyl-10,11,12,13-tetrahydrodipyrido[3,2-a:2',3'-c]phenazine)-4,7,10-tris(ethyl-N-acetylalanine)-1,4,7,10-tetraazacyclododecane

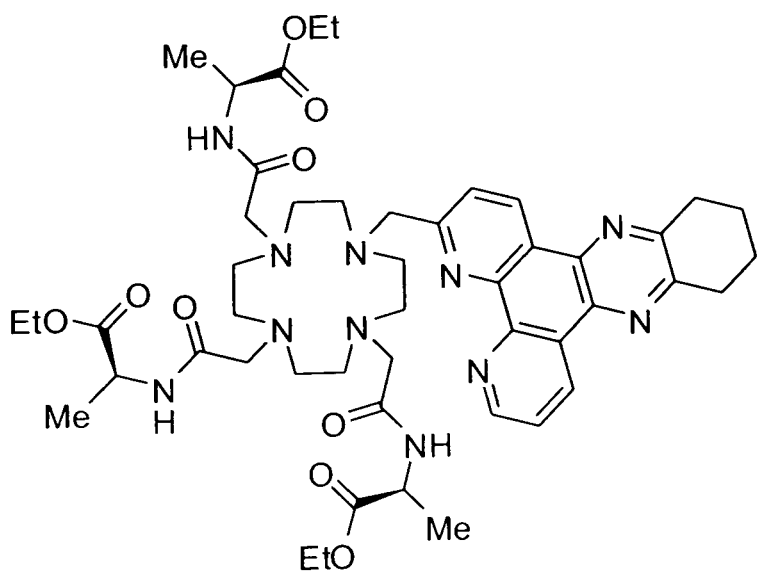

Potassium carbonate (116 mg, 0.840 mmol) and a catalytic amount of KI were added to a solution of 1-(3-methyl-10,11,12,13-tetrahydrodipyrido[3,2-a:2`,3`-c]phenazine)-1,4,7,10-tetraazacyclododecane (79.1 mg, 0.168 mmol) in CH_3CN (6 ml). The reaction mixture was heated at 60°C and a solution of *N*-chloroacetyl-L-alanine ethyl ester (97.6 mg, 0.504 mmol) in CH_2Cl_2 (6 ml) was added. The reaction mixture was boiled under reflux overnight, under argon. The solution was filtered and the salts washed with CH_2Cl_2. The product was purified by chromatography on neutral alumina. (gradient elution: CH_2Cl_2 to 1 % CH_3OH/CH_2Cl_2, R_F = 0.55, 7.5 % CH_3OH/CH_2Cl_2) to give a yellow solid. (94 mg, 0.10 mmol, 59 %). ^{1}H NMR (400 MHz, $CDCl_3$): 0.90-1.58 (18H, m, $CH_2C\underline{H}_3$, $CHC\underline{H}_3$), 2.06 (4H, m, H10, H13), 2.24-3.18 (16H, br m, CH_2 ring), 3.21 (4H, m, H11, H12), 3.42-4.45 (17H, m, CH_2CO, CH_2-dpqC, CH), 7.60 (1H, m, H2), 7.77 (1H, br m, H7), 7.89 (1H, br m, H6), 9.24 (1H, m, H1), 9.43 (1H, m, H8). ^{13}C NMR (75 MHz, $CDCl_3$): 14.1 (CH_3), 14.2 (CH_3), 17.1 (CH_3), 17.1 (CH_3), 17.5 (CH_3), 22.8 (C10, C13), 32.9 (C11, C12), 48.3-57.4 (CH_2 ring, CH_2CO, $C\underline{H}_2CH_3$), 61.3 (CH_2-dpqC), 124.2 (C2), 124.9 (C Ar), 126.7 (C Ar), 127.6 (C7), 133.2 (C8), 134.1 (C1), 137.4 (C Ar), 146.4 (C Ar), 146.9 (C Ar), 151.6 (C6), 154.3 (C Ar), 157.5 (C Ar), 160.9 (C Ar), 169.0 (C=O), 172.5 (C=O), 172.7 (C=O). m/z (ES^+): 491 (MCa^{2+}), 508 (MCu^{2+}) 965 (MNa^+).

15. 1-(3-Methyl-10,11,12,13-tetrahydrodipyrido[3,2-a:2',3'-c]phenazine)-4,7,10-tris(diethyl-*N*-acetyl-L-glutamate)-1,4,7,10-tetraazacyclododecane

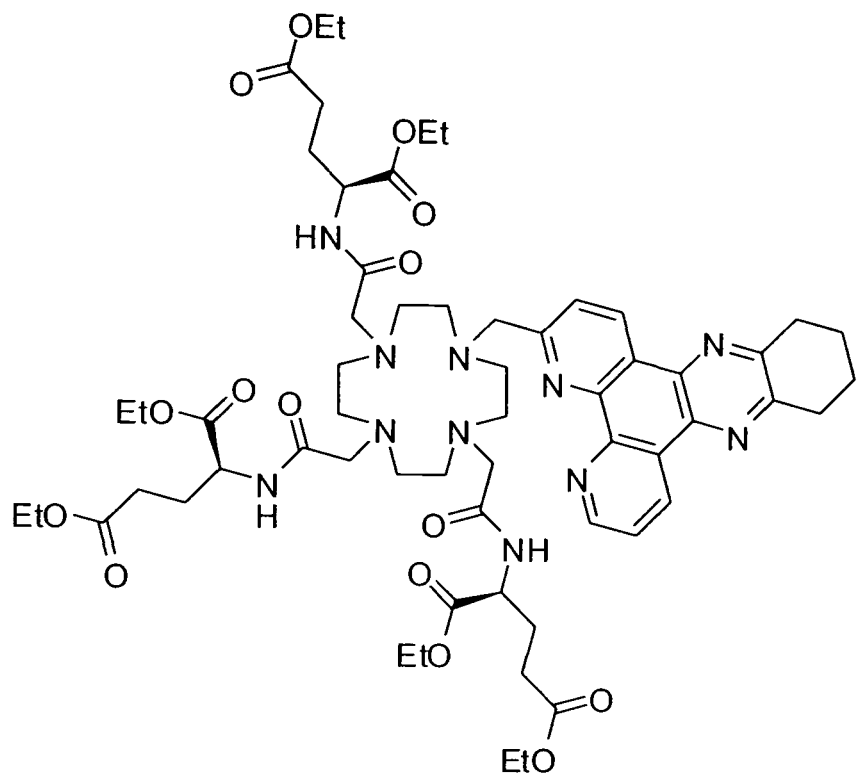

Potassium carbonate (129 mg, 0.935 mmol) and a catalytic amount of KI were added to a solution of 1-(3-methyl-10,11,12,13-tetrahydrodipyrido[3,2-a:2',3'-c]phenazine)-1,4,7,10-tetraazacyclododecane (87.8 mg, 0.187 mmol) in CH_3CN (7 ml). The reaction mixture was heated at 60°C and a solution of *N*-chloroacetyl-L-glutamic acid diethyl ester (157 mg, 0.561 mmol) in CH_2Cl_2 (7 ml) was added. The reaction mixture was boiled under reflux overnight, under argon. The solution was filtered and the salts washed with CH_2Cl_2. The product was purified by chromatography on neutral alumina to yield a pale yellow solid (gradient elution: CH_2Cl_2 to 1 % CH_3OH/CH_2Cl_2, R_F = 0.54, 7.5 % CH_3OH/CH_2Cl_2), (105 mg, 0.089 mmol, 48 %), m.p. 82-84°C. ^{1}H NMR (300 MHz, $CDCl_3$): 0.96-1.34 (18H, m, CH_3), 1.74-2.56 (16H, m, $C\underline{H}_2CH_3$, H10, H13), 2.82-3.42 (20H, br m, CH_2 ring, H11, H12), 3.72-4.64 (21H, m, CH_2CO, CH_2-dpqC, $CHCH_2C\underline{H}_2$, $CHC\underline{H}_2CH_2$, $C\underline{H}CH_2CH_2$), 7.68 (1H, m, H2), 7.76 (1H, br m, H7), 7.95 (1H, br m, H6), 9.35 (1H, m, H1), 9.45 (1H, m, H8). ^{13}C NMR (75 MHz, $CDCl_3$): 14.1 (CH_3), 14.2 (CH_3), 22.8 (C10, C13), 26.2 (CH_2), 30.4 (CH_2), 30.6 (CH_2), 32.9 (C11, C12), 50.4-60.7 (CH_2 ring, CH_2CO, $C\underline{H}_2CH_3$), 61.6 (CH_2-dpqC), 124.2 (C2), 124.7 (C Ar), 126.7 (C Ar), 127.7 (C7),

133.2 (C8), 134.1 (C1), 137.4 (C Ar), 146.3 (C Ar), 146.9 (C Ar), 151.9 (C6), 154.2 (C Ar), 157.5 (C Ar), 160.9 (C Ar), 169.4 (C=O), 171.3 (C=O), 171.6 (C=O), 172.4 (C=O), 172.8 (C=O). m/z (ES^+): 620 (MCa^{2+}), 632 (MCu^{2+}), 1223 (MNa^+)

16. [EuPh$_3$dpqC]Cl$_3$, [Eu.1]

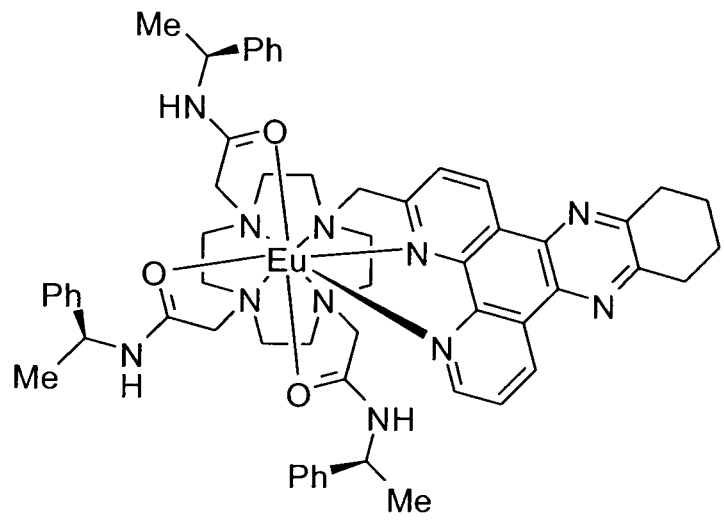

A solution of 1-(3-methyl-10,11,12,13-tetrahydrodipyrido[3,2-a:2',3'-c]phenazine)-4,7,10-tris[(S)-1-(1-phenyl)ethylcarbamoylmethyl]-1,4,7,10-tetraazacyclododecane (31.8 mg, 0.033 mmol) and Eu(OTf)$_3$ (20.0 mg, 0.033 mmol) in dry CH_3CN (5 ml) was boiled under reflux under argon overnight at 80°C. The solution was then added dropwise to ether (~ 20 ml) with stirring, the precipitate centrifuged and the solvent decanted. The solid was re-dissolved in CH_3CN and the process repeated to yield an off-white solid product (39 mg, 0.025 mmol, 76 %). m/z (ES^+): 628 ($MOTf^{2+}$), 1402 ($MOTf_2^+$). This complex was converted to the more water soluble chloride salt by ion exchange chromatography in water using an Amberlite IRA resin. λ_{max} (H_2O) 348 nm; τ (H_2O) = 1.04ms; τ (D_2O) = 1.59 ms, ϕ (H_2O) = 16%, ϕ(D_2O) = 20%. ^1H NMR (CD_3OD) Partial assignment: δ 37.51 (1H, s, H_{ax}), 36.88 (1H, s, H_{ax}), 31.43 (1H, s, H_{ax}), 27.03 (1H, s, H_{ax}), 26.45 (H6-dpqC), 15.17 (dpqC), 14.39, 10.27, 9.56, -2.06, -2.62, -3.78, -4.14, -7.40, -7.71, -8.08, -15.71, -16.24, -16.84, -17.13, -17.85, -18.49, -24.32. HRMS (+ m/z): $[MCF_3SO_3]^{2+}$ calcd for $C_{58}H_{68}N_{11}O_6F_3SEu$, 627.7081: found, 627.7080.

17. [EuAlaEt$_3$dpqC](CF$_3$SO$_3$)$_3$

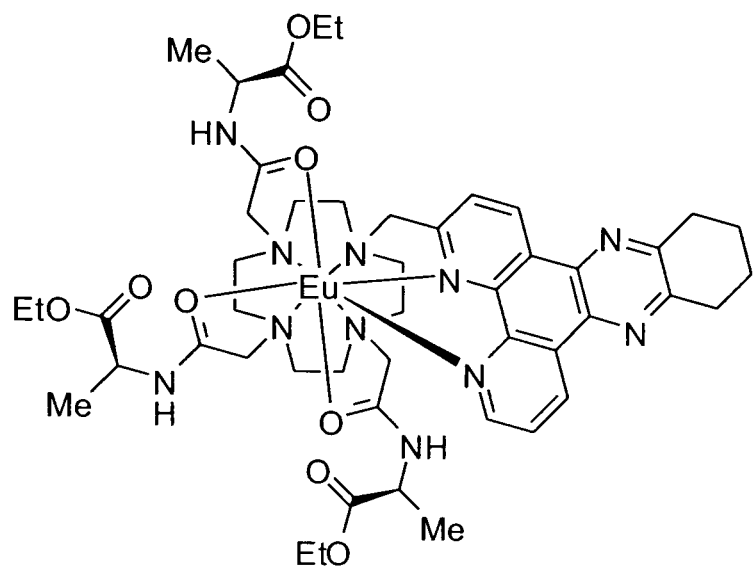

A solution of 1-(3-methyl-10,11,12,13-tetrahydrodipyrido[3,2-a:2',3'-c]phenazine)-4,7,10-tris(ethyl-N-acetylalanine)-1,4,7,10-tetraazacyclododecane (27.7 mg, 0.029 mmol) and Eu(OTf)$_3$ (17.4 mg, 0.029 mmol) in dry CH_3CN (5 ml) was boiled under reflux under argon overnight at 80°C. The solution was then added dropwise to ether (~ 20 ml) with stirring, the precipitate centrifuged and the solvent decanted. The solid was redissolved in CH_3CN and the process repeated to yield an off-white solid product (23mg, 0.015 mmol, 51 %). m/z (ES^+): 365 (M^{3+}), 621 ($MOTf^{2+}$). The product was hydrolysed immediately to give the zwitterionic complex (see **22**).

18. [EuGluEt$_3$dpqC](CF$_3$SO$_3$)$_3$

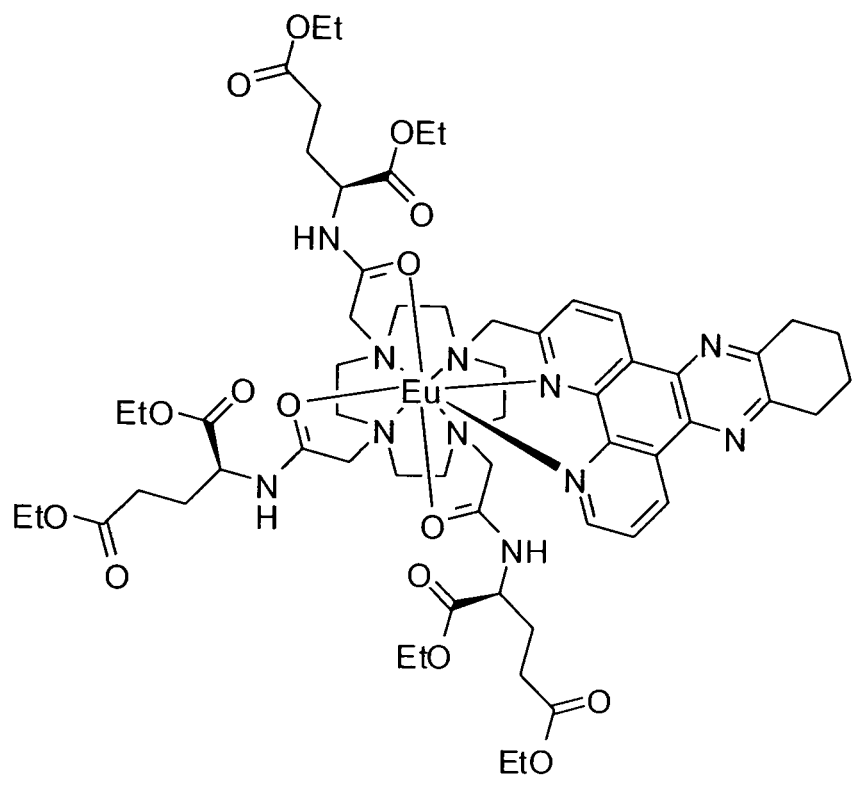

An analogous procedure to that described in **17** was followed using 1-(3-methyl-10,11,12,13-tetrahydrodipyrido[3,2-a:2',3'-c]phenazine)-4,7,10-tris(diethyl-*N*-acetyl-L-glutamate)-1,4,7,10-tetraazacyclododecane (25.4 mg, 0.021 mmol) and Eu(OTf)$_3$ (12.5 mg, 0.021 mmol) in dry CH_3CN (5 ml). The product was obtained as an off-white solid (36 mg, 0.02 mmol, 94 %). m/z (ES^+): 451 (M^{3+}), 751 ($MOTf^{2+}$). The product was hydrolysed immediately to give the anionic complex (see **23**).

19. [TbPh$_3$dpqC]Cl$_3$, [Tb.1]

An analogous procedure to that described in **17** was followed using 1-(3-methyl-10,11,12,13-tetrahydrodipyrido[3,2-a:2',3'-c]phenazinyl)-4,7,10-tris[(S)-1-(1-phenyl)ethylcarbamoylmethyl]-1,4,7,10-tetraazacyclododecane (30.9 mg, 0.032 mmol) and Tb(OTf)$_3$ (19.6 mg, 0.032 mmol) in dry CH_3CN (5 ml). The product was obtained as a pale-yellow solid (39.5 mg, 0.0253 mmol, 79 %). λ_{max} (H_2O) 348 nm; τ (H_2O) = 1.56 ms, τ (D_2O) = 1.72 ms, $\phi(H_2O)$ = 40 %, $\phi(D_2O)$ = 48 %. ^1H NMR (CD_3OD): δ 118.57, 93.49, 73.02, 67.19, 64.91, 63.33, 54.31, 37.96, -2.26, -7.03, -7.28, -8.11, -9.07, -9.35, -15.62, -17.19, -41.84, -73.53, -79.19, -110.18. m/z (ES^+):

371 (M^{3+}), 631 ($MOTf^{2+}$), 1411 ($M[OTf]_2^+$). HRMS (+ m/z): $[M + CF_3SO_3]^{2+}$ calcd for $C_{58}H_{68}N_{11}O_6F_3STb$, 630.7101; found, 630.7099.

20. [TbAlaEt$_3$dpqC](CF$_3$SO$_3$)$_3$

An analogous procedure to that described in **17** was followed using 1-(3-methyl-10,11,12,13-tetrahydrodipyrido[3,2-a:2',3'-c]phenazine)-4,7,10-tris(ethyl-N-acetylalanine)-1,4,7,10-tetraazacyclododecane (25.4 mg, 0.027 mmol) and $Tb(OTf)_3$ (16.4 mg, 0.027 mmol) in dry CH_3CN (5 ml). The product was obtained as an off-white solid (14.8 mg, 0.0957 mmol, 35 %). m/z (ES^+): 367 (M^{3+}), 625 ($MOTf^{2+}$), 1399 ($M[OTf]_2^+$). The product was hydrolysed immediately to give the zwitterionic complex (see **24**).

21. [TbGluEt$_3$dpqC](CF$_3$SO$_3$)$_3$

An analogous procedure to that described in **17** was followed using 1-(3-methyl-10,11,12,13-tetrahydrodipyrido[3,2-a:2',3'-c]phenazine)-4,7,10-tris(diethyl-*N*-acetyl-L-glutamate)-1,4,7,10-tetraazacyclododecane (22.9 mg, 0.0190 mmol) and $Tb(OTf)_3$ (11.5 mg, 0.0190 mmol) in dry CH_3CN (5 ml). The product was obtained as an off-white solid (34.1 mg, 0.189 mmol, 99 %). m/z (ES^+): 453 (M^{3+}), 754 ($MOTf^{2+}$), 1657 ($MOTf_2^+$). The product was hydrolysed immediately to give the anionic complex (see **25**).

*The series of anionic/zwitterionic complexes **22** – **25** were prepared in the following manner, containing sodium chloride that was not considered significant in assessing their photophysical properties. In each case, hydrolysis was followed by monitoring the disappearance of the ESMS peaks corresponding to the parent cationic complex. The zwitterionic and anionic complexes appeared to have poor mobility in either negative or positive ion mode.*

22. $EuAla_3dpqC$, [Eu.2]

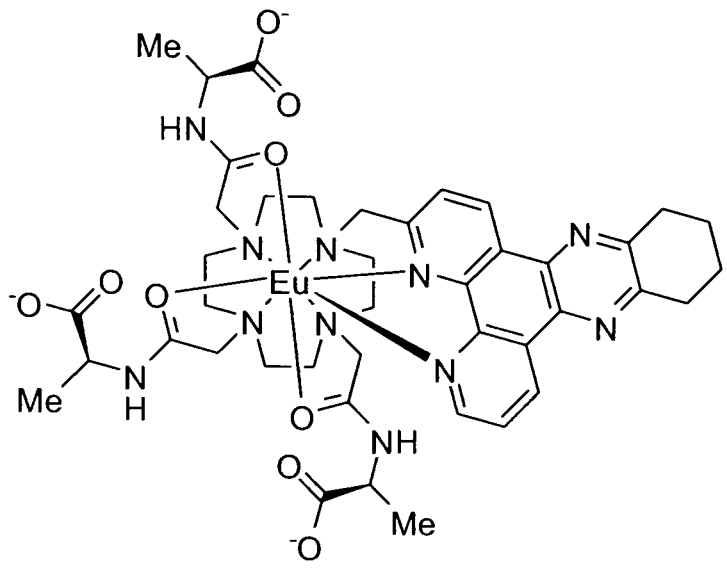

To $EuAlaEt_3dpqC\ (CF_3SO_3)_3$ (23.0 mg, 0.0150 mmol) was added a 0.02 M solution of sodium hydroxide (3.00 ml, 0.0600 mmol) and the mixture stirred overnight. The solution was neutralised using dil. HCl and the product was obtained following evaporation of the solvent under reduced pressure. λ_{max} (H_2O) 348 nm; τ (H_2O) = 0.96 ms, ϕ (H_2O) = 18 %.

23. $[EuGlu_3dpqC]Na_3$, [Eu.4]

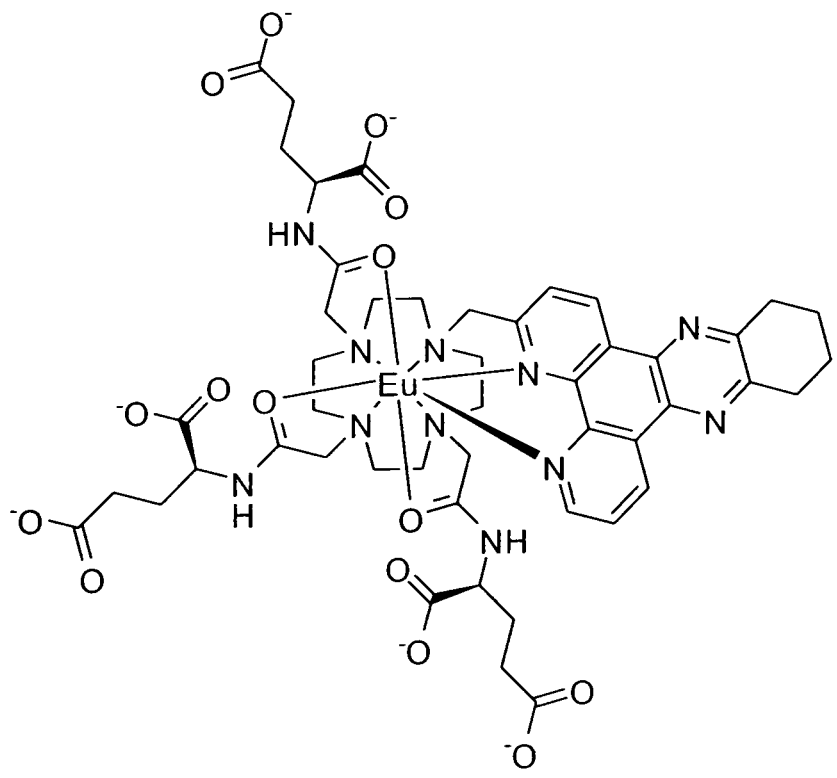

Complex EuGluEt$_3$dpqC $(CF_3SO_3)_3$ (35.6 mg, 0.0198 mmol) was hydrolysed using a procedure identical to that described for compound **22.** λ_{max} (H_2O) 348 nm; τ (H_2O) = 1.0 ms, ϕ (H_2O) = 15 %.

24. TbAla$_3$dpqC, [Tb.2]

Complex Tb(Ala-Et)$_3$dpqC $(CF_3SO_3)_3$ (14.8 mg, 0.0096 mmol) was hydrolysed using a procedure identical to that described for compound **22.** λ_{max} (H_2O) 348 nm; τ (H_2O) = 1.49 ms, ϕ (H_2O) = 36 %.

25. [TbGlu$_3$dpqC]Na$_3$, [Tb.4]

Complex Tb(Glu-Et)$_3$dpqC $(CF_3SO_3)_3$ (34.1 mg, 0.0189 mmol) was hydrolysed using a procedure identical to that described for compound **22.** λ_{max} (H_2O) 348 nm; τ (H_2O) = 1.59 ms, ϕ (H_2O) = 34 %.

26. 1-(3-Methyl-10,11,12,13-tetrahydrodipyrido[3,2-a:2',3'-c]phenazine)-4,7,10-tris-*tert*-butoxycarbonylmethyl-1,4,7,10-tetraazacyclododecane

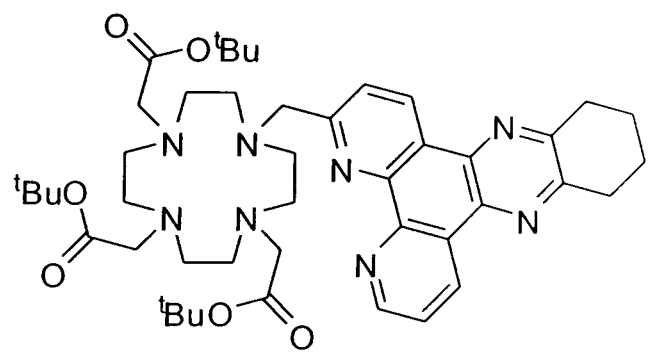

Potassium carbonate (401 mg, 2.90 mmol) and a catalytic amount of KI were added to a solution of 1,4,7-tris-*tert*-butoxycarbonylmethyl-1,4,7,10-tetraazacyclododecane , **22**, (299 mg, 0.580 mmol) in CH_3CN (15 ml). The mixture was heated at 60°C and a solution of 3-chloromethyl-10,11,12,13-tetrahydrodipyrido-[3,2a:2',3'-c]-phenazine (223 mg, 0.580 mmol) in CH_2Cl_2 (20 ml) was added. The reaction mixture was boiled under reflux overnight, under argon. The solution was filtered and the

salts washed with CH_2Cl_2. evaporation of the solvent afforded the crude residue. The product ester was purified by chromatography on silica gel to yield a very pale yellow solid (gradient elution: CH_2Cl_2 to 3.3 % CH_3OH/CH_2Cl_2, R_F = 0.47, 10 % CH_3OH/CH_2Cl_2. (68 mg, 0.084 mmol, 15 %), m.p. 137-139°C. ^{1}H NMR (300 MHz, $CDCl_3$): 1.08 (18H, s, CH_3), 1.41 (9H, s, CH_3), 2.05 (4H, m, H10, H13), 2.25-3.58 (28H, br m, CH_2 ring, H11, H12), 7.68 (1H, m, H7), 7.75 (1H, m, H2), 8.76 (1H, dd, J = 4.2, 1.2, H6), 9.42 (1H, m, H1), 9.48 (1H, m, H8). ^{13}C NMR (100 MHz, $CDCl_3$): 27.9 (CH_3), 50.9-60.4 (CH_2 ring), 81.6-82.7 (CH_2CO), 123.6 (C2), 123.9 (C Ar), 126.2 (C Ar), 127.7 (C Ar), 133.5 (C Ar), 133.9 (C Ar), 137.2 (C8), 137.5 (C1), 145.8 (C Ar), 146.4 (C Ar), 151.0 (C6), 154.2 (C Ar), 154.5 (C Ar), 160.4 (C Ar), 172.5 (C=O), 172.9 (C=O).). m/z (ES^+): 836 (MNa^+).

27. EuDO3AdpqC, [Eu.3]

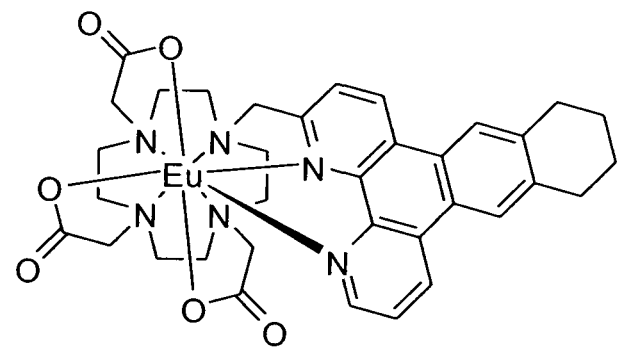

Trifluoroacetic acid (4 ml) was added to a solution of 1-(3-methyl-10,11,12,13-tetrahydrodipyrido[3,2-a:2',3'-c]phenazine)-4,7,10-tris-tert-butoxycarbonylmethyl-1,4,7,10-tetraazacyclododecane (33.8 mg, 0.042 mmol) in CH_2Cl_2 (2 ml). The mixture was stirred overnight at room temperature. The solvent was evaporated and the residue re-dissolved in CH_2Cl_2 for 3 times to facilitate elimination of excess acid and *tert*-butyl alcohol. The product, was checked by ^{1}H NMR to ensure complete ester hydrolysis, and was used for complexation immediately. ^{1}H NMR (300 MHz, CD_3OD): 2.06 (4H, m, H10, H13), 2.90-3.96 (28 H, br m, CH_2 ring, CH_2, CH_2-dpqC, H11, H12), 8.21 (2H, m, H7, H2), 9.19 (1H, m, H6), 9.38 (1H, d, H1), 9.72 (1H, m, H8). The ligand was dissolved in a mixture of methanol and water (1:1, 10 ml) and the pH raised to 5.5 by addition of a 1 M solution of KOH. $EuCl_3.6H_2O$ (15.4 mg, 0.042 mmol) was added and the mixture heated at 90°C overnight. After being

allowed to cool to room temperature the pH of the mixture was raised to 10.0 using dilute KOH solution and the mixture further stirred for 1 hour in order to precipitate excess lanthanide as its hydroxide salt. The solid in the suspension was removed by syringe filtration and the pH of the resulting clear solution again reduced to 5.5. The solution was freeze-dried to yield a pale yellow solid product. 10 mg were further purified by chromatography on alumina for use in quantum yield determination (gradient elution: CH_2Cl_2 to 30 % CH_3OH/CH_2Cl_2, R_F = 0.33 30 % CH_3OH/CH_2Cl_2), to give a colourless complex. Recovery was only 10 %. λ_{max} (H_2O) 348 nm; τ (H_2O) = 1.06 ms ; $\phi(H_2O)$ = 18 %.

28. TbDO3AdpqC, [Tb.3]

TbDO3AdpqC was prepared using the same quantities and followed an identical procedure to that desribed for the synthesis of compound **27**. λ_{max} (H_2O) 348 nm; τ (H_2O) = 1.46 ms ; $\phi(H_2O)$ = 33 %

29. 1,7-Bis(benzyloxycarbonyl)-1,4,7,10-tetraazacyclododecane[6]

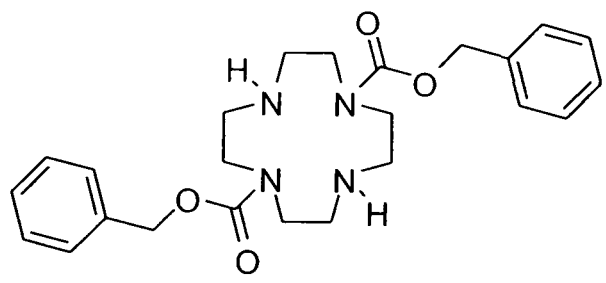

Cyclen (5 g, 0.029 mol) was dissolved in a mixture of H_2O (50 ml) and dioxane (20 ml). Na_2HPO_4 (14 g, 0.099 moles) was added and the pH of the solution adjusted to approximately 2.5 by addition of c. HCl. Benzyl chloroformate (12 g, 0.070 mol) was then added dropwise within 2.5 h to give a colourless, transparent solution. The solution was stirred at room temperature for 18 h; during this time a quantity of white solid precipitated from the mixture. The solvent was removed under reduced pressure to yield a white semi-solid. This was washed with diethyl ether (3 x 50 ml) (the mixture sonicated for 5 mins). H_2O (100 ml) was added and the pH made slightly basic by addition of a concentrated aqueous NaOH solution. The product was

extracted from the aqueous mixture with diethyl ether (3 x 150 ml). The organic layer was dried over Na_2SO_4, filtered and evaporated to yield the product as a viscous oil (0.5 g, 0.0238 mol, 82 %). M.p. 113 – 116°C. ^{1}H NMR (500 MHz, $CDCl_3$): 7.40 – 7.30 (m, 10H, Ph), 5.14 (s, 4H, OCH_2), 3.41 (br m, 8H, NCH_2), 2.95 – 2.72 (br m, 8H, NCH_2). ^{13}C NMR (125.7 MHz, $CDCl_3$): 156.9, 156.8 (C=O), 136.8, 136.7 (Ph(q)), 128.6, 128.5, 128.1, 128.0, 127.9, 127.5 (Ph), 67.2, 67.1 (OCH_2), 51.2, 50.8, 50.7, 50.3, 49.7, 49.2, 48.6, 48.3 (NCH_2). m/z (ES^+) 441 (MH^+), 881 (M_2H^+).

30. 1,7-Benzyloxycarbonyl-4,10-(1-(1-phenyl)ethylcarbamoylmethyl)-1,4,7,10-tetraazacyclododecane

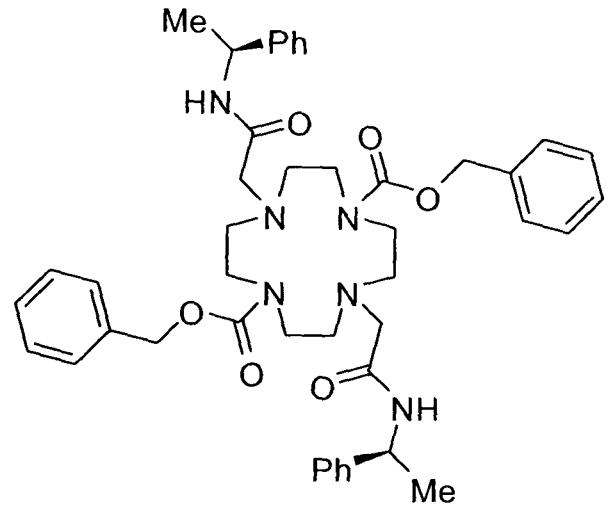

Cs_2CO_3 (1.85 g, 5.67 mmol) and 2-chloro-N-[(S)-1-phenylethyl]ethanamide (1.12 g, 5.57 mmol) were added to a solution of 1,7-bis(benzyloxycarbonyl)-1,4,7,10-tetraazacyclododecane (1.13 g, 2.58 mmol) in CH_3CN (5 cm^3). The mixture was heated at 80°C with stirring for 48 h. After the mixture had cooled the inorganic salts were removed by filtration and the solvent removed to yield the crude product. Purification by chromatography on silica (gradient elution: CH_2Cl_2 to 3 % CH_3OH/CH_2Cl_2. R_f = 4 % CH_3OH/CH_2Cl_2) gave the product as a solid (1.39 g, 1.79 mmol, 69 %). M.p. 64 – 66 °C. ^{1}H NMR (300 MHz, $CDCl_3$): 7.50 – 7.20 (m, 22H, Ph + NHCO), 5.11 (m, 2H, CH), 3.41 (br, 8H, ring CH_2), 3.14 (s, 4H, NCH_2), 2.73 (br, 8H, ring CH_2), 1.43 (d, 6H, J = 5.7 Hz, CH_3). ^{13}C NMR (75.4 MHz, $CDCl_3$): 170.0 (OC=O), 156.8 (NC=O), 143.7 (Ph(q)), 136.3 (CH_2Ph(q)), 128.6, 128.3, 128.2, 127.2, 126.3, 67.3 (O$\underline{C}H_2$Ph), 59.0 (N$\underline{C}H_2$C=O), 56.1, 55.2, 54.7, 48.8, 47.6, 46.8

(all CH_2 ring), 48.5 (CH), 21.8 (CH_3). m/z (ES^+) 763 (MH^+), 785 (MNa^+). HRMS (+ m/z): $[M+H]^+$ calcd for $C_{44}H_{55}N_6O_6$, 763.4187; found, 763.4178.

31. 1,7-(1-(1-Phenyl)ethylcarbamoylmethyl)-1,4,7,10-tetraazacyclododecane[3]

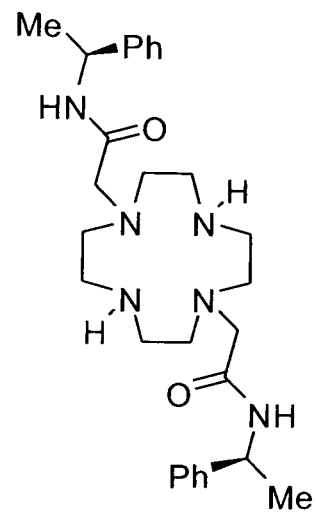

1,7-Benzyloxycarbonyl-4,10-(1-(1-phenyl)ethylcarbamoylmethyl)-1,4,7,10-tetraazacyclododecane (1.39 g, 1.79 mmol) was dissolved in ethanol (~ 30 ml). $Pd(OH)_2$-C (~120 mg) was added and the mixture hydrogenated at 45 psi for 48 hours. The solution was then filtered through celite and the solvent removed to yield the product (0.88 g, 1.78 mmol, 99 %), m.p. 140 – 143°C. ^1H NMR (500 MHz, $CDCl_3$): 7.94 (d, 2H, J = 8.5 Hz, CONH), 7.34 (d, 4H, J = 7.5 Hz, Ph(o)), 7.28 (t, 4H, J = 7.5 Hz, Ph(m)), 7.20 (t, 2H, J = 7.5 Hz, Ph(p)), 5.04 (m, 2H, CH), 3.27 (s, 4H, NCH_2CO), 2.73 (s, 8H, CH_2 ring), 2.64 (s, 8H, CH_2 ring) 1.44 (d, 6H, J = 7.0 Hz, CH_3). ^{13}C NMR (125.7 MHz, $CDCl_3$): 170.4 (C=O), 143.8 (Ph(q), 128.5 (Ph(m)), 127.1 (Ph(p)), 126.5 (Ph(o)), 60.1 (NCH_2), 52.7 (CH_2 ring), 48.7 (CH), 46.8 (CH_2 ring), 21.7 (CH_3). m/z (ES^+) 495 (MH^+). HRMS (ES^+) (+ m/z): $[M + Na]^+$ calculated for $C_{28}H_{42}N_6O_2$, 495.3447; found 495.3431.

32. 1-(3-Methyl-10,11,12,13-tetrahydrodipyrido[3,2-a:2',3'-c]phenazine)-4,10-(1-(1-phenyl)ethylcarbamoylmethyl)-1,4,7,10-tetrazacyclododecane

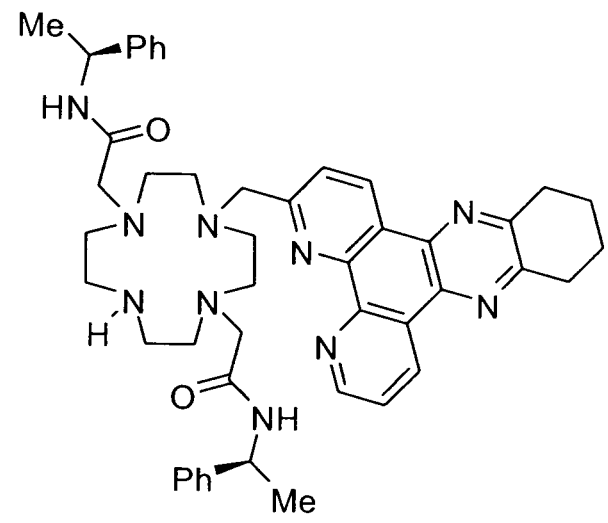

1,7-(1-(1-Phenyl)ethylcarbamoylmethyl)-1,4,7,10-tetraazacyclododecane (100 mg, 0.202 mmol), 3-chloromethyl-10,11,12,13-tetrahydrodipyrido-[3,2a:2',3'-c]-phenazine (67.6 mg, 0.202 mmol) and K_2CO_3 (27.9 mg, 0.202 mmol) were dissolved in CH_3CN (10 ml) and refluxed for 2 days with a $CaCl_2$ drying tube. The reaction mixture was filtered and the solvent removed to yield the crude product. Purification was by chromatography on alumina yielded the product as an off-white solid (54.1 mg, 68 μmol, 34 %). (gradient elution: CH_2Cl_2 to 0.5 % CH_3OH/CH_2Cl_2). ^{1}H NMR (500 MHz, $CDCl_3$): 9.56 (d, 1H, J = 8.0, H8), 9.43 (d,1H, J = 8.0, H1), 8.96 (m, 1H, H6), 8.77 (br, 1H, CONH), 8.62 (br, 1H, CONH), 7.84 (m, H, H7), 7.60 (d, 1H, J = 8.0, H2), 7.40 – 7.04 (m, 10H, Ph), 5.00 (m, 2H, CH), 3.72 – 2.22 (br m, 26H, NCH_2CO, CH2-dpqC, CH_2 ring), 2.09 (br m, 4H, CH_2), 1.38 (br, 6H, CH_3). ^{13}C NMR (125.7 MHz, $CDCl_3$): 170.1 (C=O), 160.1 (C Ar), 155.1 (C Ar), 155.0 (C Ar), 150.4 (C Ar), 146.2 (C Ar), 146.0 (C Ar), 144.3 (Ph(q)), 137.3 (C Ar), 137.0 (C Ar), 134.8 (C1), 134.6 (C8), 128.5 – 128.3 (Ph(m)), 127.0 – 126.2 (Ph(o, p), 125.4 (C7), 124.7 (C2), 61.1 (CH_2-dpqC), 55.8 (ring CH_2), 52.8 (ring CH_2), 51.4 (NCH_2), 49.3 (NCH_2), 48.5 (CH), 47.1 (CH), 32.9 (C11, C12), 22.7 (CH_3), 22.6 (C10, C13). m/z (ES^+) 428 $(MCu)^{2+}$, 793 $(MH)^+$.

33. (4-Aminobutyl) carbamic acid tert-butyl ester[7]

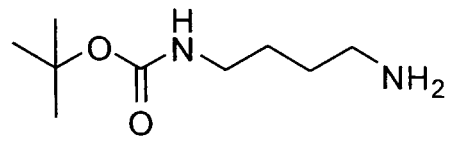

1,4-Diaminobutane (4.4 g, 0.05 mol), was dissolved in a solution of Et_3N and methanol (10 % Et_3N in MeOH, 110 ml). A solution of di-tert-butyl-dicarbonate (3.63 g, 0.017 mol) in methanol (10 ml) was added dropwise to the mixture with vigorous stirring, and the mixture was stirred at room temperature overnight. The methanol and Et_3N were removed in vacuo to yield an oily residue that was dissolved in CH_2Cl_2 (100 ml) and washed with a solution of aqueous Na_2CO_3 (2 x 100 ml). The organic layer was dried over anhydrous Na_2SO_4, filtered and the solvent removed in vacuo. Purification by flash column chromatography gave a colourless oil (2.22 g, 11.97 mmol, 70 %) (gradient elution: $CHCl_3$ to 1:10:89 NH_4OH:CH_3OH:$CHCl_3$, R_F = 0.38 1:10:89 NH_4OH:CH_3OH:$CHCl_3$). ^1H NMR (300 MHz, $CDCl_3$): 4.73 (br s, 1H, NHCO), 3.13 (dt, 2H, CH_2NH), 2.68 (t, 2H, CH_2NH_2), 1.41 (m, 4H, $(CH_2)_2CH_2NH_2$), 1.39 (s, 9H, $(CH_3)_3$), 1.21 (s, 2H, NH_2).

34. N-(4-Chloroacetimidobutyl)-tert-butyloxycarbonamide

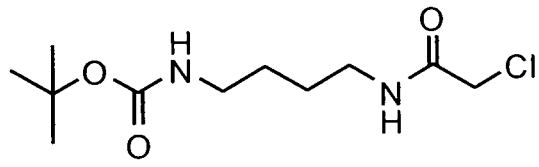

To (4-aminobutyl) carbamic acid tert-butyl ester (2.22 g, 11.97 mmol) in 6 ml of CH_2Cl_2 was added NaOH (0.47 g, 11.97 mmol) in 0.6 ml H_2O. To the cooled solution was added chloroacetylchloride (1.31 g, 11.97 mmol) in 6cm^3 CH_2Cl_2 whilst maintaining a temperature of <-10°C. After 1 h the precipitated white product which had formed was collected by filtration and dried under reduced pressure. The organic layer was washed with H_2O, dried over anhydrous K_2CO_3 and the solvent removed to yield more of the title compound as a colourless solid (1.73 g, 6.53 mmol, 55 %). ^1H NMR (300 MHz, $CDCl_3$): 6.69 (s, 1H, $CH_2N\underline{H}COCH_2$), 4.62 (s, 1H, $CH_2N\underline{H}CO_2$), 4.05 (s, 2H, CH_2Cl), 3.37 (q, 2H, J = 6.2, $C\underline{H}_2NHCO_2$), 3.14 (q, 2H, J = 6.2,

$C\underline{H}_2NHCO_2$), 1.56 (m, 4H, $(CH_2)_2CH_2NHCO$), 1.44 (s, 9H, $(CH_3)_3$). ^{13}C NMR (75 MHz, $CDCl_3$): 166.1 (C=O amide), 156.2 (C=O carbamate), 42.8 (NCH_2), 40.2 (C(q)), 39.6 (NCH_2), 28.5 ($(CH_3)_3$), 27.6 (CH_2), 26.7 (CH_2).

35. 1-(4-(*tert*-Butyloxycarbamoyl-butyl-carbamoylmethyl)-7-(3-methyl-10,11,12,13-tetrahydrodipyrido[3,2-a:2',3'-c]phenazine)-4,10-(1-(1-phenyl)ethylcarbamoylmethyl)-1,4,7,10-tetraazacyclododecane

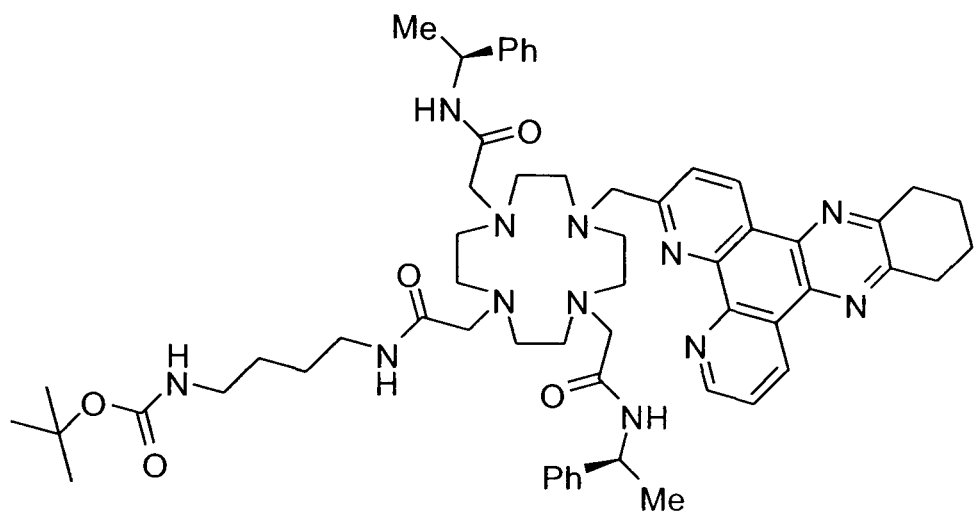

1-(3-Methyl-10,11,12,13-tetrahydrodipyrido[3,2-a:2',3'-c]phenazine)-4,10-(1-(1-phenyl)ethylcarbamoylmethyl)-1,4,7,10-tetrazacyclododecane (54.1 mg, 6.83×10^{-5} mol), N-(4-chloroacetimidobutyl)-tert-butyloxycarbonamide (18.1 mg, 6.83×10^{-5} mol), Cs_2CO_3 (22.3 mg, 68 µmol) and a catalytic amount of KI were dissolved in a mixture of CH_2Cl_2 and CH_3CN (1:1, 8 ml) and the mixture boiled under reflux for 24 hours. The salt was removed by filtration and the solvent removed in vacuo to yield the crude product. Purification by chromatography on alumina yielded the product as a glassy solid (40 mg, 39 µmol, 57 %). (gradient elution: CH_2Cl_2 to 0.5 % CH_3OH/CH_2Cl_2, $R_f = 0.47$, 5 % CH_3OH/CH_2Cl_2). ^1H NMR (500 MHz, $CDCl_3$): 9.44 (m, 2H, H8, H1), 9.23 (m, 1H, H6), 7.95 (br m, 2H, CONH), 7.72 (m, 1H, H7), 7.68 (d, 1H, J = 8.5, H2), 7.16 – 6.70 (m, 11H, Ph, $N\underline{H}COCH_2$), 4.85 (m, 2H, CH), 4.80 (t, 1H, $NHCO_2$), 4.26 – 4.00 (m, 6H, NCH_2CO, CH_2-dpqC), 3.56 (br, 2H, NCH_2CO), 3.26 – 2.80 (br m, 24H, ring CH_2, H11, H12, $CO_2NHC\underline{H}_2$, $C\underline{H}_2NHCO$), 2.08 (br m, 4H, H10, H13), 1.50 (m, 4H, $(C\underline{H}_2)_2CH_2NHCO$), 1.40 (s, 9H, $(CH_3)_3$), 1.30 – 1.16 (br, 6H, CH_3). ^{13}C NMR (125.7 MHz, $CDCl_3$): 168.0 (C=O amide), 167.7 (C=O amide), 156.3 (C=O carbamate), 154.4 (C Ar), 152.0 (C Ar), 146.9 (C Ar), 146.3 (C

Ar), 143.5 (C Ar), 142.8 (Ph(q)), 137.6 (C Ar), 137.4 (C Ar), 134.1 (C1), 133.2 (C8), 128.8 – 128.3 (Ph(m)), 127.2 – 126.2 (Ph(o, p)), 124.5 (C7), 124.2 (C2), 61.6 (CH_2-dpqC), 56.5 (ring CH_2), 55.7 (ring CH_2), 50.3 (NCH_2), 49.1 (NCH_2), 48.5 (CH), 40.2 (NCH_2 linker), 39.1 (NCH_2 linker), 32.9 (C11, C12), 28.6 ((CH_3)$_3$), 27.7 (CH_2), 26.5 (CH_2), 22.9 (CH_3), 22.2 (C10, C13). m/z (ES^+) 531 $(MCa)^{2+}$, 542 $(MCu)^{2+}$. HRMS (+ m/z): $[M + Na]^+$ calculated for $C_{58}H_{76}O_5N_{12}Na$ 1043.593; found 1043.595.

36. 1-(4-Aminobutylcarbamoylmethyl)-7-(3-methyl-10,11,12,13 tetrahydrodipyrido[3,2-a:2',3'-c]phenazine)-4,10-(1-(1-phenyl)ethylcarbamoylmethyl)-1,4,7,10-tetraazacyclododecane

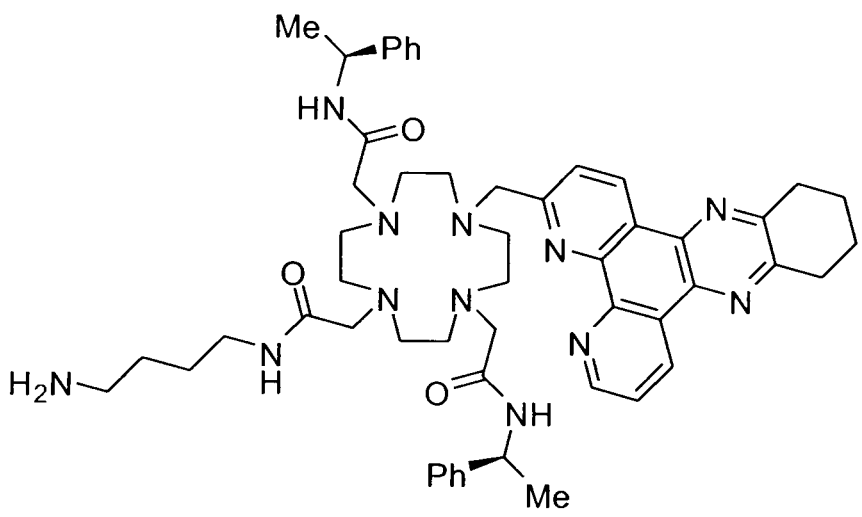

1-(4-(*tert*-Butyloxycarbamoyl-butyl-carbamoylmethyl)-7-(3-methyl-10,11,12,13-tetrahydrodipyrido[3,2-a:2',3'-c]phenazine)-4,10-(1-(1-phenyl)ethylcarbamoylmethyl)-1,4,7,10-tetraazacyclododecane (21.5 mg, 2.11 x 10^{-5} mol) was dissolved in a mixture of CH_2Cl_2 (1.5 ml) and TFA (3 ml) and was stirred overnight at room temperature. The solvent and acid were removed under reduced pressure. The residue was redissolved 3 times in CH_2Cl_2 (3 ml) to facilitate elimination of excess acid and tert-butyl alcohol. The crude product was taken into an aqueous KOH solution (1 M, 5 ml) and was extracted 3 times with CH_2Cl_2 (5 ml) to yield an orange oily product. (12.9 mg, 1.40 x 10^{-5} mol, 66 %). The product was used directly for complexation. ^{1}H NMR (300 MHz, $CDCl_3$): 9.49 (d, 1H, J = 7.8, H8), 9.36 (d, 1H, J = 8.4, H1), 9.22 (m, 1H, H6), 7.90 – 7.00 (m, 14H, H7, H2, CONH, Ph), 5.10 (m, 2H, CH), 4.08 (s, 2H, CH_2-dpqC), 3.50 – 2.32 (m, 30 H, ring CH_2, NCH_2CO, H11, H12, $NH_2C\underline{H}_2$, $CONHC\underline{H}_2$), 2.10 (br m, 4H, H10, H13), 1.76 –

1.14 (m, 10H, $(CH_2)_2CHNHCO$, CH_3). m/z (ES^+) 480 $(MCa)^{2+}$, 492 $(MCu)^{2+}$. 921 $(MH)^+$, 943 $(MNa)^+$.

37. $[TbPh_2dpqC\_NH_2]Cl_3$, [Tb.5]

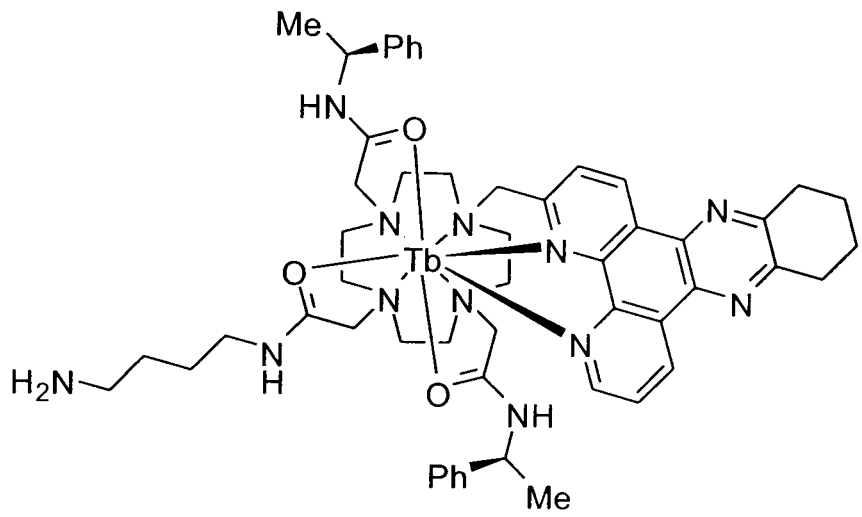

1-(4-Aminobutylcarbamoylmethyl)-7-(3-methyl-10,11,12,13 tetrahydrodipyrido[3,2-a:2',3'-c]phenazine)-4,10-(1-(1-phenyl)ethylcarbamoylmethyl)-1,4,7,10-tetraazacyclododecane (12.9 mg, 1.400 x 10^{-5} mol) and $Tb(OTf)_3.6H_2O$ (8.49 mg, 1.400 x 10^{-5} mol) were dissolved in CH_3CN and mixture heated at 80°C overnight. After cooling, the volume of solvent was reduced to < 0.5 ml and the solution added dropwise to ether (~ 20 ml) with stirring. The precipitate was centrifuged and the solvent decanted; the solid was redissolved in CH_3CN and the process repeated to yield the product as a pale yellow solid (20.1 mg, 1.32 x 10^{-5} mol, 94 %). m/z (ES^+) 363 $(M)^{3+}$, 549 $(MF)^{2+}$, 614 $(MOTf)^{2+}$, 1377 $(MOTf_2)^+$, 1527 $(MOTf_3H)^+$.

$[TbPh_2dpqC\_NH_2]3OTf$ (20.1 mg, 1.32 x 10^{-5} mol) was converted to the more soluble chloride form by ion exchange using 'Dowex' 1-X8 (Cl^-) standard grade ion exchange resin and was eluted with purite water. Preparation of the resin involved overnight reflux in methanol, followed by washing with 1M HCl and with successive portions of H_2O until the eluent had a constant pH. Removal of the water by freeze drying yielded the product as a pale yellow solid (13 mg, 1.14 x 10^{-5} mol, 86 %).. m/z (ES^+) 539 $(M)^{2+}$, 549 $(MF)^{2+}$. λ_{max} (H_2O) 348 nm; τ_{Tb} (H_2O) = 1.5 ms

38. 3-Chloromethyl-10,11,12,13-tetrahydrodipyrido-[3,2a:2',3'-c]-phenazine-N-oxide

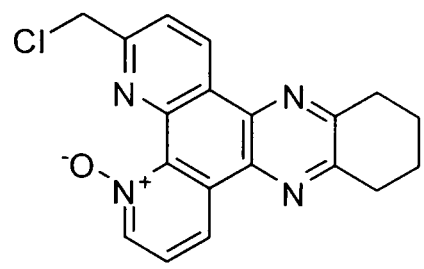

A stirred solution of 3-chloromethyl-10,11,12,13-tetrahydrodipyrido-[3,2a:2',3'-c]-phenazine (22 mg, 6.58 x 10^{-5} mol) in glacial acetic acid (1.4 ml) and H_2O_2 (0.4 ml) was heated to 65°C. After approximately 30 mins, the solution was allowed to cool to room temperature, diluted with distilled water (3 ml) and concentrated in vacuo. The dilution and concentration cycle was repeated 3 times. The residue was neutralised with saturated aqueous Na_2CO_3 and extracted into CH_2Cl_2 (3 x 5 ml). The combined extracts were dried over anhydrous Na_2SO_4 and the solvent removed under vacuum to afford a yellow-brown solid. The product was purified by column chromatography on alumina (gradient elution: CH_2Cl_2 to 0.5 % CH_3OH/CH_2Cl_2, R_f = 0.6, 2.5 % CH_3OH/CH_2Cl_2) and was obtained as a yellow solid. ^{1}H NMR (300 MHz, $CDCl_3$): δ 2.11 (4H, m, H10, 13), 3.24 (4H, m, H11, 12), 5.11 (2H, s, CH_2Cl), 7.67 (1H, dd, J = 8.4, 6.3, H7), 8.10 (1H, d, J = 8.4, H2), 8.83 (1H, d, J = 6.3, H6), 9.15 (1H, d, J = 8.4, H8), 9.56 (1H, d, J = 8.4, H1). ^{13}C NMR (75 MHz, $CDCl_3$): δ 22.7 (C11, 12), 33.5 (C10, 13), 47.8 (CH_2), 122.2 (Ar), 123.7 (Ar), 124.2 (Ar), 126.4 (Ar), 132.2 (Ar), 134.1 (Ar), 136.6 (Ar), 136.8 (Ar), 142.2 (Ar), 142.4 (Ar), 154.8 (Ar), 156.0 (Ar), 157.9 (Ar). m/z (ES^+) 351 $(MH)^+$.

39. 1-(3-methyl-10,11,12,13-tetrahydrodipyrido[3,2-a:2',3'-c]phenazine-N-oxide)-4,7,10-tris-(*tert*-butoxycarbonylmethyl)-1,4,7,10-tetraazacyclododecane

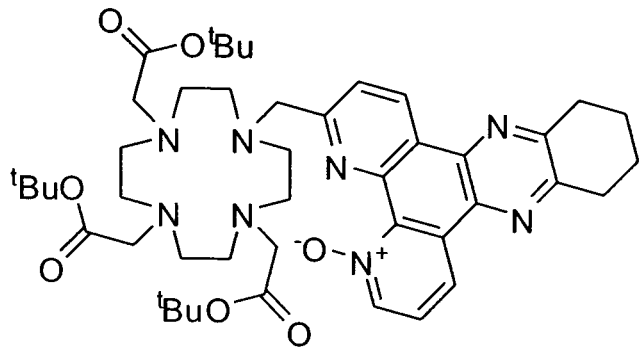

A stirred solution of 1-(3-methyl-10,11,12,13-tetrahydrodipyrido[3,2-a:2',3'-c]phenazine)-4,7,10-tris-(*tert*-butoxycarbonylmethyl))-1,4,7,10-tetraazacyclododecane (32.1 mg, 3.95 x 10^{-5} mol) in glacial acetic acid (0.84 ml) and H_2O_2 (0.24 ml) was heated to 65°C. After approximately 30 mins, the solution was allowed to cool to room temperature, diluted with distilled water (2 ml) and concentrated in vacuo. The dilution and concentration cycle was repeated 3 times. The residue was neutralised with saturated aqueous Na_2CO_3 and extracted into CH_2Cl_2 (3 x 5 ml). The combined extracts were dried over anhydrous Na_2SO_4 and the solvent removed under reduced pressure to yield the product (26.5 mg, 3.20 x 10^{-5}, 81 %) which was used directly in the formation of the europium complex. λ_{max} (H_2O) = 375 nm (cf. 348 nm for **26**)

40. EuDO3AdpqC_NO, [Eu.7]

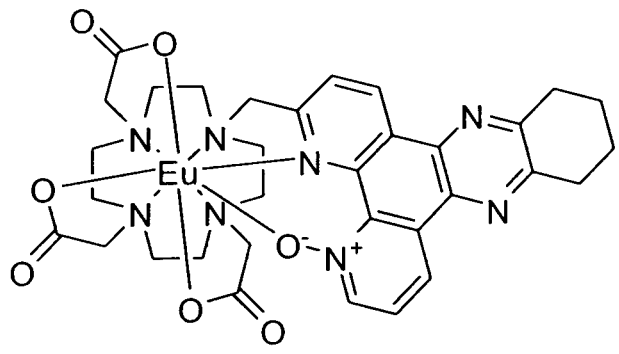

Trifluoroacetic acid (1 ml) was added to a solution of 1-(3-methyl-10,11,12,13-tetrahydrodipyrido[3,2-a:2',3'-c]phenazine-N-oxide)-4,7,10-tris-tert-

butoxycarbonylmethyl-1,4,7,10-tetraazacyclododecane (12.6 mg, 1.52 x 10^{-5} mol) in CH_2Cl_2 (1 ml). The mixture was stirred overnight at room temperature. The solvent was evaporated and the residue redissolved in CH_2Cl_2 for 3 times to facilitate elimination of excess acid and tert-butyl alcohol. The product was checked by ^1H NMR to confirm the disappearance of the signal corresponding to the tert-butyl groups and was used for complexation immediately. The ligand was dissolved in a mixture of methanol and water (1:1, 5 ml) and the pH raised to 5.5 by addition of a 1 M solution of KOH. $EuCl_3.6H_2O$ (5.57 mg, 1.52 x 10^{-5} mol) was added and the mixture heated at 90°C overnight. After being allowed to cool to room temperature the pH of the mixture was raised to 10.0 using dilute KOH solution and the mixture further stirred for 1 hour. The solid in the suspension was removed by syringe filtration and the pH of the resulting clear solution again reduced to 5.5. The solution was freeze dried to yield a solid product. m/z (ES^+) 833 $(MNa)^+$, 849 $(MK)^+$. λ_{max} = 375 nm. The complex is unstable with respect to reduction. (See chapter 2.3.2.2 for discussion).

41. TbDO3AdpqC_NO, [Tb.7]

Complex TbDO3AdpqC_NO, [Tb.7] was prepared as for the europium analogue **40**. λ_{max} (H_2O) = 375 nm. m/z (ES^+) 839 (MNa^+), 855 (MK^+). The complex is unstable with respect to reduction. (See chapter 2.3.2.2 for discussion).

42. 1-(3-Methyl-10,11,12,13-tetrahydrodipyrido[3,2-a:2',3'-c]phenazine)- 4,7,10-tris(methyl-ethyloxyphospihnatomethyl)-1,4,7,10- tetraazacyclododecane

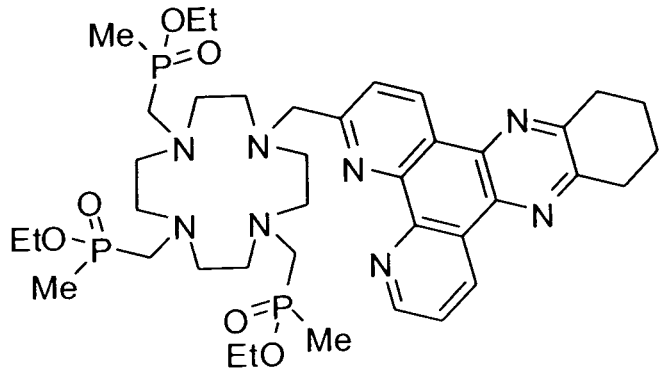

To a solution of 1-(3-methyl-10,11,12,13-tetrahydrodipyrido[3,2-a:2`,3`-c]phenazine)-1,4,7,10-tetraazacyclododecane (50 mg, 1.06 x 10^{-4} mol) in dry THF (25 ml) was added methyldiethoxyphosphine (72.3 mg, 5.31 x 10^{-4} mol) and paraformaldehyde (19.9 mg) and the mixture was heated to reflux (16 h) in a Soxhlet apparatus, equipped with 4 Å molecular sieves, under argon. After removal of the solvent under reduced pressure the residue was purified by column chromatography on neutral alumina (gradient elution: CH_2Cl_2 to 2.4 % CH_3OH/CH_2Cl_2) to yield a yellow oil (22.1 mg, 2.66 x 10^{-5} mol, 25 %). ^{1}H NMR (300 MHz, $CDCl_3$): δ 1.27 (9H, t, J = 7.2, OCH_2CH_3), 1.48 (9H, d, J = 14, PCH_3), 2.04 (4H, br m, H10, H13), 2.6 – 3.2 (22 H, br, ring CH_2 and PCH_2), 3.24 (4H, br m, H11, H12), 3.81 (2H, d, J = 4.8, CH_2dpqC), 4.10 (6H, m, OCH_2CH_3), 7.70 (1H, m, dpqC), 8.02 (1H, m, dpqC), 9.22 (1H, m, dpqC), 9.43 (2H, m, dpqC). ^{31}P NMR (81 MHz, $CDCl_3$): δ 53.2 (3P, br). m/z (ES^+) 435 $(MCa)^{2+}$.

43. 1-(3-Methyl-10,11,12,13-tetrahydrodipyrido[3,2-a:2',3'-c]phenazine)-4,7,10-tris(phosphinoxymethyl)-1,4,7,10-tetraazacyclododecane

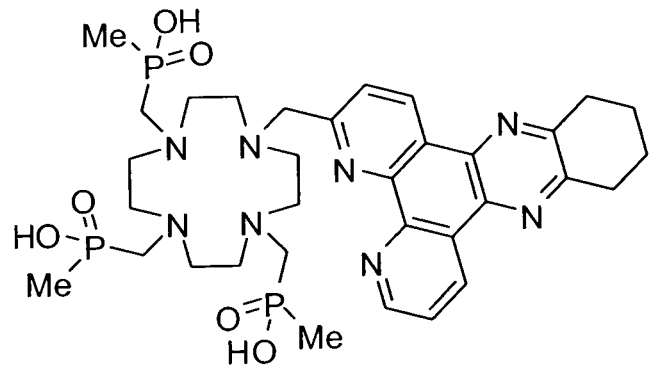

1-(3-Methyl-10,11,12,13-tetrahydrodipyrido[3,2-a:2',3'-c]phenazine)-4,7,10-tris(methyl-ethyloxyphospihnatomethyl)-1,4,7,10-tetraazacyclododecane (22.1 mg, 2.66 x 10^{-5} mol) was dissolved in KOD (0.02 M, 1 ml) and the mixture was boiled under reflux overnight. The product was obtained following evaporation of the solvent under reduced pressure and was complexed immediately. Hydrolysis was carried out in KOD in order that the reduction could be monitored by NMR. ^{31}P NMR (81 MHz, D_2O): δ 37.7 (3P, br).

44. TbPMe$_3$dpqC, [Ln.8]

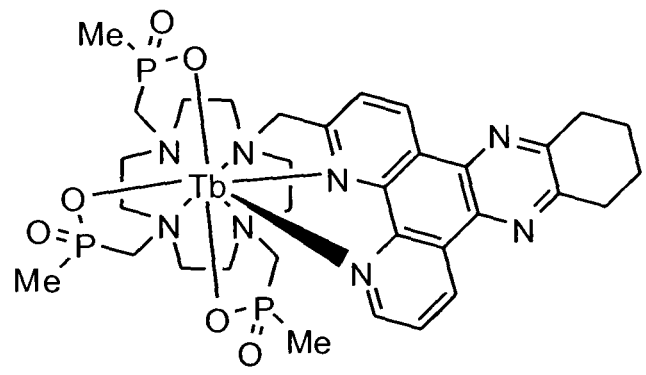

1-(3-Methyl-10,11,12,13-tetrahydrodipyrido[3,2-a:2',3'-c]phenazine)-4,7,10-tris(phosphinoxymethyl)-1,4,7,10-tetraazacyclododecane (19.9 mg, 2.66 x 10^{-5} mol) was dissolved in a mixture of methanol and water (1:1, 3 ml) and the pH raised to 5.5 by addition of a 1 M solution of KOH. $Tb(OAc)_3.xH_2O$ (15.3 mg) was added and the mixture heated at 90°C overnight. After being allowed to cool to room temperature the pH of the mixture was raised to 10.0 using dilute KOH solution and the mixture further stirred for 1 hour. The solid in the suspension was removed by syringe filtration and the pH of the resulting clear solution again reduced to 5.5. The solution was freeze dried to yield the solid product. λ_{max} (H_2O) 348 nm; τ (H_2O) = 2.90 ms ; ϕ(H_2O) = 49 %.

45. 1,4,7-tris(Trifluoromethylcarbonyl)-1,4,7,10-tetraazacyclododecane[8]

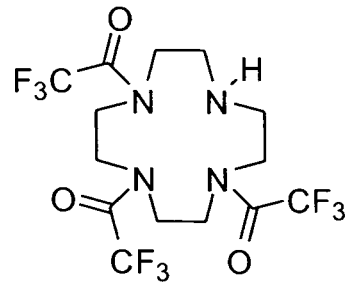

Ethyl trifluoroacetate (16.5 g, 13.8 ml, 0.12 mol) was added dropwise to a solution of cyclen (5g, 0.029 mol) and triethylamine (4.04 ml) in dry MeOH (25 ml) cooled to 0°C. The reaction mixture was stirred at room temperature under argon for 4 hours. The solvent was removed in vacuo. The residue was purified by column chromatography on silica (CH_2Cl_2 to 5% MeOH) to give the product as a white solid (11.7 g, 0.025 mol, 86%). M.p. 77 – 80°C. ^{1}H NMR (300 MHz, $CDCl_3$): δ 2.96 (4 H, m, NCH_2), 3.55 (8 H, m, NCH_2), 3.91 (4 H, m, CH_2). ^{13}C NMR (75 MHz, $CDCl_3$): δ 43.26-52.91 (NCH_2), 116.21 (q, CF_3, J_{CF} = 210), 157.12-157.96 (m, CO). ^{19}F NMR (188 MHz, $CDCl_3$): δ -69.36 (m, CF_3) . m/z (ES^+) 483.3 (MH^+).

46. 1-*tert*-Butoxycarbonyl-4,7,10-tris(trifluoromethylcarbonyl)-1,4,7,10-tetraazacyclododecane[9]

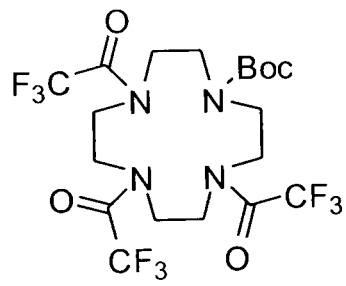

Di*tert*butyl dicarbonate (1.42 g, 6.51 mmol) was added to a solution of 1,4,7-tristrifluoroacetyl-1,4,7,10-tetraazacyclododecane (2.0 g, 4.34 mmol) and triethyl amine (0.3 ml) in dry MeOH (20 ml). The reaction mixture was stirred under argon at room temperature for 24 h after which further ditertbutyl dicarbonate (1.0 g) was added. Further additions of ditertbutyl carbonate (1.0 g) were made after 48 and 72 hours. The reaction was carried out over the period of 100 hours. The solvent was removed in vacuo. The residue was purified by column chromatography on silica (CH_2Cl_2 to 7% ethyl acetate/CH_2Cl_2. R_F = 0.56, 10 % ethyl acetate/CH_2Cl_2) to give the product as a white solid (540 mg, 0.96 mmol, 11%). M.p. 119 – 122°C. ^{1}H NMR

(300 MHz, $CDCl_3$): δ 1.47 (9 H, s, $C(CH_3)_3$), 3.20-3.95 (16 H, bm, NCH_2). ^{13}C NMR (75 MHz, $CDCl_3$): δ 27.98 (CH_3), 48.54-50.70 (NCH_2), 81.04 (C), 116.03 (q, CF_3, $J_{CF} = 210$), 156.67-158.70 (m, CO). ^{19}F NMR (188 MHz, $CDCl_3$): δ -69.70 (m, CF_3) . m/z (ES^+) 583.3 (MH^+).

47. 1-tert-Butoxycarbonyl-1,4,7,10-tetraazacyclododecane[10]

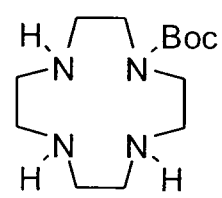

Solution of KOH (2M, 6ml) was added to a solution of 1,4,7-tristrifluoroacetyl-10-tectbutoxycarbonyl-1,4,7,10-tetraazacyclododecane (3.0 g, 5.35 mmol) in a mixture of MeOH (30 ml) and water (12 ml). The reaction mixture was stirred at room temperature under argon for 8 hours. The solvent was removed in vacuo. The residue was dissolved in CH_2Cl_2 and washed with concentrated Na_2CO_3 and NaCl solutions respectively. The organic phase was dried with K_2CO_3 and solvent was removed in vacuo to yield the product as a colourless oil. (1.0 g, 69%). ^1H NMR (300 MHz, $CDCl_3$): δ 1.39 (9 H, s, $C(CH_3)_3$), 2.64 (4 H, t, J = 4.5, NCH_2), 2.74 (8 H, q, J = 5.4, NCH_2), 3.35 (4 H, t, J = 5.4 Hz, NCH_2). m/z (ES^+) 273.3 (MH^+).

48. Benzyl diethoxyphosphine

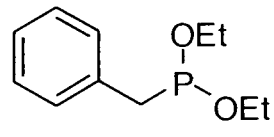

A solution of diethoxychlorophosphine (5.0 g, 31.9 mmol) in dry Et_2O (50 ml) was added dropwise to a solution of benzyl magnesium chloride in Et_2O (1 M, 32 ml), cooled to -15°C. The reaction mixture was warmed up and heated to reflux overnight. The reaction mixture was filtered and solvent was removed by distillation. The residue was purified by vacuum distillation (0.15 mbar, 52-56°C) to yield the product as a colourless liquid (2.5 g, 37 %). ^1H NMR (300 MHz, $CDCl_3$): δ 1.22 (6 H, t, J =

7.2, CH_3), 2.98 (2 H, d, J = 3.9, CH_2), 3.89 (4 H, m, OCH_2), 7.24 (5 H, m, Phenyl). ^{31}P NMR (120 MHz): δ 171.01.

49. 1,4,7-tris(Ethoxybenzylphosphinylmethyl)-10-*tert*-butyloxycarbonyl-1,4,7,10-tetraazacyclododecane

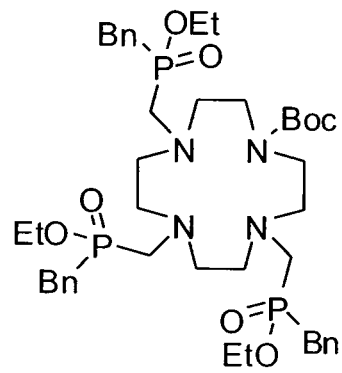

Benzyl diethoxyphosphine (1.4 g, 6.6 mmol) was added to a mixture of 1-*tert*-butyloxycarbonyl-1,4,7,10-tetraazacyclododecane (0.4 g, 1.47 mmol) and paraformaldehyde (0.3 g) in dry THF (23 ml). The reaction mixture was heated to reflux for 8 hours. The reaction mixture was filtered and the solvent was removed in vacuo. The residue was purified by column chromatography on alumina (CH_2Cl_2 to 6% CH_3OH/CH_2Cl_2) to yield the product as a colourless oil (0.3 g, 24%). ^1H NMR (300 MHz, $CDCl_3$): δ 1.18 (9 H, m, CH_3), 1.39 (9H, s, $C(CH_3)_3$), 2.60-3.80 (28 H, m, NCH_2,PCH_2), 3.95 (6 H, m, OCH_2), 7.30 (15 H, m, Phenyl). ^{31}P NMR (120 MHz): δ 50.31 (P). (ES^+) 883.4 ($M+Na^+$).

50. 1,4,7-tris(Ethoxybenzylphosphinylmethyl)-1,4,7,10-tetraazacyclododecane

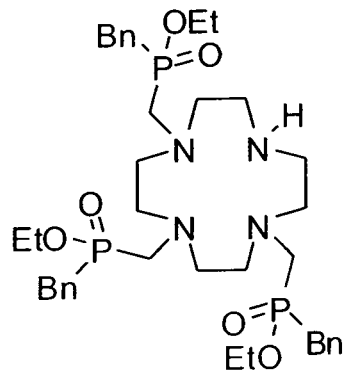

A solution of 1,4,7-tris(ethoxybenzylphosphinylmethyl)-10-*tert*-butyloxycarbonyl-1,4,7,10-tetraazacyclododecane (450 mg, 0.523 mmol) in CH_2Cl_2 (10 ml) and TFA (20 ml) was stirred at room temperature under an argon atmosphere overnight. The solvent was removed in vacuo. The residue was dissolved in CH_2Cl_2 (30 ml) and saturated Na_2CO_3 solution (30 ml). The product was extracted into CH_2Cl_2 (3 x 30 ml). The combined organic extracts were dried over K_2CO_3, filtered and the solvent removed *in vacuo* to give the product as a pale brown oil (330 mg, 0.434 mmol, 83%) which was used directly in the next step. ^{1}H NMR (300 MHz, $CDCl_3$): δ 1.18 (9 H, m, CH_3), 2.60-3.40 (28 H, m, NCH_2, PCH_2), 3.90 (6 H, m, OCH_2), 7.25 (15 H, m, phenyl). ^{31}P NMR (120 MHz): δ 51.45 (P). m/z (ES^+) 761.3 (MH^+).

51. 1-(3-Methyl-10,11,12,13-tetrahydrodipyrido[3,2-a:2',3'-c]phenazine)-4,7,10-tris(ethoxybenzylphosphinylmethyl)-1,4,7,10-tetraazacyclododecane

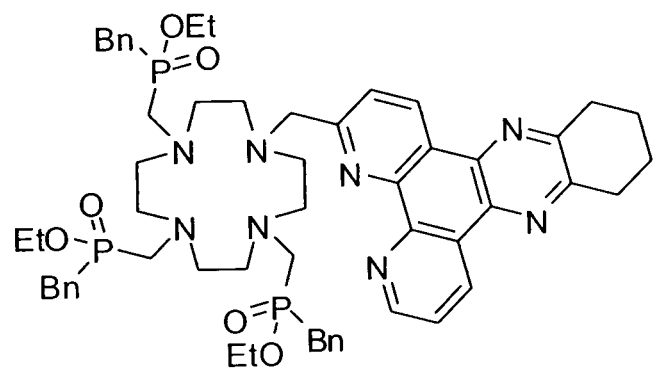

1,4,7-tris(Ethoxybenzylphosphinylmethyl)-1,4,7,10-tetraazacyclododecane (100 mg, 1.31×10^{-4} mol), 3-Chloromethyl-10,11,12,13-tetrahydrodipyrido-[3,2a:2',3'-c]-phenazine (44.0 mg, 1.31×10^{-4} mol), Cs_2CO_3 (51.3 mg, 1.57×10^{-4} mol) and a catalytic quantity of KI were dissolved in CH_2Cl_2/CH_3OH (1:1, 10 ml); the mixture was heated at 60 °C overnight. The reaction mixture was filtered and the crude product following removal of the solvent under reduced pressure. The product was purified by column chromatography on alumina (gradient elution CH_2Cl_2 to 1 % CH_3OH/CH_2Cl_2) as a brown oil (64.7 mg, 6.11×10^{-5} mol, 47 %). ^{1}H NMR (300 MHz, $CDCl_3$): δ ^{1}H NMR (300 MHz, $CDCl_3$): δ 1.04 (6H, m, OCH_2CH_3), 1.13 (3H, t, J = 7.2, OCH_2CH_3), 2.05 (4H, br m, H10, H13), 2.60 – 3.40 (26 H, br, ring CH_2, PCH_2 and H11, H12), 3.40 – 4.20 (8H, m, CH_2dpqC, OCH_2CH_3), 7.70 (1H, m,

dpqC), 8.04 (1H, m, dpqC), 9.22 (1H, m, dpqC), 9.43 (2H, m, dpqC). ^{31}P NMR (120 MHz): δ 49.0 (2P), 51.2 (1P). HRMS (+ m/z): $[M + H]^+$ calculated for $C_{57}H_{74}O_6N_8P_3$, 1059.4936; found, 1059.4938.

52. 1-(3-Methyl-10,11,12,13-tetrahydrodipyrido[3,2-a:2',3'-c]phenazine)-4,7,10-tris(benzylphosphinoxymethyl)-1,4,7,10-tetraazacyclododecane

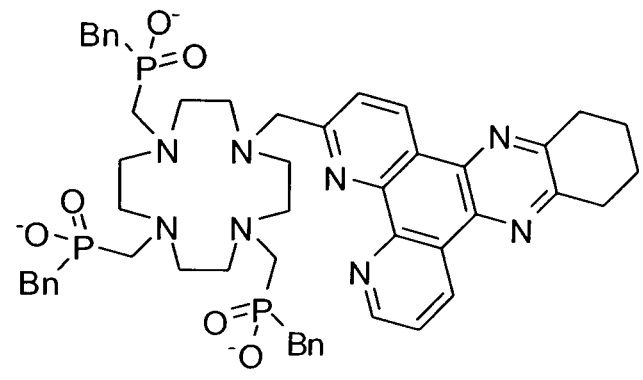

1-(3-Methyl-10,11,12,13-tetrahydrodipyrido[3,2-a:2',3'-c]phenazine)-4,7,10-tris(benzyl-ethyloxyphosphinatomethyl)-1,4,7,10-tetraazacyclododecane (64.7 mg, 6.11 x 10^{-5} mol) was dissolved in HCl (6 M, 1 ml) and the mixture was boiled under reflux overnight. The product was obtained following evaporation of the solvent under reduced pressure and was complexed immediately. Attempts were made to monitor the reaction by ^{31}P NMR, but the ligand became very insoluble upon hydrolysis and was therefore used for complexation imediately.

53. EuPBn$_3$dpqC, [Eu.9]

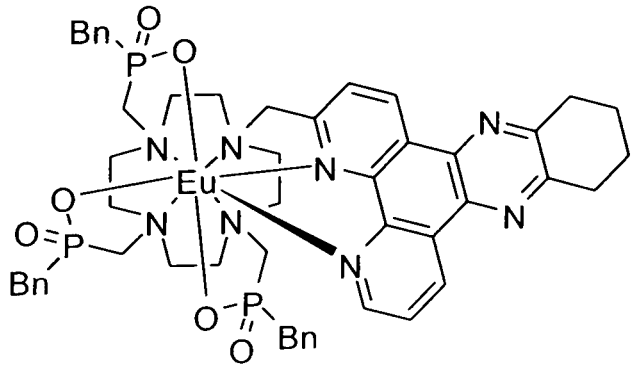

1-(3-Methyl-10,11,12,13-tetrahydrodipyrido[3,2-a:2',3'-c]phenazine)-4,7,10-tris(benzylphosphinoxymethyl)-1,4,7,10-tetraazacyclododecane (25.0 mg, 2.6 x 10^{-5} mol) was dissolved in a mixture of methanol and water (1:1, 10 ml) and the pH raised to 5.5 by addition of a 1 M solution of KOH. $EuCl_3.6H_2O$ (9.52 mg, 2.6 x 10^{-5}) was added and the mixture heated at 90°C overnight. After cooling, a considerable quantity of solid was apparent in the reaction mixture. The solvent was removed under reduced pressure; the residue was very insoluble in all but a 1:1 mixture of CH_2Cl_2 and CH_3OH under high dilution. The complex solution was filtered to remove insoluble salts. Characterisation proved very difficult given the poor solubility of the complex. A ^1H NMR spectrum was obtained in a 1:1 mixture of $CDCl_3$ and CD_3OD. λ_{max} (H_2O) 348 nm; τ (H_2O) = 1.14 ms, τ (D_2O) = 1.69 ms. ^1H NMR (300 MHz, $CDCl_3$) partial assignement: δ 25.0 (1H), 25.8 (1H), 34.0 (1H), 36.1 (1H) assigned as the four most shifted axial cyclen protons, suggestive of one main isomer in solution at ambient temperature. See chapter 2.4.1.2 for a full discussion.

54. $TbPBn_3dpqC$, [Tb.9]

Complex $TbPBn_3dpqC$, [Tb.**9**], was prepared in an analogous manner to that described for complex **53.** λ_{max} (H_2O) 348 nm; τ (H_2O) = 1.13 ms, τ (D_2O) = 1.80 ms. See chapter 2.4.1.2 for a full discussion.

References

1. G.Bobba, *Interaction of chiral lanthanide complexes with nucleic* acids, PhD Thesis, University of Durham, 2002.
2. R. S. Dickins, J. A. K. Howard, C. L. Maupin, J. M. Moloney, D. Parker, J. P. Riehl, G. Siligardi, J. A. G. Williams, *Chem. Eur. J.*, 1999, **5**, 1095.
3. R. S. Dickins, *Chiral Lanthanide Complexes*, PhD Thesis, University of Durham, 1997.
4. E. Fischer, Shultze, *Chem. Ber.*, 1907, **40**, 908.
5. (a) Ishiyama, *J. Biochem. (Tokyo)*, 1933, **17**, 285. (b) Aberhaldon, Fermentforschung, 1938, **16**, 189.
6. Z. Kovacs, A. D. Sherry, *Chem. Commun.*, 1995, 185.
7. R. A. Gardner, R. Kinkade, C. Wang, O. Phanstiel IV, *J. Org. Chem.*, 2004, **69**, 3530.
8. W. Yang, C. M. Giandomenico, M. Sartori, D. A. Moore, *Tet. Lett.*, 2003, **44**, 2481.
9. P. Atkinson, *Chemoselective Phospho-Anion Binding Studies*, PhD Thesis, University of Durham, 2005.
10. M. Sander, *Chem. Ber.*, 1960, **93**, 1220.